Universidad de Oviedo

Investigación en cáncer (Mención de calidad)

Functional relevance of mitochondrial proteases in metabolism and cancer

Doctoral Thesis

Pedro Moral Quirós

February, 2014

RESUMEN DEL CONTENIDO DE TESIS DOCTORAL

1.- Título de la Tesis	
Español/Otro Idioma: Functional relevance of mitochondrial proteases in metabolism and cancer	Inglés: Functional relevance of mitochondrial proteases in metabolism and cancer

2.- Autor	
Nombre: PEDRO MORAL QUIROS	DNI/Pasaporte/NIE:
Programa de Doctorado: Biología funcional y molecular (interdepartamental)	
Órgano responsable: INSTITUTO UNIVERSITARIO DE ONCOLOGÍA	

RESUMEN (en español)

Durante esta Tesis doctoral, hemos intentado contribuir al estudio de la función mitocondrial y su relación con la patología humana, mediante varias aproximaciones. En primer lugar, hemos generado ratones deficientes en dos proteasas mitocondriales, Oma1 y Lonp1, para analizar su relevancia funcional y su papel en la fisiología y patología humana. Estas dos proteasas mitocondriales forman parte del sistema de control de calidad mitocondrial, el cual mantiene la integridad de las mitocondrias, degradando proteínas mal plegadas, dañadas, o simplemente participando en el recambio proteico de las mismas. Mediante la generación de estos modelos murinos, hemos demostrado que OMA1 es una proteasa clave en el control del metabolismo debido a su función regulando la dinámica de las mitocondrias en respuesta a estrés. Además, hemos comprobado que esa misma función de respuesta a estrés, la cual es beneficiosa en condiciones fisiológicas, puede ser perjudicial en condiciones patológicas como el daño renal. Por otro lado, hemos generado ratones deficientes en LONP1, demostrando que esta proteasa es indispensable para la vida, ya que los ratones deficientes en este enzima proteolítico presentan letalidad embrionaria. Así mismo, utilizando los ratones haploinsuficientes y modelos celulares de ganancia y pérdida de función, hemos comprobado que la proteasa Lon es un oncogén, que participa en la reprogramación del metabolismo de las células tumorales a través de la remodelación de la actividad mitocondrial. De este modo, los ratones deficientes en estas dos proteasas nos han permitido definir su relevancia funcional en diversos procesos celulares y extraer algunas claves acerca de su implicación en el cáncer y en la regulación del metabolismo. Finalmente, hemos estudiado las alteraciones mitocondriales y metabólicas en un modelo de envejecimiento prematuro causado por deficiencia en la metaloproteasa Zmpste24. Nuestro trabajo en este sentido ha permitido definir los mecanismos subyacentes al fenotipo de lipodistrofia que presentan dichos ratones mutantes y puede abrir nuevas estrategias para el tratamiento de enfermedades devastadoras como la progeria de Hutchinson-Gilford.

RESUMEN (en Inglés)

In this Thesis, we have tried to contribute to the study of mitochondrial function and their relation with human disease through different approaches. First, we have generated mice deficient in two mitochondrial proteases, Oma1 and Lonp1, to evaluate the physiological and pathological role of those enzymes. These mitochondrial proteases belong to the quality control system, which maintains the integrity of mitochondria degrading misfolded or damaged proteins, or participating in protein turnover. By generating these mouse models, we have shown that OMA1 has a key role in the metabolic control due to its ability to regulate mitochondrial dynamics in response to stress. In addition, we have found that this stress response function, which is beneficial under physiological conditions, can be harmful under pathological situations such as kidney injury. On the other hand, we have generated mice deficient in LONP1, showing that this protease is essential for life, since mice deficient in this protease show embryonic lethality. Further, by using haploinsufficient mice and cellular models of gain- and loss-of-function, we have found that LONP1 acts as an oncogene, participating in the metabolic reprogramming of tumor cells through remodeling mitochondrial function. Therefore, the generation of mice deficient in these two proteolytic enzymes has allowed us to define their functional relevance in various cellular processes and extract some clues about their relation with metabolism regulation and cancer. Finally, we have described the mitochondrial and metabolic alterations in

a mouse model of accelerated aging caused by deficiency in Zmpste24 metalloprotease. Our work in this regard has allowed us to define the molecular mechanisms underlying the lipodystrophy phenotype characteristic of these mutant mice and may open new strategies for the treatment of devastating human diseases such as Hutchinson-Gilford progeria syndrome.

SR. DIRECTOR DEL DEPARTAMENTO DE BIOQUIMICA Y BIOLOGIA MOLECULAR

INFORME PARA LA PRESENTACIÓN DE TESIS DOCTORAL COMO COMPENDIO DE PUBLICACIONES

Año Académico: 2013 / 2014

1.- Datos personales del autor de la Tesis		
Apellidos: MORAL QUIROS	Nombre: PEDRO	
DNI/Pasaporte/NIE:	Teléfono:	Correo electrónico:

2.- Datos académicos	
Programa de Doctorado cursado: Investigación en cancer (Mención de Calidad)	
Órgano responsable: INSTITUTO UNIVERSITARIO DE ONCOLOGÍA Universidad de Oviedo	
Departamento/Instituto en el que presenta la Tesis Doctoral: BIOQUIMICA Y BIOLOGIA MOLECULAR	
Título definitivo de la Tesis	
Español:	Inglés: Functional relevance of mitochondrial proteases in metabolism and cancer
Rama de conocimiento: CIENCIAS	

3.- Director/es de la Tesis	
D/Dª: LOPEZ OTIN, CARLOS	DNI/Pasaporte/NIE:
Departamento/Instituto: BIOQUIMICA Y BIOLOGIA MOLECULAR	
D/Dª:	DNI/Pasaporte/NIE:
Departamento/Instituto/Institución:	

4.- Informe
El trabajo desarrollado por Pedro Moral Quirós a lo largo de su Tesis se ha traducido en la publicación de tres artículos científicos hasta la fecha. Se trata en todos los casos de publicaciones internacionales de alto nivel científico, revisadas y evaluadas por expertos en la materia. Además, la Tesis incluye dos manuscritos los cuales se encuentran actualmente en revisión en revistas internacionales de gran prestigio. Por ello consideramos el compendio de publicaciones como el formato más adecuado de presentación del trabajo de Tesis realizado el doctorando.

Oviedo, 17 de Febrero de 2014

Director/es de la Tesis Doctoral

Fdo.: Carlos López Otín

ACEPTACIÓN COAUTORES PRESENTACIÓN TRABAJOS FORMANDO PARTE DE TESIS DOCTORAL COMO COMPENDIO DE PUBLICACIONES

1.- Datos personales del coautor		
Apellidos: López Otín	Nombre: Carlos	
DNI/Pasaporte/NIE	Teléfono	Correo electrónico

2.- Publicaciones que formarán parte de la tesis y de las que es coautor

Pedro M. Quirós, Andrew J. Ramsay, David Sala, Erika Fernández-Vizarra, Francisco Rodríguez, Juan R. Peinado, Maria Soledad Fernández-García, José A. Vega, José A. Enríquez, Antonio Zorzano, and Carlos López-Otín. "Loss of mitochondrial protease OMA1 alters processing of the GTPase OPA1 and causes obesity and defective thermogenesis in mice" EMBO J. 2012 May 2; 31(9): 2117–2133.

Pedro M. Quirós, Andrew J. Ramsay, and Carlos López-Otín. "New roles for OMA1 metalloprotease: From mitochondrial proteostasis to metabolic homeostasis" Adipocyte. 2013 January 1; 2(1): 7–11.

Xiao Xiao, Pedro M. Quirós, Qingqing Wei1, Carlos López-Otín, and Zheng Dong. "OMA1 mediates OPA1 proteolysis and mitochondrial fragmentation in experimental models of ischemic kidney injury". (American Journal of Physiology - Renal Physiology, accepted pending revision)

Pedro M. Quirós, Yaiza Español, Rebeca Acín-Pérez, Francisco Rodríguez, Clea Bárcena, Kenta Watanabe, Enrique Calvo, Marta Loureiro, M. Soledad Fernández-García, Antonio Fueyo, Jesús Vázquez, José Antonio Enríquez and Carlos López-Otín. "ATP-dependent Lon protease promotes cancer and metastasis by reprogramming mitochondrial activity". (Cell Metabolism, manuscript under revision)

Juan R. Peinado, Pedro M. Quirós, Marina R. Pulido, Guillermo Mariño, María L. Martínez-Chantar, Rafael Vázquez-Martínez, José M. P. Freije, Carlos López-Otín, and María M. Malagón. "Proteomic profiling of adipose tissue from Zmpste24−/− mice, a model of lipodystrophy and premature aging, reveals major changes in mitochondrial function and vimentin processing". Mol Cell Proteomics. 2011 November; 10(11): M111.008094.

ACEPTACIÓN:

Carlos López Otín, en representación de todos los coautores de las publicaciones indicadas en este documento, dado que varias de ellas forman parte de colaboraciones internacionales con autores diversos y numerosos, y teniendo en cuenta que el trabajo reflejado en las mismas ha sido llevado a cabo en parte significativa por el autor de la tesis Pedro Moral Quirós, acepto que las publicaciones anteriores formen parte de la tesis doctoral titulada "Functional relevance of mitochondrial proteases in metabolism and cancer".

Oviedo, 14 de Febrero de 2014

Firma

Fdo. Carlos López Otín

RENUNCIA COAUTORES PRESENTACIÓN TRABAJOS FORMANDO PARTE DE TESIS DOCTORAL

1.- Datos personales del coautor		
Apellidos: López Otín	Nombre: Carlos	
DNI/Pasaporte/NIE	Teléfono	Correo electrónico

2.- Tesis Doctoral
Título: Functional relevance of mitochondrial proteases in metabolism and cancer
Autor: Pedro Moral Quirós
Programa de doctorado: Investigación en cáncer (Mención de calidad)

2.- Publicaciones que formarán parte de la tesis y de las que es coautor

Pedro M. Quirós, Andrew J. Ramsay, David Sala, Erika Fernández-Vizarra, Francisco Rodríguez, Juan R. Peinado, Maria Soledad Fernández-García, José A. Vega, José A. Enríquez, Antonio Zorzano, and Carlos López-Otín. "Loss of mitochondrial protease OMA1 alters processing of the GTPase OPA1 and causes obesity and defective thermogenesis in mice" EMBO J. 2012 May 2; 31(9): 2117–2133.

Pedro M. Quirós, Andrew J. Ramsay, and Carlos López-Otín. " New roles for OMA1 metalloprotease: From mitochondrial proteostasis to metabolic homeostasis" Adipocyte. 2013 January 1; 2(1): 7–11.

Xiao Xiao, Pedro M. Quirós, Qingqing Wei1, Carlos López-Otín, and Zheng Dong. "OMA1 mediates OPA1 proteolysis and mitochondrial fragmentation in experimental models of ischemic kidney injury". (American Journal of Physiology - Renal Physiology, accepted pending revision)

Pedro M. Quirós, Yaiza Español, Rebeca Acín-Pérez, Francisco Rodríguez, Clea Bárcena, Kenta Watanabe, Enrique Calvo, Marta Loureiro, M. Soledad Fernández-García, Antonio Fueyo, Jesús Vázquez, José Antonio Enríquez and Carlos López-Otín. "ATP-dependent Lon protease promotes cancer and metastasis by reprogramming mitochondrial activity ". (Cell Metabolism, manuscript under revision)

Juan R. Peinado, Pedro M. Quirós, Marina R. Pulido, Guillermo Mariño, María L. Martínez-Chantar, Rafael Vázquez-Martínez, José M. P. Freije, Carlos López-Otín, and María M. Malagón. " Proteomic profiling of adipose tissue from Zmpste24 − / − mice, a model of lipodystrophy and premature aging, reveals major changes in mitochondrial function and vimentin processing". Mol Cell Proteomics. 2011 November; 10(11): M111.008094.

RENUNCIA:	
Carlos López Otín, como director de la tesis de Pedro Moral Quirós y dado que varias de las publicaciones indicadas forman parte de colaboraciones internacionales con autores diversos y numerosos, hago constar que en lo que de nosotros dependa en el	

ámbito de la Universidad de Oviedo, dichas publicaciones no serán utilizadas en el futuro como parte de otra Tesis doctoral presentada como compendio de publicaciones por ninguno de los coautores no doctores.

Oviedo, 17 de Febrero de 2014

Firma

Fdo. Carlos López Otín

Abbreviations

bp	base pair
AAA	ATPases associated with diverse cellular activities
AD	Alzheimer disease
AKI	acute kidney disease
ATP	adenosine triphosphate
BAT	brown adipose tissue
BNGE	blue native gel electrophoresis
CCCP	carbonyl cyanide m-chlorophenyl hydrazone
CI	complex I
CII	complex II
CIII	complex III
CIV	complex IV
CS	citrate synthase
DCF	2'-7' dichlorofluorescein
DMBA	7,12-dimethylbenz(a)anthracene
DMEM	Dulbecco's Modified Eagle's medium
DNA	deoxyribonucleic acid
DNP	2,4-dinitrofenol
DSS	dextran sodium sulfate
DTNB	5,5'-dithiobis-(2-nitrobenzoic acid)
EDTA	ethylenediaminetetraacetic acid
ETC	electron transport chain
FDR	false discovery rate
HGPS	Hutchinson–Gilford progeria syndrome
HRP	horseradish peroxidase
H&E	hematoxylin and eosin
IM	inner membrane
IMS	intermembrane space
iTRAQ	isobaric tags for relative and absolute quantitation
KCN	potassium cyanide
KEGG	Kyoto Encyclopedia of Genes and Genomes
MALDI	matrix-assisted laser desorption/ionization
MOMP	mitochondrial outer membrane permeabilization

MPP	mitochondrial processing peptidase
MS	mass spectrometry
NAD	nicotinamide adenine dinucleotide
NADH	NAD reduced
NADP	nicotinamide adenine dinucleotide phosphate
NADPH	NADP reduced
OM	outer membrane
OXPHOS	oxidative phosphorylation
PBS	phosphate-buffered saline
PCR	polymerase chain reaction
PD	Parkinson disease
PFA	paraformaldehyde
PLB	passive lysis buffer
PQC	protein quality control
PVDF	polyvinylidene difluoride
QC	quality control
RNA	ribonucleic acid
ROS	reactive oxygen species
RQ	respiratory quotient / relative quotient
SDS	sodium dodecyl sulfate
SEM	standard error of the mean
TBS	tris-buffered saline
TMPD	tetramethyl-p-phenylenediamine
TMRM	tetramethylrhodamine methyl ester
ToF	time of flight
TPA	12-o-tetradecanoylphorbol-13-acetate
UPS	ubiquitin-proteasome system

Contents

Introduction

Mitochondria are subcellular eukaryotic organelles derived from an α-proteobacteria engulfed by the precursor of the modern eukaryotic cells. These organelles have evolved within our cells in endosymbiosis during billions of years maintaining part of their ancestral characteristics, such as their own genome, known as mitochondrial DNA (mtDNA). In addition, mitochondria have also conserved the capacity to produce ATP, being the central core of energy metabolism within the cell. However, the endosymbiotic evolution has resulted in profound changes in the mitochondrial genome and proteome, which have acquired new components and functions from the host cell (Wallace, 2005). Although mitochondria have been studied extensively since its discovery, over a hundred years ago, during the last decades many works have shown new features that have changed the paradigm around the static mitochondrial function. Furthermore, many diseases have been associated with mutations or deregulations in mitochondrial proteins. These events have revealed the need to explore more in depth the mitochondrial function to understand the mechanism of regulation of these new features and the underlying causes of their associated diseases (Pagliarini and Rutter, 2013).

Mitochondrial structure

Mitochondria comprise two phospholipid bilayers, the outer (OM) and inner membrane (IM), which separate two aqueous compartments, the intermembrane space (IMS) and the matrix (Friedman and Nunnari, 2014). The matrix contains the mtDNA which consists in a small circular genome encoding 13 proteins, 2 ribosomal RNA and 22 transfer RNA genes. The mtDNA-encoded proteins are components of the mitochondrial respiratory complexes, while the mitochondrial RNAs are essential components of the mitochondrial translation machinery. The mitochondrial OM is relatively smooth and very similar to the eukaryotic bilayer in phospholipid composition, whereas the IM retains some characteristics of its bacterial origin, such as the specific phospholipid cardiolipin (Claypool, 2009). Moreover, IM expands its surface forming numerous structures towards the matrix, called cristae, to increase the surface area and membrane proteins required for the multiple functions occurring there. Mitochondria also contain some complex or scaffold proteins that stabilize their internal structure, such as prohibitins in the inner membrane, the multicomplex MitOS/MICOS/MINOS in the cristae junctions and the OPA1 protein in the cristae (Frezza et al., 2006; von der Malsburg et al., 2011; Osman et al., 2009).

In contrast to classical visions of mitochondria, described as isolated entities with a bean shape, it is now well established that these organelles form a complex and connected network in the cell whose structure varies depending on the cell type and tissue, as well as on the metabolic state. The dynamic capacity of mitochondria, along with the specialized machinery developed in their outer and inner membrane, allow them to be shuttled by the

cytoskeleton and be physically connected with various cellular organelles and structures such as plasma membrane, peroxisomes, autophagosomes, lysosomes or endoplasmic reticulum (Westermann, 2010).

Mitochondrial function

Mitochondria are responsible for generating the bulk of cellular energy in the form of ATP through oxidative phosphorylation (OXPHOS). The generation of energy in the cells is based on the use of reducing equivalents of hydrogen, in form of NADH and $FADH_2$, generated by an intricate system that coordinates glucose, fatty acid and amino acid oxidation. In the mitochondria inner membrane, the electrons of these reducing equivalents pass through an electron transport chain (ETC) and finally react with oxygen to generate water. The ETC is composed of four mitochondrial respiratory complexes (complexes I-IV) and some mobile carriers, through which the electrons pass via redox reactions. NADH reducing equivalents enter into mitochondrial ETC through complex I, whereas $FADH_2$ reducing equivalents enter through complex II. The electron transport through the complex I, III and IV is coupled to a pump of protons across the mitochondrial inner membrane, generating a proton gradient used by complex V (ATPase) to generate ATP. This proton gradient, established between the IMS and the matrix, is also used for other purposes, such as the import of calcium and proteins into mitochondria or the generation of heat (Wallace et al., 2010).

Although the function of OXPHOS has been known for many years, the organization of respiratory complexes in the inner membrane has generated much discussion and study. Nowadays, it is widely accepted that mitochondrial complexes are associated into greater entities, called supercomplexes (SCs). However, the model that could explain the assembly and function of the OXPHOS complexes is still debated. The “plasticity model” is the most plausible scenario in this regard and combines two original models in which single complexes (“fluid model”) and different types of supercomplexes (“solid model”) coexist in the inner membrane (Acín-Pérez et al., 2008). According to this integrative model, SCs can be formed by the combination of two different complexes, like complex I and III or complex III and IV, or by the combination of the three complexes I, III, and IV, in a structure known as respirasome. The formation of these SCs allows a more efficient and fast transport of electrons through the ETC and a reduction in ROS, leading to a better response in metabolic adaptations (Lapuente-Brun et al., 2013; Acin-Perez and Enriquez, 2013).

Besides ATP generation, mitochondria are also implicated in several pathways of intermediate metabolism within the cell, such as beta-oxidation of fatty acids or synthesis of pyrimidines and steroids, as well as in the regulation of different pathways of the cellular metabolism. In addition, mitochondria also generate and regulate reactive oxygen species

(ROS), maintain homeostasis and calcium buffering, and participate in essential cellular processes such as apoptosis, cellular differentiation and signaling, immune response, cell cycle or cell growth (McBride et al., 2006). Consistent with the wide diversity of functional roles played by these organelles, mitochondrial dysfunctions are linked with several pathological conditions such as degenerative diseases, metabolic disorders, immunological deficiencies and cancer, but also with the normal process of aging, thereby playing a key role in the balance between life and death (Nunnari and Suomalainen, 2012).

Mitochondrial quality control

During evolution, mitochondria have developed a complex protein quality control system that maintains mitochondrial function and homeostasis (Baker et al., 2011). The role of this control system, mainly mediated by chaperones and proteases, is to restore mitochondrial proteostasis and function, acting at different levels depending on whether the damage is induced at molecular, organellar or cellular level. When this control system fails, mitochondria become sick, generating signals of damage to the cell which converge in the loss of homeostasis, triggering pathological processes or, ultimately, the death. Among all the proteins that participate in this system, mitochondrial proteases play essential roles in almost all steps of the mitochondrial quality control, and are also implicated in the regulation of different processes at organellar and cellular level, such as mitochondrial dynamics, mitophagy or apoptosis (Anand et al., 2013).

Protease-mediated quality control

Mitochondrial proteases and chaperones are responsible for the first line of defense against damage in mitochondria. These organelles contain more than a thousand proteins, of which only 13 components of the OXPHOS system are encoded in mtDNA (Pagliarini et al., 2008). The remaining proteins have to be translated in the cytoplasm and then imported, processed, and assembled in the mitochondria (Schmidt et al., 2010). Therefore, mitochondria and nucleus must coordinate their genomes in order to synthesize and import the mitochondrial components necessary to maintain their functionality. Thus, mitochondrial proteases and chaperones participate in the import and trafficking of proteins from cytosol to mitochondria, the folding of imported proteins and the unfolding and subsequent degradation of damaged and misfolded proteins, as well as in the protein turnover, facilitating the proper functionality of mitochondria (Baker et al., 2011).

Mitochondrial proteases

Proteases are essential hydrolytic enzymes that break the peptide bonds joining the amino acids together in proteins (López-Otín and Overall, 2002). Of the nearly 600 proteases present in the human degradome, there are roughly 30 located in mitochondria. Although the functional relevance of many of them is still unknown, a series of studies first performed in yeast, and then in mammals, have underscore the key role of some of these proteolytic enzymes in the mitochondrial function. However, the lack of mouse models of gain- or loss-of-function for many of these proteases keeps their physiological function largely unknown.

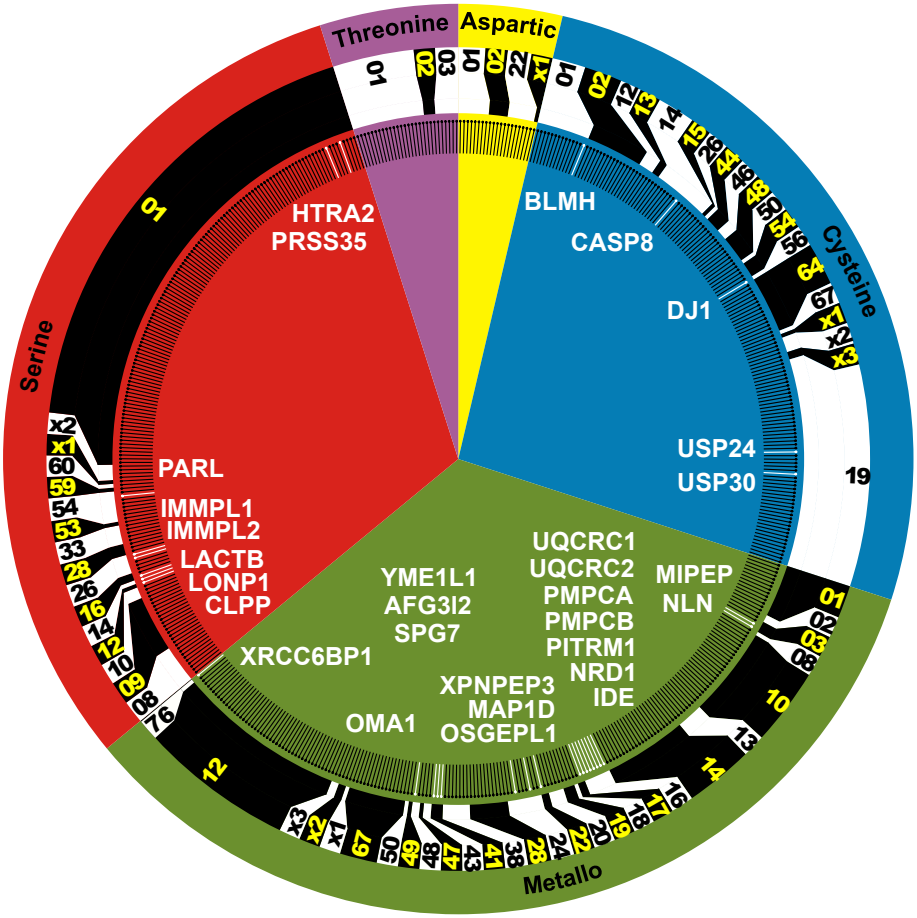

Figure 1: Distribution of mitochondrial proteases in the human degradome.

Most of the mitochondrial proteases are involved in the mitochondrial quality control system. There are four-major ATP-dependent proteases that participate actively in this process: i-AAA and m-AAA proteases, which are located in the inner membrane with their catalytic sites exposed to the intermembrane space and the matrix, respectively, and ClpP and the Lon protease, both located in the matrix. Lon protease (LONP1) is a highly conserved serine peptidase that contributes to protein quality control processes from bacteria to eukaryotic cells (Lu et al., 2003). LONP1 plays an important role in the degradation

of misfolded and damaged proteins in the matrix, supporting cell viability under different stress conditions (Venkatesh et al., 2012). LONP1 function has been studied in depth in bacteria and yeast, and there are several proposed substrates for this enzyme in mammals, such as aconitase, cytochrome c oxidase isoform COX4-1 or TFAM (Bota and Davies, 2002; Fukuda et al., 2007; Matsushima et al., 2010). However, the functional relevance of Lon protease in mammals remains unclear. The second protease in the mitochondrial matrix is ClpP, a serine protease that together with the chaperone ClpX, forms the complex ClpXP which is implicated in the degradation of misfolded proteins (Haynes et al., 2007). The i- and m-AAA are metalloproteases that form hexamers in the IM and have the capacity to recognize unfolded proteins due to the characteristics of their AAA domains (Gerdes et al., 2012). The m-AAA protease is composed of two different subunits in humans, AFG3L2 and paraplegin (or SPG7), whereas i-AAA protease is only composed of a single subunit, YME1L1 (Koppen et al., 2007; Stiburek et al., 2012). Their substrates are mainly membrane-spanning and membrane-associated subunits of the ETC. In addition, m-AAA protease processes the mitochondrial ribosomal protein MrpL32, which requires a second proteolytic cleavage for its maturation after its import to mitochondria (Bonn et al., 2011). Moreover, both proteases have been related to the processing of the fusion protein OPA1 (Ehses et al., 2009; Song et al., 2007). Notably, after proteolytic degradation by these ATP-dependent proteases, some oligopeptidases, such as PITRM1, have been associated with the further processing of polypeptides to small peptides in order to complete the degradation of misfolded proteins (Stahl et al., 2002). Additionally, there are several ATP-independent proteases that collaborate in the maintenance of mitochondrial homeostasis, such as HTRA2 or ATP23 in the IMS, or PARL and OMA1 in the IM. The function of these proteases is not completely clear, but it is widely accepted that all of them play different roles in the mitochondrial quality control (Anand et al., 2013).

Together with these proteases belonging to the quality control machinery, there is another important subgroup of mitochondrial proteases whose function is related to the processing and activation of imported proteins. These mitochondrial processing peptidases, which include PMPCA/B and IMMP1L/2L, are responsible for removing mitochondrial import signals - amphipathic sequences mainly located in the N-terminal of some proteins - necessary to their correct target and entry into mitochondria through the TOM and TIM complexes (Gakh et al., 2002). Finally, other proteases such as MIPEP or XPNPEP3, collaborate with the processing peptidases inducing a further proteolytic cleavage required in certain proteins after being imported into the mitochondrial space (Vögtle et al., 2009).

Mitochondrial unfolded protein response

The balance between nuclear protein synthesis and the import and assembly into mitochondria must be perfectly coordinated, especially in the assembly of OXPHOS complexes,

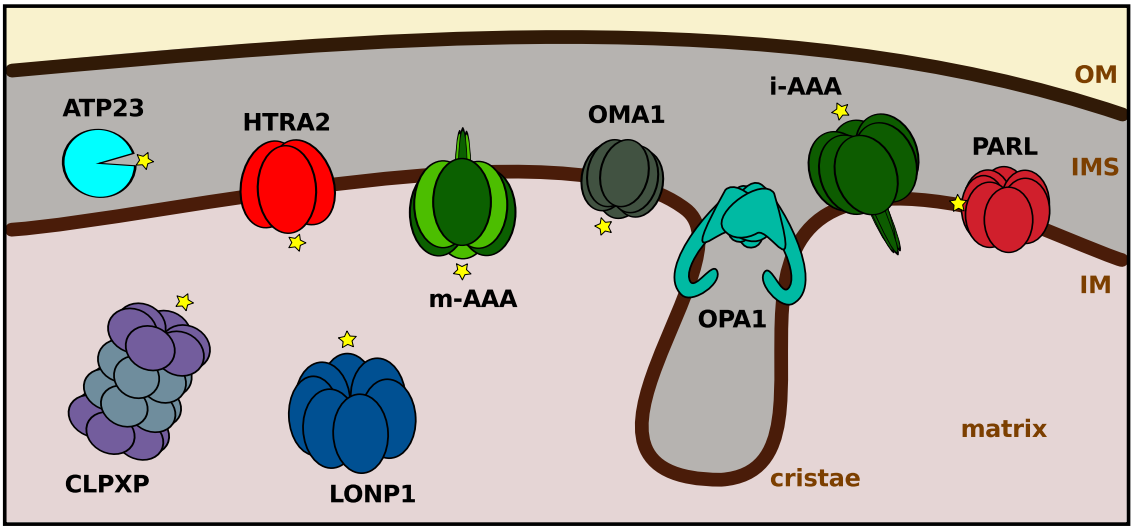

Figure 2: Mitochondrial quality control proteases. Representation of the main mitochondrial quality control proteases and the fusion protein OPA1. Star denotes the location of the active center of proteolytic enzymes.

which have components encoded by different genomes. The imbalance in the expression of nuclear or mitochondrial OXPHOS subunits leads to accumulation of unassembled or unfolded proteins and the subsequent mitochondrial stress and dysfunction. This equilibrium perturbation, also known as mitonuclear imbalance, induces the mitochondrial unfolded protein response (UPRmt) (Houtkooper et al., 2013; Mouchiroud et al., 2013). The UPRmt activates the transcription of nuclear encoded mitochondrial quality control components along with other genes in order to re-establish mitochondrial proteostasis (Haynes and Ron, 2010). Although the UPRmt was discovered in mammalian cells, its function has been more extensively studied in Caenorhabditis elegans, where its activation increases longevity (Houtkooper et al., 2013). In worms, UPRmt involves a protease-mediated digestion of unfolded or unassembled proteins into peptides and the transport of these peptides to the cytoplasm, where they induce a transcriptional response that leads to the expression of components of the mitochondrial quality control system, such as ClpXP protease and the mitochondrial chaperone mtHsp60 (Haynes et al., 2007).

Mitochondrial dynamics

Mitochondria are highly dynamic organelles that continually undergo processes of fusion and fission. Thus, and depending on the cell type, tissue or metabolic state, mitochondria adopt morphologies ranging from small punctuate organelles to a highly connected network (Westermann, 2010). Linked to the quality control mechanism exerted by proteases and chaperones, the regulation of mitochondrial dynamics generates another point of control at organellar level. Accordingly, mitochondrial dynamics can result in more efficient organelles through induction of mitochondrial fusion, or can protect the mitochondrial

network under some stress conditions by coordinating mitochondrial fission (Friedman and Nunnari, 2014). The study of mitochondrial dynamics during recent years has permitted the identification of several components of the fusion and fission machinery, as well as some components that participate in the regulation of these processes. In mammals, the fission process is largely controlled by the dynamin-related GTPase DRP1, located in the cytoplasm (Smirnova et al., 1998). This GTPase is recognized and recruited to mitochondria by specific mitochondrial receptors in the outer membrane, such as MFF, FIS1 or MID49/51, forming a ring-like structure that constricts mitochondrial membranes producing the fission event (Losón et al., 2013). On the other hand, the fusion process is mainly performed by three large GTPases, mitofusin 1 and 2 (MFN1 and MFN2) in the outer membrane and OPA1 in the inner membrane (Chen et al., 2003; Cipolat et al., 2004). Both dynamic processes must be highly controlled to maintain the balance between fusion and fission events, as well as to enable a rapid response to a wide variety of stimuli in the cell. Thus, a decrease in ATP levels, loss of mitochondrial membrane potential or apoptotic stimuli, induce fragmentation of the mitochondrial network due to inhibition of the fusion process (Youle and van der Bliek, 2012). Conversely, the fission process is inhibited in response to starvation, increasing the connection of the mitochondrial tubular network to protect mitochondria from degradation by mitophagy (Gomes et al., 2011). The fusion event has been widely studied in the context of OPA1, a very important protein for mitochondrial function and homeostasis, which is associated with different degenerative diseases (Landes et al., 2010). OPA1 functions are controlled by alternative splicing events and by proteolysis of these isoforms (Ishihara et al., 2006). In mammals, OPA1 produces eight different isoforms, some of which are proteolytically processed generating short isoforms (S-OPA1), while others keep their large structure as long isoforms (L-OPA1). To produce the fusion event is necessary to maintain equimolar amounts of the long and short isoforms, thereby only some of the long isoforms are processed to generate short isoforms. Under stress conditions, all L-OPA1 isoforms are cleaved exclusively generating S-OPA1 isoforms and inhibiting the fusion event. Many proteases have been associated with the physiological processing and stress inactivation of OPA1, such as m-AAA, YME1L1, PARL or OMA1 (Cipolat et al., 2006; Ehses et al., 2009; Head et al., 2009; Song et al., 2007).

Besides OPA1, the other GTPases involved in mitochondrial dynamics are also regulated by proteolysis. Both DRP1 and mitofusins are subjected to different types of post-translational modifications adding new systems of complexity in their regulation. For instance, the E3 ubiquitin ligase MARCH5 ubiquitinates DRP1, FIS1 and mitofusins, while parkin ubiquitinates DRP1 (Park et al., 2010; Poole et al., 2008). The involvement of ubiquitin ligases suggests a possible activity of some deubiquitinating enzymes affecting mitochondrial dynamics, such as USP30 (Nakamura and Hirose, 2008). In addition, DRP1 is sumoylated by the mitochondrial-anchored protein ligase (MAPL), whereas the sestrin-

specific protease 5 (SENP5) removes SUMO from DRP1, regulating its activity and stability in the mitochondrial outer membrane (Braschi et al., 2009; Zunino et al., 2007).

Importantly, mitochondrial dynamics is also involved in other cellular functions, such as the distribution of the mitochondrial pool during cell division, the mitochondrial transport in the cell or the increase in the transmission of membrane potential (Westermann, 2010). These functions indicate that the regulation of fusion and fission processes must be highly regulated and coordinated not only by the mitochondrial quality control machinery, but also by other cellular mechanisms. The importance of mitochondrial networks is highlighted by the fact that mutations in components involved in maintaining mitochondrial dynamics result in neurodegenerative diseases (Itoh et al., 2013).

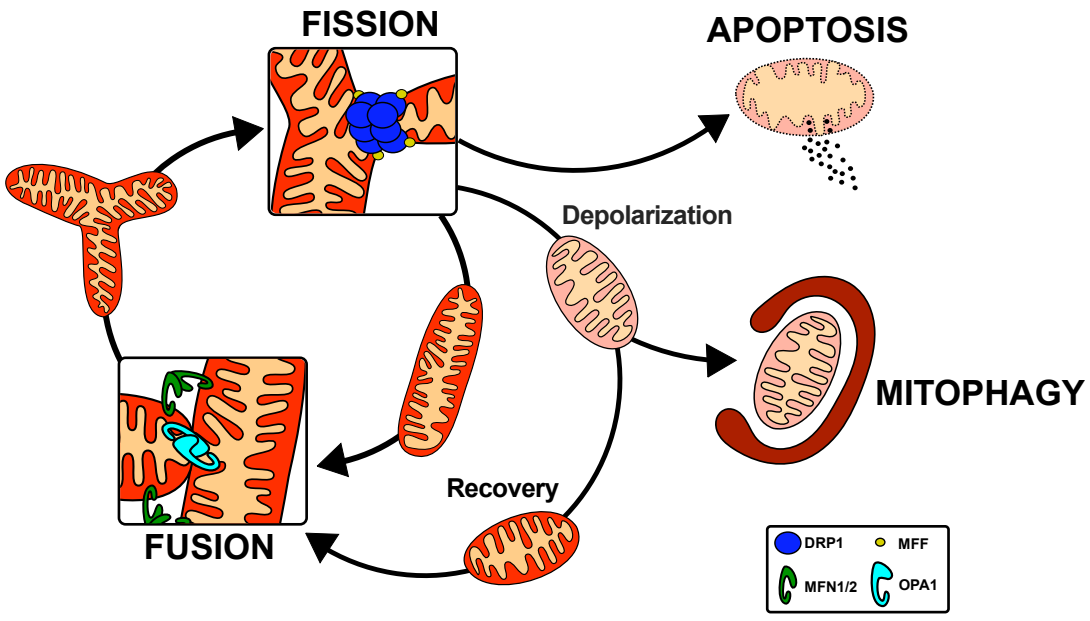

Figure 3: Mitochondrial life cycle. Representation of fusion and fission processes and their relationship with mitophagy and apoptosis.

Mitophagy

Mitophagy is a process by which damaged mitochondria are selectively degraded by the autophagy machinery. Linked to mitochondrial dynamics, mitophagy removes damaged mitochondria with low membrane potential whose function cannot be rescued and which have been previously segregated from the network by mitochondrial fission (Twig et al.,

2008). In addition, mitochondria can be removed by the autophagy machinery in a non-selective degradation due to nutritional requirements in the cell, such as deprivation of nutrients (Mariño et al., 2014). The selective regulation of mitophagy depends on the recruitment of autophagy proteins to the mitochondrial outer membrane through specific receptors. Although the molecular mechanisms underlying this process are not completely well understood, it is assumed that the main regulation depends on the E3 ubiquitin ligase parkin and PINK1 (PTEN-induced kinase 1) (Youle and Narendra, 2011). In normal conditions, PINK1 is imported and inserted into the mitochondria inner membrane, through TOM and TIM complexes by a mechanism dependent on mitochondrial membrane potential. Consequently, PINK1 is degraded in the inner membrane by PARL and another as yet unidentified protease. Loss of the mitochondrial membrane potential inhibits the import and degradation of PINK1 (Jin et al., 2010), thus remaining in the outer membrane. Then, PINK1 is recognized by parkin, which is recruited to mitochondria and mediates the polyubiquitination of different outer membrane proteins, such as mitofusins or VDAC1 (Voltage-Dependent Anion-Channel 1). Subsequently, autophagy proteins such as HDAC or p62 are also recruited to mitochondria, binding to the ubiquitinated proteins and linking them to the autophagy machinery for degradation (Youle and Narendra, 2011). Interestingly, ubiquitination of some proteins, such as mitofusins, can also recruit the proteasome and p97 machinery, indicating that the ubiquitin-proteasome system (UPS) is also involved in the mitochondrial quality control, even degrading outer membrane proteins or participating in the mitophagy process (Tanaka et al., 2010).

Apoptosis

Finally, when all previous steps of quality control fail, stressed cells undergo apoptosis. As described previously, mitochondrial dynamics induces the fission of the mitochondrial network after some kind of deleterious stress signals. In addition, mitochondrial fission is also induced in apoptotic cells (Frank et al., 2001). During apoptosis, pro-apoptotic members of the BCL-2 family BAX/BAK are translocated from cytosol to mitochondria forming pores in the outer membrane and leading to the mitochondrial outer membrane permeabilization (MOMP). This MOMP induces the release of cytochrome c and other pro-apoptotic factors from the intermembrane space, promoting caspase activation and cell death (Mariño et al., 2014). Accordingly, it is described that BAX/BAK oligomerization is accumulated in foci where DRP1 and mitofusins are localized, and that DRP1 can stimulate BAX oligomerization and cytochrome c release, independently of their GTPase activity, indicating the convergence of both processes (Karbowski et al., 2002). On the other hand, mitochondrial fusion protects against apoptosis, due to the inhibition of fragmentation and the stabilization of OPA1, which maintains the integrity of cristae junctions inhibiting the release of pro-apoptotic proteins (Frezza et al., 2006). In addition, the anti-apoptotic protein BCL-2 plays a role in mitochondrial dynamics, stimulating fusion events (Autret and Martin,

2009). These data illustrate a crosstalk between mitochondrial dynamics and apoptosis.

In summary, the mitochondrial quality control system protects mitochondria against damages acting at different molecular and cellular levels. This system, consisting of a series of linked mechanisms, ensures a proper mitochondrial function. Conversely, defects in the mitochondrial quality control system induce mitochondrial damage, and trigger several pathological conditions.

Mitochondrial diseases

Mitochondrial diseases can be defined as inherited disorders resulting from mutations in mtDNA or nDNA that impair mitochondrial function. There are nearly 300 monogenic diseases associated with mitochondrial proteins, half of which are caused by mutations in mitochondrial and nuclear genes encoding OXPHOS components (Koopman et al., 2012). The resulting mutations induce defects in mitochondrial respiratory chain function, which finally trigger a broad and diverse set of pathologies. Neurons are especially susceptible to mitochondrial damage, because they are highly dependent on the mitochondrial function. Thus, many mutations or defects in mitochondrial proteins cause neurodegenerative diseases (Rugarli and Langer, 2012). Nevertheless, mitochondrial dysfunction and respiratory defects are also common in other pathologies, which are not directly associated with mutations in mitochondrial proteins but affect their function and can also be considered as mitochondrial diseases. These include metabolic disorders, cardiac diseases, immunological defects or cancer, as well as the aging process (Wallace, 2011; Lopez-Otin et al., 2013).

Monogenic diseases

Most of the gene mutations that affect mitochondrial function follow a Mendelian inheritance and can be autosomal or recessive. However, mutations in mtDNA genes follow a maternal inheritance, because mitochondria are transmitted maternally. Thousands of mutations have been identified in the human mtDNA, from which hundreds have clinical relevance (Wallace, 2013). These mutations affect genes encoding both proteins and mitochondrial tRNAs and rRNAs, having at least one human disease associated with each of the 37 mtDNA genes (Koopman et al., 2013). The phenotypic characteristics of these diseases are very heterogeneous and have a wide range of disease onset and severity. This heterogeneity can be explained by the heteroplasmy – the presence of a mixture of native and mutated mtDNA in the same cell – which arises due to the multiple copies of mtDNA within each mitochondria (Schon et al., 2012). The heteroplasmy can render differences among tissues or members of the same family who present the same mutation (Sharpley et al., 2012).

Mutations in nDNA-encoded mitochondrial genes have been related to a broad spectrum of pathologies, ranging from severe neurological and lethal syndromes to metabolic problems or predisposition to degenerative diseases (Koopman et al., 2012). These mutations affect genes encoding proteins related to the OXPHOS system, replication and transcription of the mtDNA, protein synthesis, metabolism, mitochondrial dynamics, biogenesis and quality control. The decrease in respiration and OXPHOS defects are a common feature of almost all the mitochondrial diseases. This pleiotropic consequence is explained because respiration has a plethora of mitochondrial proteins involved in its correct execution (Pagliarini et al., 2008). Moreover, defects in proteins of the mitochondrial quality control system will induce the same dysfunction, due to the absence of protein turnover and the accumulation of misfolded and aggregated proteins (Andreux et al., 2013). Some examples of the most relevant mitochondrial pathologies are summarized herein, with special attention to those caused by defects in mitochondrial proteases or proteins related to the mitochondrial quality control system.

Table 1: Mitodegradomopathies

Gene	Function	Associated Disease	Reference
SPG7	PQC/dynamics	Hereditary spastic paraplegia	(Casari et al., 1998)
AFG3L2	PQC	Spastic ataxia-neuropathy syndrome	(Pierson et al., 2011)
	dynamics	Spinocerebellar ataxia SCA28	(Di Bella et al., 2010)
CLPP	PQC	Perrault syndrome	(Jenkinson et al., 2013)
PARL	PQC	Parkinson disease	(Shi et al., 2011)
PARK7	PQC	Parkinson disease type VII	(Bonifati et al., 2003)
UQCRC2	OXPHOS	Mitochondrial complex III deficiency	(Miyake et al., 2013)
CASP8	Apoptosis	Autoimmune lymphoproliferative syndrome	(Varfolomeev et al., 1998)
HTRA2	Apoptosis	Parkinson disease	(Strauss et al., 2005)
PITRM1	MPP	Alzheimer disease	(Pinho et al., 2010)
XPNPEP3	MPP	Nephronophthisis-like nephropathy	(O'Toole et al., 2010)
IMMP2L	MPP	Gilles de la Tourette syndrome	(Petek et al., 2001)

PQC: Protein Quality Control. MPP: Mitochondrial Processing Peptidase

Mitodegradomopathies

Consistent with the essential roles of mitochondrial proteases for mitochondrial function, alterations in the mitochondrial proteolytic system underlie multiple pathological conditions (López-Otín and Bond, 2008). Importantly, among the more than a hundred human hereditary diseases associated with proteases (http://degradome.uniovi.es/), 12 are caused by mutations or defects in mitochondrial proteases (Table 1). These diseases can be defined as mitodegradomopathies. Because more than half of mitochondrial proteases have yet unknown physiological function, the high percentage of human diseases associated with these proteolytic enzymes highlights their importance for mitochondrial and cellular homeostasis.

Neurodegenerative diseases

A common feature in the degenerative disorders, such as Parkinson disease (PD) or Alzheimer (AD) disease is the loss of proteostasis (Powers et al., 2009). This loss, due to an excessive protein misfolding or to defects in the degradation machinery, induces the accumulation of protein aggregates triggering a pathological process. Given the observation that the protein aggregates related to PD or AD may appear into mitochondria, it is plausible that mutations or defects in any of the mitochondrial QC components, essential to remove misfolded proteins or defective mitochondria, may underlie some of these human diseases (Kwong et al., 2006). In fact, mutations in mitochondrial proteases, such as DJ1 (*PARK7*) or HRTA2 (*PARK13*), have been associated with PD due to possible defects in the clearance of α-synuclein deposits in mitochondria (Table 1). Furthermore, defects in mitophagy, due to mutations in *PINK1* or *PARK2*, the gene encoding parkin, are the major causes of an autosomal recessive form of early-onset PD (Kitada et al., 1998; Valente et al., 2004). In addition, mutations and defects in PARL protease are also associated with PD, due to its function processing PINK1 (Table 1). Likewise, the oligopeptidase PITRM1 has been implicated in AD (Table 1), being the main peptidase degrading the amyloid β aggregates, despite the translocation of amyloid β to mitochondria is unclear (Falkevall et al., 2006).Similarly to the above discussed degenerative disorders, other neurological syndromes are caused by defects in components of the mitochondrial quality control system. For example, mutations in *AFG3L2* and *SPG7*, encoding components of the m-AAA protease complex, cause spastic paraplegia and ataxia syndromes with different degrees of severity (Table 1). Furthermore, mutations in *CLPP*, which encodes another mitochondrial ATP-dependent protease, cause Perrault syndrome, an heterogeneous autosomal-recessive condition characterized by sensorineural hearing loss and ovarian failure (Table 1). Likewise, mutations in *HSPD1*, which encodes the mitochondrial chaperonin HSP60, cause an autosomal dominant form of hereditary spastic paraplegia and an autosomal recessive form of Pelizaeus-Merzbacher-like disease (Hansen et al., 2007; Magen et al., 2008). In addition, deregulation of fusion or fission events is also implicated in several human diseases, most of them related to neurological disorders. Thus, mutations in *MFN2* cause the Charcot-Marie-Tooth disease type 2A2 and a hereditary motor and sensory neuropathy (Züchner et al., 2004, 2006). Similarly, a mutation in *DRP1* causes a postnatal death with neurodevelopmental disorder (Waterham et al., 2007). Finally, mutations in *OPA1* cause an autosomal dominant optic atrophy and other forms of optic atrophy with or without deafness, ophthalmoplegia, myopathy, ataxia and neuropathy (Delettre et al., 2000; Payne et al., 2004).

Mitochondrial dysfunction and metabolic alterations

Metabolic alterations, such as type 2 diabetes mellitus, are very common in many mitochondrial diseases, appearing as secondary physiological effects due to the mitochondrial

dysfunction (Liesa and Shirihai, 2013). Although there have not been described mutations in proteins of the mitochondrial quality control system associated with metabolic alterations, dysfunctions in this system have also a profound impact in metabolism due to the loss of mitochondrial homeostasis. The loss of proteostasis induces defects in OXPHOS proteins as well as in mitochondrial enzymes, triggering the alterations in the cellular metabolism which likely contribute to physiological deregulations and metabolic disorders. Thus, defects in the mitochondrial PARL protease, in components of the mitochondrial dynamics, such as mitofusins, or in mediators of the mitochondrial biogenesis, such as PGC1a, have been related to type 2 diabetes mellitus and obesity (Civitarese et al., 2010; Lin et al., 2004; Sebastián et al., 2012). Nevertheless, we cannot exclude that mutations in any component of the mitochondrial quality control machinery could be the primary cause of specific metabolic alterations, but the severe neurological conditions that usually derive from these mutations can mask the metabolic defect. In this regard, the generation of conditional mouse models of some of these proteins, such as OPA1 or mitofusins, has shown that defects in mitochondrial dynamics in specific cells or tissues can induce systemic metabolic alterations (Schneeberger et al., 2013; Zhang et al., 2011).

Mitochondrial dysfunction and cancer

Deregulation of cellular energetics has emerged as a new "Hallmark of Cancer", leading the study of metabolism and mitochondria to the first line of tumor biology (Hanahan and Weinberg, 2011). As discussed above, mitochondria are the central core of the metabolic regulation in the cell and, because some defects in mitochondria alter the metabolism, it is not surprising that changes in the metabolism of tumor cells are caused by defects or modifications in the mitochondrial function (Wallace, 2012). The main alteration observed in tumor cells involving mitochondrial function is the glycolytic switch, in which tumor cells shift their metabolism from oxidative phosphorylation to glycolytic metabolism (Vander Heiden et al., 2009). However, this metabolic reprogramming is not unique, because depending on the type and tumor stage, cancer cells can adapt their metabolism and transform their mitochondria from a highly oxidative organelle to an anabolic machine that generates ATP only through glycolysis. Many mutations in mitochondrial proteins have been described as inductors of the metabolic switch, due to inactivation of the OXPHOS system or the activation or inhibition of different metabolic pathways (Zhang et al., 2012; Yan et al., 2009). Accordingly, an increase in the expression of some proteins of the mitochondrial quality control machinery, such as Lon protease or the HSP90 chaperone TRAP1, have also been associated with tumor cells (Chae et al., 2012; Cheng et al., 2013). In addition, changes in the mitochondrial morphology, due to alterations of the mitochondrial dynamic proteins, seem to play a key role in the invasion, migration and proliferation of different tumor cells, as well as in the resistance to mitophagy and apoptosis (Zhao et al., 2013). Moreover, mutations in *CASP8*, encoding a mitochondrial apoptotic protease, have been associated with hepatocellular car-

cinoma and with the protection against breast and lung cancer (Soung et al., 2005; Sun et al., 2007; Varfolomeev et al., 1998), supporting the idea of the different roles of proteolytic enzymes in tumor biology (López-Otín and Hunter, 2010).

Mitochondrial dysfunction and aging

Mitochondrial dysfunction has been recently featured as one of the nine hallmarks responsible for the aging process (Lopez-Otin et al., 2013). Although the mitochondrial dysfunction has been associated with aging for many years, especially due to the free radical hypothesis of aging and the mitochondrial theory of aging, the molecular mechanisms underlining this association have changed substantially over the last years. As described in the "Hallmarks of Aging", mitochondrial dysfunction together with deregulated nutrient sensing and cellular senescence are antagonistic hallmarks, induced as a response to mitigate the damage caused by the primary hallmarks, but which can be deleterious and exacerbate the damage when occurring chronically or at high levels. These primary hallmarks, which include genomic instability, telomere attrition, epigenetic alterations and loss of proteostasis, also affect the mitochondrial function directly, mainly mediated by the generation of mtDNA mutations and the loss of mitochondrial proteostasis.

Mitochondrial function declines with age and this decline is accompanied by a decrease in respiration, mtDNA, protein levels and mitochondrial mass, as well as alterations in mitochondrial morphology (Bratic and Larsson, 2013). The mitochondrial dysfunction can be induced by different effectors, such as mtDNA mutations, destabilization of OXPHOS complexes, decrease in mitochondrial biogenesis or alterations in mitochondrial dynamics and mitophagy. Because mitochondrial quality control is involved in the maintenance of all of these processes, defects in some of these components may also contribute or even cause the mitochondrial dysfunction observed in the aging process (Baker and Haynes, 2011). Accordingly, many works suggest that the modulation of quality control proteins could increase or decrease longevity. Thus, it is remarkable the case of Lon protease, which increases the healthspan and lifespan of the fungus *Podospora anserina* when is overexpressed, and induces accelerated aging in yeast when it is disrupted (Erjavec et al., 2013; Luce and Osiewacz, 2009). Surprisingly, deletion of ClpP in *P. anserina* increases the lifespan (Fischer et al., 2013). Finally, activation of UPRmt signaling due to a mitonuclear imbalance, together with the mitohormesis induced by ROS, also modulate longevity in worms and flies increasing healthspan and lifespan (Houtkooper et al., 2013; Mouchiroud et al., 2013; Owusu-Ansah et al., 2013).

All these data illustrate the essential roles of the mitochondrial quality control system maintaining mitochondrial and cellular homeostasis. However, despite all functions and pathologies associated with some of these components, the functional relevance of many of

them still remains unknown. Thus, expanding the study of these mitochondrial components appears necessary, not only to know the functional and molecular mechanisms, but also to analyze their possible relevance in different human physiological and pathological conditions.

Objectives

During the last years, studies on mitochondrial biology have revealed the critical role of these organelles for cellular homeostasis. In addition, the discovery of mutations or defects in numerous mitochondrial proteins underlying many human diseases and the observation of mitochondrial dysfunctions associated with other pathologies, has prompted to study in depth how mitochondria control and maintain their functionality. In this regard, many new components and functions have been added to the mitochondrial quality control system, the mechanism controlling the mitochondrial function. Recent studies have identified some mitochondrial proteases which play essential roles in this quality control system. However, the large complexity of the proteolytic landscape has made that the molecular and physiological relevance of several of these mitochondrial proteases still remains unknown. On this basis, and due to the interest of our laboratory in the functional analysis of proteolytic enzymes, we have opened a new line of investigation focused on mitochondrial proteases. Accordingly, the present Thesis work has addressed the generation and phenotypic characterization of two mitochondrial proteases belonging to the mitochondrial quality control system, in order to unravel their in vivo functional relevance. Moreover, the availability in our laboratory of a mouse model of premature aging, showing many metabolic alterations, has focused our attention on the analysis of mitochondrial and metabolic alterations present in these mice as a model of lipodystrophy.

The main objectives of this Doctoral Thesis were:

- Generation of mice deficient in Oma1 to elucidate the putative role of this metalloprotease in the mitochondrial quality control system.
- Evaluation of physiological and pathological alterations in *Oma1*-deficient mice.
- Generation of mice deficient in Lonp1 to analyze the *in vivo* functional relevance of this quality control protease.
- Analysis of the potential implication of Lonp1 in tumor development using *Lonp1*-deficient mice and *in vitro* models.
- Characterization of mitochondrial and metabolic alterations in *Zmpste24*-deficient mice as a model of lipodystrophy.

Experimental procedures

Molecular Biology Methods

General methods

The basic molecular biology techniques employed in this work, including digestion with restriction enzymes, DNA ligations, agarose gel electrophoresis or Southern blot hybridization, which are not detailed below, were performed following manufacturers' instructions or standard protocols.

DNA constructs

Mouse cDNA from LONP1 was cloned tagged with a FLAG epitope in the carboxy terminus and subcloned into the pMX retroviral vector (pMX). The construct was verified by capillary sequencing. For RNA interference experiments, five shRNA vectors were purchased for human and mouse LONP1 (RHS4533-NM_004793 for human and RMM4534-NM_028782 for mouse; Open Biosystems, Thermo Scientific), and the ability of individual and combinations of the shRNAs to repress the expression of LONP1 was evaluated by Western-blot and quantitative RT-PCR after lentiviral infection.

RNA preparation

Collected tissues or cells were immediately homogenized in Trizol (Life Technologies) and processed in the same day through alcohol precipitation according to the manufacturer's instructions. RNA pellets were then washed in cold 80% ethanol and stored at -80 ºC until further use. Following re-suspension of RNA in nuclease-free water (Life Technologies), the samples were quantified and evaluated for purity (260/280 nm ratio) using a NanoDrop ND-1000 spectrophotometer (NanoDrop Technologies).

Real-time quantitative PCR

cDNA was synthesized using 1-2 µg of total RNA, 0.14 mM random hexamer primer, 0.2 mM of each deoxynucleoside triphosphate and Superscript II reverse transcriptase (Life Technologies). Quantitative PCR (qPCR) was performed using TaqMan® gene expression assay (Life Technologies) or Power SYBR® Green PCR Master Mix (Life Technologies), following manufacturer's instructions, using an Applied Biosystems 7300HT Real-Time PCR System. As an internal control, gene expression was normalized to the β-actin gene using TaqMan® gene expression assay or specific oligonucleotides for Power SYBR® Green. Relative expression is represented as relative quantification, using RQ value ($RQ=2^{-\Delta\Delta Ct}$) or with percentage relative to the wild-type animals.

Transcriptional profiling and gene expression analysis

The full transcriptome analysis was conducted using Affymetrix Mouse Gene 1.0 ST Array according to the protocols recommended by the manufacturer (Affymetrix). Total RNA was isolated as described above from mice tissues maintained under the same high-fat diet and light/dark cycle conditions. The RNA integrity was assessed using Agilent 2100 Bioanalyzer (Agilent). Labeling and hybridizations were performed according to protocols from Affymetrix. Washing and scanning were performed using Fluidics Station 400 and GeneChip Scanner (Affymetrix). After scanning, rawdata were processed with RMAExpress (http://RMAExpress.bmbolstad.com), using default settings. DAVID, Ingenuity and OpenOffice software were used for data analysis. The DAVID web portal was used to calculate statistical enrichment of KEGG pathways and Gene Ontology biological processes for each group. The network analyses were generated through the use of Ingenuity Pathways Analysis (Ingenuity® Systems; www.ingenuity.com).

Western blotting

Cultured cells were washed twice with 1× PBS and lysed in RIPA buffer containing 50 mM Tris buffer, pH 7.4, 150 mM NaCl, 1% Triton X-100, 0.1 % SDS, 10 mM EDTA, and complete protease inhibitor cocktail (Roche Applied Science). Mice tissues were immediately frozen in liquid nitrogen after extraction, then homogenized in RIPA buffer, and complete protease inhibitor cocktail (Roche Applied Science). Once homogenized, lysed cells or tissues were centrifuged at 13,000 g at 4 °C for 10 min, and supernatants were collected. The protein concentration of the supernatant was evaluated by bicinchoninic acid technique (BCA protein assay kit; Pierce Biotechnology Inc.). Protein samples (15 μg) were loaded into SDS-polyacrylamide gels. After electrophoresis, gels were electrotransferred onto PVDF or nitrocellulose membranes, blocked with 5% nonfat dried milk in TBS-T (TBS with 0.05% Tween-20) and incubated with primary antibodies following the commercial instructions. After 3 washes with TBS-T, membranes were incubated with the corresponding secondary antibody in 1.5% milk in TBS-T, and developed with Immobilon Western Chemiluminescent HRP substrate (Millipore) in a LAS-3000 Imaging System (Fujifilm). Optical densities of the immunoreactive bands were measured using ImageJ 1.40g analysis software or Multigauge Software (Fujifilm). The antibodies against LONP1 were obtained from Atlas Antibodies; against alpha-tubulin and beta-actin were from Sigma-Aldrich; against Flag, PARP, cleaved caspase-3, AMPKα, Phospho-AMPKα (Thr172), Bcl-2 and ACO2 were from Cell Signaling; against OPA1 and DRP1 were from BD Bioscience; against MFN2 was from Abcam; against PRDX3, prelamin A, CPT1, UCP-1, and PCK1 were from Santa-Cruz Biotechnology; against vimentin was from Biomedal SL. Finally, the antibody against ME1 was from Proteintech.

Lactate, glucose and ATP measurements

Extracellular lactate levels were measured by a colorimetric assay and glucose levels were determined using the Accu-Chek II glucometer (Roche Diagnostics). Briefly, 5 x 10^4 cells were seeded in triplicates into 24-well plates for 48 h in the presence or absence of 500 μM of $CoCl_2$. After that, media were collected and the content of glucose and lactate was determined, normalizing to cell number and subtracting the time zero content of each one. Lactate measurement was performed in a hydrazine/glycine buffer (0.5 M glycine, 0.4 M hydrazine, pH 9.0), containing 17 mg/mL NAD and 11.4 mg/mL lactate dehydrogenase (LDH). The absorbance due to formation of NADH was monitored in a Power Wave XS Microplate reader (Biotek) at 340 nm during 1 h at 25 ºC. The presence of lactate on samples was correlated with the lactate concentrations from a standard curve. Cellular ATP levels were determined using the ATP kit (Molecular probes, Invitrogen) according to the instructions of the manufacturer. Briefly, cells were collected by trypsinization and lysed using passive lysis buffer (PLB) (Promega). The lysates were centrifuged at 12,000 g at 4 ºC for 5 min, and supernatants were collected. The protein concentration of the supernatant was evaluated by BCA protein assay kit (Pierce Biotechnology). We used 1-3 μg of lysed material for ATP determination with a D-luciferin/firefly luciferase reaction mix, and luminescence was measured in a Luminometer TD20/20 and compared to a freshly prepared ATP standard curve.

Mitochondrial DNA copy number quantification

We quantified mtDNA by real-time PCR using ABI PRISM 7300 Sequence Detector System (Life Technologies) and Power SYBR® Green PCR Master Mix (Life Technologies). Total DNA was used as a template and amplified with specific oligodeoxynucleotides for mt-Co2 and Sdha. We calculated the mtDNA copy number per cell using Sdha amplification as a reference for nuclear genome.

ROS determination

The intracellular reactive oxygen species (ROS) levels were determined using the 2,7'-dichloroflourescein diacetate (DCF-DA) dye (Sigma). Tissue or cellular samples were homogenized using PLB (Promega). The lysates were centrifuged at 12,000 × g for 5 min at 4 °C, and supernatants were collected. Protein concentration in the supernatants was evaluated by the bicinchoninic acid technique as described above). Supernatants (50 μg) were mixed with 25 μm DCF-DA and then incubated at 37 °C for 30 min in the dark. Fluorescence at 485/535 was measured using a LS55 PerkinElmer LifeScience spectrofluorometer.

Mitochondria membrane potential assay

Mitochondrial membrane potential was determined using the tetramethylrhodamine methyl ester (TMRM) fluorogenic probe (Sigma). Cells were harvested, washed with PBS, and resuspended in media containing 200 nM TMRM and incubated at 37 °C for 15 min. After that, cells were washed and resuspended in PBS. Samples were placed on ice and analyzed by flow cytometry or fluorometry (540em; 595ex). For negative control we added 20 μM of CCCP, 30 min before treatment with TMRM. Mitochondrial membrane potential was represented as a percentage of positive cells.

Oxygen consumption measurements

Endogenous respiration measurements in intact cells or polarography in digitonin-permeabilized cells were performed using a Clark type oxygen electrode (Hansatech) as previously described (Acín-Pérez et al., 2003). Briefly, for the O_2 consumption determinations in intact cells to measure the maximum respiration capacity, exponentially growing cells were collected by trypsinization and centrifugation, and resuspended at 6.5 x 10^6 cells per mL in 0.75 mL of DMEM containing glucose (4.5 g/L), supplemented with 10% FBS. The cell suspension was transferred to the electrode's 1.5 mL water-jacketed chamber containing a small magnetic bar, thermostated at 37 ºC. Recording of oxygen consumption was carried out for 150 s. Then, 65 nmol 2,4-dinitrophenol (DNP, Sigma) were added to uncouple the respiration and oxygen consumption was monitored for an additional 150 s to determine the maximum O_2 consumption. For polarographic measurements of the individual respiratory complexes, cells were collected by trypsinization and centrifugation, and resuspended at 2-5 x 10^6 cells per mL in Respiration Buffer (250 mM HEPES, pH 7.1; 250 mM sucrose, 10 mM $MgCl_2$, 1 mM ADP and 2 mM potassium phosphate). Cells were permeabilized using 10-20 μg digitonin per 10^6 cells and the oxygen consumption rates were determined using specific substrates and inhibitors for each of the respiratory complexes: glutamate+malate and rotenone for complex I; succinate+glycerol-3-phosphate and antimycin A for complex III; TMPD and KCN for complex IV.

Seahorse analysis of mitochondrial function

Oxygen consumption was measured in 2 x 10^4 intact cells using a Seahorse Bioscience XF96 extracellular flux analyzer, following manufacturer's instructions. Briefly, after a 12 min equilibration, three measurements of 3 min were performed, separated by 3 min of mixing. Maximal membrane potential was assessed by addition of 1 μM oligomycin, and uncoupled mitochondrial respiration was induced by injection of 1 μM CCCP. To stop the mitochondrial dependent oxygen consumption both 1 μM rotenone and antimycin were used.

Electrophoretic analysis of mitochondrial supercomplexes assembly

Mitochondrial membranes were isolated from 5×10^6 cells as previously described (Nijtmans et al., 2002). Mitochondrial membrane proteins were applied and run on a 3-13% first dimension gradient blue native gel electrophoresis (BNGE) as previously described (Schägger, 1995). After electrophoresis, the complexes were electroblotted onto PVDF membranes and sequentially probed with specific antibodies against complex I, anti-NDUFA9; complex III, anti-core1; complex IV, anti-COX5a; complex II, anti-Fp; complex V, anti-F1-ATPase (ATP5B), all from Abcam and anti-Tom20 from Santa Cruz.

Spectrophotometric analysis of mitochondrial complexes

Measurements of mitochondrial complexes enzymatic activities were assessed individually in the spectrophotometer as described elsewhere (Birch-Machin and Turnbull, 2001). Briefly, NADH-dehydrogenase activity rotenone sensitive (CI activity) was measured at 340 nm (ε = 6.22 mM-1cm-1) in a mix containing 25 mM K_2HPO_4, 5 mM $MgCl_2$, 3 mM KCN, 2.5 mg/mL BSA, pH 7.2; 0.13 mM NADH, 0.13 mM UQ1 and 0.2 µg/mL antimycin A. Rotenone sensitivity was measured under the same conditions adding 5 µM rotenone. Succinate dehydrogenase activity (CII activity) was measured at 600 nm (ε = 19.2 $mM^{-1}cm^{-1}$) in a mix containing 25 mM K_2HPO_4, 5 mM $MgCl_2$, 3 mM KCN, 2.5 mg/mL BSA, pH 7.2; 0.03 mM DCPIP (dichlorophenol indophenol), 10 mM succinate, 2 µg/mL antimycin A and 5 µM rotenone. Cytochrome c oxidase activity (COX; CIV activity) was measured at 550 nm (ε = 21 $mM^{-1}cm^{-1}$) in a mix containing 100 mM K2HPO4 pH 7.4 and reduced cytochrome c (1 mg/mL, freshly made). NADH cytochrome c oxido-reductase activity (CI+III) was measured at 550 nm (ε = 21 $mM^{-1}cm^{-1}$) in a mix containing 25 mM K_2HPO_4, 5 mM $MgCl_2$, 3 mM KCN, 2.5 mg/mL BSA, pH 7.2; 0.2 mM KCN, 0.1 mM cytochrome c and 0.1 mM NADH. Succinate cytochrome c oxido-reductase activity (CII+III) was measured at 550 nm (ε = 21 $mM^{-1}cm^{-1}$) in a mix containing 25 mM K_2HPO_4, 5 mM $MgCl_2$, 3 mM KCN, 2.5 mg/mL BSA, pH 7.2; 0.2 mM KCN, 0.1 mM cytochrome c, 3 mM succinate and 5 µM rotenone. Citrate synthase activity (CS) was measured at 412 nm (ε = 13.6 $mM^{-1}cm^{-1}$) in a mix containing 10 mM Tris-HCl pH 8, 0.023 mg/mL acetyl CoA, 0.1 mM DTNB (5,5-dithio-bis-2-nitrobenzoic acid), 0.25 mM oxalacetate and 0.1 % Triton X-100.

Aconitase activity

Aconitase activity was determined as previously described (Gardner et al., 1994). Briefly, 10 µg of mitochondria were used to measure aconitase activity following the linear increase in absorbance at 340 nm during 60 min at 25 ºC in a reaction mixture containing 50 mM Tris-HCl (pH 7.4), 6 mM sodium citrate, 0.2% Triton X-100, 0.6 mM $MnCl_2$, 0.2 mM NADP and 2 U/mL of NADP-dependent isocitrate dehydrogenase.

Fatty acid synthesis assay

Fatty acid synthesis was determined as previously described (Sabbisetti et al., 2009), with some modifications. Briefly, cells were plated in 6-well plate at $3x10^5$ cells per dish and incubated overnight. The next day, cells were incubated with 3 μCi of [1-^{14}C] acetate during 4 h. After that, cells were harvested and resuspended in 500 μL of PBS, and 20 μL aliquots were taken to assess protein content. Then, cells were pelleted and lipids were extracted following Folch method, adding 1 mL of chloroform:methanol (2:1) with occasional vortexing. After 20 min incubation, 200 μL of PBS were added, the samples were mixed and centrifuged, and the lower phase was counted for ^{14}C using scintillation counter. Each experiment was performed in triplicates and normalized with protein content.

Palmitate oxidation measurement

Oxidation of [1-^{14}C] palmitic acid by tissue homogenates was performed as previously described (Hirschey et al., 2010). Briefly, liver and BAT samples were extracted and homogenized in sucrose/Tris/EDTA buffer, incubated for 120 min in the reaction mixture (pH 8.0) containing [1-^{14}C] palmitic acid, and measured for acid-soluble metabolites. Palmitate oxidation rates in primary brown adipocytes were quantified as described (Antinozzi et al., 1998) and corrected for total cellular protein content.

Proteomic methods for adipose tissue

Isoelectric focusing and two-dimensional-PAGE. For gel-based proteomic studies, adipose tissue biopsies from four Zmpste24$^{-/-}$and four wild-type mice were washed in PBS immediately after removal and directly frozen in liquid nitrogen and stored at −80 °C. Samples were processed following a specific protocol previously optimized by us for adipose tissue (Peinado et al., 2010). Three hundred and fifty micrograms (50 μL) of protein from both wild-type and Zmpste24$^{-/-}$ mice, were diluted in 300 μL of Rehydratation Buffer and 0.8% of 3–10NL IPG buffer (GE Healthcare). Immobilized pH gradient strips (18 cm, pH 3–10 NL) were rehydrated overnight in a Ettan IPGPhor 3 System (GE Healthcare) following a stepwise voltage: 300 V for 3 h, linear gradient to 1000 V for 4 h, linear gradient to 8000 V for 2 h, and 8000 V until total Vh (40,000) is reached. Strips were equilibrated in SDS Equilibration Buffer (75 mM Tris, pH 8.8, 6 M urea, 30% glycerol, 2% SDS) containing 2% dithiothreitol for 15 min, followed by a 15 min wash with equilibration buffer containing 2.5% iodoacetamide. Thereafter, proteins were separated on 12% Tris-glycine gels using an Ettan Dalt Six device (GE Healthcare). These conditions resolved proteins with a MW higher than 20 kDa. After migration, gels were stained with SYPRO Ruby dye and/or 0.1% Coomassie brilliant blue G-250, 10% ammonium sulfate, 2% phosphoric acid, and 20% methanol. Both stainings gave similar results. Staining of phosphoproteins was performed using Pro-Q Diamond stain (Bio-Rad Laboratories) according to manufacturer's

instructions. Three hundred micrograms of adipose tissue extracts were set as the minimum protein amount required for a correct identification of phosphorylated proteins. Images of gels stained with Coomassie, SYPRO Ruby or Pro-Q Diamond were captured with the FX system (Bio-Rad).

Identification of proteins and data analysis. Spots were excised automatically in a ProPic station (Genomic Solutions) and subjected to MS analysis. MALDI-ToF-MS analyses were carried out on a 4800 MALDI-ToF/ToF Analyzer (Applied Biosystems/MDS SCIEX). Gel specimens were destained twice (30 min, 37 °C) with 200 mM ammonium bicarbonate/40% acetonitrile. Gel pieces dehydrated for 5 min with pure acetonitrile and dried out over 4 h were automatically digested with trypsin according to standard protocols in a ProGest station (Genomic Solutions). MS and MS/MS analyses of peptides of each sample were analyzed in a 4700 Proteomics Station (Applied Biosystems) in automatic mode. Samples were deposited onto MPep Chips prespotted with α-cyano-4-hydroxy-cinnamic acid (Sunyx) using the thin layer affinity method and analyzed with the following setting: for the MS data, m/z range 800 to 4000 with an accelerating voltage of 20 kV and delayed extraction, peak density of maximum 50 peaks per 200 Da, and minimal signal-to-noise (S/N) ratio of 10 and maximum peak at 65. Peak lists for MS/MS data sets were generated using the 4000 Series Explorer (TM) RAC Software, version 3.5.3 (Applied Biosystems/MDS SCIEX). For the analysis of vimentin isoforms the m/z range was increased from 400 to 4000. Peak lists were submitted to Mascot database in order to identify the proteins (Database, NCBInr 12012010 (10320603 sequences; 3520860234 residues); taxonomy, Mammalia (757310 sequences)). Analysis was limited to peptides of six or more amino acids and maximum one missed cleavage site. Mass tolerance for precursor ions was set to 100 ppm and mass tolerance for fragment ions to 0.2 Da; oxidation of methionine was searched as variable modification and carbamidomethylation of cysteine was set as fixed modification. MS/MS data were also searched against the ENSEMBL Mus musculus database using the open source software X!Tandem (http://www.thegpm.org) with similar settings to those employed for Mascot. Peptide false discovery rates were determined by a target decoy approach using a reversed database concatenated to the parent forward database (Elias and Gygi, 2007). A cutoff expectation value of $\leq$1.0 (significance threshold; expressed as the negative logarithm of E-value) was chosen for individual MS/MS spectra that resulted in a false discovery rate of $\leq$1%. Other post-translational modifications (i.e. phosphorylation) were also investigated using Expasy proteomic server (FindMod and Aldente). To determine whether protein carbamylation occurred during the preparation of the samples, representative protein extracts from mouse adipose tissue were analyzed by High-Performance Liquid Chromatography and Tandem Mass spectrometry using LTQ-Orbitrap XL mass spectrometer (Thermo Fisher Scientific Inc.) equipped with a nanoelectrospray ion source (nESI). 2-DE gel analysis was performed by PDQuest software (Bio-Rad), version 8.0. Spots which gave significant re-

sults ($p < 0.05$) were verified visually to exclude artifacts. Furthermore, statistically significant spots were rechecked by two-tailed unpaired Student's t test after reevaluation of density with ImageJ 1.40g software. For further evaluation, proteins identified by the proteomic study were analyzed using a pathway analysis software (Ingenuity Pathway Analysis (IPA); Ingenuity Systems) to reveal their potential relationships with other proteins and/or intracellular pathways.

Proteomic methods for cells

Protein digestion and iTRAQ labeling. Protein digestion was performed as described (Bonzon-Kulichenko et al., 2011), with minor modifications. The resulting soluble protein extracts from cell lysates or mitochondria-enriched samples were run on a SDS-PAGE gel (10% resolving gel and 4% stacking gel) at 50V. The electrophoresis was stopped when the front dye had barely passed into the resolving gel, ensuring concentration of all proteins into a unique band. Staining was performed using GelCode® Blue Stain Reagent (Thermo Scientific). Gel pieces were cut into cubes (2 mm). For the protein digestion, modified porcine trypsin (Promega) was added at a final ratio of 1:20 (trypsin-protein). Digestion proceeded overnight at 37 ºC in 100 mM ammonium bicarbonate, pH 8.8. The resulting tryptic peptides were extracted twice by 1 h incubation at room temperature in 100% acetonitrile and 5% formic acid and dried-down. Samples were desalted with C18 RP cartridges and vacuum dried. The concentration of peptides was determined by measuring amide bonds in protein chains with the Direct Detect® Spectrometer (Millipore). A total of 200 µg of each peptide mixture were labeled with different iTRAQ tags according to the manufacturer protocol. LONP1-overexpressed derived samples (LON) were labeled with 115 iTRAQ tag, while the 117 iTRAQ tag was used to label the LONP1-knockdown samples (shLon). The iTRAQ tags 114 and 116 were used to label the corresponding controls, respectively. After labeling, the samples were vacuum dried and finally dissolved in trifluoroacetic acid 1% for both desalting and iTRAQ reagent excess removal in reversed-phase C-18 cartridges.

Identification and quantification of proteins. Tryptic peptide mixtures were subjected to nano-liquid chromatography coupled to mass spectrometry for protein identification and quantification. Peptides were separated on a C-18 reversed phase (RP) nano-column (75 µm I.D. and 50 cm, Acclaim PepMap100, Thermo Scientific) and analyzed in a continuous acetonitrile gradient consisting of 0-30% B in 240 min, 50-90% B in 3 min (B = 90% acetonitrile, 0.5% acetic acid). A flow rate of ca. 200 nL/min was used to elute peptides from the RP nano-column to an emitter nanospray needle for real time ionization and peptide fragmentation on a Q-Exactive mass spectrometer (Thermo Fisher). An enhanced FT-resolution spectrum (resolution=70000) followed by the MS/MS spectra from most intense fifteen parent ions were analyzed along the chromatographic run (272 min). Dynamic exclusion was set at 30 s. For protein identification, tandem mass spectra were extracted and

charge state deconvoluted by Proteome Discoverer 1.4.0.288 (Thermo Fisher Scientific). All MS/MS samples were analyzed using SEQUESTTM (Thermo Fisher Scientific). Searching engines were set up to search Mouse_human keratin.fasta (119,718 entries). All searchings were performed assuming full trypsin digestion. Two mixed cleavages were allowed, and an error of 300 ppm or 15 ppm was set for full MS or MS/MS spectra searches, respectively. Oxidation in M, and deamidation in Q or N were selected as dynamic modifications. Database searching results were analyzed using the probability ratio method (Martínez-Bartolomé et al., 2008) and FDR was calculated using a decoy database and the refined method (Navarro and Vázquez, 2009). Proteins that contained similar peptides and could not be differentiated based on MS/MS analysis alone were grouped to satisfy the principles of parsimony. Statistical analysis of quantitative proteomics data were performed using the QuiXoT package, an in-house developed software based on a statistical model previously described (Jorge et al., 2009). In this model, the accuracy of individual quantifications is taken into account by expressing protein abundance changes in units of standard deviation, using the standardized variable zq, to which we also refer as the z-score.

Immunostaining

Normal and tumor colorectal samples were obtained from the tumor bank of the Instituto Universitario de Oncología del Principado de Asturias (IUOPA) and used to evaluate LONP1 expression. The automated system DISCOVERY® (Ventana Medical Systems) was used to carry out the immunohistochemical protein detection. Sections were deparaffinized and rehydrated in EZ Prep® (Ventana Medical Systems) for 20 min. Antigen retrieval was done by heating (CC1 HCl-Tris buffer solution, pH 9.0) (Ventana Medical Systems). Endogenous peroxidase activity was blocked with H2O2 solution (Inhibitor®, Ventana Medical System) for 4 min. Samples were incubated with primary antibody at 37 ºC: polyclonal anti-LONP1 (Atlas Antibodies). Slides were incubated with the secondary antibody (OmniMap® Ventana Medical Systems) for 30 min at room temperature. Then the samples were visualized with 3-3'-diaminobenzidine. Finally, samples were counterstained with hematoxylin, dehydrated and mounted in Entellan (Merck). Sections were photographed (20X) under a light microscope (Nikon-Eclipse 80i).

Cell Biology Methods

Cell culture

Murine embryo fibroblasts (MEFs) were extracted from E13.5 mouse embryos. Briefly, embryos were sterilized with ethanol, washed with PBS, and triturated with razor blades. Samples were then incubated in Dulbecco's modified Eagle's medium (DMEM; Gibco) overnight at 37 °C and 5% CO2. The next day, cultured cells were trypsinized and washed.

Finally, MEFs were incubated at 37 °C and 5% CO2 and used for the corresponding experiments. Adult murine fibroblasts (AFs) were extracted from 12-week-old mice ears. Ears were sterilized with ethanol, washed with PBS, and triturated with razor blades. Samples were then incubated with 600 µL of 4 mg/mL collagenase D (Roche Applied Science) and 4 mg/mL dispase II (Roche Applied Science) in DMEM for 45 min at 37 °C and 5% CO2. After filtering and washing, 6 mL of DMEM with 10% fetal bovine serum (Invitrogen), and 1% antimycotic-antibiotic (Invitrogen) were added, and the mixture was incubated at 37 °C and 5% CO2. Once extracted, cells were cultured in DMEM containing 10% fetal bovine serum at 37 °C and 5% CO2. Brown preadipocytes were isolated from newborn mice by collagenase digestion and were differentiated to mature adipocytes as previously described (Fasshauer et al., 2000). Immortalized MEFs, AFs and preadipocytes were generated by SV40 transformation. Cancer cell lines 293T, HCT116, HCT15, HT29, SW480, SW620, DLD-1, RKO and FHC were purchased from the American Type Culture Collection. The luciferase-expressing cell line B16F10 Luc2 was purchased from Caliper Life Sciences. Cells were routinely maintained in DMEM containing 10% fetal bovine serum (FBS), 100 U/mL penicillin and 100 µg/mL streptomycin (Life Technologies).

Proliferation assay

To quantify cell proliferation, a Cell Titer 96 Non Radioactive cell proliferation kit was used following manufacturer's instructions (Promega Corp.). Briefly, HCT116 and B16F10 cells infected with the corresponding vectors were seeded into 96-well plates at a density of 5x103 cells per well (100 µL) and incubated at 37 ºC, 5% CO2 for 4 days. Cell proliferation was quantified by measuring the conversion of a tetrazolium salt into formazan in living cells. At the desired time points (0 h, 24 h, 48 h and 72 h), 15 µL of Dye solution was added into each well (n=5) and cells were incubated at 37 ºC for 2 h. Then, 100 µL of solubilization/stop mixture was added into each well. After 1 h of incubation at 37 ºC, absorbance was measured at 570 nm with a Power Wave XS Microplate reader (Biotek). Then, each point was normalized to time 0 h and mean ± SEM was calculated and represented. Statistical significance was assessed using a non-parametric Mann Whitney-Wilcoxon test. For classical proliferation assay, growth capacity was determined in 6-well test plates in which 6 x 104 cells were plated per well in 2.5 mL of DMEM medium and incubated at 37 °C for 72 h. Cells were daily counted by using a Neubauer chamber. Population doubling time was calculated using the algorithm provided by http://www.doubling-time.com.

Viral package and cell infection

Lentiviruses and retrovirus were packaged in HEK-293T cells using a VSVG-based and pCL-Ampho package system respectively, kindly provided by Dr. J.M. Silva (Columbia University, New York, USA). Cells were transfected using TransITs-LT1 Transfection Rea-

gent (Mirus Bio LLC) and a mixture of 2 μg of the desired plasmid and 1 μg of each viral helper, following manufacturer's instructions. Transfection medium was removed 24 h after transfection and fresh medium was added to the plate. Cell supernatants were collected at 24 and 48 h and filtered through a 0.45-μm sterile filter. Cells were seeded in 6-well plates at 20–30% confluence 24 h before infection. The following day, 1 mL of viral supernatant supplemented with 5 mg/mL of polybrene (Millipore) was added to growing cells. This step was repeated twice and cells were left to recover for 24 h in growth media before puromycin selection (2 μg/mL).

Microscopy analysis

For fluorescence microscope analyses, mitochondrial morphology was examined after transfection of vector containing mito-DsRed, and images were obtained using a laser-scanning confocal microscope (TCS-SP2-AOBS; Leica) using HCX PL APO Ibd BL ×63 NA 1.4 objective lense. Images were acquired with LCS Suite version 2.61 (Leica), and then modified with ImageJ, using the maxima projection of 0.2 μm stacks images after convolve, median filter and despeckle modification. Brightness/contrast was adjusted using ImageJ. For transmission electron microscopy analysis, BAT samples were dissected from control and cold-stress-induced mice and fixed in 3% glutaraldehyde in 0.1 M sodium cacodylate (pH 7.2) for 1 h at 4 °C. After 3 washes in 0.1 M Sorensen's phosphate buffer, samples were postfixed with 1% osmium tetroxide for 1 h and rinsed 3 times in Sorensen's buffer. Tissues were dehydrated in graded ethanol and infiltrated in 50% propylene oxide/50% resin for 1 h, then placed in resin for 1 h, and embedded in a resin-based mold for polymerization overnight in a 37 °C oven. Ultra-thin sections (85 nm) were taken from each sample and analyzed on a Jeol (JEM-1011) transmission electron microscope at 80 kV. Images were modified using ImageJ and Gimp 2.6 software.

Animal Model Methods

Generation of mouse models

For the generation of Oma1-deficient mice, we first constructed the targeting vector in pKO scrambler V916 (Lexicon Genetics). A 4.3 kb SalI-NotI fragment from 5'-flanking region, exon 1 and part of intron 1 was used as the 5'-homologous region, whereas a 3.2 kb XhoI-ClaI fragment containing part of intron 2 and exon 3 was used as the 3'-region of homology. The 2.4 kb neo cassette was used as a positive marker and replaced a 2.9 kb fragment containing exon 2 of the Oma1 gene. The thymidine kinase marker was used as negative selection. The targeting vector was linearized by digestion with NotI, electroporated into G4 embryonic stem cells, and selected for homologous recombination with G418 and ganciclovir. Positive clones were screened by Southern-blot after PvuII digestion of ge-

nomic DNA and probed with radiolabeled 3'-external probe. A 7.5 kb fragment was detected from wild-type allele and a 4.3 kb fragment from mutant allele. The targeted ES cells clones were expanded and subsequently injected into blastocysts to generate chimeras. Chimeric males were mated with C57BL/6N female mice and the offspring heterozygous for Oma1 were used to generate homozygous null mice. The Lonp1-heterozygous mice were provided by Texas Institute for Genomic Medicine. In all cases, mice genotypes were determined by PCR analysis. We used genomic DNA from tail samples for PCR genotyping using 3 primers under the following conditions: denaturation at 94 ºC for 15 s, annealing at 62 ºC for 15 s, and extension at 72 ºC for 45 s, 30 cycles. For Oma1, we used the following primers: a common forward 5'-gagtgctgtttctctgggtgt-3', a wild type-specific reverse 5'-tgccctaaactgaaggtgtg-3', and a mutant-specific reverse 5'- tagaccgcggctagaggta-3'. The bands amplified were 379 pb for wild-type allele and 252 pb for the mutant allele. For Lonp1, we used: wild type-specific forward 5'-ccctgactgcagagattgtgaa-3', mutation-specific forward 5'-caggacatagcgttggctacc-3' and common reverse 5'-ttcagtgccagtgccttagagt-3'. The bands amplified were 200 bp for wild-type allele and 300 bp for the mutant allele. Mutant mice deficient in Zmpste24 metalloproteinase have been previously described (Pendás et al., 2002).

Animal care

All animal procedures were approved in accordance with the guidelines of the Committee for Animal Experimentation of the Universidad de Oviedo and the Institutional animal care and user committees of Charlie Norwood VA Medical Center and Medical College of Georgia at Georgia Regent University.

Diet-induced obesity

For diet-induced obesity, four-week-old Oma1-deficient mice and their wild-type littermates (C57BL/6/129Sv) were kept in microisolation cages on a 12 h day-night cycle and fed a high-fat diet containing 42% fat (Harlan TD 88137). Mice were weighted once a week for all the experiments. After 24 weeks, mice were sacrificed by cervical dislocation.

Renal ischemia/reperfusion and renal function

Male mice (8-week-old) were subjected to 25 min of bilateral renal ischemia as detailed in previous studies (Wei et al., 2013; Wei and Dong, 2012). Mice were sacrificed at indicated time points of reperfusion to collect blood samples and kidney tissues. For renal function measurement, blood samples were collected from tail clip or at the time of sacrifice. After clotting at room temperature, serum was collected after centrifugation at 12000g for 5 min. Blood urea nitrogen and serum creatinine were measured with analytical kits from Stanbio Laboratory. For histological analysis, kidneys were collected freshly and fixed with 4% PFA. Tubular damage was scored as follows: 1: 0-25% of damage; 2: 26-50% of damage;

3:51-75% of damage and 4: >75% of damage. The slides were checked in a blind manner and the representative images were taken with a light microscope.

Colon carcinogenesis protocol

For colon carcinogenesis protocol, 6-week-old mice were injected intraperitoneally with 10 mg/kg AOM (azoxymethane; Sigma-Aldrich). 4 days after AOM administration, dextran sodium sulfate (DSS; MP Biomedicals) at 2% was administered in the drinking water for five consecutive days. Thereafter, mice received reverse osmosis water. Two DSS cycles more were administered with intervals of 16 days on water between cycles at 2% and 1.5% of DSS respectively. During the course of the experiment, mice were monitored for body weight, rectal prolapse, diarrhea, and macroscopic bleeding as indicative of clinical score (Neufert et al., 2007). Ten days after the last DSS cycle, mice were euthanized and colons were resected, flushed with PBS and measured in length. Colons were fixed in 4% PFA and transversal sections were hematoxylin and eosin (H&E) stained. Number of tumors was count and grade of inflammatory lesions was analyzed in each mice.

Skin papillomas

Skin carcinogenesis was induced using DMBA/TPA as previously described (Balbín et al., 2003). Briefly, 8-week-old mice backs were shaved and treated those 2 days later with a single application of DMBA followed by bi-weekly applications of TPA for 12 weeks. The number and size of papillomas per mouse was recorded weekly. Two weeks after the end of TPA treatment, mice were sacrificed and papillomas were removed, fixed in 4% PFA and subsequently stained with H&E to analyze the grade of lesions.

Experimental metastasis protocol

Lung metastasis experimental model was performed as previously described (Gutierrez-Fernandez et al., 2008). Briefly, mice were anesthetized and 25,000 B16F10-luc2 tumor cells (100 μL) were injected through the jugular vein. Mice were sacrificed after 21 days and lungs were collected for histological analysis. Serial sections of the lung (at least 10 sections spaced 100 μm) were stained with H&E, and metastatic foci were counted. Metastases were classified in small (<10 cells), medium (between 10 and 50 cells), and large (>50 cells). For histological analysis, tissues were fixed in 4% PFA in PBS and stored in 70% ethanol. Fixed tissues were embedded in paraffin by standard procedures. Blocks were sectioned (5 μm) and stained with H&E.

Xenograft models

Xenograft studies were performed as previously described (Fraile et al., 2013). Briefly, 2×10^6 HCT116 cells infected with different constructs of pMX or shRNA vectors were injected subcutaneously into the flanks of six-week-old athymic Nude-Foxn1nu/nu mice (Charles River). Tumor size was measured twice a week with a caliper and tumor volume was determined using the formula: $V=0.4 \times A \times B^2$, where A is the largest and B is the smallest dimension of the tumor. Significant differences were assessed by a linear mixed-effects model.

Glucose and insulin tolerance test

Prior to studies, mice were fasted overnight. For glucose tolerance test (IPGTT), mice received an intraperitoneal injection of glucose (2 mg/g body weight). In insulin tolerance test (IPITT) studies, mice received an intraperitoneal injection of 1U of insulin per Kg of body weight. Blood glucose levels were determined as describe above. Areas under the curve during IPGTT and IPITT were then calculated by the linear trapezoidal method.

Indirect calorimetry

Energy expenditure and ambulation were assessed using Micro-Oxymax multiple sensor (Columbus Instruments). Mice kept on standard rodent chow were housed individually in Oxymax chambers and kept on a 12:12-h light-dark cycle. Constant airflow (0.5 L/min) was drawn through each chamber. After one day of acclimation, O_2 consumption, CO_2 production, RQ, heat and ambulation parameters were recorded during 72 h, using software provided by Columbus Instruments.

Blood and plasma parameters

Animals fed on regular and high-fat diet were fasted overnight and used for measurements of blood and plasma parameters. Blood glucose was measured with Accu-Chek glucometer (Roche Diagnostics) using blood from the tail vein. For all the other measured parameters, blood was extracted directly from heart after anesthetizing mice with halothane. For plasma extraction, blood was immediately centrifuged after collection at 3,000 g and 4 ºC, and the supernatant was collected and stored at -80 ºC until analysis. For plasma insulin, leptin and free fatty-acid measurements, we used Millipore ELISA Kits. All protocols were performed according to manufacturer´s instructions. Levels of hepatic transaminases, cholesterol and triglycerides were determined in the Servicio de Bioquímica, Hospital Universitario Central de Asturias, Oviedo-Spain.

Serum metabolomics

Serum samples from eight Zmpste24$^{+/+}$and Zmpste24$^{-/-}$ male mice were analyzed. A global metabolite profiling UPLC®-MS methodology was employed, where all endogenous metabolite related features, characterized by mass-to-charge ratio m/z and retention time Rt, were included in a subsequent multivariate analysis procedure used to study metabolic differences between the different groups of samples (Theodoridis et al., 2008). Where possible, Rt-m/z features corresponding to putative biomarkers were later identified. Sample preparation, LC-MS system, data processing and multivariate data analysis were performed as described previously (Barr et al., 2010). The top 50 candidate markers resulting from this procedure were selected and subjected to additional statistical testing (fold changes and Wilcoxon rank sum test p values). Finally, the following procedures were used in an attempt to identify selected markers: a) Mass spectra recorded in the positive and negative ion modes were analyzed to determine the most likely parent (as opposed to metal adducts or fragments) ion m/z value and b) The exact mass information obtained, corrected to within a 5 ppm error, was checked against the ChemSpider10 online database, using the subdatabases: KEGG, Lipid Maps and Human Metabolome database. Where possible, hit lists were further reduced by comparison of theoretical/measured isotopic patterns.

Histological analysis

Tissues were fixed in 4% paraformaldehyde in phosphate-buffered saline and stored in 70% ethanol. Fixed tissues were embedded in paraffin by standard procedures. Blocks were sectioned (5 μm) and stained with hematoxylin and eosin (H&E). For adipose tissue evaluation, portions of gonadal and subscapular fat pads and pieces of skin were processed as described above. The number of adipocytes and their mean diameter were determined in 3-μm tissue sections by computer-assisted image analysis. For each sample, different sections were analyzed and 100 adipocytes were measured. The area of cells was calculated considering the maximum and minimum diameter of each adipocyte. For triglyceride detection, liver samples were fixed with 4% formaldehyde and left overnight at 4 ºC. After that, samples were treated with 15% sucrose in PBS for 4 h, and then with 30% sucrose solution overnight, embedded in Tissue-Tek OCT compound (Sakura Finetechnical Co. Ltd.) and stored at -70 ºC. Finally, samples were sectioned at 5 μm thickness with cryostat (CM3050 S, Leica) and cryosections were stained with Oil Red O. For BAT droplets quantification, pictures from BAT sections stained with H&E were analyzed with Image J software.

Statistical Methods

All experimental data are reported as means and the error bars represent the standard error of the mean (SEM). Differences between mean values were analyzed by two-tailed

Student's t test, except in the cases that indicate other statistical test. A value of $P < 0.05$ was considered significant and statistically significant differences are shown with asterisks. All statistical analyses were done using LibreOffice, the statistical package R (http://www.r-project.org) and the application Rstudio (http://www.rstudio.org).

Results

I. Generation and characterization of *Oma1*-deficient mice

Oma1 was identified in yeast as a mitochondrial protease with activities overlapping with m-AAA protease. The function of Oma1 was first associated with the proteolytic degradation of misfolded proteins, being part of the quality control system in the inner membrane of mitochondria. However, the identification of human OMA1 as one of the proteases involved in the degradation of the fusion protein OPA1 suggested a new role for this enzyme in mitochondrial dynamics. In this work, we describe the generation of mice deficient in *Oma1* and the identification of an unexpected key role of this mitochondrial protease in the control of energy metabolism. In addition, we demonstrate that OMA1 plays an essential and non-redundant proteolytic inactivation of OPA1 regulating mitochondrial dynamics under stress conditions.

Article 1: Pedro M. Quirós, Andrew J. Ramsay, David Sala, Erika Fernández-Vizarra, Francisco Rodríguez, Juan R. Peinado, Maria Soledad Fernández-García, José A. Vega, José A. Enríquez, Antonio Zorzano, and Carlos López-Otín. "Loss of mitochondrial protease OMA1 alters processing of the GTPase OPA1 and causes obesity and defective thermogenesis in mice".

EMBO J. 2012 May 2; 31(9): 2117–2133.

Personal contribution to this work

I have been the main responsible for all the experiments shown in this work. I generated, established, managed, genotyped and characterized the Oma1 mouse colony. I performed all subsequent experimental work, including diet-induced obesity studies, metabolic analysis, thermogenic experiments, as well as all morphological and functional cell-based experiments. Additionally, I collaborated in the analysis of mitochondrial function and supervised the energy expenditure studies. Finally, I analyzed the data, prepared the figures and wrote the manuscript under the supervision of Prof. Carlos López-Otín.

The EMBO Journal (2012), 1–17 | © 2012 European Molecular Biology Organization | All Rights Reserved 0261-4189/12
www.embojournal.org

THE
EMBO
JOURNAL

Loss of mitochondrial protease OMA1 alters processing of the GTPase OPA1 and causes obesity and defective thermogenesis in mice

Pedro M Quirós[1], Andrew J Ramsay[1], David Sala[2,3,4], Erika Fernández-Vizarra[5,6], Francisco Rodríguez[1], Juan R Peinado[1,10], Maria Soledad Fernández-García[7], José A Vega[8], José A Enríquez[6,9], Antonio Zorzano[2,3,4] and Carlos López-Otín[1,*]

[1]Departamento de Bioquímica y Biología Molecular, Facultad de Medicina, Instituto Universitario de Oncología, Universidad de Oviedo, Oviedo, Spain, [2]Institute for Research in Biomedicine (IRB Barcelona), Barcelona, Spain, [3]Departament de Bioquímica i Biologia Molecular, Facultat de Biologia, Universitat de Barcelona, Barcelona, Spain, [4]CIBER de Diabetes y Enfermedades Metabólicas Asociadas (CIBERDEM), Instituto de Salud Carlos III, Spain, [5]IIS Aragón, Unidad de Investigación Traslacional I + CS, Hospital Universitario Miguel Servet, Zaragoza, Spain, [6]Departamento de Bioquímica y Biología Molecular, Facultad de Ciencias, Universidad de Zaragoza, Zaragoza, Spain, [7]Servicio de Anatomía Patológica, Hospital Universitario Central de Asturias, Oviedo, Spain, [8]Departamento de Morfología y Biología Celular, Facultad de Medicina, Universidad de Oviedo, Oviedo, Spain and [9]Centro Nacional de Investigaciones Cardiovasculares Carlos III, Madrid, Spain

Mitochondria are dynamic subcellular organelles that convert nutrient intermediates into readily available energy equivalents. Optimal mitochondrial function is ensured by a highly evolved quality control system, coordinated by protein machinery that regulates a process of continual fusion and fission. In this work, we provide *in vivo* evidence that the ATP-independent metalloprotease OMA1 plays an essential role in the proteolytic inactivation of the dynamin-related GTPase OPA1 (optic atrophy 1). We also show that OMA1 deficiency causes a profound perturbation of the mitochondrial fusion–fission equilibrium that has important implications for metabolic homeostasis. Thus, ablation of OMA1 in mice results in marked transcriptional changes in genes of lipid and glucose metabolic pathways and substantial alterations in circulating blood parameters. Additionally, *Oma1*-mutant mice exhibit an increase in body weight due to increased adipose mass, hepatic steatosis, decreased energy expenditure and impaired thermogenenesis. These alterations are especially significant under metabolic stress conditions, indicating that an intact OMA1-OPA1 system is essential for developing the appropriate adaptive response to different metabolic stressors such as a high-fat diet or cold-shock. This study provides the first description of an unexpected role in energy metabolism for the metalloprotease OMA1 and reinforces the importance of mitochondrial quality control for normal metabolic function.

The EMBO Journal advance online publication, 20 March 2012; doi:10.1038/emboj.2012.70
Subject Categories: proteins; cellular metabolism
Keywords: ageing; apoptosis; degradome; metabolism; mitochondrial dynamics

Introduction

Mitochondria are fundamental and highly dynamic organelles of eukaryotic cells that play critical roles in energy generation, control of intermediate metabolism, homeostasis of intracellular calcium and regulation of apoptosis events (Mammucari and Rizzuto, 2010; Wallace *et al*, 2010). Additionally, mitochondria are also the primary source of endogenous reactive oxygen species (Orrenius *et al*, 2007). Due to these multiple functions, it is not surprising that mitochondrial alterations have been associated with many pathological conditions including cancer, neurodegenerative disorders and cardiovascular diseases (Green and Kroemer, 2004; Wallace, 2005; Chen and Chan, 2009; Fulda *et al*, 2010). To maintain their functional activities, mitochondria have developed a quality control mechanism, in which several proteolytic enzymes play important roles (Tatsuta and Langer, 2008). These mitochondrial proteases, together with some mitochondrial chaperones, monitor the folding and assembly of mitochondrial proteins and selectively degrade misfolded and non-assembled polypeptides from the organelle (Voos, 2009). Among the proteolytic enzymes implicated in the mitochondrial quality control system, there are several ATP-dependent proteases such as Yme1L and m-AAA proteases located in the inner membrane, or ClpP and Lonp1 that carry out their functions in the matrix (Koppen and Langer, 2007). The functional relevance of these mitochondrial enzymes is underscored by the finding that deficiencies in m-AAA proteases *SPG7* and *AFG3L2* are responsible for important neurodegenerative diseases such as hereditary spastic paraplegia or a dominant form of spinocerebellar ataxia (Casari *et al*, 1998; Di Bella *et al*, 2010).

In addition to the key role of mitochondrial proteases in the quality control system characteristic of these organelles, these enzymes may also regulate the activity of some mitochondrial proteins through their ability to perform highly specific reactions of proteolytic processing, which contribute to the maturation or inactivation of these substrates. This may be the case of OMA1, a proteolytic enzyme located in the inner mitochondrial membrane, which was first identified in yeast as a protease with **o**verlapping activities with **m**-**A**AA proteases (Kaser *et al*, 2003). OMA1 is a zinc metalloprotease of the M48 family, which exhibits multiple transmembrane

*Corresponding author. Departamento de Bioquímica y Biología Molecular, Facultad de Medicina, Universidad de Oviedo, 33006 Oviedo, Spain. Tel.: +34 985 104201; Fax: +34 985 103564;
E-mail: clo@uniovi.es
[10]Present address: Departamento de Ciencias Médicas, Facultad de Medicina, Universidad de Castilla-La Mancha, Ciudad Real, Spain

Received: 20 September 2011; accepted: 17 February 2012

domains and significant amino-acid sequence similarity with FACE1/ZMPSTE24, a protease involved in the processing of prelamin-A and whose mutations cause premature ageing disorders (Navarro *et al*, 2005; Varela *et al*, 2005, 2008). Yeast OMA1 seems to play a role in mitochondrial quality control through a mechanism similar to that of m-AAA proteases, although in an ATP-independent manner. This activity has been proposed to be part of a salvage system of quality control, reminiscent of that performed in *Escherichia coli* by HtpX, a stress protease with overlapping activities with the AAA protease FtsH (Shimohata *et al*, 2002). Recently, a series of *in vitro* studies have permitted the conclusion that OMA1, in collaboration with m-AAA protease isoenzymes, contributes to the proteolytic processing of OPA1 (optic atrophy 1), a dynamin-related GTPase involved in mitochondrial inner membrane fusion as well as in the regulation of mitochondrial morphology and in the protection of cells from apoptosis (Ehses *et al*, 2009; Head *et al*, 2009).

To further characterize the *in vivo* role of this mitochondrial metalloprotease, we have generated mutant mice deficient in OMA1. These mice are viable and fertile, but exhibit a marked obesity with metabolic alterations, reduced energy expenditure and altered thermogenic response. Furthermore, we have found that OMA1 plays an essential and non-redundant role in the *in vivo* proteolytic inactivation of the GTPase OPA1. Finally, we describe studies of mitochondrial activity and function in brown fat tissue and primary adipocytes deficient in OMA1. On the basis of these findings, we propose that OMA1 participates in mitochondrial quality control regulating mitochondrial dynamics, and its absence induces mitochondrial dysfunctions, which have an important impact on mouse metabolic homeostasis.

Results

Generation of mice deficient in OMA1

To evaluate the *in vivo* roles of OMA1 mitochondrial protease, we engineered a targeting vector to generate a null allele of *Oma1*. This vector was designed to replace exon 2 of the *Oma1* gene with a *neo* cassette (Supplementary Figure S1A). The linearized construct was electroporated into G4 embryonic stem cells and after homologous recombination, we obtained seven positive targeted clones that were used to generate chimeric mice. These mice were then bred to C57BL/6 mice to generate heterozygous mice. After intercrossing these heterozygous mice, we generated $Oma1^{-/-}$ animals at the expected Mendelian ratio. Homozygosity for the mutation was confirmed by Southern blot and PCR analysis (Supplementary Figure S1B and C).

Despite the *Oma1* deficiency, these mutant mice developed normally, with males and females being fertile, and their survival rates indistinguishable from those of their wild-type littermates (Supplementary Figure S2A). During the time period we studied the animals, we did not observe any physical indicators of neurological abnormalities. Moreover, histopathological analysis of the brain, specifically the hippocampus, from 18-month-old mice did not reveal any neuronal loss, nor increment in ubiquitin staining in *Oma1*-deficient mice compared with their littermates controls. Finally, all samples analysed for both genotypes displayed changes consistent with normal ageing (Supplementary Figure S2B). These findings demonstrate that OMA1 is dispensable for embryonic and adult mouse development, as well as for normal growth and fertility, possibly due to functional redundancy with other peptidases present in the inner membrane of mitochondria.

Diet-induced obesity in $Oma1^{-/-}$ mice

In the course of phenotypic characterization of *Oma1*-deficient mice, we noticed a significant increase in the body weight of $Oma1^{-/-}$ mice as compared with their wild-type littermates kept on standard chow (Supplementary Figure S2C). This observation encouraged us to evaluate a putative role for OMA1 in adipose tissue biology. Accordingly, wild-type and *Oma1* knockout mice were fed a high-fat diet and total body weights were determined for 24 weeks. We started our study with 4-week-old mice, which displayed similar weights and adipose deposit composition in males and females of each genotype (Supplementary Figure S2D). At 8 weeks, we observed significant weight differences in $Oma1^{-/-}$ males when compared with controls, and these marked changes continued until the end of the experiment. In the case of $Oma1^{-/-}$ females, there was also an increase of weight when compared with the corresponding controls, but lower than in male mice (Figure 1A and B). Statistical analysis revealed that the gain of weight observed at the end of the experiment was significantly higher in both male and female mice deficient in *Oma1* than in their littermate controls (Figure 1C).

To determine whether the increase of body weight observed in *Oma1*-deficient mice was due to an increase in fat content, gonadal and subscapular fat pad deposits were separately weighted. We only detected an increase of gonadal fat pads weight and their weight normalized to total body weight in *Oma1*-null mice (Figure 1D and E), whereas subscapular fat pads and their weight relative to total body weight did not reach statistical significant differences. Histological analysis of white adipose tissue (WAT) from gonadal and subcutaneous deposits showed a marked adipocyte hypertrophy in $Oma1^{-/-}$ mice (Figure 1F), which was confirmed by morphometric measurement of adipocyte area (Figure 1G). Analysis of brown adipose tissue (BAT) of *Oma1*-deficient mice did not show any significant alteration in fat content (Supplementary Figure S3A), indicating that the obesity-induced phenotype was only related to WAT hypertrophy. Interestingly, those $Oma1^{-/-}$ mice exhibiting the most severe obesity phenotype often presented granuloma-like lesions in the intestinal mesenteric fat. Further histological analysis of these granulomatous lesions revealed the presence of fat necrosis foci containing foamy histiocytes and cholesterol crystals (Supplementary Figure S3B). Similar lesions have been described previously as crown-like structures, which appear to manifest as a result of increased inflammation and adipocyte cell death (Cinti *et al*, 2005). All these findings suggest that the absence of OMA1 protease leads to profound alterations in WAT homeostasis after nutritional challenges.

Metabolic changes in $Oma1^{-/-}$ mice

To further evaluate the phenotypic alterations observed in $Oma1^{-/-}$ mice, we performed an analysis of biochemical parameters and metabolic enzymes in the liver of these mutant mice under both standard and high-fat diet. First, and because in many animal models of obesity blood glucose tends to be above normal due to obesity-induced insulin

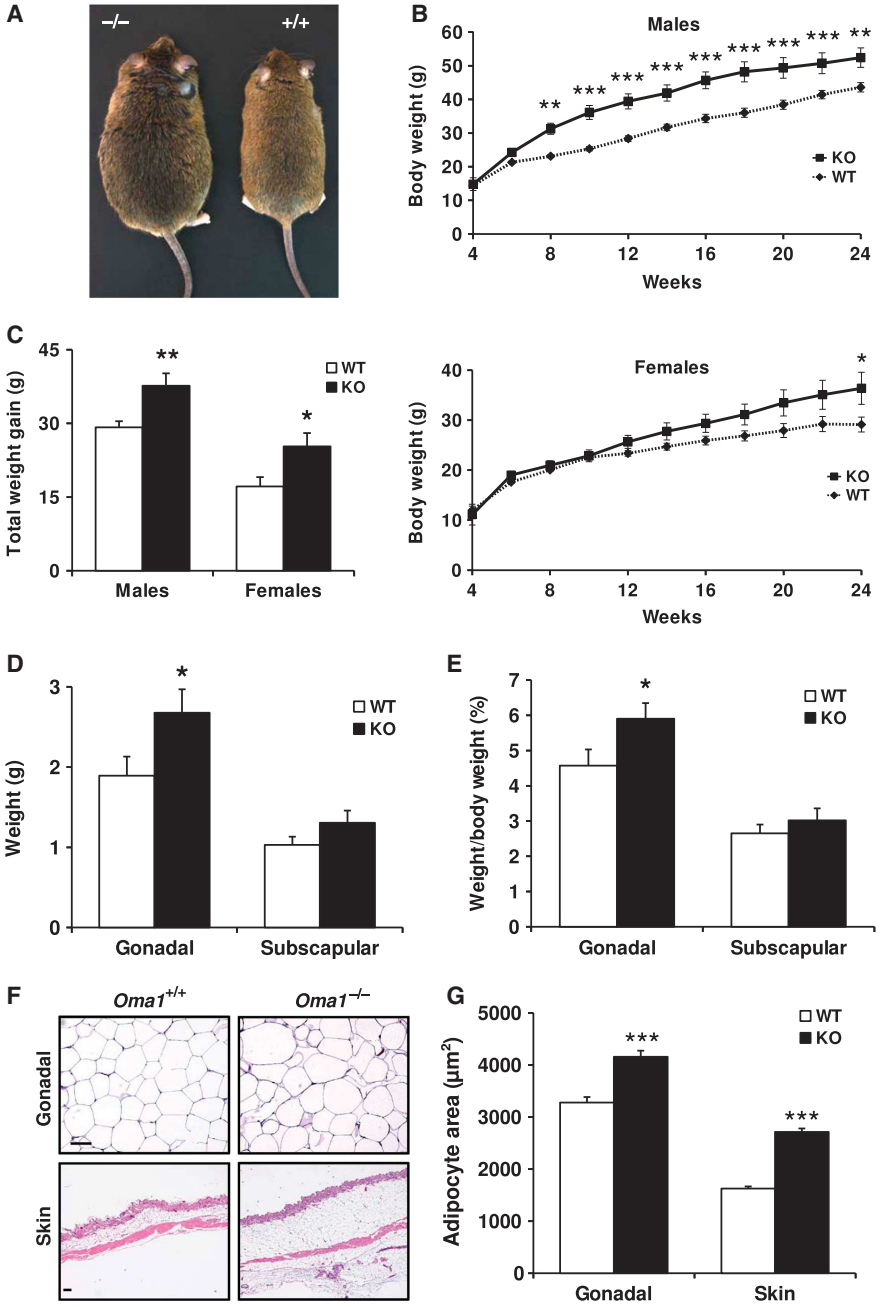

Figure 1 Increase of body weight and fat content in *Oma1*$^{-/-}$ mice after diet-induced obesity. (**A**) Photograph of representative *Oma1*$^{+/+}$ and *Oma1*$^{-/-}$ mice after high-fat diet induced obesity. (**B**) Body weight curves of males and females of *Oma1*$^{+/+}$ (♦) and *Oma1*$^{-/-}$ (■) mice ($n = 8$–12). (**C**) Lean body mass in the same animals. (**D**) Gonadal and subscapular fat mass and (**E**) gonadal and subscapular fat mass as a percentage of total body weight of the same animals at the end of the experiment. (**F**) H&E sections of gonadal WAT and skin of *Oma1*$^{+/+}$ and *Oma1*$^{-/-}$ mice. Original magnifications WAT: × 200; skin: × 40. Scale bar: 60 µm. (**G**) Mean of adipocyte area in gonadal WAT and skin. Results are mean ± s.e.m. ($n = 6$–12). *$P < 0.05$; **$P < 0.01$; ***$P < 0.001$.

resistance, we measured blood glucose levels in *Oma1*$^{-/-}$ adult mice, but we did not observe any differences with control mice in both standard and high-fat diet conditions (Figure 2A). Furthermore, analysis of liver parameters did not reveal significant differences in levels of hepatic transaminases under standard chow diet. However, under high-fat diet, we observed an increment in the levels of both Ala- and Asp-transaminases (Figure 2B). Total levels of cholesterol in mutant mice did not exhibit significant differences with those of control animals under chow and high-fat diet (Figure 2C). Nevertheless, levels of triglycerides were significantly higher in *Oma1*$^{-/-}$ mice compared with littermate controls, in both

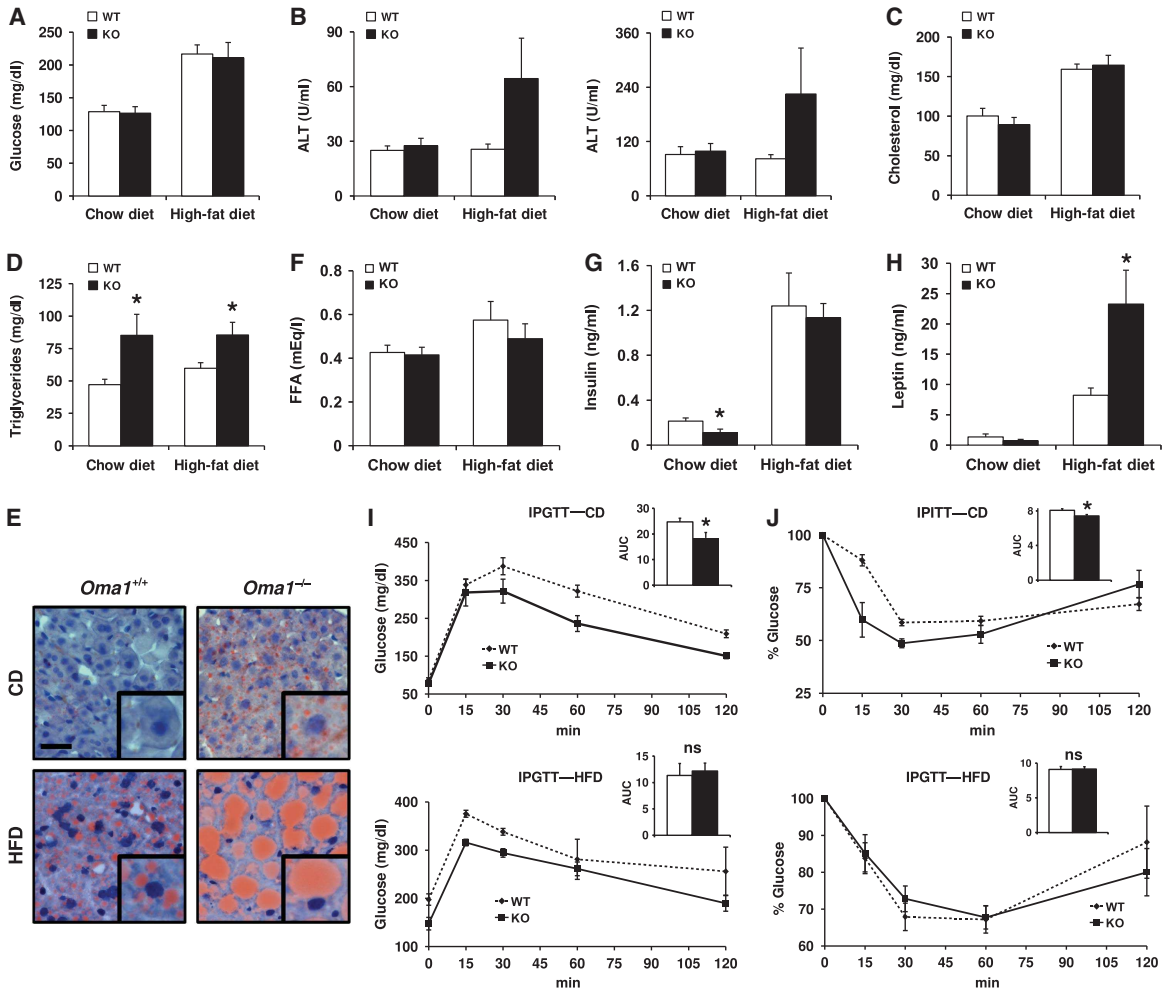

Figure 2 Lipid metabolism and glucose tolerance alterations in *Oma1*$^{-/-}$ mice under standard chow and high-fat diet. Analysis of serum and plasma parameters of *Oma1*$^{+/+}$ and *Oma1*$^{-/-}$ mice (12–20 weeks old, $n = 6$–12 for each group). Mice were fed on standard chow and high-fat diet, and analysis was determined after an overnight fast. (**A**) Blood glucose levels in *Oma1*$^{+/+}$ and *Oma1*$^{-/-}$ mice. (**B**) Serum levels of alanine aminotransaminase (ALT) and aspartate aminotransaminase (AST), (**C**) cholesterol and (**D**) triglycerides. (**E**) Oil Red O staining of histological sections of liver from *Oma1*$^{+/+}$ and *Oma1*$^{-/-}$ mice under chow diet (CD) and high-fat diet (HFD). Scale bar: 20 μm. Levels of (**F**) free fatty acids, (**G**) insulin and (**H**) leptin in plasma of *Oma1*$^{+/+}$ and *Oma1*$^{-/-}$ mice. (**I**) IPGTT and (**J**) IPITT in wild-type and *Oma1*$^{-/-}$ male mice (8–12 weeks old, $n = 6$–8). AUC, area under the curve (arbitrary units). Bars represent mean values ± s.e.m. ns denotes no significant difference. *$P < 0.05$.

standard and high-fat diet (Figure 2D). Consistent with this, Oil Red O staining revealed a marked steatosis in the liver of *Oma1*$^{-/-}$ mice maintained on a normal chow diet, which increased significantly under a high-fat diet (Figure 2E). Levels of free fatty acids were comparable between genotypes on both diets (Figure 2F). Interestingly, analysis of insulin and leptin plasma levels showed different patterns under standard and high-fat diet. Thus, under standard rodent chow, both insulin and leptin plasma levels were reduced in mutant mice. However, under high-fat diet, insulin levels did not show differences despite the increment levels in control and mutant mice. Furthermore, leptin levels were significant enhanced as expected in an obese mouse model (Figure 2G and H).

The absence of hyperglycaemia in *Oma1*-deficient mice, together with their low insulin levels under standard chow diet, suggested the possibility of an increased insulin sensitivity of *Oma1*$^{-/-}$ mice. Accordingly, intraperitoneal glucose tolerance tests (IPGTTs) revealed that *Oma1*$^{-/-}$ mice showed improved glucose clearance compared with control mice (Figure 2I). Intraperitoneal insulin tolerance tests (IPITTs) confirmed that *Oma1*$^{-/-}$ mice presented increased insulin sensitivity (Figure 2J), which is consistent with their low insulin levels. Remarkably, these advantages in glucose metabolism were lost when *Oma1*-deficient mice were fed a high-fat diet. Thus, the metabolic tests in mutant mice showed a decrease in glucose tolerance and the same insulin insensitivity than control mice (Figure 2I and J, lower panels). Insulin tolerance was also analysed at 8 weeks, with animals displaying similar insulin responses to those observed at 12 weeks (data not shown). In addition, obese *Oma1*$^{-/-}$ mice showed the same higher levels of insulin than

controls (Figure 2F), which explains the observed insulin insensitivity.

To further investigate these metabolic alterations observed in *Oma1*-deficient mice, we performed oligonucleotide-based microarrays to analyse transcriptional changes in adipose tissue from *Oma1*$^{-/-}$ mice kept under high-fat diet. As can be seen in Supplementary Table S1, we found a marked up-regulation in the expression of genes encoding proteins related with lipid metabolism and transport such as fatty-acid binding protein 1 (FABP1) and several apolipoproteins and cytochromes. Further, bioinformatic analysis revealed that a number of the up-regulated genes in *Oma1*-deficient mice are associated with two metabolic pathways (peroxisome proliferator-activated receptors α and γ, and retinol pathway), which can be related to the obesity phenotype observed in these mutant mice (Supplementary Figure S4). Collectively, these results indicate that mutant mice deficient in OMA1 mitochondrial protease exhibit significant alterations in lipid metabolism, characterized by an increase in triglycerides and hepatic steatosis, as well as an improved glucose clearance likely derived from an increased sensitivity to insulin.

Energy balance and thermogenesis are altered in Oma1-deficient mice

To determine the possible causes of the obesity and metabolic dysfunction observed in *Oma1*-deficient mice, we performed analyses of their food-intake and energy balance in mice maintained on a control chow diet. We did not find significant differences in food-intake of *Oma1*$^{-/-}$ mice relative to control littermates (Figure 3A). However, indirect calorimetry studies indicated that *Oma1*-deficient mice showed reduced oxygen consumption and CO_2 production, which correlated with a significant reduction in heat production in these mice (Figure 3B–D). These alterations occurred in the absence of changes in respiratory quotient values (Figure 3E) and could not be explained by changes in ambulation (Figure 3F). Thus, we decided to study thermogenic activity of BAT under basal and cold-stress conditions. As expected, wild-type mice showed an increase in body temperature at night under basal conditions (22°C), which was not observed in *Oma1*-deficient mice (Figure 3G). To further evaluate their adaptive thermogenic response, *Oma1*$^{+/+}$ and *Oma1*$^{-/-}$ mice were subjected to cold exposure at 4°C monitoring their temperature for 12 h. As can be seen in Figure 3H, *Oma1*$^{-/-}$ mice showed a significant decrease in body core temperature when compared with controls from 3 to 12 h. We analysed UCP1 protein levels after cold-stress but we did not find any differences, indicating that the observed failure in thermogenic response was not due to a decrease in UCP1-mediated uncoupling (data not shown). However, histological analysis of BAT showed that while control mice depleted lipid droplets under cold-stress, *Oma1*-deficient animals retained most of them (Figure 3I and J). Taken together, these results indicate that *Oma1* ablation causes reduced energy expenditure under stress conditions, which may explain the susceptibility of these mice to obesity and their impaired adaptive thermogenic response.

Next, we examined whether reduced respiration of *Oma1*-deficient mice could be explained by alterations in the expression of genes coding for mitochondrial proteins or for the nuclear co-activator PGC1α, an essential transcriptional regulator of mitochondria and oxidative metabolic programmes (Finck and Kelly, 2006; Uldry *et al*, 2006; Fernandez-Marcos and Auwerx, 2011). To this end, we obtained tissues from wild-type and *Oma1*-deficient mice chronically subjected to a high-fat diet (20 weeks) and analysed the expression of selected genes by real-time qPCR. BAT samples showed reduced expression of β-oxidation genes, *Cpt1b* and *Vlcad* in the *Oma1*-deficient group (Table I). Livers from *Oma1*-deficient mice showed a reduced expression of *Ndufa9*, *Uqcrc2* and *CoxIV* (Table I). Furthermore, we detected increase in *Pgc1a* and decrease in *Pgc1b*, together with an increase in lipogenic genes *Fasn* and *Scd1* in *Oma1*-deficient mice compared with controls (Table I). In addition, we also detected reduced expression of *Sdha* and *Atp5a1* in skeletal muscle from *Oma1*-null mice (Supplementary Table S2). Collectively, these data indicate that *Oma1* deficiency causes a reduced expression of nuclear genes encoding mitochondrial proteins, decrease in β-oxidation genes and increase in lipogenic genes, which may explain the low oxygen consumption and obesity phenotype of these animals. Notably, *Oma1* deletion also led to a marked decrease in the expression of genes encoding proteins involved in mitochondrial fusion (*Mfn2* or *Opa1*) or in mitochondrial fission (*Drp1*). In fact, *Mfn2* was markedly down-regulated in BAT and WAT from *Oma1*-null mice, whereas *Opa1* was down-regulated in BAT, WAT and skeletal muscle (Table I; Supplementary Table S2). Additionally, *Drp1* was down-regulated in BAT, skeletal muscle and liver from *Oma1*-deficient mice (Table I; Supplementary Table S2).

Alteration of OPA1 processing in Oma1$^{-/-}$ *mice*

Recent *in vitro* studies have shown that OMA1 cooperates with m-AAA proteases in the proteolytic inactivation of OPA1 (Ehses *et al*, 2009; Head *et al*, 2009). To evaluate how mouse OMA1 induces this proteolytic inactivation, we first compared the levels of the different isoforms of OPA1 in murine embryonic fibroblasts (MEFs) from *Oma1*$^{+/+}$ and *Oma1*$^{-/-}$ mice. In *Oma1*$^{+/+}$ cells, we detected the five characteristic isoforms of OPA1 (labelled a–e) (Figure 4A). After treatment of these cells with the protonophore carbonylcyanide m-chlorophenylhydrazone (CCCP), an inducer of loss of mitochondrial membrane potential, we detected the conversion of bands b–e (Figure 4A). This proteolytic event involves the processing of large (L-OPA1) to short (S-OPA1) isoforms of OPA1 and protects cells from mitochondrial fusion under stress conditions. Interestingly, we could not detect the S-OPA1 isoform corresponding to band c in *Oma1*$^{-/-}$ MEFs, concomitant with a decrease in the production of band e (Figure 4A). Furthermore, we did not observe the cleavage of L-OPA1 (band b) to S-OPA1 isoforms (band e) in *Oma1*$^{-/-}$ cells treated with CCCP (Figure 4A). Similar results were obtained when cells were treated with staurosporine, a known apoptosis inducer, or with oligomycin, an inhibitor of ATP synthesis (Figure 4B). Analysis of tissue samples from *Oma1*-deficient mice also revealed alterations in OPA1 processing, characterized by the absence of isoform c in all cases (Supplementary Figure S5A and B). Interestingly, analysis of WAT samples from high-fat diet showed an increase in isoform e and a decrease in L-OPA1 isoforms in control mice, a characteristic pattern of stress conditions, whereas *Oma1*-deficient mice maintained all L-OPA1 isoforms intact (Supplementary Figure S5C). Accordingly, we conclude that

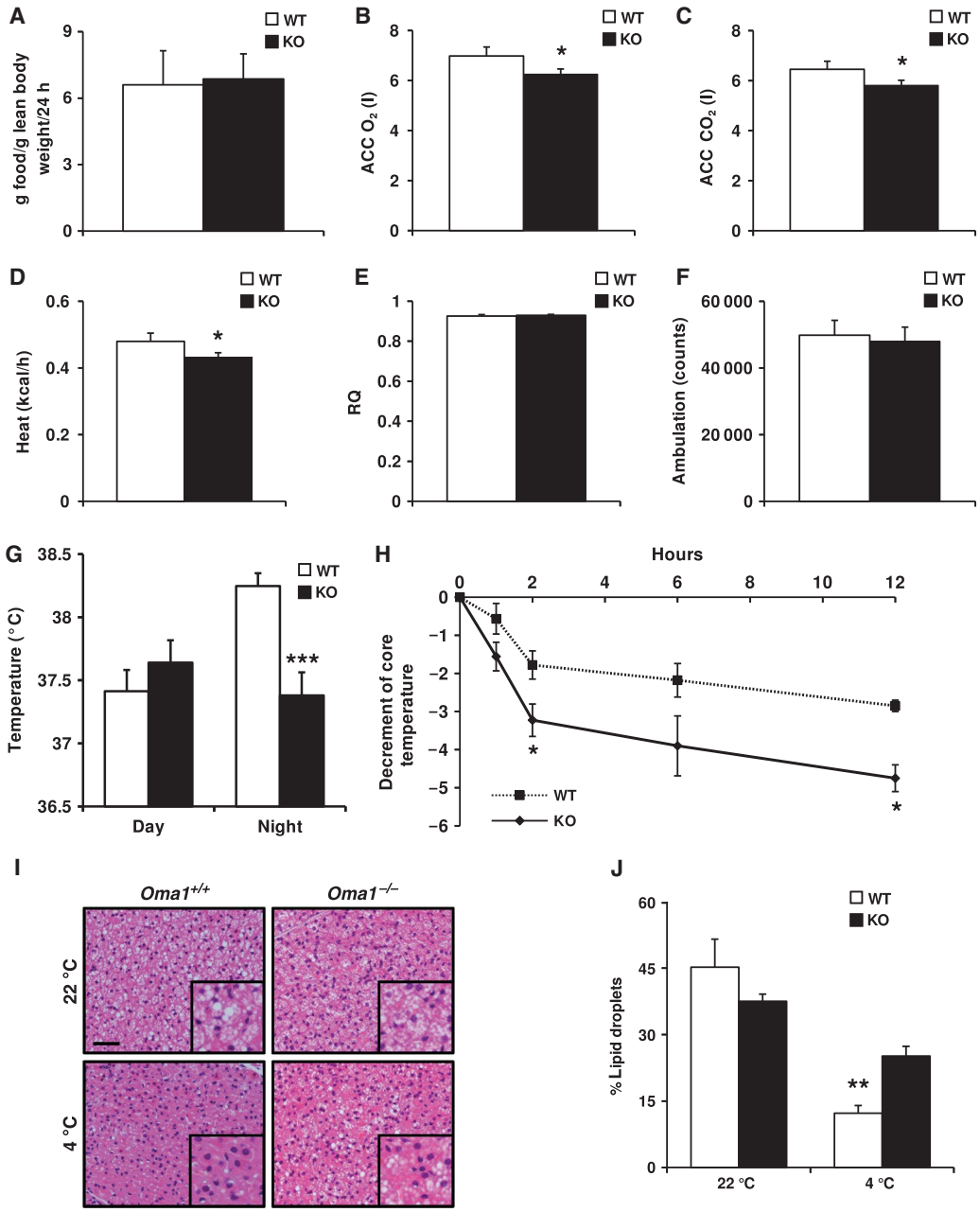

Figure 3 Decrease of energy expenditure and impaired thermogenesis in *Oma1*$^{-/-}$ mice. (**A**) Food-intake of 2-month-old *Oma1*$^{+/+}$ and *Oma1*$^{-/-}$ mice kept on standard rodent chow ($n=6$). (**B**) Whole body oxygen consumption (ACC O_2), (**C**) carbon dioxide production (ACC CO_2), (**D**) heat production, (**E**) respiratory quotient (RQ) and (**F**) ambulatory movement of 2-month-old *Oma1*$^{+/+}$ and *Oma1*$^{-/-}$ mice during dark period of 3 days kept on standard rodent chow ($n=6$–8). (**G**) Basal rectal temperature of *Oma1*$^{+/+}$ and *Oma1*$^{-/-}$ mice measured during daytime (1000 hours) and night (2200 hours) for 3 consecutive days ($n=5$). (**H**) Body temperature curve of 2-month-old *Oma1*$^{+/+}$ and *Oma1*$^{-/-}$ mice exposed to 4°C during 12 h ($n=6$). (**I**) Representation of BAT histology stained with H&E of *Oma1*-deficient mice and controls before and after cold exposure for 3 h. Scale bar: 50 μm. (**J**) The cumulative area occupied by all lipid droplets in each of the tissue sections was determined using image J and presented as a percentage of the total area analysed ($n=4$). $^{*}P<0.05$; $^{**}P<0.01$; $^{***}P<0.001$.

OMA1 mediates the *in vivo* cleavage and inactivation of OPA1.

To further investigate the molecular consequences of *Oma1* deletion on mitochondrial structure and function, we examined mitochondrial morphology in immortalized MEFs from *Oma1*$^{+/+}$ and *Oma1*$^{-/-}$ mice. We observed that *Oma1*$^{-/-}$ MEFs show a lower percentage of mitochondrial fragmentation than control MEFs, as well as an increase in tubular connections (Figure 4C and D; Supplementary Figure S5D). We also examined the mitochondrial morphology of

Table I Expression of mitochondrial genes in BAT and liver of *Oma1*$^{+/+}$ and *Oma1*$^{-/-}$ under high-fat diet

	Brown adipose tissue		Liver	
	Oma1$^{+/+}$	Oma1$^{-/-}$	Oma1$^{+/+}$	Oma1$^{-/-}$
Mitochondrial dynamics				
Mfn2	1 ± 0.18	0.55 ± 0.09*	1 ± 0.25	0.64 ± 0.11
Opa1	1 ± 0.37	0.47 ± 0.05	1 ± 0.12	0.94 ± 0.30
Drp1	1 ± 0.17	0.56 ± 0.07*	1 ± 0.21	0.41 ± 0.07*
OXPHOS genes				
Ndufa9	1 ± 0.30	0.93 ± 0.07	1 ± 0.11	0.67 ± 0.14*
SdhA	1 ± 0.42	0.64 ± 0.10	1 ± 0.14	1.18 ± 0.33
Uqcrc2	1 ± 0.39	0.84 ± 0.08	1 ± 0.16	0.61 ± 0.12*
CoxIV	1 ± 0.29	1.13 ± 0.12	1 ± 0.05	0.77 ± 0.09*
Atp5a1	1 ± 0.35	0.73 ± 0.05	1 ± 0.12	0.91 ± 0.18
Metabolic regulators				
Pgc1a	1 ± 0.11	0.82 ± 0.24	1 ± 0.01	1.62 ± 0.19*
Pgc1b	1 ± 0.16	0.64 ± 0.12	1 ± 0.19	0.53 ± 0.07*
β-*Oxidation genes*				
Mcad	1 ± 0.17	0.83 ± 0.13	1 ± 0.08	0.82 ± 0.17
Vlcad	1 ± 0.14	0.65 ± 0.65*	1 ± 0.11	0.92 ± 0.14
Cpt1a			1 ± 0.15	1.07 ± 0.21
Cpt1b	1 ± 0.08	0.67 ± 0.13*		
Cpt2	1 ± 0.11	0.82 ± 0.24	1 ± 0.10	0.84 ± 0.11
Lipogenic genes				
Fasn	1 ± 0.11	0.82 ± 0.24	1 ± 0.14	2.79 ± 0.45**
Acc1	1 ± 0.06	0.91 ± 0.21	1 ± 0.06	1.27 ± 0.13
Scd1	1 ± 0.13	0.81 ± 0.04	1 ± 0.11	2.16 ± 0.47*

Gene expression relative to β-actin. Data represent mean ± s.e.m. of at least five mice per group. *$P<0.05$; **$P<0.01$.

MEFs from mutant and control mice after treatment with CCCP. We observed that the CCCP-induced mitochondrial fragmentation is lower in *Oma1*$^{-/-}$ cells than in their corresponding controls (Figure 4E). Likewise, mutant cells predominantly maintain the tubular network morphology when compared with cells from wild-type mice (Figure 4E). Furthermore, after treatment with this inducer of membrane potential loss, we still observed a significant percentage of *Oma1*$^{-/-}$ cells that conserved the highly connected mitochondrial morphology (Figure 4E). Collectively, these results provide evidence that *Oma1*$^{-/-}$ cells are unable to perform the protease-mediated process of inactivation of OPA1 and are also refractory to the stress signals induced by CCCP, maintaining the mitochondrial tubular network morphology.

It has been previously reported that OPA1 is cleaved concomitantly with cytochrome c release during apoptosis (Cipolat *et al*, 2006; Baricault *et al*, 2007; Griparic *et al*, 2007). As can be seen in Figure 4B, proteolytic processing of OPA1 in *Oma1*-deficient cells was blocked after induction of apoptosis with staurosporine. To further evaluate the putative impact of *Oma1* deficiency on apoptosis, *Oma1*$^{-/-}$ cells were treated with staurosporine and the number of apoptotic cells was determined. The percentage of pyknotic nuclei was significantly lower in *Oma1*-deficient cells than in controls (Figure 4F). Western blot analysis of PARP cleavage and activated caspase-3 levels confirmed the decreased sensitivity to apoptosis of *Oma1*-deficient cells after treatment with staurosporine and etoposide (Figure 4G). Taken together, these results indicate that *Oma1* deficiency impairs cellular sensitivity to apoptosis.

Analysis of mitochondrial function in Oma1$^{-/-}$ *cells*

To determine whether the deficiency in OMA1 metalloproteinase has any effect on mitochondrial activity, we performed a series of functional experiments using *Oma1*$^{-/-}$ MEFs. First, we assessed the proliferation rate of *Oma1*-deficient MEFs but we did not observe significant differences with control cells (Supplementary Figure S6A). Similarly, we did not find significant differences in OXPHOS function in the absence of OMA1. In fact, coupled and CCCP-uncoupled respiration rates were comparable between *Oma1*$^{+/+}$ and *Oma1*$^{-/-}$ cells, as well as oligomycin- and KCN-insensitive oxidation (Supplementary Figure S6B). Furthermore, the ratio between uncoupled and coupled respiration (Supplementary Figure S6C) and the polarography measurements of mitochondrial complexes did not show significant differences between *Oma1*$^{+/+}$ and *Oma1*$^{-/-}$ cells (Supplementary Figure S6D). Moreover, ATP levels in mutant cells were very similar to those of control cells under both basal and oxidative stress conditions (Supplementary Figure S6E). Collectively, these results indicate that OMA1 does not play a major role in the maintenance of OXPHOS function. Analysis of mitochondrial inner membrane potential ($\Delta\Psi$m) using TMRM fluorescence probe did not show differences between *Oma1*$^{+/+}$ and *Oma1*$^{-/-}$ cells, in neither control nor CCCP-stimulated uncoupling conditions (Supplementary Figure S6F). However, we could detect a significant loss of mtDNA in *Oma1*-deficient cells (Supplementary Figure S6G). This decrease could not be explained by a decrease in mitochondrial mass as the activity of citrate synthase (Supplementary Figure S6H), a known marker of mitochondrial mass, and MitoTracker flow cytometry analysis (Supplementary Figure S6I) was comparable in cells from both genotypes. Thus, it is reasonable to speculate that the loss of OMA1 alters the copy number of mtDNA, likely as a consequence of defective OPA1 processing and the subsequent changes in the mitochondrial morphology.

To study mitochondrial function in tissues, we analysed mitochondrial respiration rates in mitochondria isolated from livers of *Oma1*$^{+/+}$ and *Oma1*$^{-/-}$ mice on control and high-fat diet. Thus, we measured the respiration rates in states 3 and 4 using two different combinations of substrates (glutamate + malate and succinate). Similar to the above cell analysis, we did not observe differences between the two genotypes in respiration control rate or ATP synthesis per O_2 consumed—represented as P/O rate—under control and high-fat diets (Figure 5A and B; Supplementary Figure S7A). These results demonstrate that abnormalities observed in *Oma1*-deficient mice were not due to defects in the OXPHOS system. To analyse other possible pathways that could explain the phenotype observed in *Oma1*-deficient mice, we assessed fatty-acid utilization in the BAT and liver of *Oma1*$^{-/-}$ mice on both control and high-fat diets. As shown in Figure 5C and D, *Oma1*-deficient mice on a high-fat diet had a significant decrease in fatty-acid β-oxidation in BAT and liver compared with wild-type controls. Under a control diet, a significant decrease in fatty-acid utilization was found only in the BAT of *Oma1*$^{-/-}$ mice, indicating that the dysfunction in β-oxidation was due to primary defects in BAT and not a result of an inflammatory state caused by the obesity phenotype. However, and because the impaired β-oxidation was only observed in the livers of *Oma1*$^{+/+}$ on a high-fat diet, we cannot exclude that inflammation may contribute to defective fatty-acid utilization in this tissue.

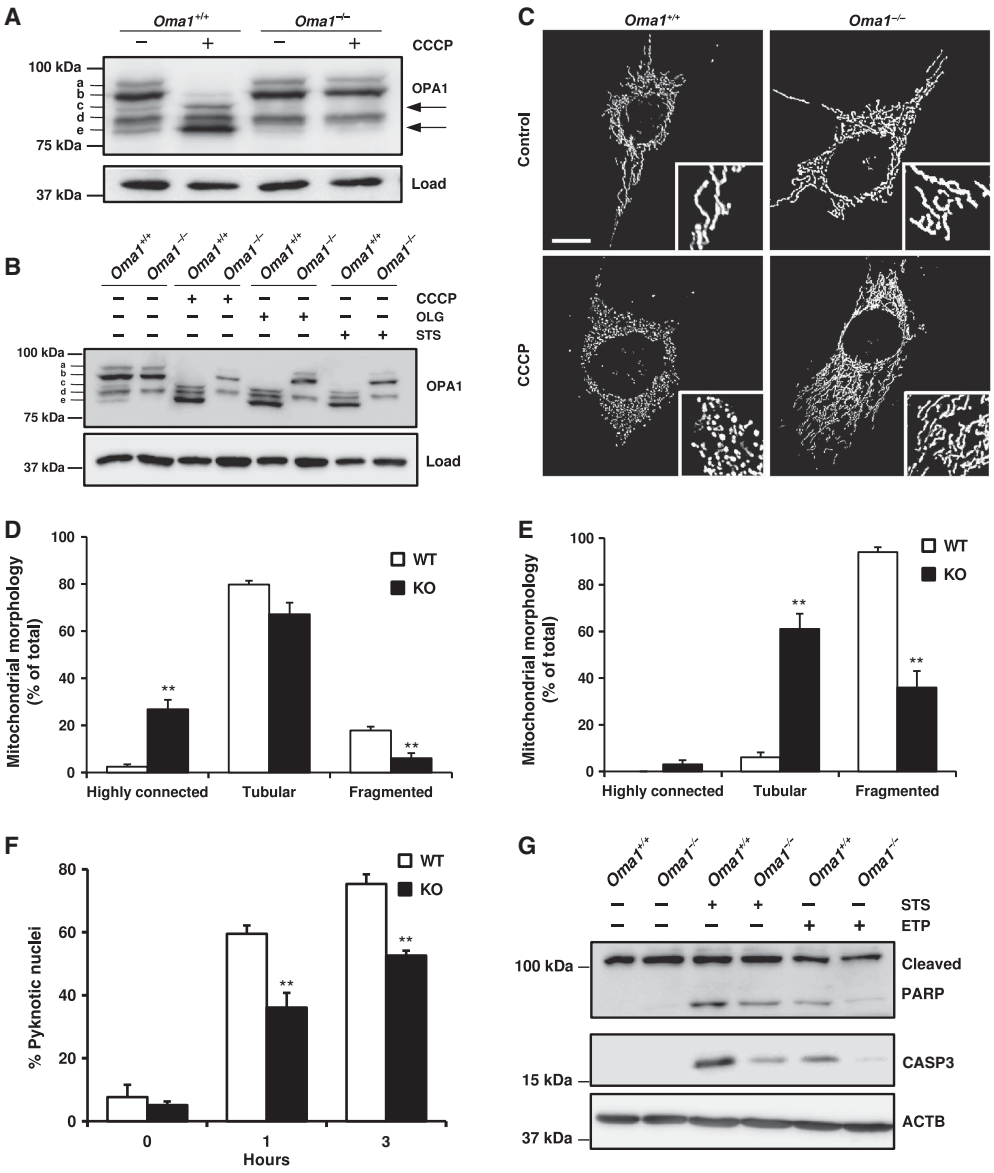

Figure 4 Impaired OPA1 processing induces mitochondrial morphology alterations and apoptosis resistance in *Oma1*$^{-/-}$ mice. (**A**) Western blot analysis of OPA1 processing in *Oma1*$^{+/+}$ and *Oma1*$^{-/-}$ MEFs after treatment with 20 μM of CCCP for 60 min. (**B**) Western blot analysis of OPA1 processing after treatment of *Oma1*$^{+/+}$ and *Oma1*$^{-/-}$ MEFs with 20 μM CCCP, 20 μM oligomycine (OLG) and 1 μM staurosporine (STS) during 3 h. (**C**) Confocal images of *Oma1*$^{+/+}$ and *Oma1*$^{-/-}$ MEFs in control cells and after CCCP treatment. Insets represent characteristic mitochondrial morphologies observed in each situation. Scale bar: 10 μm. (**D**) Mitochondrial morphology of *Oma1*$^{+/+}$ and *Oma1*$^{-/-}$. MEFs were visualized after transfection with a vector containing mito-DsRed, and (**E**) after treatment with 20 μM of CCCP during 3 h. More than 100 cells were scored. Bars represent mean values ± s.e.m. and are shown as a percentage of the total, of three independent experiments (**$P<0.01$). (**F**) Percentage of apoptotic cells was determined by counting pyknotic nuclei after treatment of *Oma1*$^{+/+}$ and *Oma1*$^{-/-}$ MEFs with 1 μM staurosporine during each time point. More than 150 cells were counted. Bars represent mean values ± s.e.m. and are shown as a percentage of the total, of three independent experiments (**$P<0.01$). (**G**) Western blot analysis of PARP and activated caspase-3 as apoptosis markers in *Oma1*$^{+/+}$ and *Oma1*$^{-/-}$ MEFs, after treatment of these cells with 1 μM staurosporine and 100 μM etoposide (ETP) during 3 and 16 h, respectively. Figure source data can be found in Supplementary data.

Additionally, we measured citrate synthase activity in both liver and BAT from *Oma1*$^{+/+}$ and *Oma1*$^{-/-}$ mice on control and high-fat diet, and did not find differences under these conditions between the two genotypes (Supplementary Figure S7B and C). These results demonstrate that differences in β-oxidation were due to specific mitochondrial defects and not attributable to a decrease in mitochondrial mass.

Having identified a significant inability of *Oma1*-deficient mitochondria to oxidize fatty acids under control and high-fat diets in BAT, we next chose to explore the impact of Oma1 ablation on the morphology of mitochondria in this tissue by electron microscopy. Measurements of mitochondrial size showed a significant increase in mitochondrial area from *Oma1*$^{-/-}$ BAT compared with controls (Figure 5E and F).

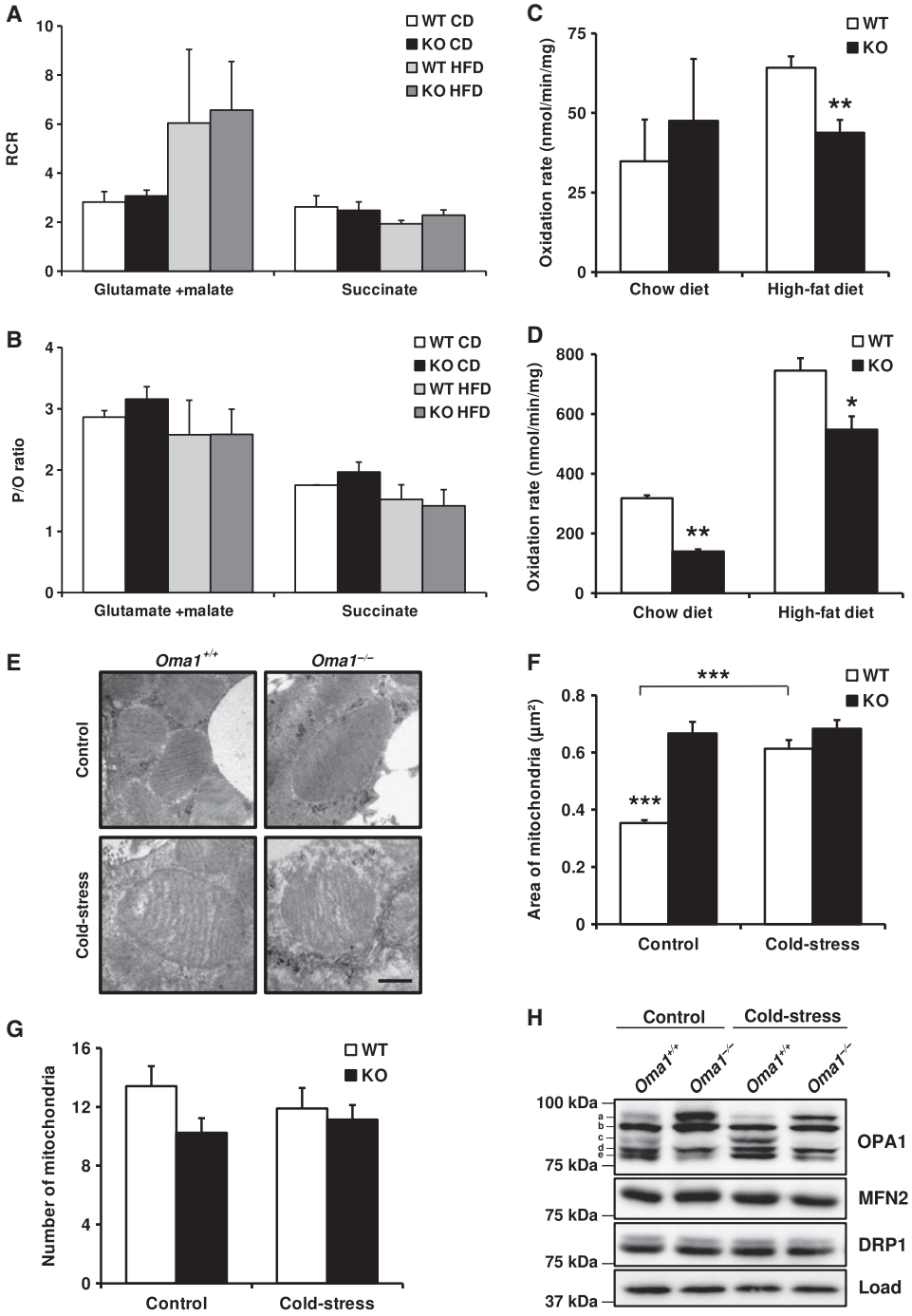

Figure 5 Mitochondrial alterations in liver and BAT after obesity and cold-stress. Analysis of OXPHOS function in mitochondria isolated from liver of *Oma1*$^{+/+}$ and *Oma1*$^{-/-}$ mice on control and high-fat diet. (**A**) Mitochondrial respiration control rate (RCR) and (**B**) P/O ratio, using glutamate + malate or succinate as substrates. Reduced fatty-acid utilization in *Oma1*-deficient mice. Mitochondrial fatty-acid oxidation was measured by the incubation of ^{14}C-palmitate (100 μM) in liver (**C**) and BAT (**D**) extracts from mice under control diet and high-fat diet ($n = 4$). (**E**) Electron microscopy (EM) images from BAT of *Oma1*$^{+/+}$ and *Oma1*$^{-/-}$ mice on control and cold-stress. Scale bar: 0.4 μm. Mitochondrial morphology quantification in EM was measured with ImageJ, represented as (**F**) area of mitochondria and (**G**) number of mitochondria per field, using at least 12 different pictures of each condition. (**H**) Western blot analysis of OPA1, MFN2 and DRP1 in BAT samples extracted from mice after control and cold-stress treatment. Bars represent mean values ± s.e.m. *$P < 0.05$; **$P < 0.01$; ***$P < 0.001$. Figure source data can be found in Supplementary data.

Moreover, we found that after cold-stress, *Oma1*$^{+/+}$ BAT increased the size of mitochondria while *Oma1*$^{-/-}$ BAT maintained an identical mitochondrial size (Figure 5F). All of these changes were produced without significant differences in the mitochondrial number between control and *Oma1*-deficient mice (Figure 5G). Focusing on OPA1 processing after cold-stress, *Oma1*$^{+/+}$ mice displayed a small but appreciable loss of isoform 'a' and a clear accumulation of isoform 'c', the isoform exclusively generated by OMA1 in response to cold-stress (Figure 5H). This pattern of OPA1 processing was absent in *Oma1*$^{-/-}$ BAT, indicating that cold-stress initiates OMA1-mediated processing of OPA1. Moreover, while OPA1 remodelling was detected in BAT, neither MFN2 nor DRP1 proteins showed a clear difference in either condition. Collectively, these results indicate that *Oma1*-null mice are unable to develop the appropriate mitochondrial dynamic response required for cold-stress-induced thermogenesis.

OMA1-OPA1 system is necessary for brown adipocytes function

To explore the connection observed in BAT between OPA1 processing by OMA1 and β-oxidation function, we next analysed fatty-acid utilization in primary brown adipocytes from *Oma1*$^{+/+}$ and *Oma1*$^{-/-}$ mice. Brown preadipocytes were isolated from newborn mice, immortalized and differentiated into mature brown adipocytes. We then analysed palmitate oxidation rates as an indicator of β-oxidation function in *Oma1*$^{+/+}$ and *Oma1*$^{-/-}$ mature brown adipocytes. In agreement with our experiments in BAT (Figure 5D), *Oma1*-deficient adipocytes displayed significantly lower palmitate oxidation rates in comparison to wild-type control cells (Figure 6A). Next, to delineate the importance of OPA1 for brown adipocyte function, we ablated OPA1 protein levels in *Oma1*$^{+/+}$ using siRNA and then analysed palmitate oxidation rates. This protocol involved first differentiating the primary brown preadipocytes for 2 days with insulin, T3, IBMX, dexamethasone and indomethacin, and then transfecting the cells with an siRNA targeting OPA1 mRNA or a scrambled control. The cells were maintained for a further 72 h with insulin and T3 to complete adipocyte differentiation and then analysed for palmitate oxidation rates. This approach reduced OPA1 protein levels by ∼75% in the final mature brown adipocytes (Figure 6B). Interestingly, knockdown of OPA1 decreased palmitate oxidation rates by ∼25% in *Oma1*$^{+/+}$ brown adipocytes compared with cells transfected with the scrambled siRNA (Figure 6C). This indicates that OPA1 is required for the correct functioning of brown adipocyte β-oxidation. Further, to specifically demonstrate the relevance of OPA1 processing by OMA1 in brown adipocyte function, we restored OPA1 in these cells by reintroducing wild-type OPA1 or a mutant OPA1 isoform not cleavable by OMA1. Brown adipocytes were transfected with OPA1 siRNA to remove endogenous OPA1 protein as outlined previously, then 24 h later, we transfected a mammalian expression vector containing a wild-type full-length cDNA of OPA1 (OPA1-S1) or a mutant cDNA isoform of OPA1 without the S1 cleavage site that is utilized by OMA1 (OPA1-ΔS1) (Ishihara *et al*, 2006). Both constructs were insensitive to the siRNA targeting mouse Opa1 due to their human origin and lack of homology in the targeted region and contained a Flag epitope for detection by western blot (Figure 6B). Thus, reintroduction of full-length OPA1 in adipocytes partially restored the levels of palmitate oxidation (Figure 6C). However, mutant OPA1-ΔS1 did not demonstrate a similar ability to increase the levels of palmitate oxidation, displaying similar oxidation rates to those observed in OPA1-depleted cells (Figure 6C). These results indicate that β-oxidation in brown adipocytes requires the OMA1-OPA1 system, and an absence of OPA1 or its proteolytic regulator OMA1, impairs mitochondrial function.

In summary, our results indicate a pivotal role for the OMA1 protease in mitochondrial homeostasis by regulating the mitochondrial dynamics that is essential for lipid metabolism as well as to maintain body temperature and energy expenditure under cold-stress conditions.

Discussion

We describe herein the generation and phenotypic characterization of mutant mice deficient in OMA1, a mitochondrial metalloprotease proposed to be involved in protein quality control. Despite the wide tissue distribution of OMA1, the disruption of this gene does not cause the severe abnormalities observed in mice deficient in other mitochondrial proteases such as SPG7, AFG3L2 or PARL (Ferreirinha *et al*, 2004; Cipolat *et al*, 2006; Maltecca *et al*, 2008). However, further analysis of *Oma1*$^{-/-}$ mice revealed an unexpected contribution of this protease to metabolic homeostasis. In fact, *Oma1*-deficient mice exhibit a progressive increase in body weight when compared with control animals, and these differences are further enhanced when mice from both genotypes are maintained on a high-fat diet. Histological analysis showed a marked hypertrophy of adipocytes from *Oma1*$^{-/-}$ mice. These mutant animals also exhibited hepatic steatosis as well as a significant increase in plasma triglycerides and a decrease in circulating leptin and insulin levels. Moreover, glucose and insulin tolerance tests revealed that *Oma1*-null mice display improved glucose tolerance and increased insulin sensitivity. Furthermore, after high-fat diet induced obesity, *Oma1*-deficient mice lost glucose tolerance protection and developed insulin insensitivity, displaying higher levels of leptin than those found in obese controls. Finally, hepatic steatosis and triglyceride levels were also dramatically enhanced in mutant mice after high-fat diet.

The finding of this array of metabolic changes in *Oma1*$^{-/-}$ mice prompted us to explore their putative links to the absence of this mitochondrial metalloproteinase, which had not been previously associated with metabolic homeostasis. In this regard, there is growing evidence that a number of metabolic disorders are caused by alterations of mitochondrial function and dynamics (Detmer and Chan, 2007; Suen *et al*, 2008; Hyde *et al*, 2010; Westermann, 2010). There are many proteins implicated in the regulation of the appropriate balance between mitochondrial fission and fusion. In mammals, mitochondrial fission is largely controlled by the dynamin-related GTPase DRP1 (Chang and Blackstone, 2010), whereas mitochondrial fusion mainly depends on the activity of three large GTPases, the mitofusins (MFN1 and MFN2) and OPA1 (Hoppins and Nunnari, 2009; Zorzano *et al*, 2010). On the basis of these previous findings, we speculated that the absence of OMA1 could alter the levels of some of these proteins involved in modulating mitochondrial

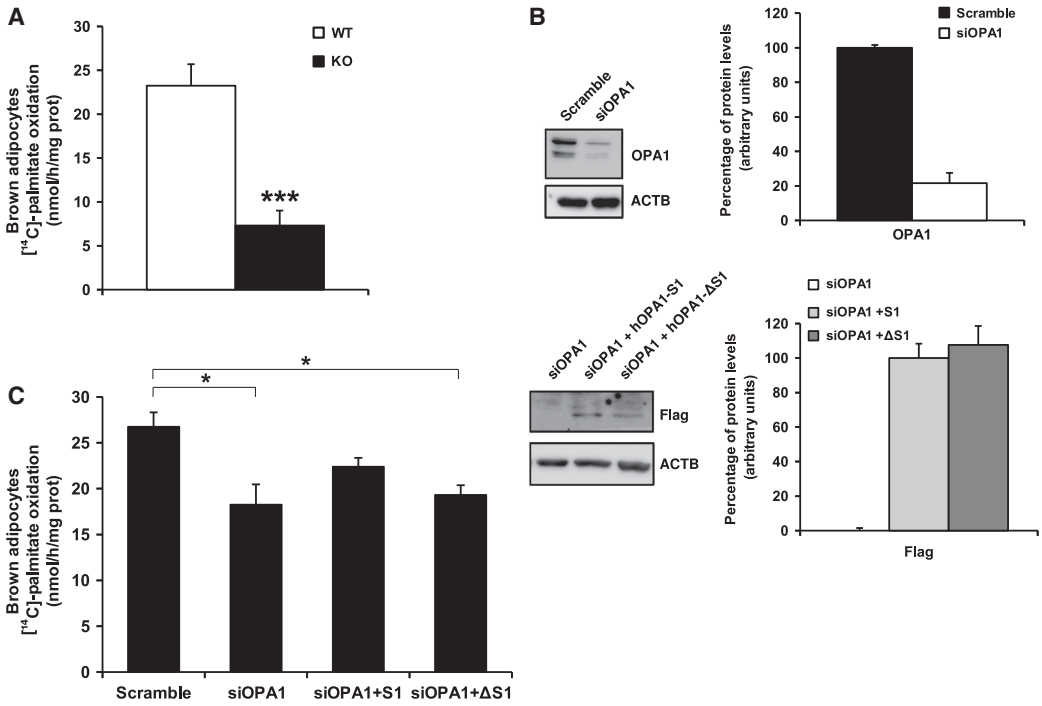

Figure 6 β-Oxidation in brown adipocytes depends on OMA1 and OPA1 function. (**A**) Analysis of palmitate oxidation rate in brown adipocytes obtained from *Oma1*$^{+/+}$ and *Oma1*$^{-/-}$ mice ($n=3$). (**B**) OPA1, Flag-tag and actin western blot analyses from wild-type adipocytes after transfection with an siRNA scrambled control (Scramble) or Opa1 siRNA (siOPA1) (top panel, Opa1 western blot) or siOPA1 samples retransfected with hOPA1-S1 or hOPA1-ΔS1 (bottom panel, Flag western blot). To the right of each representative western blot, is the densitometry analysis from three independent experiments, normalized to actin levels. (**C**) Palmitate oxidation rate in wild-type brown adipocytes after 72 h of the above transfections. Bars represent mean values ± s.e.m. of three independent experiments. $*P<0.05$; $***P<0.001$. Figure source data can be found in Supplementary data.

dynamics, shifting the balance towards fusion or fission events, and finally resulting in the metabolic alterations observed in *Oma1*-mutant mice. In fact, our proteomic analysis of cells and tissues from *Oma1*$^{-/-}$ mice revealed that OMA1 plays an *in vivo* non-redundant role in the proteolytic processing of OPA1, which leads to its functional inactivation under stress conditions, thus extending recent *in vitro* findings showing that OPA1 can be targeted by OMA1 (Ehses *et al*, 2009; Head *et al*, 2009). There are at least five OPA1 isoforms in mammalian cells, including two long forms (L-OPA1) and three short isoforms (S-OPA1) (Duvezin-Caubet *et al*, 2006; Ishihara *et al*, 2006; Griparic *et al*, 2007; Song *et al*, 2007). The precise molecular balance between these long and short isoforms is necessary for mitochondrial fusion to occur. However, under stress conditions such as loss of mitochondrial membrane potential, low levels of mitochondrial ATP or induction of apoptosis, L-OPA1 isoforms are cleaved to S-OPA1 isoforms and mitochondrial fusion is blocked (Song *et al*, 2007). Our finding that *Oma1*$^{-/-}$ MEFs lack one isoform ('c') and have a decrease in another isoform ('e') of the three S-OPA1 isoforms, clearly indicate that OMA1 is responsible for the *in vivo* proteolytic processing of L-OPA1 isoforms. Notably, even under stress conditions, *Oma1*$^{-/-}$ cells display the same pattern of OPA1 isoforms characterized by the lack of processing of L-OPA1, which finally results in the shift of mitochondrial dynamics towards fusion events. Tissue samples from *Oma1*-deficient mice also lack one S-OPA1 isoform in all cases (isoform 'c'), although the pattern of OPA1 bands exhibits some differences with that of MEFs, which can be due to variations in compensatory or redundant proteolytic activities operating in the different cells and tissues from *Oma1*-null mice under normal conditions. The OPA1-processing deficiency was also clearly evident in BAT samples from mutant mice after cold-stress and in WAT samples after high-fat diet, as assessed by the maintenance of all L-OPA1 isoforms and the absence of any increase in S-OPA1 bands. Collectively, these results demonstrate that both cells and tissues from *Oma1*-null mice exhibit an *in vivo* impairment of OPA1 inactivation, which is especially significant under stress conditions. Consistent with this proteolytic processing deficiency, *Oma1*$^{-/-}$-deficient cells show an increase of highly connected and less-fragmented mitochondria when compared with control cells. Likewise, after treatment of cells with CCCP, which induces loss of mitochondrial membrane potential, most mitochondria from *Oma1*-deficient cells maintain their archetypal tubular network, whereas those present in control cells show a fragmented morphology. We found the same protection against mitochondrial fission when *Oma1*-mutant cells were treated with a respiratory chain inhibitor such as oligomycin or with an apoptosis inducer such as staurosporine, demonstrating that even under different stress conditions, the absence of OMA1 imposes a pro-fusion phenotype in mitochondria from *Oma1*-mutant mice.

In addition to its mitochondrial pro-fusion activity, OPA1 plays an important role in the maintenance of cristae junctions of the organelle, protecting cells from apoptosis by preventing cytochrome c release and mitochondrial depolarization (Olichon *et al*, 2003; Cipolat *et al*, 2006; Frezza *et al*, 2006). Accordingly, we also examined whether the defects in L-OPA1 proteolytic processing observed in *Oma1*-deficient cells could have an impact on apoptosis in these cells. In fact, *Oma1*$^{-/-}$ cells display low sensitivity to apoptosis compared with control cells, thus demonstrating that the absence of OMA1 metalloprotease has a profound impact on both pro-fusion and anti-apoptotic activities of OPA1. The proposed implication of OMA1 in the OPA1-mediated control of cristae remodelling and cytochrome c release during apoptosis likely derives from its ability to cleave L-OPA1 isoforms. In fact, these transmembrane isoforms keep in check the cristae junctions through the formation of stabilizing oligomeric structures with soluble short isoforms of OPA1 (Cipolat *et al*, 2006; Frezza *et al*, 2006). Since *Oma1*-deficient cells maintain their L-OPA1 isoforms intact, even under stress conditions, and still have available some soluble S-OPA1 isoform, the tight structural organization of cristae junctions is completely preserved. This situation prevents the redistribution and release of cristae-stored cytochrome c and finally results in apoptosis impairment. Notably, we also observed a significant decrease of mtDNA levels in *Oma1*$^{-/-}$ cells, which was not a consequence of any putative mitochondrial mass decrease between normal and mutant cells. The recent finding that OPA1 is also linked to mtDNA stability (Landes *et al*, 2010) suggests that the OPA1-processing deficiency found in mitochondria from *Oma1*$^{-/-}$ cells could contribute to explain why these cells are prone to mtDNA loss.

Interestingly, despite all these mitochondrial abnormalities observed in *Oma1*$^{-/-}$ cells, including inhibition of mitochondrial fission and loss of mtDNA, mitochondria deficient in OMA1 metalloprotease do not display marked respiratory defects, indicating that this enzyme is dispensable for OXPHOS function. This somewhat paradoxical situation is not unprecedented, as mitochondria deficient in rhomboid PARL1 protease do not exhibit primary respiratory defects in a variety of cell types, although this enzyme is also involved in OPA1 processing (Cipolat *et al*, 2006). These observations reinforce the usefulness of *in vivo* models to define the specific functions of proteins, which form part of complex and redundant regulatory pathways like those involving proteolytic systems (Lopez-Otin and Bond, 2008; Lopez-Otin and Hunter, 2010). In fact, over recent years, several mitochondrial proteases from different catalytic classes, including the serine protease PARL1 and several ATP-dependent and -independent metalloproteases, have been implicated in the constitutive or regulated proteolytic processing of mammalian OPA1 (Cipolat *et al*, 2006; Ishihara *et al*, 2006; Griparic *et al*, 2007; Song *et al*, 2007). These studies were initially based on *in vitro* experiments involving cell cultures and pointed to a large degree of overlapping functions between candidate OPA1-processing proteases. However, the recent introduction of studies based on animal models of protease deficiency such as those presented herein, has finally demonstrated the non-redundant *in vivo* role of enzymes such as OMA1 in the proteolytic regulation of the mitochondrial function of the dynamin-related GTPase OPA1.

It is also remarkable that the absence of significant pathological alterations in adult mice deficient in OMA1 facilitated the identification of the obesity phenotype, which has led us to propose a new and unexpected role for this mitochondrial protease in metabolic control. How can we explain that the deficient OPA1 processing observed in *Oma1*-null mice leads to an obesity phenotype? Our data indicate that *Oma1* deficiency causes reduced energy expenditure, which agrees with previous results, indicating that a reduction in energy expenditure causes obesity in animal models (Lowell *et al*, 1993; Feldmann *et al*, 2009). Accordingly, we suggest that the reduced energy expenditure in *Oma1*-deficient mice may account for their increased adipose mass. In addition, *Oma1* deficiency causes a reduced expression of nuclear genes encoding for mitochondrial proteins and key metabolic transcription co-activators, and this may be instrumental in the reduced energy expenditure shown in *Oma1*-null mice. Moreover, deregulation in lipid metabolism due to defects in β-oxidation genes observed in *Oma1*-deficient mice contributes to the obesity and thermoregulation defects. In this respect, we can speculate that altered OPA1 processing induces changes in mitochondrial dynamics, modifying expression levels of dynamic proteins to compensate or counteract this deficiency. Thus, under physiological conditions and in the absence of any relevant stressor, the lack of OMA1 induces changes in mitochondrial dynamics without seriously affecting any physiological function. In this situation, *Oma1*-deficient mice display a modest increase in body weight, improvement in glucose metabolism, hepatic steatosis, decrement in energy expenditure and low body temperature. However, under stress conditions such as a high-fat diet, the lack of OMA1 induces obesity, loss of glucose metabolism improvement and decrease in β-oxidation that induce the marked increase in the expression of genes of the lipogenic pathway and manifests as the significant hepatic steatosis observed in *Oma1*-deficient mice. Likewise, cold-stress induces impaired thermogenic response diminishing core body temperature, due to defects in β-oxidation and dysfunction in mitochondrial dynamics in response to cold-stress. Interestingly, a recent *in vitro* study using 3T3-L1 adipocytes has described a new function for OPA1 as a dual-specificity A-kinase anchoring protein, which interacts with perilipin and PKA forming a supramolecular complex involved in the lipolysis of lipid droplets (Pidoux *et al*, 2011). We did not observe any change in perilipin phosphorylation in *Oma1*-deficient BAT in comparison to normal tissue (data not shown), although this does suggests that perilipin functions normally in *Oma1*$^{-/-}$ BAT and likely does not contribute to the numerous defects we have described in these mutant mice, it may function in other tissues, for example white adipose, a possibility that will require further detailed examination in the future. Finally, and in relation to the putative implications of these findings for human metabolic control, several genome-wide linkage studies have found evidence of a quantitative trait locus for human obesity phenotypes in the region harbouring *OMA1* (Saar *et al*, 2003; Choquette *et al*, 2008). Nevertheless, further epidemiological studies will also be necessary to clarify the putative relevance of *OMA1* mutations or polymorphisms in abnormal weight control and glucose metabolism in humans.

In summary, the generation and characterization of *Oma1*-deficient mice has contributed to clarifying the

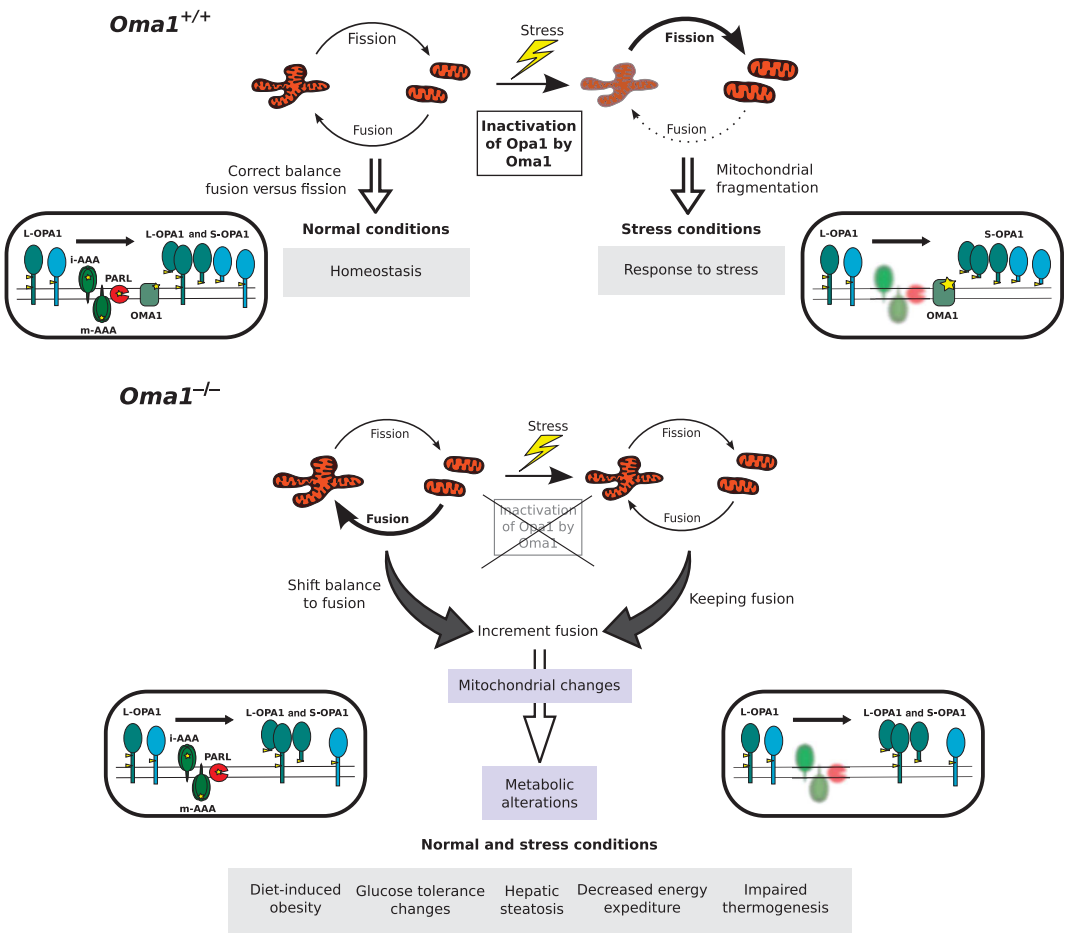

Figure 7 Schematic model summarizing the functional relevance of OMA1 in mitochondrial dynamics and metabolic homeostasis.

in vivo functional role of this metalloproteinase in mitochondrial quality control and metabolic homeostasis (Figure 7). The first steps in these processes are performed by mitochondrial peptidases, which play direct roles in the degradation of misfolded and damaged proteins or participate in the proteolytic processing of proteins that form part of the mitochondrial dynamics machinery. OMA1 belongs to this second category of mitochondrial proteases due to its ability to target OPA1. Accordingly, *Oma1*-deficient cells have marked alterations in mitochondrial dynamics due to the incomplete processing of L-OPA1. This perturbation of the fusion–fission equilibrium in *Oma1*$^{-/-}$ cells has clear implications for metabolic homeostasis and causes a series of energy metabolic derangements, which finally result in abnormal weight control, hepatic steatosis and defective thermogenesis. The absence of OMA1 is especially significant under stress conditions, indicating that an intact OMA1-OPA1 system is essential for developing the appropriate adaptive response to different metabolic stressors such as high-fat diet or cold-shock. However, we cannot discard that, despite all of these metabolic derangements observed, other potential substrates/interacting proteins for OMA1 may be involved in this process. The marked transcriptional changes observed in genes of lipid and glucose metabolic pathways and the substantial alterations in circulating blood parameters found in *Oma1*-mutant mice, are likely part of an exacerbated or anomalous adaptive response, which finally fails in the absence of OMA1 and leads to the phenotypes observed in these mice including obesity and defective thermogenesis. Hopefully, the identification of OMA1 as a proteolytic enzyme involved in the regulation of energy metabolism may open new ways for a better understanding of human obesity, a major medical problem that is reaching epidemic dimensions worldwide.

Materials and methods

Generation of Oma1$^{-/-}$ *mice*

We first constructed the targeting vector in pKO scrambler V916 (Lexicon Genetics). A 4.3-kb *Sal*I–*Not*I fragment from 5′-flanking region, exon 1 and part of intron 1 was used as the 5′-homologous region, whereas a 3.2-kb *Xho*I–*Cla*I fragment containing part of intron 2 and exon 3 was used as the 3′-region of homology. The 2.4-kb *neo* cassette was used as a positive marker and replaced a 2.9-kb fragment containing exon 2 of the *Oma1* gene. The thymidine kinase marker was used as negative selection (Supplementary Figure S1A). The targeting vector was linearized by digestion with *Not*I, electroporated into G4 embryonic stem cells,

and selected for homologous recombination with G418 and ganciclovir. Positive clones were screened by Southern blot after *Pvu*II digestion of genomic DNA and probed with radiolabelled 3′-external probe. A 7.5-kb fragment was detected from wild-type allele and a 4.3-kb fragment from mutant allele. The targeted ES cells clones were expanded and subsequently injected into blastocysts to generate chimeras. Chimeric males were mated with C57BL/6 female mice and the offspring heterozygous for *Oma1* were used to generate homozygous null mice. In all cases, mice genotypes were determined by PCR analysis of tail DNA.

Animal care

All animal procedures were approved in accordance with the guidelines of the Committee for Animal Experimentation of the Universidad de Oviedo. For diet-induced obesity, 4-week-old *Oma1*-deficient mice and their wild-type littermates (C57BL/6/129Sv) were kept in microisolation cages on a 12-h day–night cycle and fed a high-fat diet containing 42% fat (Harlan TD 88137). Mice were weighted once a week for all the experiments. After 24 weeks, mice were sacrificed by cervical dislocation.

Histological analysis

Tissues were fixed in 4% paraformaldehyde in phosphate-buffered saline (PBS) and stored in 70% ethanol. Fixed tissues were embedded in paraffin by standard procedures. Blocks were sectioned (5 μm) and stained with haematoxylin and eosin (H&E). For adipose tissue evaluation, portions of gonadal and subscapular fat pads and pieces of skin were processed as described above. The number of adipocytes and their mean diameter were determined in 3 μm tissue sections by computer-assisted image analysis. For each sample, different sections were analysed and 100 adipocytes were measured. The area of cells was calculated considering the maximum and minimum diameter of each adipocyte. For triglyceride detection, liver samples were fixed with 4% formaldehyde and left overnight at 4°C. After that, samples were treated with 15% sucrose in PBS for 4 h, and then with 30% sucrose solution overnight, embedded in Tissue-Tek OCT compound (Sakura Finetechnical Co. Ltd.) and stored at −70°C. Finally, samples were sectioned at 5 μm thickness with cryostat (CM3050 S, Leica) and cryosections were stained with Oil Red O. For BAT droplets quantification, pictures from BAT sections stained with H&E were analysed with Image J software.

Blood and plasma parameters

Animals fed on regular and high-fat diet were fasted overnight and used for measurements of blood and plasma parameters. Blood glucose was measured with Accu-Chek glucometer (Roche Diagnostics) using blood from the tail vein. For all the other measured parameters, blood was extracted directly from heart after anaesthetizing mice with halothane. Plasma was obtained as previously described. Briefly, blood was immediately centrifuged after collection at 3000 *g* and 4°C, and the supernatant was collected and stored at −80°C until analysis. For plasma insulin, leptin and free fatty-acid measurements, we used Millipore ELISA Kits. All protocols were performed according to the manufacturer's instructions. Levels of hepatic transaminases, cholesterol and triglycerides were determined in the Servicio de Bioquímica, Hospital Universitario Central de Asturias, Oviedo, Spain.

Glucose and insulin tolerance test

Prior to studies, mice were fasted overnight. For IPGTT, mice received an intraperitoneal injection of glucose (2 mg/g body weight). In IPITT studies, mice received an intraperitoneal injection of 1 U of insulin per kg of body weight. Blood glucose levels were determined as describe above. Areas under the curve during IPGTT and IPITT were then calculated by the linear trapezoidal method.

Indirect calorimetry

Energy expenditure and ambulation were assessed using Micro-Oxymax multiple sensor (Columbus Instruments). $Oma1^{+/+}$ and $Oma1^{-/-}$ mice kept on standard rodent chow were housed individually in Oxymax chambers and kept on a 12:12-h light–dark cycle. Constant airflow (0.5 l/min) was drawn through each chamber. After 1 day of acclimation, O_2 consumption, CO_2 production, RQ, heat and ambulation parameters were recorded during 72 h, using software provided by Columbus Instruments.

RNA preparation

Collected tissue was immediately homogenized in TRI reagent (Sigma-Aldrich, St Louis, MO, USA) and processed in the same day through alcohol precipitation according to the manufacturer's instructions. RNA pellets were then washed in cold 80% ethanol and stored at −80°C until further use. Following resuspension of RNA in nuclease-free water (Ambion, Austin, TX, USA), the samples were quantified and evaluated for purity (260/280 nm ratio) using a NanoDrop ND-1000 spectrophotometer (NanoDrop Technologies, Wilmington, DE, USA), and 100 mg of each sample was further purified using RNeasy spin columns according to the manufacturer's instructions (Qiagen, Valencia, CA, USA).

Transcriptional profiling and gene expression analysis

The full transcriptome analysis was conducted using Affymetrix Mouse Gene 1.0 ST Array according to the protocols recommended by the manufacturer (Affymetrix, Santa Clara, CA, USA). Total RNA was isolated as described above from mice tissues maintained under the same high-fat diet and light/dark cycle conditions. The RNA integrity was assessed using Agilent 2100 Bioanalyzer (Agilent, Palo Alto, CA, USA). Labelling and hybridizations were performed according to the protocols from Affymetrix. Washing and scanning were performed using Fluidics Station 400 and GeneChip Scanner (Affymetrix). After scanning, raw data were processed with RMAExpress (http://RMAExpress.bmbolstad.com), using default settings. DAVID, Ingenuity and OpenOffice software were used for data analysis. The DAVID web portal was used to calculate statistical enrichment of KEGG pathways and Gene Ontology biological processes for each group (Dennis *et al*, 2003; Huang da *et al*, 2009). The network analyses were generated through the use of Ingenuity Pathways Analysis (Ingenuity® Systems; http://www.ingenuity.com).

Real-time quantitative PCR

cDNA was synthesized using 1–5 μg of total RNA, 0.14 mM random hexamer primer, 0.2 mM of each deoxynucleoside triphosphate and Superscript II reverse transcriptase (Invitrogen, Carlsbad, CA, USA). Quantitative reverse transcription–PCR (qRT–PCR) was carried out in triplicate for each sample using 20 ng of cDNA, TaqMan® Universal PCR master mix (Applied Biosystems, San Francisco, CA, USA), and 1 μl of the specific TaqMan custom gene expression assay for the gene of interest (Applied Biosystems). To quantitate gene expression, PCR was performed at 95°C for 10 min, followed by 40 cycles at 95°C for 15 s, 60°C for 30 s and 72°C for 30 s using an ABI Prism 7300 sequence detector system. As an internal control, gene expression was normalized to the mouse β-actin gene using the Mouse β-actin Endogenous Control (VIC®/MGB Probe, Primer Limited) TaqMan gene expression assay (Applied Biosystems). Relative expression of the analysed genes was calculated according to the manufacturer's instructions. Briefly, the analysed gene expression was normalized to β-actin in wild-type or $Oma1^{-/-}$ derived samples, using the following formula: the mean value of $2\Delta^{\text{CTgene (}\textit{Gene}\text{ of interest)}} - \Delta^{\text{CTgene (β-}\textit{actin}\text{)}}$ for at least six different wild-type animals were considered 100% for each analysed gene and the same values for $Oma1^{-/-}$ mice tissues were referred to those values as previously described.

Western blotting

Mice tissues were immediately frozen in liquid nitrogen after extraction, then homogenized in 50 mM Tris buffer, pH 7.4, containing 150 mM NaCl, 1% Triton X-100, 10 mM EDTA and complete protease inhibitor cocktail (Roche Applied Science). Once homogenized, tissue extracts were centrifuged at 13 000 *g* and 4°C for 5 min, and supernatants were collected. The protein concentration of the supernatant was evaluated by bicinchoninic acid technique (BCA protein assay kit; Pierce Biotechnology Inc.). A protein sample (15 μg) was loaded on SDS–polyacrylamide gels. After electrophoresis, gels were electrotransferred onto PVDF filters, and the filters were blocked with 5% non-fat dried milk in TBS-T (TBS with 0.05% Tween-20) and incubated with primary antibodies following the commercial instructions. After three washes with TBS-T, filters were incubated with the corresponding secondary antibody in 1.5% milk in TBS-T, and developed with Immobilon Western Chemiluminescent HRP substrate (Millipore) in a LAS-3000 Imaging System (Fujifilm). The antibodies against OPA1 and DRP1 were from BD Bioscience, and the antibody against MFN2

was from Abcam. All the other antibodies used in this work were from Cell Signaling.

Cell culture and microscopy analysis

Primary MEFs were extracted from E13.5 embryos. Briefly, embryos were sterilized with ethanol, washed with PBS and triturated with razor blades. Samples were then incubated in Dulbecco's modified Eagle's medium (DMEM) (Gibco) overnight at 37°C and 5% CO_2. The next day, cultured cells were trypsinized and washed. Finally, MEFs were incubated at 37°C and 5% CO_2 and used for the corresponding experiments. Adult murine fibroblasts (AFs) were extracted from 12-week-old mice ears. Ears were sterilized with ethanol, washed with PBS and triturated with razor blades. Samples were then incubated with 600 μl of 4 mg/ml collagenase D (Roche Applied Science) and 4 mg/ml dispase II (Roche Applied Science) in DMEM (Gibco) for 45 min at 37°C and 5% CO_2. After filtering and washing, 6 ml of DMEM with 10% fetal bovine serum (Invitrogen), and 1% antimycotic-antibiotic (Invitrogen) were added, and the mixture was incubated at 37°C and 5% CO_2. Once extracted, cells were cultured in DMEM containing 10% fetal bovine serum at 37°C and 5% CO_2. Brown preadipocytes were isolated from newborn mice by collagenase digestion and were differentiated to mature adipocytes as previously described (Fasshauer *et al*, 2000). Immortalized MEFs, AFs and preadipocytes were generated by SV40 transformation. For fluorescence microscope analyses, mitochondrial morphology was examined after transfection of vector containing mito-DsRed, and images were obtained using a laser-scanning confocal microscope (TCS-SP2-AOBS; Leica) using HCX PL APO Ibd BL ×63 NA 1.4 objective lens. Images were acquired with LCS Suite version 2.61 (Leica), and then modified with ImageJ, using the maxima projection of 0.2 μm stacks images after convolve, median filter and despeckle modification. Brightness/contrast was adjusted using ImageJ.

Transmission electron microscopy

BAT samples were dissected from control and cold-stress-induced mice and fixed in 3% glutaraldehyde in 0.1 M sodium cacodylate (pH 7.2) for 1 h at 4°C. After three washes in 0.1 M Sorensen's phosphate buffer, samples were postfixed with 1% osmium tetroxide for 1 h and rinsed three times in Sorensen's buffer. Tissues were dehydrated in graded ethanol and infiltrated in 50% propylene oxide/50% resin for 1 h, then placed in resin for 1 h, and embedded in a resin-based mould for polymerization overnight in a 37°C oven. Ultra-thin sections (85 nm) were taken from each sample and analysed on a Jeol (JEM-1011) transmission electron microscope at 80 kV. Images were modified using ImageJ and Gimp 2.6 software.

Proliferation assays

Growth capacity was determined in six-well test plates in which 6×10^4 cells were plated per well in 2.5 ml of DMEM medium and incubated at 37°C for 72 h. Cells were daily counted by using a Neubauer chamber. Population doubling time was calculated using the algorithm provided by http://www.doubling-time.com.

Mitochondrial ATP content

Cellular ATP levels were determined using the ATP determination kit (Molecular probes, Invitrogen) according to the instructions of the manufacturer. Briefly, MEFs were collected by trypsinization and lysed using PLB (Promega). The lysates were centrifuged at 12 000 *g* and 4°C for 5 min, and supernatants were collected. The protein concentration of the supernatant was evaluated by bicinchoninic acid technique (BCA protein assay kit, Pierce Biotechnology, Rockford, IL, USA). We used 3 μg of lysated material for ATP determination with a D-luciferin/firefly luciferase reaction mix, and luminescence was measured in a Luminometer TD20/20 and compared with a freshly prepared ATP standard curve.

Mitochondrial DNA copy number quantification

We quantified mtDNA by real-time PCR using ABI PRISM 7300 Sequence Detector System (Applied Biosystems) and TaqMan Universal PCR master mix (Applied Biosystems). Total DNA was used as a template and amplified with specific oligodeoxynucleotides for *mt-Co2* and *Sdha*. We calculated the mtDNA copy number per cell using *Sdha* amplification as a reference for nuclear genome (Moreno-Loshuertos *et al*, 2006).

Citrate synthase activity

We determined mitochondrial citrate synthase activity in whole MEFs lysates and tissues homogenates. Briefly, MEFs were collected by trypsinization, washed twice with PBS and resuspended in buffer A (0.25 M sucrose and 20 mM MOPS-KOH, pH 7.4). Then, we added digitonin to a final concentration of 0.1 mg/ml, and cells were kept on ice for 5 min and centrifuged at 5000 *g* and 4°C for 5 min. The pellets were resuspended in buffer B (0.25 M sucrose, 1 mM EDTA and 20 mM MOPS-KOH, pH 7.4), kept on ice 5 min and centrifuged again at 10 000 *g*. The final mitochondrial fraction pellets were resuspended in 10 mM of potassium phosphate buffer (pH 7.4) and samples were freezed-thawed three times in liquid nitrogen before use. For tissue analysis, homogenates were prepared as described in palmitate oxidation protocol. Citrate synthase activity was determined spectrophotometrically at 30°C as the reduction rate of 100 μM DTNB (5,5′-dithio-bis-2-nitrobenzoic acid) at 412 nm ($\varepsilon = 13.8$/mM/cm) after the addition of 400 μM acetyl-Coenzyme A and 500 μM oxalacetate (Sigma-Aldrich).

Oxygen consumption measurements

Endogenous respiration measurements in intact cells or polarography in digitonin-permeabilized cells were performed using a Clark type oxygen electrode (Hansatech) as previously described (Hofhaus *et al*, 1996; Acin-Perez *et al*, 2003). Briefly, for the O_2 consumption determinations in intact cells to measure the maximum respiration capacity, exponentially growing cells were collected by trypsinization and centrifugation, and resuspended at 6.5×10^6 cells/ml in 0.75 ml of DMEM containing glucose (4.5 g/l), supplemented with 10% FBS. The cell suspension was transferred to the electrode's 1.5 ml water-jacketed chamber containing a small magnetic bar, thermostated at 37°C. Recording of oxygen consumption was carried out for 150 s. Then, 65 nmol 2,4-dinitrophenol (DNP; Sigma) were added to uncouple the respiration and oxygen consumption was monitored for an additional 150 s to determine the maximum O_2 consumption. For polarographic measurements of the individual respiratory complexes, cells were collected by trypsinization and centrifugation, and resuspended at $2–5 \times 10^6$ cells/ml in Respiration Buffer (250 mM HEPES, pH 7.1; 250 mM sucrose, 10 mM $MgCl_2$, 1 mM ADP and 2 mM potassium phosphate). Cells were permeabilized using 10–20 μg digitonin per 10^6 cells and the oxygen consumption rates were determined using specific substrates and inhibitors for each of the respiratory complexes: glutamate + malate and rotenone for complex I; succinate + glycerol-3-phosphate and antimycin A for complex III; TMPD and KCN for complex IV.

Palmitate oxidation measurement

Oxidation of [1-^{14}C]-palmitic acid by tissue homogenates was performed as previously described (Hirschey *et al*, 2010). Briefly, liver and BAT samples were extracted and homogenized in sucrose/Tris/EDTA buffer, incubated for 120 min in the reaction mixture (pH 8.0) containing [1-^{14}C]-palmitic acid, and measured for acid-soluble metabolites. Palmitate oxidation rates in primary brown adipocytes were quantified as described (Antinozzi *et al*, 1998) and corrected for total cellular protein content.

Statistical analysis

All experimental data are reported as mean and the error bars represent the standard error of the mean (s.e.m.). Differences between mean values were analysed by two-tailed Student's *t*-test. A value of $P < 0.05$ was considered significant. Statistical significant differences are shown with asterisks.

Accession numbers

The Affymetrics GeneChip data set is publicly available from the Gene Expression Omnibus (GEO; http://www.ncbi.nlm.nih.gov/geo/) with the accession number GSE27525.

Supplementary data

Supplementary data are available at *The EMBO Journal* Online (http://www.embojournal.org).

Acknowledgements

We thank G Mariño, AR Folgueras, A Astudillo and JM Freije for helpful comments and T Langer for OPA1 expression plasmids. We

also thank FV Álvarez, JC Fernández and E Lapuente-Brun for help in blood analysis and cell culture, and M Fernández, D Puente, A Moyano, R Feijoo and MS Pitiot for excellent technical assistance. This work was supported by grants from Ministerio de Ciencia e Innovación-Spain and the European Union (FP7-Microenvimet). The Instituto Universitario de Oncología was supported by Obra Social Cajastur-Asturias and Acción Transversal del Cáncer-RTICC, Spain. CL-O is an Investigator of the Botin Foundation.

Author contributions: PMQ and AJR performed the experiments and analysed the data; FR participated in the generation of knockout mice; DS and AZ designed and carried out energy expenditure and ambulation experiments in mice; EFV and JAE carried out and analysed oxygen consumption measurements; JRP collaborated in blood analysis; MSFG analysed histological samples; JAV carried out electronic microscopy analysis; PMQ, AJR and CLO conceived, designed and wrote the paper.

Conflict of interest

The authors declare that they have no conflict of interest.

References

Acin-Perez R, Bayona-Bafaluy MP, Bueno M, Machicado C, Fernandez-Silva P, Perez-Martos A, Montoya J, Lopez-Perez MJ, Sancho J, Enriquez JA (2003) An intragenic suppressor in the cytochrome c oxidase I gene of mouse mitochondrial DNA. *Hum Mol Genet* **12:** 329–339

Antinozzi PA, Segall L, Prentki M, McGarry JD, Newgard CB (1998) Molecular or pharmacologic perturbation of the link between glucose and lipid metabolism is without effect on glucose-stimulated insulin secretion. A re-evaluation of the long-chain acyl-CoA hypothesis. *J Biol Chem* **273:** 16146–16154

Baricault L, Segui B, Guegand L, Olichon A, Valette A, Larminat F, Lenaers G (2007) OPA1 cleavage depends on decreased mitochondrial ATP level and bivalent metals. *Exp Cell Res* **313:** 3800–3808

Casari G, De Fusco M, Ciarmatori S, Zeviani M, Mora M, Fernandez P, De Michele G, Filla A, Cocozza S, Marconi R, Durr A, Fontaine B, Ballabio A (1998) Spastic paraplegia and OXPHOS impairment caused by mutations in paraplegin, a nuclear-encoded mitochondrial metalloprotease. *Cell* **93:** 973–983

Chang CR, Blackstone C (2010) Dynamic regulation of mitochondrial fission through modification of the dynamin-related protein Drp1. *Ann NY Acad Sci* **1201:** 34–39

Chen H, Chan DC (2009) Mitochondrial dynamics—fusion, fission, movement, and mitophagy—in neurodegenerative diseases. *Hum Mol Genet* **18:** R169–R176

Choquette AC, Lemieux S, Tremblay A, Chagnon YC, Bouchard C, Vohl MC, Perusse L (2008) Evidence of a quantitative trait locus for energy and macronutrient intakes on chromosome 3q27.3: the Quebec Family Study. *Am J Clin Nutr* **88:** 1142–1148

Cinti S, Mitchell G, Barbatelli G, Murano I, Ceresi E, Faloia E, Wang S, Fortier M, Greenberg AS, Obin MS (2005) Adipocyte death defines macrophage localization and function in adipose tissue of obese mice and humans. *J Lipid Res* **46:** 2347–2355

Cipolat S, Rudka T, Hartmann D, Costa V, Serneels L, Craessaerts K, Metzger K, Frezza C, Annaert W, D'Adamio L, Derks C, Dejaegere T, Pellegrini L, D'Hooge R, Scorrano L, De Strooper B (2006) Mitochondrial rhomboid PARL regulates cytochrome c release during apoptosis via OPA1-dependent cristae remodeling. *Cell* **126:** 163–175

Dennis Jr G, Sherman BT, Hosack DA, Yang J, Gao W, Lane HC, Lempicki RA (2003) DAVID: database for annotation, visualization, and integrated discovery. *Genome Biol* **4:** P3

Detmer SA, Chan DC (2007) Functions and dysfunctions of mitochondrial dynamics. *Nat Rev Mol Cell Biol* **8:** 870–879

Di Bella D, Lazzaro F, Brusco A, Plumari M, Battaglia G, Pastore A, Finardi A, Cagnoli C, Tempia F, Frontali M, Veneziano L, Sacco T, Boda E, Brussino A, Bonn F, Castellotti B, Baratta S, Mariotti C, Gellera C, Fracasso V *et al* (2010) Mutations in the mitochondrial protease gene AFG3L2 cause dominant hereditary ataxia SCA28. *Nat Genet* **42:** 313–321

Duvezin-Caubet S, Jagasia R, Wagener J, Hofmann S, Trifunovic A, Hansson A, Chomyn A, Bauer MF, Attardi G, Larsson NG, Neupert W, Reichert AS (2006) Proteolytic processing of OPA1 links mitochondrial dysfunction to alterations in mitochondrial morphology. *J Biol Chem* **281:** 37972–37979

Ehses S, Raschke I, Mancuso G, Bernacchia A, Geimer S, Tondera D, Martinou JC, Westermann B, Rugarli EI, Langer T (2009) Regulation of OPA1 processing and mitochondrial fusion by m-AAA protease isoenzymes and OMA1. *J Cell Biol* **187:** 1023–1036

Fasshauer M, Klein J, Ueki K, Kriauciunas KM, Benito M, White MF, Kahn CR (2000) Essential role of insulin receptor substrate-2 in insulin stimulation of Glut4 translocation and glucose uptake in brown adipocytes. *J Biol Chem* **275:** 25494–25501

Feldmann HM, Golozoubova V, Cannon B, Nedergaard J (2009) UCP1 ablation induces obesity and abolishes diet-induced thermogenesis in mice exempt from thermal stress by living at thermoneutrality. *Cell Metab* **9:** 203–209

Fernandez-Marcos PJ, Auwerx J (2011) Regulation of PGC-1{alpha}, a nodal regulator of mitochondrial biogenesis. *Am J Clin Nutr* **93:** 884S–8890

Ferreirinha F, Quattrini A, Pirozzi M, Valsecchi V, Dina G, Broccoli V, Auricchio A, Piemonte F, Tozzi G, Gaeta L, Casari G, Ballabio A, Rugarli EI (2004) Axonal degeneration in paraplegin-deficient mice is associated with abnormal mitochondria and impairment of axonal transport. *J Clin Invest* **113:** 231–242

Finck BN, Kelly DP (2006) PGC-1 coactivators: inducible regulators of energy metabolism in health and disease. *J Clin Invest* **116:** 615–622

Frezza C, Cipolat S, Martins de Brito O, Micaroni M, Beznoussenko GV, Rudka T, Bartoli D, Polishuck RS, Danial NN, De Strooper B, Scorrano L (2006) OPA1 controls apoptotic cristae remodeling independently from mitochondrial fusion. *Cell* **126:** 177–189

Fulda S, Galluzzi L, Kroemer G (2010) Targeting mitochondria for cancer therapy. *Nat Rev Drug Discov* **9:** 447–464

Green DR, Kroemer G (2004) The pathophysiology of mitochondrial cell death. *Science* **305:** 626–629

Griparic L, Kanazawa T, van der Bliek AM (2007) Regulation of the mitochondrial dynamin-like protein Opa1 by proteolytic cleavage. *J Cell Biol* **178:** 757–764

Head B, Griparic L, Amiri M, Gandre-Babbe S, van der Bliek AM (2009) Inducible proteolytic inactivation of OPA1 mediated by the OMA1 protease in mammalian cells. *J Cell Biol* **187:** 959–966

Hirschey MD, Shimazu T, Goetzman E, Jing E, Schwer B, Lombard DB, Grueter CA, Harris C, Biddinger S, Ilkayeva OR, Stevens RD, Li Y, Saha AK, Ruderman NB, Bain JR, Newgard CB, Farese Jr RV, Alt FW, Kahn CR, Verdin E (2010) SIRT3 regulates mitochondrial fatty-acid oxidation by reversible enzyme deacetylation. *Nature* **464:** 121–125

Hofhaus G, Shakeley RM, Attardi G (1996) Use of polarography to detect respiration defects in cell cultures. *Methods Enzymol* **264:** 476–483

Hoppins S, Nunnari J (2009) The molecular mechanism of mitochondrial fusion. *Biochim Biophys Acta* **1793:** 20–26

Huang da W, Sherman BT, Lempicki RA (2009) Systematic and integrative analysis of large gene lists using DAVID bioinformatics resources. *Nat Protoc* **4:** 44–57

Hyde BB, Twig G, Shirihai OS (2010) Organellar vs cellular control of mitochondrial dynamics. *Semin Cell Dev Biol* **21:** 575–581

Ishihara N, Fujita Y, Oka T, Mihara K (2006) Regulation of mitochondrial morphology through proteolytic cleavage of OPA1. *EMBO J* **25:** 2966–2977

Kaser M, Kambacheld M, Kisters-Woike B, Langer T (2003) Oma1, a novel membrane-bound metallopeptidase in mitochondria with activities overlapping with the m-AAA protease. *J Biol Chem* **278:** 46414–46423

Koppen M, Langer T (2007) Protein degradation within mitochondria: versatile activities of AAA proteases and other peptidases. *Crit Rev Biochem Mol Biol* **42:** 221–242

Landes T, Leroy I, Bertholet A, Diot A, Khosrobakhsh F, Daloyau M, Davezac N, Miquel MC, Courilleau D, Guillou E, Olichon A,

Lenaers G, Arnaune-Pelloquin L, Emorine LJ, Belenguer P (2010) OPA1 (dys)functions. *Semin Cell Dev Biol* **21:** 593–598

Lopez-Otin C, Bond JS (2008) Proteases: multifunctional enzymes in life and disease. *J Biol Chem* **283:** 30433–30437

Lopez-Otin C, Hunter T (2010) The regulatory crosstalk between kinases and proteases in cancer. *Nat Rev Cancer* **10:** 278–292

Lowell BB, S-Susulic V, Hamann A, Lawitts JA, Himms-Hagen J, Boyer BB, Kozak LP, Flier JS (1993) Development of obesity in transgenic mice after genetic ablation of brown adipose tissue. *Nature* **366:** 740–742

Maltecca F, Aghaie A, Schroeder DG, Cassina L, Taylor BA, Phillips SJ, Malaguti M, Previtali S, Guenet JL, Quattrini A, Cox GA, Casari G (2008) The mitochondrial protease AFG3L2 is essential for axonal development. *J Neurosci* **28:** 2827–2836

Mammucari C, Rizzuto R (2010) Signaling pathways in mitochondrial dysfunction and aging. *Mech Ageing Dev* **131:** 536–543

Moreno-Loshuertos R, Acin-Perez R, Fernandez-Silva P, Movilla N, Perez-Martos A, Rodriguez de Cordoba S, Gallardo ME, Enriquez JA (2006) Differences in reactive oxygen species production explain the phenotypes associated with common mouse mitochondrial DNA variants. *Nat Genet* **38:** 1261–1268

Navarro CL, Cadinanos J, De Sandre-Giovannoli A, Bernard R, Courrier S, Boccaccio I, Boyer A, Kleijer WJ, Wagner A, Giuliano F, Beemer FA, Freije JM, Cau P, Hennekam RC, Lopez-Otin C, Badens C, Levy N (2005) Loss of ZMPSTE24 (FACE-1) causes autosomal recessive restrictive dermopathy and accumulation of Lamin A precursors. *Hum Mol Genet* **14:** 1503–1513

Olichon A, Baricault L, Gas N, Guillou E, Valette A, Belenguer P, Lenaers G (2003) Loss of OPA1 perturbates the mitochondrial inner membrane structure and integrity, leading to cytochrome c release and apoptosis. *J Biol Chem* **278:** 7743–7746

Orrenius S, Gogvadze V, Zhivotovsky B (2007) Mitochondrial oxidative stress: implications for cell death. *Annu Rev Pharmacol Toxicol* **47:** 143–183

Pidoux G, Witczak O, Jarnaess E, Myrvold L, Urlaub H, Stokka AJ, Kuntziger T, Tasken K (2011) Optic atrophy 1 is an A-kinase anchoring protein on lipid droplets that mediates adrenergic control of lipolysis. *EMBO J* **30:** 4371–4386

Saar K, Geller F, Ruschendorf F, Reis A, Friedel S, Schauble N, Nurnberg P, Siegfried W, Goldschmidt HP, Schafer H, Ziegler A, Remschmidt H, Hinney A, Hebebrand J (2003) Genome scan for childhood and adolescent obesity in German families. *Pediatrics* **111:** 321–327

Shimohata N, Chiba S, Saikawa N, Ito K, Akiyama Y (2002) The Cpx stress response system of Escherichia coli senses plasma membrane proteins and controls HtpX, a membrane protease with a cytosolic active site. *Genes Cells* **7:** 653–662

Song Z, Chen H, Fiket M, Alexander C, Chan DC (2007) OPA1 processing controls mitochondrial fusion and is regulated by mRNA splicing, membrane potential, and Yme1L. *J Cell Biol* **178:** 749–755

Suen DF, Norris KL, Youle RJ (2008) Mitochondrial dynamics and apoptosis. *Genes Dev* **22:** 1577–1590

Tatsuta T, Langer T (2008) Quality control of mitochondria: protection against neurodegeneration and ageing. *EMBO J* **27:** 306–314

Uldry M, Yang W, St-Pierre J, Lin J, Seale P, Spiegelman BM (2006) Complementary action of the PGC-1 coactivators in mitochondrial biogenesis and brown fat differentiation. *Cell Metab* **3:** 333–341

Varela I, Cadinanos J, Pendas AM, Gutierrez-Fernandez A, Folgueras AR, Sanchez LM, Zhou Z, Rodriguez FJ, Stewart CL, Vega JA, Tryggvason K, Freije JM, Lopez-Otin C (2005) Accelerated ageing in mice deficient in Zmpste24 protease is linked to p53 signalling activation. *Nature* **437:** 564–568

Varela I, Pereira S, Ugalde AP, Navarro CL, Suarez MF, Cau P, Cadinanos J, Osorio FG, Foray N, Cobo J, de Carlos F, Levy N, Freije JM, Lopez-Otin C (2008) Combined treatment with statins and aminobisphosphonates extends longevity in a mouse model of human premature aging. *Nat Med* **14:** 767–772

Voos W (2009) Mitochondrial protein homeostasis: the cooperative roles of chaperones and proteases. *Res Microbiol* **160:** 718–725

Wallace DC (2005) A mitochondrial paradigm of metabolic and degenerative diseases, aging, and cancer: a dawn for evolutionary medicine. *Annu Rev Genet* **39:** 359–407

Wallace DC, Fan W, Procaccio V (2010) Mitochondrial energetics and therapeutics. *Annu Rev Pathol* **5:** 297–348

Westermann B (2010) Mitochondrial fusion and fission in cell life and death. *Nat Rev Mol Cell Biol* **11:** 872–884

Zorzano A, Liesa M, Sebastian D, Segales J, Palacin M (2010) Mitochondrial fusion proteins: dual regulators of morphology and metabolism. *Semin Cell Dev Biol* **21:** 566–574

II. Metabolic control by mitochondrial protease OMA1

The proper regulation of mitochondrial dynamics is essential to maintain mitochondrial homeostasis. Under some stress conditions, mitochondria are divided to protect mitochondrial network. However, and because the balance between fusion and fission must be perfectly coordinated in order to induce the mitochondrial fragmentation it is necessary to concomitantly inhibit the fusion events. OMA1 protease mediates the inactivation of mitochondrial fusion by proteolytic processing of OPA1. Defects in this system induce alterations under some stress conditions, including metabolic changes such as high-fat diet or cold-stress, which can underlie some metabolic-related diseases. Our finding of this novel and unexpected role of OMA1 as a key factor controlling energy metabolism, prompted us to compile all these data in a mini-review.

Article 2: Pedro M. Quirós, Andrew J. Ramsay, and Carlos López-Otín. "New roles for OMA1 metalloprotease: From mitochondrial proteostasis to metabolic homeostasis".

Adipocyte. 2013 January 1; 2(1): 7–11.

Personal contribution to this work

In this work, I have been the main responsible for compiling the data, preparing the figures and writing the manuscript that describes the functional relevance of OMA1 in the control of energy metabolism. This review was prepared under the supervision of Dr. Andrew J. Ramsay and Prof. Carlos López-Otín.

MINI-REVIEW

Adipocyte 2:1, 7–11; January/February/March 2013; © 2013 Landes Bioscience

New roles for OMA1 metalloprotease
From mitochondrial proteostasis to metabolic homeostasis

Pedro M. Quirós, Andrew J. Ramsay and Carlos López-Otín*

Departamento de Bioquímica y Biología Molecular; Facultad de Medicina; Instituto Universitario de Oncología; Universidad de Oviedo; Oviedo, Spain

Keywords: obesity, brown adipose tissue, protease, mitochondrial dynamics

The mitochondrial quality control system is essential for the preservation and regulation of mitochondrial function. This system is formed by a complex machinery that controls and maintains protein function and regulates mitochondrial morphology through a coordinated system of continual fusion and fission events. Impairments in the mitochondrial quality control system through either mutation or deficiency in any of its components, can lead to mitochondrial dysfunction. However, the physiological consequences of these deficiencies remain unknown in most cases. Here, we briefly review the role of the OPA1-OMA1 system in mitochondrial biology, and summarize our recent report on the generation and phenotypic characterization of a model deficient in OMA1, an ATP-independent mitochondrial metalloprotease that participates in mitochondrial quality control. Interestingly, *Oma1*-deficient mice display an obesity phenotype, characterized by hepatic steatosis, decrease in energy expenditure and defective thermogenic regulation. In addition, our study has provided in vivo evidence of OMA1 function as a mitochondrial quality control protease, inactivating OPA1 under stress conditions and inhibiting mitochondrial fusion. Further, we have demonstrated the essential role of the OMA1-OPA1 system for brown adipose function and how this system regulates metabolic homeostasis in mice.

Mitochondria are the central core of energy metabolism within the cell, producing ATP through oxidative phosphorylation, as well as participating in many pathways of intermediate metabolism, calcium regulation and other processes such as apoptosis.[1] For this reason, mitochondria have developed a complex quality control system, comprised of a network of proteases and chaperones, which regulate the assembly, folding and turnover of mitochondrial proteins to maintain proper function.[2,3] Mitochondria are highly dynamic organelles that continually undergo a process of fusion and division. As such, depending on the cell type, tissue or moment, mitochondria adopt morphologies ranging from small punctuate organelles to a highly connected network.[4] Linked to the quality control mechanism exerted by proteases and chaperones, the regulation of mitochondrial dynamics generates another point of control. Thus, mitochondrial dynamics can result in more efficient organelles through induction of mitochondrial fusion, or can protect the mitochondrial network under some stress conditions by coordinating mitochondrial fission. Due to the range and importance of the functions in which mitochondria participate, a highly evolved process of cellular safeguarding has developed. As an illustrative example, if mitochondrial damage continues unabated and its function cannot be rescued, small mitochondria generated by fission can be removed by mitophagy, or apoptotic signals can be orchestrated to remove damaged cells and protect organismal viability.[5,6] Given the importance of the quality control machinery, it is plausible that mutations in any of its protein components could induce mitochondrial dysfunction and underlie human diseases.

The study of mitochondrial dynamics during recent years has permitted the identification of several components of the fusion and fission machinery, as well as some components that participate in the regulation of these processes. In mammals, the fusion process is principally performed by three large GTPases, mitofusin 1 and 2 (MFN1 and MFN2) in the outer membrane and OPA1 in the inner membrane.[7,8] The fission process is largely controlled by the dynamin-related GTPase DRP1, located in the cytoplasm, which is recruited to mitochondria and recognized by specific mitochondrial receptors in the outer membrane, MFF or FIS1.[9,10] Both dynamic processes have to be highly controlled to maintain the balance between fusion and fission events, as well as to enable a rapid response to a wide variety of stimuli in the cell. Thus, a decrease in ATP levels, loss of mitochondrial membrane potential or apoptotic stimuli, induce fragmentation of the mitochondrial network due to inhibition of the fusion process.[11] Conversely, the fission process is inhibited in response to starvation, increasing the connection of the mitochondrial tubular network to protect mitochondria from degradation and increase cell viability.[12] Deregulation of fusion or fission events is implicated in several human diseases, most of them related to neurological disorders, as neurons appear to be particularly susceptible to mitochondrial defects.[13] Thus, Charcot-Marie-Tooth type 2A, autosomal dominant optic atrophy or postnatal death with neurodevelopmental disorder, are due to mutation in *MFN2*, *OPA1* and *DRP1*, respectively.[14-17] Moreover, *OPA1* mutations are also associated with different forms of optic atrophy with or without deafness, ophthalmoplegia, myopathy, ataxia and neuropathy,[18,19] as well as with susceptibility to normal tension glaucoma[20,21] Indeed, mutations in other proteases of the

*Correspondence to: Carlos López-Otín; Email: clo@uniovi.es
Submitted: 06/27/12; Revised: 08/27/12; Accepted: 08/28/12
http://dx.doi.org/10.4161/adip.21999

mitochondrial inner membrane that belong to quality control systems and are associated with OPA1 processing, have a clear neurological phenotype, such as spastic paraplegia and a dominant form of spinocerebellar ataxia caused by mutations in *SPG7* and *AFG3L2*, respectively.[22,23]

Despite recent advances in our understanding of mitochondrial dynamics, the generation of animal models is essential to understand the entirety of this molecular process and its functional relevance in pathophysiology. In this regard, we have recently reported that OMA1, a mitochondrial metalloprotease that processes the GTPase OPA1 in response to stress stimuli, has a new key role in metabolic homeostasis.[24] OMA1 was identified in yeast as a mitochondrial protease of overlapping activity with the m-AAA protease,[25] a mitochondrial quality control protease located in the inner membrane.[26] Subsequent in vitro studies in mammalian cells determined that OMA1 proteolytically inactivates OPA1, inhibiting the fusion process and catalyzing mitochondrial fragmentation.[27,28] However, the physiological role of this protease remained unknown. Thus, we generated a knockout mouse model of *Oma1* in order to delineate the in vivo roles and relevance in mitochondrial function and quality control of this protease. Surprisingly, *Oma1*-deficient mice showed an unexpected metabolic phenotype, characterized by increase in body weight and hepatic steatosis, together with defective energy balance and thermogenic regulation. Under control conditions, *Oma1*-deficient mice displayed a slight body weight increase and hepatic steatosis. However, on a high-fat diet, *Oma1* knockout mice developed a marked obesity phenotype with a significant increase in body weight and fat mass compared with controls. Further, gonadal and skin adipocytes showed a clear hypertrophy, and hepatic steatosis was enhanced together with an increase in triglyceride levels in blood. In addition, *Oma1*$^{-/-}$ mice displayed reduced energy expenditure, which is in accordance with previous studies in mouse models as a possible cause of an obesity phenotype.[29,30] Further, the metabolic alterations observed in *Oma1*-deficient mice were accompanied by a decrease in the expression of genes controlling mitochondrial dynamics and oxidative phosphorylation, metabolic regulation, β-oxidation and an increase in lipogenic genes in both liver and brown adipose tissues. These gene changes were similarly consistent with previous observations in other murine models in which an obesity phenotype was related to mitochondrial dysfunction.[31] Moreover, thermogenic control and adaptive thermogenic response to cold-stress were both altered, indicating a possible dysfunction in brown adipose tissue function regulating heat production.

Interest in brown adipose tissue has gained significant momentum over the last few years due to recent studies correlating its function to, not only the generation of heat in animals and newborns, but also as an integral tissue for regulating metabolic homeostasis and as a possible control point for obesity.[32,33] In our studies of *Oma1*-deficient mice, brown adipose tissue showed reduced β-oxidation rates in both normal and high-fat diets. These results indicated a dysfunction in brown adipose tissue due to deficiency of the OMA1 protease, under both normal and stress conditions. We analyzed mitochondrial structure by electron microscopy, and found that *Oma1*-deficient mice displayed an increase in mitochondrial size without changes in the number of mitochondria. It has been previously described that under cold-stress conditions, mitochondria elongate, increasing fusion in an attempt to protecting the mitochondrial network.[34] However, analysis of mitochondrial structure after cold-stress of brown adipose tissue from *Oma1*-deficient mice did no display an increase in mitochondrial size in contrast to control mice, indicating a dysfunction in the response to cold-induced stress by the mitochondrial dynamic machinery. In addition, using in vitro experiments with brown adipocytes, we confirmed that both OMA1 and OPA1 are required for β-oxidation, and that this function was dependent on OPA1 isoforms generated by OMA1 activity. Further, analysis of mitochondrial respiratory rates and ATP production were not altered in the liver under normal or high-fat diets; however, β-oxidation rates were significantly reduced in liver under high-fat diet treatment. These results confirmed that the OMA1-OPA1 system is required for the proper function of brown adipose tissue and for keeping metabolic homeostasis in mice.

The deficiency in OMA1 alters the balance between fusion and fission, and can be the origin of the metabolic alterations observed in our mouse model. Thus, we have demonstrated in vivo that OMA1 has a non-redundant role in the proteolytic inactivation of OPA1 under stress conditions. OPA1 functions are controlled by alternative splicing and proteolysis of the different isoforms. Thereby, OPA1 is characterized by at least five different isoforms, two long isoforms (L-OPA1; a and b), and three short isoforms (S-OPA1; c–e).[11,35] Under stress conditions, such as loss of mitochondrial membrane potential or apoptotic stimuli, L-OPA1 isoforms are cleaved to S-OPA1 isoforms by OMA1 activity, inhibiting the fusion event.[36,37] This inhibition is due to the fact that, for an inner membrane fusion event to occur, OPA1 requires at least one of each of the long and short isoforms, forming a complex structure to induce the fusion of membranes. At present, several mitochondrial proteases have been implicated in the processing and regulation of OPA1 levels, such as PARL1, m-AAA and YME1L1.[27,35,38] Analysis of *Oma1*-deficient cells demonstrated the absence of one of the short isoforms of OPA1 and a decrease in the expression of the other under basal conditions (**Fig. 1**; c and e, respectively). Moreover, under stress conditions, *Oma1*-deficient cells displayed no proteolysis of OPA1 to generate the shorter isoforms. This observation reinforces that under normal conditions, several inner membrane proteases could regulate the generation of some S-OPA1 isoforms, although in response to stress conditions the inactivation of OPA1 is exclusively due to OMA1 function.

As fusion and fission are interdependent, inhibition of one of the two creates disequilibrium in the balance of these two events. Under normal conditions mitochondria adopt a tubular morphology that fragments in response to fission predominance. Conversely, inhibition of fission increases the tubular connection of mitochondria due to increased fusion. Analysis of mitochondria from *Oma1*-deficient MEFs showed, predominantly, an archetypal tubular morphology with a significant increase in the

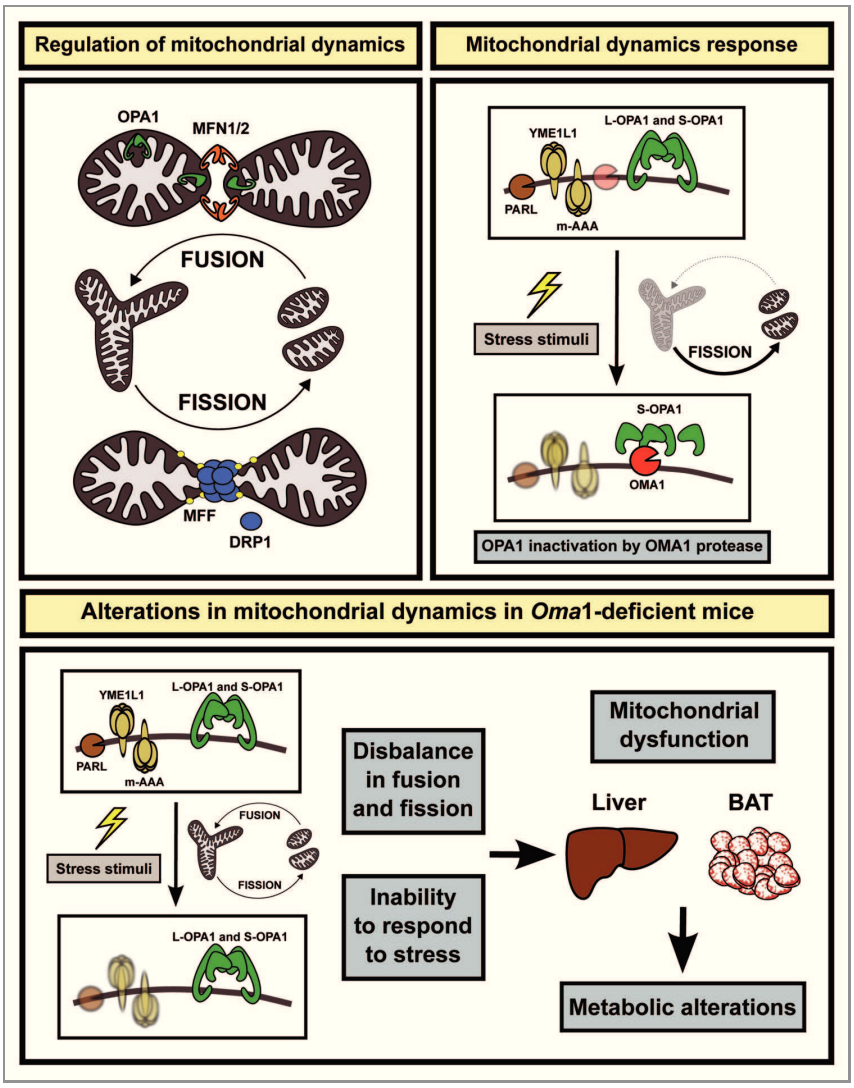

Figure 1. Schematic representation of mitochondrial dynamics regulation, the mitochondrial dynamics response mediated by OMA1 and the alterations observed in *Oma1*-deficient mice due to alterations in mitochondrial dynamics equilibrium under stress conditions.

elongated mitochondrial morphologies. Further, under stress conditions, *Oma1*$^{-/-}$ MEFs maintain their tubular morphology due to absent fusion. Intriguingly, the stabilization of L-OPA1 isoforms in *Oma1*-deficient MEFs protected cells from apoptotic stimuli, due to maintenance of cristae morphology and prevention of cytochrome c release.[38,39] Thus, the OMA1-OPA1 system is critical to maintain mitochondrial function and has an important role in mitochondrial quality control, exerting its function on mitochondrial dynamics and apoptosis levels. The alterations in this control system due to *Oma1* ablation induce mitochondrial dysfunction under stress conditions due to inability to adequately respond to stress stimuli, such as metabolic stress induced by high-fat diet or cold-stress.

Future Perspectives

Oma1-deficient mice have provided the first in vivo evidence linking dysfunction in the mitochondrial quality control system with an obesity phenotype and deregulated thermogenic control. Interestingly, recent publications have shown that OPA1 function is necessary for mitochondrial glucose-stimulated ATP production in pancreatic β cells,[40] and for mediating adrenergic control of lipolysis, as a dual-specificity A-kinase anchoring protein in lipid droplets.[41] Collectively, these findings further emphasize the importance of the OMA1-OPA1 system for metabolic homeostasis. Looking toward the future, the possibility must be entertained that OMA1 has other additional substrates and interaction partners that can contribute to

the quality control system or to other mitochondrial pathways. The potential identification of novel regulatory proteins belonging to the OMA1 proteostasis network would provide further insights into mitochondrial function and could also shed new light on human pathologies. Accordingly, *Oma1* knockout generation has allowed the discovery of an unexpected role of this mitochondrial quality control protease as a new key regulator of metabolic homeostasis. Hopefully, the use of this and other mouse models of mitochondrial quality control components will let us further understand this complex system and its associated human diseases.

Disclosure of Potential Conflicts of Interest

No potential conflicts of interest were disclosed.

Acknowledgments

This work was supported by grants from Ministerio de Economía y Competitividad-Spain and the European Union (FP7-Microenvimet). The Instituto Universitario de Oncología is supported by Obra Social Cajastur-Asturias and Acción Transversal del Cáncer-RTICC, Spain. C.L.-O. is an Investigator of the Botin Foundation.

References

1. Wallace DC, Fan W, Procaccio V. Mitochondrial energetics and therapeutics. Annu Rev Pathol 2010; 5: 297-348; PMID:20078222; http://dx.doi.org/10.1146/annurev.pathol.4.110807.092314
2. Anand R, Langer T, Baker MJ. Proteolytic control of mitochondrial function and morphogenesis. Biochim Biophys Acta 2012; In press; PMID:22749882; http://dx.doi.org/10.1016/j.bbamcr.2012.06.025
3. Baker MJ, Tatsuta T, Langer T. Quality control of mitochondrial proteostasis. Cold Spring Harb Perspect Biol 2011; 3:a007559; PMID:21628427; http://dx.doi.org/10.1101/cshperspect.a007559
4. Westermann B. Mitochondrial fusion and fission in cell life and death. Nat Rev Mol Cell Biol 2010; 11:872-84; PMID:21102612; http://dx.doi.org/10.1038/nrm3013
5. Youle RJ, Narendra DP. Mechanisms of mitophagy. Nat Rev Mol Cell Biol 2011; 12:9-14; PMID:21179058; http://dx.doi.org/10.1038/nrm3028
6. Suen DF, Norris KL, Youle RJ. Mitochondrial dynamics and apoptosis. Genes Dev 2008; 22:1577-90; PMID:18559474; http://dx.doi.org/10.1101/gad.1658508
7. Chen H, Chan DC. Physiological functions of mitochondrial fusion. Ann N Y Acad Sci 2010; 1201: 21-5; PMID:20649534; http://dx.doi.org/10.1111/j.1749-6632.2010.05615.x
8. Hoppins S, Nunnari J. The molecular mechanism of mitochondrial fusion. Biochim Biophys Acta 2009; 1793:20-6; PMID:18691613; http://dx.doi.org/10.1016/j.bbamcr.2008.07.005
9. Otera H, Wang C, Cleland MM, Setoguchi K, Yokota S, Youle RJ, et al. Mff is an essential factor for mitochondrial recruitment of Drp1 during mitochondrial fission in mammalian cells. J Cell Biol 2010; 191: 1141-58; PMID:21149567; http://dx.doi.org/10.1083/jcb.201007152
10. Chang CR, Blackstone C. Dynamic regulation of mitochondrial fission through modification of the dynamin-related protein Drp1. Ann N Y Acad Sci 2010; 1201:34-9; PMID:20649536; http://dx.doi.org/10.1111/j.1749-6632.2010.05629.x
11. Song Z, Chen H, Fiket M, Alexander C, Chan DC. OPA1 processing controls mitochondrial fusion and is regulated by mRNA splicing, membrane potential, and Yme1L. J Cell Biol 2007; 178:749-55; PMID:17709429; http://dx.doi.org/10.1083/jcb.200704110
12. Gomes LC, Di Benedetto G, Scorrano L. During autophagy mitochondria elongate, are spared from degradation and sustain cell viability. Nat Cell Biol 2011; 13:589-98; PMID:21478857; http://dx.doi.org/10.1038/ncb2220
13. Rugarli EI, Langer T. Mitochondrial quality control: a matter of life and death for neurons. EMBO J 2012; 31:1336-49; PMID:22354038; http://dx.doi.org/10.1038/emboj.2012.38
14. Züchner S, Mersiyanova IV, Muglia M, Bissar-Tadmouri N, Rochelle J, Dadali EL, et al. Mutations in the mitochondrial GTPase mitofusin 2 cause Charcot-Marie-Tooth neuropathy type 2A. Nat Genet 2004; 36:449-51; PMID:15064763; http://dx.doi.org/10.1038/ng1341
15. Delettre C, Lenaers G, Griffoin JM, Gigarel N, Lorenzo C, Belenguer P, et al. Nuclear gene OPA1, encoding a mitochondrial dynamin-related protein, is mutated in dominant optic atrophy. Nat Genet 2000; 26:207-10; PMID:11017079; http://dx.doi.org/10.1038/79936
16. Waterham HR, Koster J, van Roermund CW, Mooyer PA, Wanders RJ, Leonard JV. A lethal defect of mitochondrial and peroxisomal fission. N Engl J Med 2007; 356:1736-41; PMID:17460227; http://dx.doi.org/10.1056/NEJMoa064436
17. Alexander C, Votruba M, Pesch UE, Thiselton DL, Mayer S, Moore A, et al. OPA1, encoding a dynamin-related GTPase, is mutated in autosomal dominant optic atrophy linked to chromosome 3q28. Nat Genet 2000; 26:211-5; PMID:11017080; http://dx.doi.org/10.1038/79944
18. Verny C, Loiseau D, Scherer C, Lejeune P, Chevrollier A, Gueguen N, et al. Multiple sclerosis-like disorder in OPA1-related autosomal dominant optic atrophy. Neurology 2008; 70:1152-3; PMID:18287570; http://dx.doi.org/10.1212/01.wnl.0000289194.89359.a1
19. Yu-Wai-Man P, Griffiths PG, Gorman GS, Lourenco CM, Wright AF, Auer-Grumbach M, et al. Multi-system neurological disease is common in patients with OPA1 mutations. Brain 2010; 133:771-86; PMID:20157015; http://dx.doi.org/10.1093/brain/awq007
20. Aung T, Ocaka L, Ebenezer ND, Morris AG, Krawczak M, Thiselton DL, et al. A major marker for normal tension glaucoma: association with polymorphisms in the OPA1 gene. Hum Genet 2002; 110:52-6; PMID:11810296; http://dx.doi.org/10.1007/s00439-001-0645-7
21. Yu-Wai-Man P, Stewart JD, Hudson G, Andrews RM, Griffiths PG, Birch MK, et al. OPA1 increases the risk of normal but not high tension glaucoma. J Med Genet 2010; 47:120-5; PMID:19581274; http://dx.doi.org/10.1136/jmg.2009.067512
22. Casari G, De Fusco M, Ciarmatori S, Zeviani M, Mora M, Fernandez P, et al. Spastic paraplegia and OXPHOS impairment caused by mutations in paraplegin, a nuclear-encoded mitochondrial metalloprotease. Cell 1998; 93:973-83; PMID:9635427; http://dx.doi.org/10.1016/S0092-8674(00)81203-9
23. Di Bella D, Lazzaro F, Brusco A, Plumari M, Battaglia G, Pastore A, et al. Mutations in the mitochondrial protease gene AFG3L2 cause dominant hereditary ataxia SCA28. Nat Genet 2010; 42:313-21; PMID:20208537; http://dx.doi.org/10.1038/ng.544
24. Quirós PM, Ramsay AJ, Sala D, Fernández-Vizarra E, Rodríguez F, Peinado JR, et al. Loss of mitochondrial protease OMA1 alters processing of the GTPase OPA1 and causes obesity and defective thermogenesis in mice. EMBO J 2012; 31:2117-33; PMID:22433842; http://dx.doi.org/10.1038/emboj.2012.70
25. Kaser M, Kambacheld M, Kisters-Woike B, Langer T. Oma1, a novel membrane-bound metallopeptidase in mitochondria with activities overlapping with the m-AAA protease. J Biol Chem 2003; 278:46414-23; PMID:12963738; http://dx.doi.org/10.1074/jbc.M305584200
26. Rugarli EI, Langer T. Translating m-AAA protease function in mitochondria to hereditary spastic paraplegia. Trends Mol Med 2006; 12:262-9; PMID:16647881; http://dx.doi.org/10.1016/j.molmed.2006.04.002
27. Ehses S, Raschke I, Mancuso G, Bernacchia A, Geimer S, Tondera D, et al. Regulation of OPA1 processing and mitochondrial fusion by m-AAA protease isoenzymes and OMA1. J Cell Biol 2009; 187:1023-36; PMID:20038678; http://dx.doi.org/10.1083/jcb.200906084
28. Head B, Griparic L, Amiri M, Gandre-Babbe S, van der Bliek AM. Inducible proteolytic inactivation of OPA1 mediated by the OMA1 protease in mammalian cells. J Cell Biol 2009; 187:959-66; PMID:20038677; http://dx.doi.org/10.1083/jcb.200906083
29. Feldmann HM, Golozoubova V, Cannon B, Nedergaard J. UCP1 ablation induces obesity and abolishes diet-induced thermogenesis in mice exempt from thermal stress by living at thermoneutrality. Cell Metab 2009; 9:203-9; PMID:19187776; http://dx.doi.org/10.1016/j.cmet.2008.12.014
30. Lowell BB, S-Susulic V, Hamann A, Lawitts JA, Himms-Hagen J, Boyer BB, et al. Development of obesity in transgenic mice after genetic ablation of brown adipose tissue. Nature 1993; 366:740-2; PMID:8264795; http://dx.doi.org/10.1038/366740a0
31. Luvisetto S, Basso E, Petronilli V, Bernardi P, Forte M. Enhancement of anxiety, facilitation of avoidance behavior, and occurrence of adult-onset obesity in mice lacking mitochondrial cyclophilin D. Neuroscience 2008; 155:585-96; PMID:18621101; http://dx.doi.org/10.1016/j.neuroscience.2008.06.030
32. Whittle AJ, López M, Vidal-Puig A. Using brown adipose tissue to treat obesity - the central issue. Trends Mol Med 2011; 17:405-11; PMID:21602104; http://dx.doi.org/10.1016/j.molmed.2011.04.001
33. Kajimura S, Seale P, Spiegelman BM. Transcriptional control of brown fat development. Cell Metab 2010; 11:257-62; PMID:20374957; http://dx.doi.org/10.1016/j.cmet.2010.03.005

34. Zhang W, Chen Y, Yang Q, Che H, Chen X, Yao T, et al. Mitofusin-2 protects against cold stress-induced cell injury in HEK293 cells. Biochem Biophys Res Commun 2010; 397:270-6; PMID:20580691; http://dx.doi.org/10.1016/j.bbrc.2010.05.099
35. Griparic L, Kanazawa T, van der Bliek AM. Regulation of the mitochondrial dynamin-like protein Opa1 by proteolytic cleavage. J Cell Biol 2007; 178:757-64; PMID:17709430; http://dx.doi.org/10.1083/jcb.200704112
36. Duvezin-Caubet S, Jagasia R, Wagener J, Hofmann S, Trifunovic A, Hansson A, et al. Proteolytic processing of OPA1 links mitochondrial dysfunction to alterations in mitochondrial morphology. J Biol Chem 2006; 281:37972-9; PMID:17003040; http://dx.doi.org/10.1074/jbc.M606059200
37. Ishihara N, Fujita Y, Oka T, Mihara K. Regulation of mitochondrial morphology through proteolytic cleavage of OPA1. EMBO J 2006; 25:2966-77; PMID:16778770; http://dx.doi.org/10.1038/sj.emboj.7601184
38. Cipolat S, Rudka T, Hartmann D, Costa V, Serneels L, Craessaerts K, et al. Mitochondrial rhomboid PARL regulates cytochrome c release during apoptosis via OPA1-dependent cristae remodeling. Cell 2006; 126:163-75; PMID:16839884; http://dx.doi.org/10.1016/j.cell.2006.06.021
39. Frezza C, Cipolat S, Martins de Brito O, Micaroni M, Beznoussenko GV, Rudka T, et al. OPA1 controls apoptotic cristae remodeling independently from mitochondrial fusion. Cell 2006; 126:177-89; PMID:16839885; http://dx.doi.org/10.1016/j.cell.2006.06.025
40. Zhang Z, Wakabayashi N, Wakabayashi J, Tamura Y, Song WJ, Sereda S, et al. The dynamin-related GTPase Opa1 is required for glucose-stimulated ATP production in pancreatic beta cells. Mol Biol Cell 2011; 22:2235-45; PMID:21551073; http://dx.doi.org/10.1091/mbc.E10-12-0933
41. Pidoux G, Witczak O, Jarnæss E, Myrvold L, Urlaub H, Stokka AJ, et al. Optic atrophy 1 is an A-kinase anchoring protein on lipid droplets that mediates adrenergic control of lipolysis. EMBO J 2011; 30:4371-86; PMID:21983901; http://dx.doi.org/10.1038/emboj.2011.365

III. Characterization of the role of OMA1 in renal failure

Acute kidney injury (AKI) is a major kidney disease that is associated with high mortality and an increased incidence of chronic kidney disease. AKI can be caused by a renal ischemia/reperfusion, due to different physiological and pathological conditions. Recent evidences have demonstrated that the renal damage is centered on mitochondria, which remarkably contributes to renal tubular cell injury and death in AKI. In addition, the ATP-depletion observed in tubular cells resulting in mitochondrial fragmentation and apoptosis. Accordingly, to better understand the molecular mechanisms of cell injury caused by mitochondrial fragmentation and the subsequent apoptosis, we employed the mice deficient in OMA1 to explore the possible key role of this protease in renal disease regulating mitochondrial dynamics.

Article 3: Xiao Xiao, **Pedro M. Quirós**, Qingqing Wei1, Carlos López-Otín, and Zheng Dong. "OMA1 mediates OPA1 proteolysis and mitochondrial fragmentation in experimental models of ischemic kidney injury".

(American Journal of Physiology - Renal Physiology, accepted pending revision)

Personal contribution to this work

In this work, I was the responsible for the management and genotyping of the mice colony used for the experimental work aimed at evaluating the functional role of Oma1 in acute kidney injury. Likewise, I contributed to the discussion of the experiments performed in the Dr. Zheng Dong laboratory and participated in the writing of the manuscript.

OMA1 mediates OPA1 proteolysis and mitochondrial fragmentation in experimental models of ischemic kidney injury

Xiao Xiao[1,2], Pedro M. Quirós [3], Qingqing Wei[1], Carlos López-Otín[3], Zheng Dong[1,3,4]

[1] Department of Cellular Biology and Anatomy, Medical College of Georgia at Georgia Reagents University and Charlie Norwood VA Medical Center, Augusta, GA 30912; [2] Wuhan University, Wuhan, China; [3] Departamento de Bioquímica y Biología Molecular, Facultad de Medicina, Instituto Universitario de Oncología, Universidad de Oviedo, Oviedo, Spain; [4] Department of Nephrology, The Second Xiangya Hospital, Central South University, Changsha, China

Correspondence should be sent to:

Zheng Dong, PhD

Department of Nephrology, The Second Xiangya Hospital, Central South University, Changsha, China; Department of Cellular Biology and Anatomy, Medical College of Georgia at Georgia Reagents University and Charlie Norwood VA Medical Center, Augusta, GA 30912, USA

Phone: 706-721-2825

Email: zdong@gru.edu

Abstract

Acute kidney injury (AKI) is associated with mitochondrial fragmentation, which contributes to mitochondrial damage and tubular cell apoptosis. Mitochondrial fragmentation involves the cleavage of both mitochondrial outer and inner membranes. Cleavage of the outer membrane results from Drp-1-mediated fission activation and Bak-promoted fusion arrest, but the molecular mechanism of inner membrane cleavage remains elusive. OMA1-mediated proteolysis of OPA1, a key inner membrane fusion protein, was recently suggested to account for inner membrane cleavage during cell stress. In this study, we have determined the role of OMA1 in OPA1 proteolysis and mitochondrial fragmentation in experimental models of ischemic AKI. In ATP-depletion injury, knockdown of OMA1 suppressed OPA1 proteolysis, mitochondrial fragmentation, cytochrome c release and consequent apoptosis in renal proximal tubular cells. In mice, OMA1-deficiency prevented ischemic AKI as indicated by better renal function, less tubular damage, and lower apoptosis. OPA1 proteolysis and mitochondrial injury during ischemic AKI were ameliorated in OMA1-deficient mice. Thus OMA1-mediated OPA1 proteolysis plays an important role in the disruption of mitochondrial dynamics in ischemic AKI.

Keywords: acute kidney injury; ischemia/reperfusion, mitochondria, apoptosis

OMA1 in ischemic AKI

Introduction

Acute kidney injury (AKI) is a major kidney disease that is associated with high mortality and an increased incidence of chronic kidney disease (CKD) (10, 12, 13, 33). One of the main causes of AKI in clinical settings is renal ischemia/reperfusion, which occurs during kidney transplantation, vascular occlusion in major surgeries, renal vascular obstruction, and hypoperfusion of kidneys due to dehydration, hypotension and decreased cardiac output (2, 29). Due to decreased blood flow in kidneys, ischemia leads to the deprivation of oxygen and nutrients in tissues, resulting in ATP depletion and related injury in kidney cells. Restoration of blood-flow following ischemia further induces reperfusion injury.

Despite decades of study, the cellular and molecular mechanism of AKI induced by renal ischemia/reperfusion remains elusive (2, 29). The research in recent years has demonstrated that the cell death pathway centered on mitochondrial damage contributes remarkably to renal tubular cell injury and death in AKI (11, 19, 27). Especially, it is now known that mitochondria are a class of dynamic organelles that constantly undergo fission and fusion under physiological conditions. During ATP-depletion in vitro and ischemia AKI in vivo, mitochondrial dynamics is shifted to fission, resulting in mitochondrial fragmentation, which, along with pro-death molecules such as Bax and Bak, induces mitochondrial membrane permeabilization and the release of apoptotic factors (eg. cytochrome c) to initiate the cascade of apoptosis (5, 38).

As double-membrane organelles, mitochondria maintain their dynamics at both inner and outer membranes (9, 25, 37). At the outer membrane, fission is mainly controlled by Drp1, while fusion depends on the functional interaction between mitofusin proteins (14, 30, 37). Relatively little is known about the regulation of inner membrane dynamics. Nonetheless, OPA1 is known to be the fusion protein for mitochondrial inner membrane in mammalian cells and the regulation of OPA1 depends on proteolytic processing (1, 31). In 2009, two groups reported separately that OMA1, a zinc metalloprotease located at mitochondrial inner membrane, is responsible for OPA1 proteolysis and inactivation during cell stress (15, 20). The proteolysis of OPA1 by OMA1 leads to the loss of

the long isoforms of OPA1 (L-OPA1), resulting the inactivation of OPA1 and cessation of inner membrane fusion (15, 20, 31). More recently, OMA1 has been implicated in OPA1 proteolysis in vivo in metabolic stress (28). However, it remains unclear if OMA1 mediates OPA1 proteolysis and inactivation and alterations of mitochondrial dynamics in vivo under other pathological conditions such as ischemia/reperfusion. In addition, the regulation of OPA1 and OMA1 has not been examined in renal cells or tissues. Therefore, the current study was designed to investigate the role of OMA1 in OPA1 proteolysis, mitochondrial fragmentation, and tubular cell apoptosis in experimental models of ischemic AKI.

Materials and methods

Cells and OMA1 knockdown: The immortalized rat kidney proximal tubular cell line (RPTC) used in this study was originally from Dr. Ulrich Hopfer's lab (Case Western Reserve University, Cleveland, OH). OMA1-shRNA was purchased from Origene technologies, Inc. (Rockville, MD). To generate OMA1 knockdown stable RPTC cells, OMA1-shRNA was transfected into RPTCs at the confluence of 60% using Lipofectamine LTX (Life technologies, Grand Island, NY). At 24 hours after transfection, cells were subjected to 20 □M of puromycin (Clontech Laboratories, Inc., Mountain View, CA) selection for two weeks. The knockdown effect was confirmed by immunoblot analysis with anti-OMA1 antibody (Abcam, Cambridge, MA). RPTC cells stably transfected with scramble-shRNA were used as control cells.

ATP-depletion of RPTC: RPTCs were treated with 10 mM of sodium azide (Sigma Aldrich, St. Louis, MO) for 2.5 hours in a glucose-free Krebs-Ringer bicarbonate buffer followed by reperfusion with fresh culture medium for 3 hours. Cells were then fixed with 4% paraformaldehyde and stained with Hoechst 33342 (Molecular Probes, Eugene, OR). Apoptotic cells were evaluated morphologically by phase contrast and fluorescence microscopy as described previously (7).

Animals and renal ischemia/reperfusion: The mice used in this study were housed and treated following the protocols approved by the Institutional animal care and user committees of Charlie Norwood VA Medical Center and Medical College of Georgia at Georgia Regent University. C57BL/6 mice were originally purchased from Jackson Laboratory (Bar Harbor, ME). The OMA1 germ-line knockout (OMA1-KO) mouse model was established as previously described (28). OMA1-KO mice were mated with C57BL/6 mice to generate heterozygotes as breeders for the production of WT and KO littermates for experiment. The genotypes of the mice were determined by PCR with the primers: 1. Forward: gagtgctgtttctctgggtgt; 2 Reverse for WT: tgccctaaactgaaggtgtg; 3 Reverse for KO: tagaccgcggctagaggta. The WT allele product was 379bp and the KO allele

product was 252bp. For experiment, male mice of 8 week old (WT and OMA1-KO) were subjected to 25 min of bilateral renal ischemia as detailed in previous studies (34, 36). Mice were sacrificed at indicated time points of reperfusion to collect blood samples and kidney tissues.

Renal function measurement: Blood samples were collected from tail clip or at the time of sacrifice. After clotting at room temperature, serum was collected after centrifugation at 12000g for 5 min. BUN and serum creatinine were measured with analytical kits from Stanbio Laboratory (Boerne, TX).

Histology: Kidneys were collected freshly and fixed with 4% paraformaldehyde at 4°C overnight, followed by dehydration and paraffin embedding. The paraffin embedded tissues were cut into 5-micrometer sections for the Hematoxylin and Eosin (H & E) staining. Tubular damage was scored as follows: 1: 0-25% of damage; 2: 26-50% of damage; 3:51-75% of damage and 4: >75% of damage. The slides were checked in a blind manner and the representative images were taken with a light microscope.

TUNEL staining: Paraffin-embedded kidney tissue sections were rehydrated and permeabilized with 0.1 M of sodium citrate, PH 6.0 for 60 min at 60°C. The slides were then incubated with a TUNEL reaction enzyme mixture from in situ Cell Death Detection kit (Roche Applied Science, Indianapolis, IN) for 40 min at 37°C. The slides were mounted with Prolong Gold Anti-fade Reagent (Life technologies, Grand Island, NY). For quantification, 10-20 fields were randomly selected from each tissue section and the amount of TUNEL positive cells per 1mm^2 was evaluated as before(5, 21, 35).

Analysis of mitochondrial fragmentation: To evaluate mitochondrial fragmentation in cultured cells, the pAcGFP1-Mito (Mito-Green from Clontech Laboratories, Inc., Mountain View, CA) was

transiently transfected into RPTCs. Following treatment, the cells were fixed with 4% paraformaldehyde and mounted with Prolong Gold Anti-fade Reagent (Life technologies, Grand Island, NY). The definition of fragmented mitochondria was described in our previous studies (7). Totally 100-200 cells were examined to determine the percentage of cells with fragmented mitochondria in each group and three separated experiments were conducted for statistical analysis. To analyze mitochondrial fragmentation in vivo, kidney tissues were collected and fixed for electron microscopy to count the tubular cells with fragmented mitochondria as described in our previous study (6).

Analysis of cytochrome c release: To examine cytochrome c release in RPTCs, the cells were lysed with an isotonic sucrose buffer containing 0.05% digitonin (w/v) for 5 min to collect the cytosol and mitochondrial fraction as described previously (30). To analyze cytochrome c release in mouse kidney tissues, fresh mouse kidney cortical tissues were collected to separate the cytosol and mitochondrial fractions as described in our previous study (35). The samples were analyzed by immunoblotting.

Immunoblot analysis: Protein samples were separated on the denatured SDS-PAGE gels and then transferred to PVDF membrane for immunoblot analysis. After blocking in 5% milk, the blots were incubated in primary antibodies and secondary antibodies subsequently. The specific signals were detected by chemiluminescence.

Statistics: Microsoft Excel (14.1.2) was used for all the data analysis. Student t-test with $P<0.05$ was considered as statistically significant difference.

Results

Knockdown of OMA1 suppresses ATP-depletion induced apoptosis in RPTC.

We initially examined the role of OMA1 in apoptosis following ATP-depletion in cultured renal proximal tubular cells (RPTCs). RPTCs were stably transfected with shRNAs to knockdown OMA1. As shown in Fig. 1A and B, OMA1-shRNA transfection induced ~50% decrease of OMA1 expression comparing to the scramble shRNA transfection. Both OMA1 knockdown cells and scrambled sequence transfected cells were treated with sodium azide (a mitochondrial respiration inhibitor) in glucose-free medium to induce ATP depletion, followed by recovery in full culture medium (5). The treatment induced 35% apoptosis in scrambled sequence transfected cells, but only 15% in OMA1 knockdown cells (Fig 1C and D). Consistently, scrambled sequence transfected cells had a significantly higher level of cleaved/active caspase-3 than the OMA1 knockdown cells (Fig 1E: lane 5 vs. 6). These results indicate that the loss of OMA1 alleviates the apoptosis induced by ATP-depletion in RPTCs, supporting a role of OMA1 in tubular cell apoptosis in this model.

Knockdown of OMA1 inhibits OPA1 proteolysis and mitochondrial fragmentation during ATP-depletion.

Cytochrome c release from mitochondria to cytosol is a hallmark of the intrinsic pathway of apoptosis (8). As shown in Fig .2A, cytochrome c was released during azide treatment of RPTCs (lane 3) and this release was inhibited in OMA1 knockdown cells (lane 4). As OMA1 has been implicated in OPA1 cleavage during mitochondrial injury and stress (15, 20, 28), we further examined the spectrum of OPA1 isoforms in those cells. Two long isoforms (L1 and L2) and three short isoforms (S1, S2 and S3) of OPA1 were detected by immunoblot analysis in control cells (Fig 2B: lanes 1, 2). Following azide treatment, the long isoforms of OPA1 disappeared and, concomitantly, there was a marked accumulation of OPA1-S3 short form (Fig. 2B: lane 3), indicative

of OPA1 proteolysis. Notably, the OPA1 proteolysis was suppressed in OMA1 knockdown cells (Fig 2B: lane 4).

OPA1 is the key fusion protein for mitochondrial inner membrane. Excessive proteolysis leads to the inactivation of OPA1 followed by the arrest of inner membrane fusion, contributing to inner membrane cleavage(1). We reasoned that the preservation of OPA1 in OMA1-knockdown cells (Fig. 2B) would prevent mitochondrial fragmentation as a consequence of lack of inner membrane cleavage. To monitor mitochondrial morphology, the cells were transfected with Mito-Green to label mitochondria and then subjected to azide treatment. Representative images of cells with filamentous (right panel) and fragmented (left panel) mitochondria are shown in Fig. 2C. By cell counting, we detected some (less than 25%) cells with fragmented mitochondria under control conditions, which were not affected by OMA1 knockdown. After azide treatment, 52% cells showed fragmented mitochondria, which was suppressed to 37% when OMA1 was knocked down (Fig 2D).

Together, these in vitro experimental results suggest that under ATP-depletion condition, OMA1 may regulate apoptosis by mediating OPA1 proteolysis and inducing mitochondrial fragmentation and pro-apoptotic factors leakage in kidney tubular cells.

OPA1 proteolysis occurs during renal ischemia/reperfusion in mice.

To assess whether OMA1-dependent OPA1 proteolysis plays a pathological role in vivo, we examined a mouse model of renal ischemia/reperfusion. C57BL/6 mice were subjected to 25 minutes of bilateral renal ischemia followed by 48 hours of reperfusion. Fig. 3A and B show that after ischemia/reperfusion the blood urea nitrogen (BUN) and serum creatinine values significantly increased as compared with control. Meanwhile, the kidney injury molecule-1 (Kim-1), a biomarker of kidney proximal tubular injury (32), was markedly induced at 48 hours of reperfusion (Fig. 3C). The loss of renal function was accompanied with OPA1 proteolysis. As shown in Fig. 3D, after ischemia/reperfusion, the long isoforms of OPA1 (L1 and L2) showed obvious decreases, while the shortest OPA1 (S3, arrowed) accumulated (Fig 3D).

OMA1 knockout protects renal function and reduces OPA1 proteolysis in ischemic AKI.

Since OPA1 proteolysis occurs in ischemic AKI in mouse, we determined whether the proteolysis is OMA1 dependent. To this end, we used a recently described OMA1 knockout mouse model (28). The deficiency of OMA1 in this model was verified by genotyping (Fig 4A). OMA1 knockout did not induce noticeable defects in renal function and histology at the age of 8 weeks of our experiments (Fig. 4B and C, Fig. 5A). Male littermates of OMA1-knockout (KO) and wild-type (WT) were subjected to 25 minutes of bilateral renal ischemia. At 24 hours of reperfusion, BUN in WT mice increased to 159 mg/dl, compared with 93 mg/dl in KO mice (Fig 4B). The BUN in WT mice further increased to over 200 mg/dl at 48 hours of reperfusion, while that of KO started to decrease. Consistently, serum creatinine in KO mice (0.52 mg/dl) was significantly lower than that of WT mice (1.35 mg/dl) (Fig. 4C). Immunoblot analysis showed a dramatic induction of Kim-1 in the kidney tissues of WT mice after ischemia/reperfusion, which was marked lower in KO tissues (Fig. 4D). Notably, OPA1 proteolysis during renal ischemia/reperfusion was also ameliorated in KO tissues (Fig. 4E), suggesting a role of OMA1 in mediating OPA1 proteolysis and ischemic AKI.

Tubular damage and apoptosis are attenuated in OMA1-KO mice during renal ischemia/reperfusion.

In histology, renal ischemia/reperfusion induced significant tubular damage in WT mice, as indicated by lysis of tubules and massive cast formation (Fig. 5A: left lower panel). Tubular damage was also detected in OMA1-KO tissues (Fig. 5A: right lower panel). In semi-quantification, WT tissues had a tubular damage score of 2 vs. 1.25 for KO tissues (Fig. 5B). We further evaluated renal apoptosis by TUNEL assay. After renal ischemia/reperfusion, ~50 TUNEL positive cells were detected in each mm^2 of WT kidney tissues, whereas 35 in OMA1-KO tissues (Fig 5C and D). These results indicate that OMA1 deficiency protects kidneys from ischemic injury.

Resistance of OMA1-KO tissues to mitochondrial fragmentation and cytochrome c release in ischemic AKI.

Our results shown above support a role of OMA1 in tubular cell injury and death in ischemic AKI. Mechanistically, OMA1 mediates OPA1 proteolysis under the disease condition. OPA1 is a mitochondria inner membrane fusion protein, which plays an important role in cytochrome c retention in mitochondria (16). Thus, to further understand the involvement of OMA1 in ischemia AKI, we examined mitochondrial morphology and cytochrome c release in the WT and KO kidneys (Fig 6A and B). By electron microscopy, we observed proximal tubular cells in kidneys with filamentous or fragmented mitochondria (Fig 6A). The basal level of tubular cells with fragmented mitochondria was about 10% in both WT and OMA1-KO mice. Renal ischemia induced mitochondrial fragmentation in 26.1% of tubular cells in WT mice, but only 18.2% in KO mice (Fig 6B), supporting a role of OMA1 in mitochondrial fragmentation. We further examined cytochrome c release in WT and OMA1-KO mouse kidneys. No cytochrome c release from mitochondria was detected in sham-operated kidneys (Fig. 6C: lanes 1, 2). After 25 minutes of ischemia and 16 hours of reperfusion, there was significant release of cytochrome c in WT mouse kidneys (lane 3), which was partially suppressed in OMA1-KO mouse kidneys (lane 4).

Discussion

Tubular cell apoptosis contributes significantly to the pathogenesis of AKI (19, 27). Especially, the intrinsic pathway of apoptosis plays an important role in tubular apoptosis under this disease condition. The intrinsic pathway is characterized by Bax/Bak-mediated mitochondrial membrane permeabilization and the release of apoptogenic factors, such as cytochrome c. Our recent work demonstrated that Bax or Bak-deficient mice are protected from AKI following renal ischemia/reperfusion (35). Interestingly, prior to mitochondrial membrane permeabilization, mitochondria become fragmented during tubular cell apoptosis, and inhibition of mitochondrial fragmentation prevents mitochondrial damage and reduces apoptosis and kidney injury, supporting a pathogenic role of mitochondrial fragmentation (5). We and others further showed that fragmented mitochondria are sensitized to Bax "attack" of mitochondria (3, 17), providing an explanation as to how mitochondrial fragmentation participates in apoptosis. Of note, all these studies focused on the molecular events at mitochondrial outer membrane.

In the present study, we have examined the role of OMA1 in the proteolysis of OPA1, a key mitochondrial inner membrane fusion protein. We firstly used an ATP-depletion model to demonstrate the involvement of OMA1 in OPA1 proteolysis and mitochondria fragmentation during renal tubular cell apoptosis. Further in vivo study confirmed the role of OMA1 in a mouse model of renal ischemia/reperfusion. Compared with wild-type mice, OMA1-KO mice exhibited better kidney function, less tubular damage and apoptosis in response to ischemic challenge. These effects were associated with the preservation of OPA1, suppression of mitochondrial fragmentation, and decrease of cytochrome c release and apoptosis in OMA1-KO tissues. Collectively, these in vitro and in vivo observations suggest that OMA1 mediates OPA1 proteolysis, contributing to mitochondrial fragmentation and consequent mitochondrial damage and cell death in pathological conditions.

As highly dynamic organelles, mitochondria frequently undergo fission and fusion in normal physiological conditions and the dynamics is important to the homeostasis, function and viability of

mitochondria and the cell (9, 25, 37). Mitochondrial fission depends on the activation of fission proteins such as Drp1, while fusion is controlled by mitofusin proteins at the outer membrane and OPA1 at the inner membrane. In response to cell stress, mitochondrial fission is activated and fusion arrested, resulting in fragmentation of the organelles. Inhibition of mitochondrial fragmentation by blocking Drp1 or expressing mitofusins prevents mitochondrial damage and apoptosis, supporting a critical role of mitochondrial fragmentation in cell injury and death under pathological conditions. Notably, blockade of mitochondrial fragmentation leads to the prevention of apoptosis and tissue damage in disease models (5, 18, 24, 26), further supporting a pathogenic role of mitochondrial fragmentation.

Mitochondria are double membrane bound and, as a result, mitochondrial fragmentation during cell stress involves the cleavage of both the outer and inner membranes. The cleavage of the outer membrane is a combined result of fission activation and fusion arrest. During cell stress, Drp1 is activated by mechanisms including dephosphorylation to induce outer membrane fission. Meanwhile, mitofusins are inactivated by interacting with regulatory proteins such as Bak (4, 7). In contrast, relatively little is known about inner membrane cleavage. In mammalian cells, OPA1 is the key fusion protein at mitochondrial inner membrane. The current understanding is that the cleavage of mitochondrial inner membrane depends on the inactivation of OPA1 (22).

OPA1 exists in cells in multiple forms due to alternative splicing and proteolytic processing (1, 31). In immunoblot analysis, two long and three short OPA1 isoforms can be distinguished. Interestingly, the fusion activity of OPA1 depends on the presence of both long and short OPA1 isoforms. During cell stress, OPA1 is excessively proteolyzed, leading to the loss of the long isoforms and ensuing inactivation of OPA1. Several proteases have been implicated in the cleavage of OPA1. However, in 2009 two separate studies identified OMA1 as the key protease responsible for the excessive OPA1 proteolysis during cell stress (15, 20). In mouse, OMA1 was shown to mediate OPA1 proteolysis during metabolic stress induced by high fat diet (28). Our current results demonstrate OPA1 proteolysis in experimental models of renal ischemia/reperfusion.

Importantly, this study further supports a critical role of OMA1 in OPA1 proteolysis under pathological conditions.

OMA1 is a zinc metalloprotease located in the mitochondrial inner membrane. Despite the implication of OMA1 in OPA1 proteolysis, it remains elusive as to how OMA1 is activated for OPA1 proteolysis during cell stress. In this regard, OMA1 has been proposed to be normally sequestered by prohibitin complexes and, upon cell stress, OMA1 is released (23). This scenario, while being attractive, remains to be investigated. For example, it is unclear whether OMA1 is indeed sequestered in prohibitin complexes and whether these complexes are disrupted to release OMA1 during cell stress. In addition, the factors governing the integrity of prohibitin complexes are completely unknown. Addressing these questions would gain significant new insights into the molecular regulation of mitochondrial inner membrane dynamics under patho-physiological conditions.

Acknowledgements: The study was supported in part by grants from National Natural Science Foundation of China [81370791], National Basic Research Program of China 973 Program No. 2012CB517600, and the National Institutes of Health and Department of Veterans Administration of USA.

References

1. **Belenguer P, and Pellegrini L**. The dynamin GTPase OPA1: more than mitochondria? *Biochim Biophys Acta* 1833: 176-183, 2013.
2. **Bonventre JV, and Yang L**. Cellular pathophysiology of ischemic acute kidney injury. *J Clin Invest* 121: 4210-4221, 2011.
3. **Brooks C, Cho SG, Wang CY, Yang T, and Dong Z**. Fragmented mitochondria are sensitized to Bax insertion and activation during apoptosis. *Am J Physiol Cell Physiol* 300: C447-455, 2011.

4. **Brooks C, and Dong Z**. Regulation of mitochondrial morphological dynamics during apoptosis by Bcl-2 family proteins: a key in Bak? *Cell Cycle* 6: 3043-3047, 2007.
5. **Brooks C, Wei Q, Cho S, and Dong Z**. Regulation of mitochondrial dynamics in acute kidney injury in cell culture and rodent models. *Journal of Clinical Investigation* 119: 1275-1285, 2009.
6. **Brooks C, Wei Q, Cho SG, and Dong Z**. Regulation of mitochondrial dynamics in acute kidney injury in cell culture and rodent models. *The Journal of clinical investigation* 119: 1275-1285, 2009.
7. **Brooks C, Wei Q, Feng L, Dong G, Tao Y, Mei L, Xie ZJ, and Dong Z**. Bak regulates mitochondrial morphology and pathology during apoptosis by interacting with mitofusins. *Proc Natl Acad Sci U S A* 104: 11649-11654, 2007.
8. **Budihardjo I, Oliver H, Lutter M, Luo X, and Wang X**. Biochemical pathways of caspase activation during apoptosis. *Annu Rev Cell Dev Biol* 15: 269-290, 1999.
9. **Chan DC**. Fusion and fission: interlinked processes critical for mitochondrial health. *Annu Rev Genet* 46: 265-287, 2012.
10. **Chawla LS, and Kimmel PL**. Acute kidney injury and chronic kidney disease: an integrated clinical syndrome. *Kidney Int* 82: 516-524, 2012.
11. **Che R, Yuan Y, Huang S, and Zhang A**. Mitochondrial dysfunction in the pathophysiology of renal diseases. *Am J Physiol Renal Physiol* 2013.
12. **Chertow GM, Burdick E, Honour M, Bonventre JV, and Bates DW**. Acute kidney injury, mortality, length of stay, and costs in hospitalized patients. *J Am Soc Nephrol* 16: 3365-3370, 2005.
13. **Chertow GM, Levy EM, Hammermeister KE, Grover F, and Daley J**. Independent association between acute renal failure and mortality following cardiac surgery. *The American journal of medicine* 104: 343-348, 1998.
14. **Detmer SA, and Chan DC**. Complementation between mouse Mfn1 and Mfn2 protects mitochondrial fusion defects caused by CMT2A disease mutations. *J Cell Biol* 176: 405-414, 2007.
15. **Ehses S, Raschke I, Mancuso G, Bernacchia A, Geimer S, Tondera D, Martinou JC, Westermann B, Rugarli EI, and Langer T**. Regulation of OPA1 processing and mitochondrial fusion by m-AAA protease isoenzymes and OMA1. *J Cell Biol* 187: 1023-1036, 2009.
16. **Frezza C, Cipolat S, Martins de Brito O, Micaroni M, Beznoussenko GV, Rudka T, Bartoli D, Polishuck RS, Danial NN, De Strooper B, and Scorrano L**. OPA1 controls apoptotic cristae remodeling independently from mitochondrial fusion. *Cell* 126: 177-189, 2006.
17. **Gall JM, Wang Z, Liesa M, Molina A, Havasi A, Schwartz JH, Shirihai O, Borkan SC, and Bonegio RG**. Role of mitofusin 2 in the renal stress response. *PLoS One* 7: e31074, 2012.
18. **Guo X, Disatnik MH, Monbureau M, Shamloo M, Mochly-Rosen D, and Qi X**. Inhibition of mitochondrial fragmentation diminishes Huntington's disease-associated neurodegeneration. *J Clin Invest* 123: 5371-5388, 2013.
19. **Havasi A, and Borkan SC**. Apoptosis and acute kidney injury. *Kidney Int* 80: 29-40, 2011.
20. **Head B, Griparic L, Amiri M, Gandre-Babbe S, and van der Bliek AM**. Inducible proteolytic inactivation of OPA1 mediated by the OMA1 protease in mammalian cells. *J Cell Biol* 187: 959-966, 2009.
21. **Jiang M, Wei Q, Dong G, Komatsu M, Su Y, and Dong Z**. Autophagy in proximal tubules protects against acute kidney injury. *Kidney Int* 82: 1271-1283, 2012.
22. **Landes T, Leroy I, Bertholet A, Diot A, Khosrobakhsh F, Daloyau M, Davezac N, Miquel MC, Courilleau D, Guillou E, Olichon A, Lenaers G, Arnaune-Pelloquin L, Emorine LJ, and Belenguer P**. OPA1 (dys)functions. *Seminars in cell & developmental biology* 21: 593-598, 2010.
23. **McBride H, and Soubannier V**. Mitochondrial function: OMA1 and OPA1, the grandmasters of mitochondrial health. *Curr Biol* 20: R274-276, 2010.
24. **Molina AJ, Wikstrom JD, Stiles L, Las G, Mohamed H, Elorza A, Walzer G, Twig G, Katz S, Corkey BE, and Shirihai OS**. Mitochondrial networking protects beta-cells from nutrient-induced apoptosis. *Diabetes* 58: 2303-2315, 2009.

25. **Nunnari J, and Suomalainen A**. Mitochondria: in sickness and in health. *Cell* 148: 1145-1159, 2012.
26. **Ong SB, Subrayan S, Lim SY, Yellon DM, Davidson SM, and Hausenloy DJ**. Inhibiting mitochondrial fission protects the heart against ischemia/reperfusion injury. *Circulation* 121: 2012-2022, 2010.
27. **Pabla N, and Dong Z**. Cisplatin nephrotoxicity: Mechanisms and renoprotective strategies. *Kidney Int* 73: 994-1007, 2008.
28. **Quiros PM, Ramsay AJ, Sala D, Fernandez-Vizarra E, Rodriguez F, Peinado JR, Fernandez-Garcia MS, Vega JA, Enriquez JA, Zorzano A, and Lopez-Otin C**. Loss of mitochondrial protease OMA1 alters processing of the GTPase OPA1 and causes obesity and defective thermogenesis in mice. *Embo J* 31: 2117-2133, 2012.
29. **Sharfuddin AA, and Molitoris BA**. Pathophysiology of ischemic acute kidney injury. *Nature reviews Nephrology* 7: 189-200, 2011.
30. **Smirnova E, Griparic L, Shurland DL, and van der Bliek AM**. Dynamin-related protein Drp1 is required for mitochondrial division in mammalian cells. *Mol Biol Cell* 12: 2245-2256, 2001.
31. **Song Z, Chen H, Fiket M, Alexander C, and Chan DC**. OPA1 processing controls mitochondrial fusion and is regulated by mRNA splicing, membrane potential, and Yme1L. *J Cell Biol* 178: 749-755, 2007.
32. **Vaidya VS, Ferguson MA, and Bonventre JV**. Biomarkers of Acute Kidney Injury. *Annu Rev Pharmacol Toxicol* 2007.
33. **Venkatachalam MA, Griffin KA, Lan R, Geng H, Saikumar P, and Bidani AK**. Acute kidney injury: a springboard for progression in chronic kidney disease. *American journal of physiology Renal physiology* 298: F1078-1094, 2010.
34. **Wei Q, Dong G, Chen JK, Ramesh G, and Dong Z**. Bax and Bak have critical roles in ischemic acute kidney injury in global and proximal tubule-specific knockout mouse models. *Kidney international* 84: 138-148, 2013.
35. **Wei Q, Dong G, Huang S, Ramesh G, and Dong Z**. Global deletion of Bak and specific deletion of Bax from proximal tubules protect against ischemic acute kidney injury in mice. *Kidney Int* 84: 138-148, 2013.
36. **Wei Q, and Dong Z**. Mouse model of ischemic acute kidney injury: technical notes and tricks. *American journal of physiology Renal physiology* 303: F1487-1494, 2012.
37. **Youle RJ, and van der Bliek AM**. Mitochondrial fission, fusion, and stress. *Science* 337: 1062-1065, 2012.
38. **Zhan M, Brooks C, Liu F, Sun L, and Dong Z**. Mitochondrial dynamics: regulatory mechanisms and emerging role in renal pathophysiology. *Kidney Int* 83: 568-581, 2013.

Figure Legends

Fig. 1 OMA1 knockdown suppresses ATP-depletion induced apoptosis in RPTCs. RPTCs were transfected with OMA1-shRNA or scrambled sequence shRNA plasmids to generate stable cell lines. The cells were then left untreated (Control) or treated with 10mM sodium azide sodium azide in glucose-free buffer for 2.5 hours to induce ATP depletion (A), followed by 3 hours of recovery in fresh culture medium (A/R). (**A**) Representative immunoblots showing OMA1 knockdown in OMA1-shRNA transfected cells; □-actin was probed as internal protein control. (**B**) Densitometry quantification of immunoblots confirming OMA1 knockdown in OMA1-shRNA transfected cells (n=3). *, P<0.05. (**C**) Representative images of cell morphology (upper panel) and nuclear morphology after Hoechst staining (lower panel). (**D**) Percentage of apoptosis evaluated by counting the cells with typical apoptotic morphology (n=3). *, P<0.05 vs. Control; #, P<0.05 vs. treated OMA1-shRNA cells. (**E**) Immunoblot of cleaved, active caspase 3.

Fig. 2 OMA1 knockdown inhibits ATP-depletion induced OPA1 proteolysis, mitochondrial fragmentation and cytochrome c release. OMA1 shRNA- or scrambled sequence- transfected RPTCs were left untreated (Control) or treated with 10 mM sodium azide to induce ATP-depletion. (**A**) Immunoblots of cytochrome c. Cells were fractionated into mitochondria-enriched membrane fraction and cytosolic fraction for immunoblot analysis. (**B**) Immunoblot of OPA1 in whole cell lysate. The long (L1, L2) and short (S1, S2, S3) OPA1 isoforms are indicated. □-actin was used as loading control. (**C**) Representative images of RPTCs with fragmented or filamentous mitochondria. (**D**) Quantification of percentage of cells with fragmented mitochondria (n=3). *, P<0.05 vs. Control groups; #, <0.05 vs. treated OMA1-shRNA group.

Fig. 3 OPA1 proteolysis occurs during renal ischemia/reperfusion in mice. C57BL/6 mice was subjected to 25 minutes of bilateral renal ischemia followed by 48 hours of reperfusion. (**A**) BUN increase (n=4). *, P<0.05 vs. Control; #, P<0.05 vs. 24 hours' BUN value. (**B**) Serum creatinine values at 48 hours of reperfusion (n=4). *, P<0.05 vs. Control group. (**C**) Immunoblot of Kim-1. (**D**) Immunoblot of OPA1 showing OPA1 proteolysis during renal ischemia/reperfusion. Arrows: the shortest OPA1 isoform (S3).

Fig. 4 OMA1 knockout protects renal function and reduces OPA1 proteolysis in ischemic AKI. Male littermates of wild-type (WT) and OMA1-knockout (KO) mice were subjected 25 minutes of bilateral renal ischemia and 48 hours of reperfusion. (**A**) PCR-based genotyping results to confirm OMA1 deletion in KO mice. Wild-type allele, 379bp; OMA-knockout allele, 252bp. (**B**) BUN values of WT and KO mice during renal ischemia/reperfusion (n=5 pairs). *, P<0.05 vs. control group; #, P<0.05 vs. KO mouse values. (**C**) Serum creatinine value at 48 hours of reperfusion (n=5 pairs). *, P<0.05 vs. control group. #, P<0.05 vs. treated KO mouse values. (**D**) Immunoblots of Kim-1. (**E**) Immunoblot of OPA1 showing the changes of various OPA1 isoforms during renal ischemia/reperfusion in the WT and KO mice. □acting was probed as loading control.

Fig. 5 Tubular damage and apoptosis are attenuated in OMA1-KO mice during renal ischemia/reperfusion. Kidney tissues with or without 25 minutes of ischemia and 48 hours of reperfusion were fixed and processed for paraffin embedding, followed by H & E or TUNEL staining. (**A**) Representative images of H & E staining. (**B**) kidney tubular damage score from H & E staining for WT and KO mice with ischemic AKI (n=5). *, P<0.05 vs. the KO group. (**C**) Representative images of TUNEL staining. (**D**) Quantification of apoptotic cells from TUNEL images (n=5). *, P<0.05 vs. the KO group.

Fig. 6 Resistance of OMA1-KO tissues to mitochondrial fragmentation and cytochrome c release in ischemic AKI. (**A, B**) Male littermates of wild-type (WT) and OMA1-knockout (KO) mice were subjected 25 minutes of bilateral renal ischemia and a brief period (~15 minutes) of reperfusion. Kidney tissues were fixed and processed for electron microscopy to record representative images (**A**) and quantify the cells with fragmented mitochondria in collected images (**B**). (**C**) The mice were subjected 25 minutes of bilateral renal ischemia and 16 hours of reperfusion. Kidney tissues were collected to exact mitochondrial and cytosol fractions for immunoblot analysis of cytochrome c.

Fig. 1 OMA1 knockdown suppresses ATP-depletion induced apoptosis

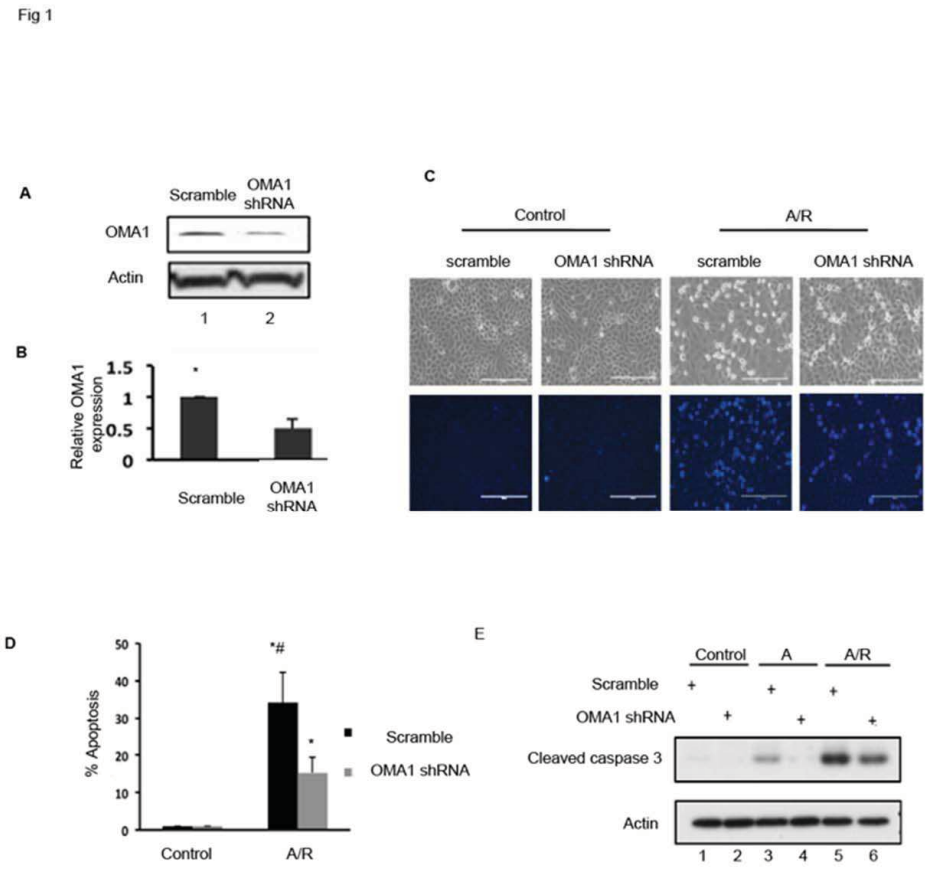

Fig. 2 OMA1 knockdown inhibits ATP-depletion induced OPA1 proteolysis, mitochondrial fragmentation and cytochrome c release

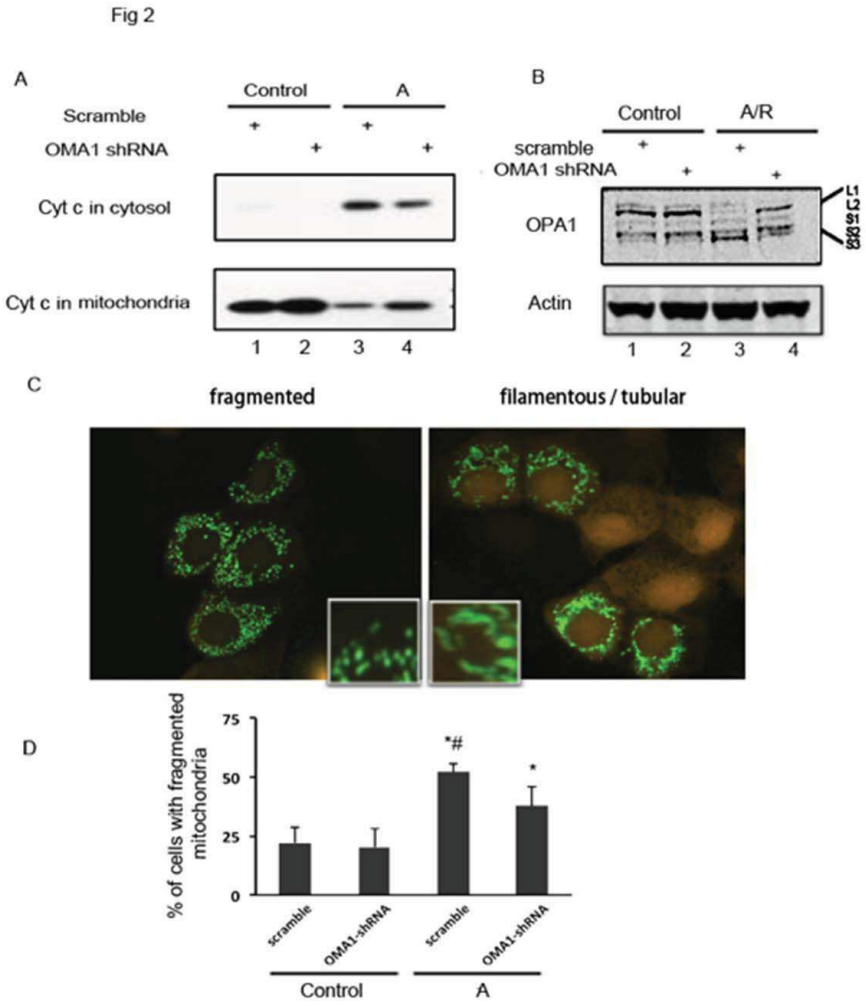

Fig. 3 OPA1 proteolysis occurs during renal ischemia/reperfusion in mice

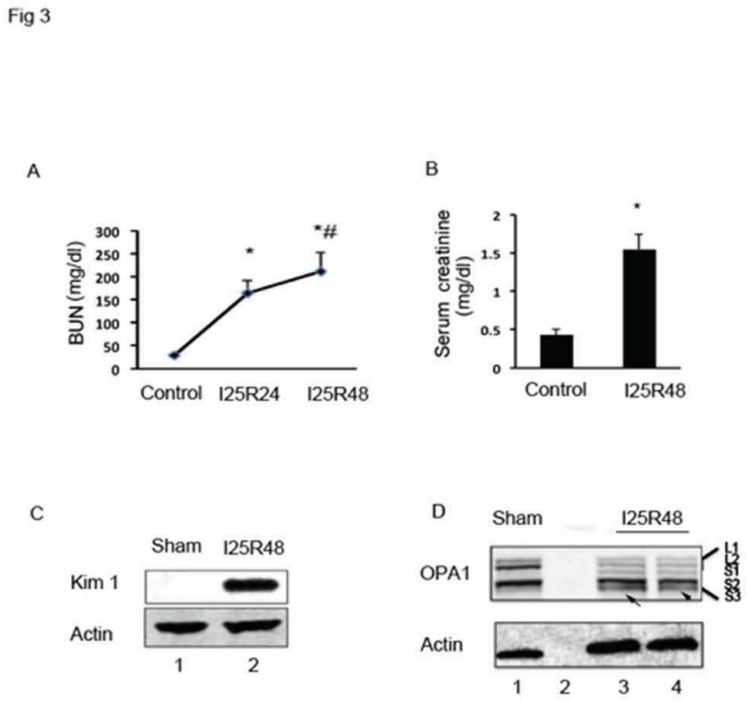

Fig. 4 OMA1 knockout protects renal function and reduces OPA1 proteolysis in ischemic AKI

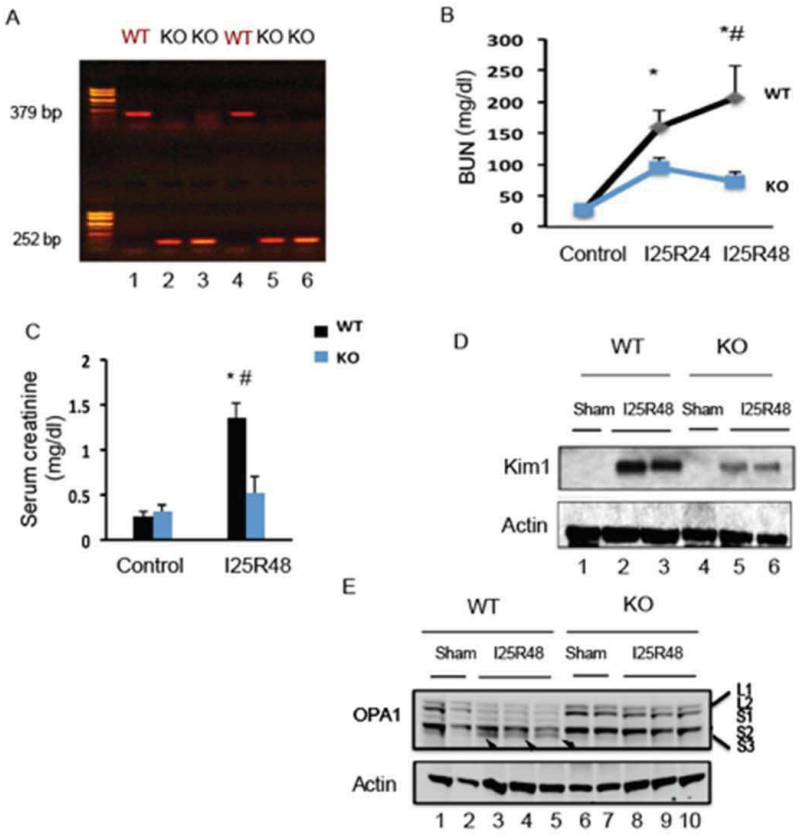

Fig. 5 Tubular damage and apoptosis are attenuated in OMA1-KO mice during renal ischemia/reperfusion

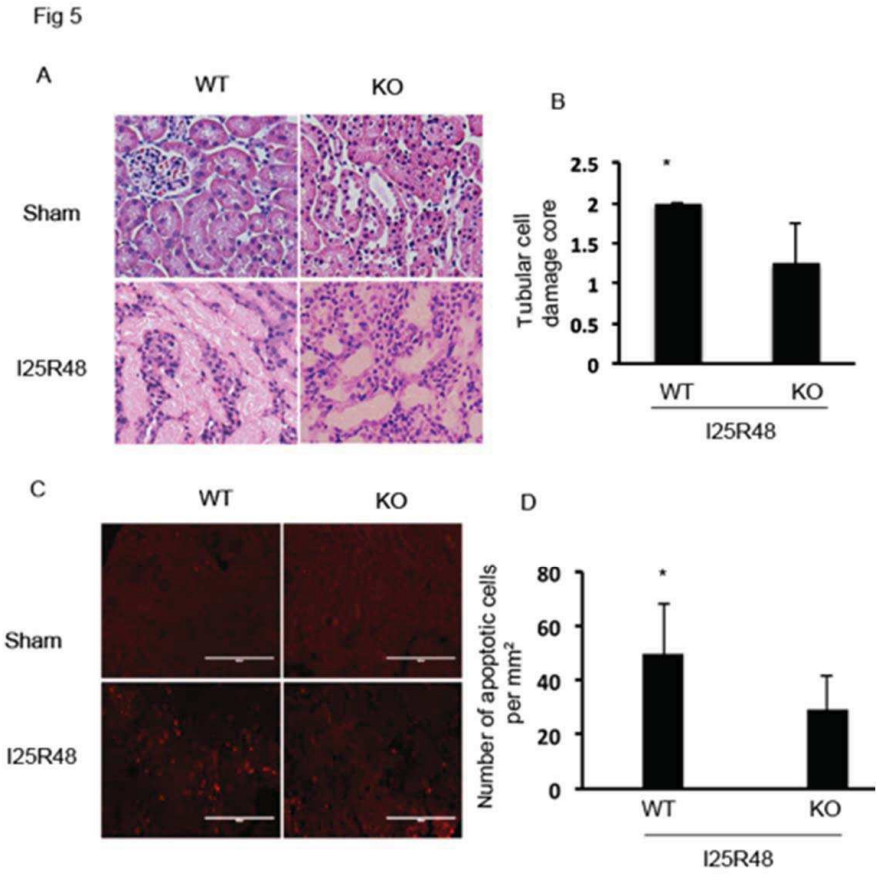

Fig. 6 Resistance of OMA1-KO tissues to mitochondrial fragmentation and cytochrome c release in ischemic AKI

Fig 6

A

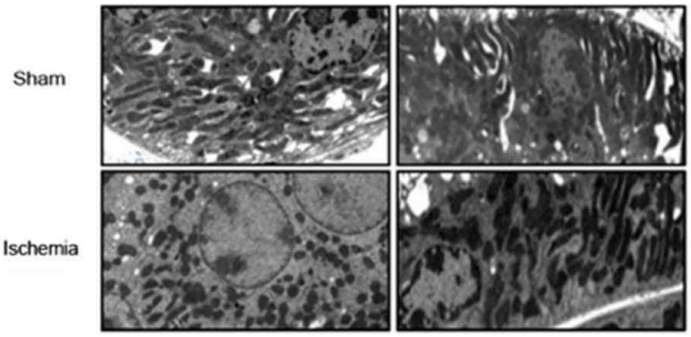

B

	WT		KO	
	Sham	Ischemia	Sham	Ischemia
# of total cells	201	211	190	198
# of cells with fragmented mitochondria	21	55	23	36
% of cells with fragmented mitochondria	10.4	26.1	12.1	18.2

C

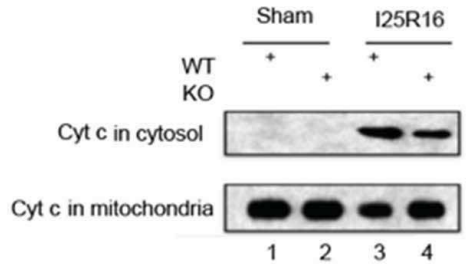

IV. Generation and cancer susceptibility of Lonp1-deficient mice

Lon protease (LONP1) is a highly conserved serine protease that contributes to protein quality control processes from bacteria to eukaryotic cells. LONP1 plays a crucial role degrading misfolded and damaged proteins and protecting mitochondrial function under stress conditions. Accordingly, changes in the expression levels of this protease gene are associated with several diseases, including cancer. Nevertheless, although the function of Lon protease is well known in lower organisms and several *in vitro* substrates have been identified for this protease in mammalian cells, the physiological function of LONP1 remains unknown. In this work, we report the generation of mice deficient in the Lon protease demonstrating the essential function of this proteolytic enzyme for embryonic development and cancer susceptibility. In addition, we show that LONP1 plays a key role in metabolic reprogramming of tumor cells by remodeling OXPHOS complexes and protecting against senescence, identifying this protease as a central regulator of mitochondrial activity in oncogenesis.

Article 4: Pedro M. Quirós, Yaiza Español, Rebeca Acín-Pérez, Francisco Rodríguez, Clea Bárcena, Kenta Watanabe, Enrique Calvo, Marta Loureiro, M. Soledad Fernández-García, Antonio Fueyo, Jesús Vázquez, José Antonio Enríquez and Carlos López-Otín. "ATP-dependent Lon protease promotes cancer and metastasis by reprogramming mitochondrial activity".

(Cell Metabolism, manuscript under revision)

Personal contribution to this work

I have been the main responsible for all the experiments shown in this work. I established, managed, genotyped and characterized the Lonp1 mouse colony. I performed all subsequent experiments, including the characterization of the lethality phenotype and the generation of the carcinogenesis protocols. I also generated the cellular models of loss- and gain-function for LONP1 and carried out the xenografts and experimental metastasis protocols. Finally, I analyzed the data, prepared the figures and wrote the manuscript under the supervision of Prof. Carlos López-Otín.

Manuscript

ATP-dependent Lon protease promotes cancer and metastasis by reprogramming mitochondrial activity

Pedro M. Quirós[1], Yaiza Español[1], Rebeca Acín-Pérez[2], Francisco Rodríguez[1], Clea Bárcena[1], Kenta Watanabe[1], Enrique Calvo[3], Marta Loureiro[3], M. Soledad Fernández-García[4], Antonio Fueyo[5], Jesús Vázquez[3], José Antonio Enríquez[2] and Carlos López-Otín[1]

[1]Departamento de Bioquímica y Biología Molecular, Facultad de Medicina, Instituto Universitario de Oncología, Universidad de Oviedo, 33006-Oviedo, Spain; [2]Department of Cardiovascular Development and Repair, Centro Nacional de Investigaciones Cardiovasculares, 28029-Madrid, Spain; [3]Cardiovascular Proteomics Laboratory, Department of Vascular Biology, Centro Nacional de Investigaciones Cardiovasculares, 28029-Madrid, Spain; [4]Servicio de Anatomía Patológica, Hospital Universitario Central de Asturias, 33006-Oviedo, Spain; [5]Area de Fisiología, Departamento de Biología Funcional, Facultad de Medicina, Instituto Universitario de Oncología, Universidad de Oviedo, 33006-Oviedo, Spain.

Running title: Control of mitochondrial activity and tumor bioenergetics by LON protease

Keyworks: aging, cancer, degradome, mitochondrial quality control, OXPHOS

Send correspondence to:
Carlos Lopez-Otin
Departamento de Bioquímica y Biología Molecular
Facultad de Medicina, Universidad de Oviedo
33006 Oviedo-SPAIN
Tel. 34-985-104201; Fax: 34-985-103564
E-mail: clo@uniovi.es

ABSTRACT

We have generated mice deficient in Lon protease (LONP1), a major enzyme of the mitochondrial quality control machinery. Homozygous deletion of Lonp1 causes early embryonic lethality, while its haploinsufficiency protects against colorectal and skin tumors. Furthermore, LONP1 knockdown inhibits cellular proliferation and tumor and metastasis formation, whereas its overexpression increases tumorigenesis. Clinical studies indicate that high levels of LONP1 are a poor prognosis marker in human colorectal cancer and melanoma. Additionally, functional analyses show that LONP1 plays a key role in metabolic reprogramming by remodeling OXPHOS complexes and protecting against senescence. Our findings demonstrate the relevance of LONP1 for cellular and organismal viability, and identify this protease as a central regulator of mitochondrial activity in oncogenesis.

Highlights

LONP1 is a mitochondrial protease essential for embryonic development
LONP1 is up-regulated in human colorectal and melanoma tumors
LONP1 loss induces mitochondrial dysfunction and triggers cellular senescence
LONP1 regulates metabolic reprogramming through remodeling mitochondrial function

INTRODUCTION

Mitochondria are subcellular organelles of eukaryotic cells responsible for generating the bulk of cellular energy in the form of ATP through oxidative phosphorylation (OXPHOS) (Wallace et al., 2010). In addition, mitochondria are involved in other pathways of intermediate metabolism, generate and regulate reactive oxygen species (ROS), maintain homeostasis and calcium buffering, and participate in essential cellular processes such as apoptosis (Galluzzi et al., 2012; Rizzuto et al., 2012; Sena and Chandel, 2012; Wallace, 2011). Consistent with the wide diversity of functional roles played by these organelles, mitochondrial dysfunctions are associated with aging and various pathological processes such as cancer and neurological diseases (Lopez-Otin et al., 2013; Wallace, 2005). To exert their functions properly, mitochondria have developed a quality control system composed of proteases and chaperones that regulate the assembly, folding and turnover of proteins, as well as the removal of damaged proteins (Tatsuta, 2009; Voos, 2013). In mammals, there are four-major ATP-dependent proteases that participate in mitochondrial quality control: Yme1 and m-AAA proteases localized in the inner membrane, and ClpP and Lon located in the matrix (Anand et al., 2013; Rugarli and Langer, 2012). Additionally, there are several ATP-independent proteases that collaborate in mitochondrial homeostasis (Cipolat et al., 2006; Quirós et al., 2012).

Lon protease (LONP1) is a highly conserved serine peptidase that contributes to protein quality control processes from bacteria to eukaryotic cells (Lu et al., 2003). LONP1 plays an important role in the degradation of misfolded and damaged proteins, and supports cell viability under oxidative, hypoxia and ER-stress conditions (Venkatesh et al., 2012). Thus, LONP1 degrades aconitase, a key enzyme of the Krebs cycle which is highly susceptible to oxidative inactivation (Bota and Davies, 2002). Likewise, LONP1 degrades the cytochrome c oxidase isoform COX4-1 under hypoxic conditions, enabling the function of COX4-2, which is more efficient under low oxygen conditions (Fukuda et al., 2007). The proteolytic function of LONP1 is also involved in cholesterol metabolism by degrading the steroidogenic acute regulatory protein and in the heme biosynthesis pathway by targeting 5-aminolevulinic acid synthase, the first rate-controlling enzyme in this pathway (Granot et al., 2007; Tian et al., 2011). Besides its

functions as a protease, LONP1 is a DNA-binding protein both in prokaryotic and eukaryotic cells (Fu and Markovitz, 1998). In particular, mammalian LONP1 binds to single strand mtDNA in G-rich consensus sequences and participates in mtDNA maintenance and gene expression regulation through association with nucleoids and interaction with mtDNA polymerase gamma and the twinkle helicase (Cheng et al., 2005; Liu et al., 2004). Moreover, LONP1 degrades mitochondrial transcription factor A (TFAM), regulating mtDNA copy number and metabolism to maintain the TFAM/mtDNA ratio necessary to control replication and transcription (Lu et al., 2013; Matsushima et al., 2010).

Consistent with LONP1 crucial role in the control of mitochondrial function under stress conditions, changes in the expression levels of this protease gene are associated with several diseases. Thus, LONP1 expression is up-regulated in different mitochondrial syndromes, such as Friedrich ataxia, MERRF (myoclonic epilepsy with ragged red fibers), and MELAS (mitochondrial encephalomyopathy, lactic acidosis and stroke-like episodes) (Felk et al., 2010; Guillon et al., 2009; Wu et al., 2010). Conversely, LONP1 expression is down-regulated in hereditary spastic paraplegia, familial amyotrophic lateral sclerosis, and aging (Erjavec et al., 2013; Fukada et al., 2004; Hansen et al., 2008; Ngo and Davies, 2007; Ngo et al., 2011). Moreover, LONP1 levels are increased in different tumor cell lines, like human mammary epithelial cells or hepatoma cells (Kita et al., 2012), as well as in different tumors, including non-small-cell lung carcinoma and lymphoma (Bernstein et al., 2012; Hu et al., 2005). Interestingly, down-regulation of LONP1 in some tumor cell lines causes apoptosis and cell death (Bota et al., 2005), indicating a possible addiction of tumor cells to LONP1 function, as occurs with other intracellular proteases associated with cancer (Bulteau and Bayot, 2011; Fraile et al., 2011; Freije et al., 2011).

To further analyze the in vivo roles of this mitochondrial protease in both normal and pathological conditions, including cancer, we have generated mutant mice deficient in Lonp1. Homozygous deletion of Lonp1 causes early embryonic lethality due to an arrest in mouse embryonic development. However, Lonp1$^{+/-}$ heterozygous mice are fertile and viable, thereby facilitating studies of cancer susceptibility which have shown that these haploinsufficient animals are protected against colon and skin carcinomas induced by chemical carcinogens. Moreover,

4

knockdown of Lon protease in colorectal and melanoma cells inhibits in vivo tumor growth and metastasis, respectively, while LONP1 overexpression promotes tumorigenesis. Finally, we provide evidence that LONP1 regulates metabolic reprogramming and controls tumor bioenergetics by remodeling OXPHOS complexes. Together, our results indicate that LONP1 is an essential protease for embryonic development and operates as a pro-tumor protease during carcinogenesis.

RESULTS

Lonp1 deletion causes embryonic lethality in mice

Mice heterozygous for the targeted allele of the mitochondrial Lon protease ($Lonp1^{+/-}$) were viable and fertile with no obvious abnormalities. These mice were intercrossed to generate homozygous mice deficient in Lonp1 (Figure S1A). However, we did not detect homozygous pups at weaning (Figure S1B), suggesting that Lonp1 homozygous deletion causes embryonic lethality. To further assess this hypothesis, we analyzed and genotyped embryos at different stages of development, from 3.5 to 9.5 days post coitum (dpc). We found that at blastocyst stage (3.5 dpc), the number of embryos of the different genotypes followed the expected Mendelian ratios. However, at 8.5 dpc, only one of the analyzed viable embryos carried the homozygous mutation, whereas at 9.5 dpc none of them carried the mutation in homozygosis (Figure 1A and Figure S1B). Moreover, analysis of non-viable mutant embryos at 8.5 dpc showed a clear reduction in size when compared with their littermate controls, looking like 7.5 dpc embryos and suggesting that their development was arrested. These differences were maintained at 9.5 dpc (Figure 1A). To clarify the embryonic lethality of $Lonp1^{-/-}$ in the gastrulation period, we performed comparative histological analysis of 5.5 to 7.5 dpc embryos from both genotypes. $Lonp1^{-/-}$ embryos from 5.5 and 6.5 dpc showed normal size and development (Figure 1B). However, at 7.5 dpc, Lonp1-null embryos showed a marked growth decrease, being much smaller than their littermate controls and exhibiting incomplete formation of embryo cavities, thereby pointing to a developmental arrest at the egg-cylinder early gastrulation stage (Figure 1B).

To further characterize the cause of lethality observed in Lonp1-null embryos, we first tried to generate ES cells or murine embryonic fibroblasts (MEFs) with homozygous deletion of Lonp1. However, after repeated experiments, we were unable to obtain any Lonp1-deficient cell line. To evaluate the putative relationship between mtDNA deficiencies and embryonic lethality in Lonp1-null mice, we analyzed mtDNA copy number in Lonp1-null embryos during development. We observed that at 3.5 dpc there were no differences between control, heterozygous and Lonp1-null embryos (Figure 1C). However, analysis at 7.5 dpc showed a decrease in mtDNA copy number in Lonp1-deficient embryos compared with control and heterozygous embryos (Figure 1C). To further evaluate the influence of LONP1 deficiency in embryo development, we analyzed the in vitro growth of embryos. Thus, we isolated preimplantation embryos by uterine flushing at blastocyst stage (3.5 dpc), from control and knockout mice. As shown in Figure 1D and Figure S1B, almost all blastocysts obtained from intercrossed heterozygous mice were normal and viable, and Lonp1-null blastocysts were indistinguishable from the corresponding controls. We then cultured blastocysts in vitro for 5 days in ES cells media, finding that virtually all analyzed embryos developed normally. However, Lonp1-deficient embryos showed a smaller size in the inner cell mass (ICM) and trophoblast cells (TB) compared with littermates (Figure 1E), indicating a growth arrest similar to that observed in the in vivo experiments. Taken together, these results indicate that LONP1 is essential for in vivo and in vitro embryo development. Embryonic absence of this protease leads to marked growth retardation and arrest likely due to mitochondrial dysfunction and loss of mtDNA, with subsequent failure to accomplish the energy requirements necessary for embryonic development.

In marked contrast to embryonic lethality of $Lonp1^{-/-}$ mice, $Lonp1^{+/-}$ mice developed normally and did not display any obvious pathological alterations. Analysis of Lonp1 expression in heterozygous mice indicated a 50% reduction at both RNA and protein levels in these animals (Figure 1F and 1G). These findings demonstrate that LONP1 haploinsufficiency is compatible with embryonic and adult mouse development, as well as with normal growth and fertility, thus opening the possibility to perform long-term studies aimed at analyzing cancer susceptibility in $Lonp1^{+/-}$ mice.

6

Lonp1-haploinsufficient mice are protected against colorectal cancer and chemically-induced skin tumors

To analyze the role of LONP1 in tumor development, we induced colon carcinoma in $Lonp1^{+/-}$ mice and in littermate $Lonp1^{+/+}$ controls, using a combined treatment with azoxymethane (AOM) and dextrane sulfate (DSS) (Figure 2A). At the end of the experiment, all Lonp1 wild-type mice, but only 72% Lonp1 heterozygous mice, developed colorectal tumors ($P < 0.05$) (Figure 2B). Moreover, $Lonp1^{+/-}$ mice had significantly fewer tumors than control animals (Figure 2C and 2D). There was also a decrease in the colon length in Lonp1 control mice compared with heterozygous mice (Figure 2E). Quantitative analysis of the clinical score during the carcinogenesis protocol revealed that $Lonp1^{+/-}$ mice exhibited milder clinical features than wild-type animals (Figure 2F). These results indicate that a decrease in Lonp1 levels protects against colorectal carcinoma in mice.

To further characterize the putative role of LONP1 in tumor development, we used an additional chemical carcinogenesis protocol to induce skin tumors. For this purpose, we subjected Lonp1-heterozygous mice and their wild-type littermate controls to a conventional 7,12-dimethylbenzanthracene and tetradecanoylphorbol acetate (DMBA/TPA) carcinogenesis protocol that induces skin papillomas. Lonp1 heterozygous mice developed significantly less papillomas during the TPA treatment, from week 9 to the end of the experiment, both in size and in total number of papillomas per mouse (Figure 2G). Moreover, Lonp1-heterozygous mice displayed significantly lower incidence in papilloma appearance ($P < 0.05$) (Figure 2H), while histological analysis of papillomas showed tumor size differences between both groups (Figure 2I). These results indicate that LONP1 has a key role in the development of colon and skin tumors, and decrease in Lonp1 levels protects against colorectal carcinoma and papilloma formation in mice.

LONP1 is upregulated in colon cancer and promotes tumor growth

To clarify the role of this mitochondrial protease in colorectal cancer, we studied LONP1 expression in different human colorectal cancer cell lines (HCT116, HCT15, HT29, SW480, SW620, DLD-1 and RKO), as well as in a colon epithelial cell line (FHC). qPCR analysis

showed high expression of LONP1 in all colon cancer cell lines compared to the control cells (Figure 3A). Interestingly, in four of the seven cell lines analyzed (HCT116, HCT15, DLD-1 and RKO), the increase in LONP1 expression relative to colon fibroblasts was more than 10-fold. These four cell lines with very high expression levels of LONP1 display microsatellite instability, while those showing less than 10-fold changes in LONP1 relative expression (HT29, SW620 and SW480) exhibit microsatellite stability phenotypes (Kleivi et al., 2004). To extend these LONP1 expression data to the protein level, we performed Western-blot analysis of these cell lines. This analysis showed increased LONP1 protein levels in all cell lines compared to control colon fibroblasts, although these protein levels did not perfectly correlate with those of RNA (Figure 3B). To analyze the relevance of Lon protease in these colon carcinoma cells, we used HCT116 cells to perform in vitro and in vivo studies of loss- and gain-of-function. Thus, we reduced Lon protease levels using lentiviral-based shRNAs against LONP1, and ectopically induced LONP1 using a retroviral system that expresses a Flag-tagged LONP1 cDNA construct. The expression of LONP1 was confirmed by qPCR analysis and western-blot analysis (Figure 3C and Figure S2A). Knockdown of LONP1 (shLon) significantly reduced cell proliferation in vitro compared to control cells (pLKO1) (Figure 3D and Figure S2B). However, ectopic expression of LONP1 (LON) did not increase proliferation when compared to its corresponding control cell line (pMX) (Figure 3D). Likewise, overexpression of LONP1 in DLD-1, a colon cancer cell line with relatively low levels of LONP1 expression, did not increase the proliferation rates (Figure S2C). We then examined the in vivo relevance of LONP1 expression on tumor growth, using a xenograft model. Thus, the shLon engineered cells were injected subcutaneously into the flanks of nude mice and the size of tumors measured. As shown in Figure 3E, tumor growth of shLon cells was significantly reduced when compared to pLKO1 control cells. On the other hand, ectopic expression of LONP1 increased growth of tumors in nude mice compared to those generated by pMX control cells (Figure 3F). These results indicate that LONP1 is necessary to maintain the proliferative rates and tumor growth of this colorectal cancer cell line.

To further evaluate the relevance of LONP1 expression in colon carcinoma, we performed an immunohistochemical analysis of human samples from normal and tumor colorectal sections. Thus, in agreement with previous data, LONP1 is expressed in normal colon samples and highly

up-regulated in colon cancer mucosa (Figure 3G). Moreover, analysis of transcriptional data from colorectal adenomas and normal mucosa (Sabates-Bellver et al., 2007), showed a significant increase in LONP1 expression in adenomas compared to their matched normal mucosa (Figure 3H). In addition, detailed analysis of reported data on survival of colorectal carcinoma patients with Duke's stages A-C, showed a positive correlation between high LONP1 expression and lower survival (Figure 3I). Collectively, these results suggest that Lonp1 up-regulation is common in colorectal cancer and may provide some advantage to tumor cells, thereby facilitating cancer development.

LONP1 is necessary for proliferation and metastasis of melanoma cells

As described above, Lonp1-heterozygous mice displayed less susceptibility to develop tumors than control mice, and the expression of LONP1 is increased during malignant transformation in both human colon and skin tumors. A deeper analysis of human cutaneous melanoma (Talantov et al., 2005), showed a significant increase in LONP1 levels in melanoma compared to normal skin or benign nevi samples (Figure 4A). Moreover, analysis of clinical outcome of melanoma patients with metastasis (Bogunovic et al., 2009), showed a positive correlation between LONP1 expression and short survival (Figure 4B). To further evaluate the functional relevance of Lon protease in tumor and metastasis formation in vivo, we used the murine B16F10 melanoma cells in which, similar to the above experiments with HCT116 colorectal cancer cells, we reduced LONP1 levels using lentiviral-based shRNA and induced ectopic expression of LONP1 using a retroviral system. A complete set of shRNA (shLon) reduced both LONP1 mRNA and protein levels approximately 90% compared with control pLKO1 shRNA, whereas ectopic expression of Lon increased the levels of protein and mRNA 10-fold (Figure 4C-D and Figure S3A). Knockdown of LONP1 diminished in vitro proliferation of B16F10 cells, whereas ectopic expression of LONP1 did not increase proliferation rates (Figure 4E and Figure S3A). We then analyzed the in vivo formation of experimental lung metastasis using this highly metastatic melanoma cell line. Thus, we intravenously injected 25,000 B16F10 cells in C57BL/6 mice, and after three weeks, mice were sacrificed and the

number of lung metastasis determined by histological analysis. As shown in Figure 4F, knockdown of LONP1 inhibited metastasis formation, reducing 10-fold the number of metastasis compared to pLKO1 control cells. Conversely, overexpression of Lon protease increased significantly the number of metastasis (Figure 4G). Together, these results indicate that LONP1 is essential for cell proliferation as well as for metastasis formation in vivo, and high levels of LONP1 are a marker of poor prognosis in human melanoma.

LONP1 induces a metabolic switch and regulates tumor bioenergetics by remodeling OXPHOS complexes

To study the role of LONP1 in the regulation of mitochondrial function in cancer, we used the above described B16F10 melanoma cells with knockdown or overexpression of Lon protease. Knockdown of LONP1 decreased cellular ATP content, whereas ectopic expression of LONP1 increased ATP content (Figure 5A and Figure S4A). Further, analysis of mitochondrial respiration showed a decrease in basal oxygen consumption in LONP1 ablated cells when compared to controls (Figure 5B and Figure S4B). Interestingly, overexpression of Lon protease also showed a decrease in mitochondrial respiration compared to control cells (Figure 5B). Stimulation with the chemical uncoupler trifluorocarbonylcyanide phenylhydrazone (FCCP) increased oxygen consumption to maximal respiration rate (MRR) in both pLKO1 and pMX control cells. Nevertheless, neither knockdown nor overexpression of Lon protease reached similar oxygen consumptions than control cells (Figure 5B and Figure S4B). In addition, both knockdown and ectopic expression of LONP1 increased the glucose consumption and lactate production compared to controls (Figure 5C-D and Figure S4C-D). These results were puzzling because both conditions, i.e. ablation and overexpression of LONP1, induce the down-regulation of respiration and the up-regulation of the glycolytic pathway. To try to understand this phenomenon, we examined mitochondrial respiratory complexes by blue-native gel electrophoresis (BNGE) in both situations. We detected a significant decrease in complex I (Figure 5E and Figure S4E) and a concomitant decrease in complex III-containing supercomplexes (Figure 5F and Figure S4E) in shLon cells. Similarly, we observed a significant decrease in complex I, II, and IV in cells

overexpressing LONP1 (Figure 5G and Figure S4F), as well as a reduction in complex III-containing supercomplexes (Figure 5H and Figure S4F). We also noticed that the relative amount of complex V in dimers was reduced in both models (Figure 5F and Figure 5H). The observed decrease in mitochondrial complexes in both models likely derives from enhanced degradation or from a reduction in their assembly and could underlie the decrease in mitochondrial respiration in both LONP1-overexpressing and LONP1-deficient cells.

We next evaluated the individual activities of mitochondrial complexes by spectrophotometric analysis of mitochondria isolated from both cells. We observed that shLon cells showed significantly lower activities of CI and combined CII+III activity (Table 1), consistent with the low levels of CI and assembled CIII measured by BNGE (Figure 5E and 5F). In contrast, overexpression of LONP1 decreased almost all individual complex activities. Thus, we observed a reduction in CII and CIV, as well as combined CI+III and CII+III activities (Table 1), consistent with the decrease observed by BNGE (Figure 5G and 5H). Moreover, knockdown of Lon protease specifically induced an increased activity of CI+III relative to CI (CI+III/CI) and decreased activity of CII+III relative to CII (CII+III/CII) (Figure 5I), suggesting that complex III is more dedicated to complex I than to complex II, favoring the use NADH equivalents and the respiration through complex I. However, overexpression of Lon protease reduced the respiration through complex I, demonstrating decreased activity of CI+III relative to CI (CI+III/CI) (Figure 5J), while respiration efficiency through complex II (CII+III/CII) remained unaltered. These changes are consistent with a metabolic reprograming of the OXPHOS system by primarily reducing the flux from NADH electrons (more catabolic), but maintaining the flux through the FAD dependent enzymes, that are also involved in anabolic (nucleotide and amino acid metabolism) and detoxifying metabolic pathways.

To further clarify the putative differences observed in the regulation of OXPHOS complexes in LONP1-overexpressing and LONP1-knockdown cells, we performed a quantitative proteomic analysis, using iTRAQ labeling and subsequent LC-MS/MS analysis. To enrich the amount of mitochondrial proteins and reduce the experimental variability, we performed these experiments in preparations of purified mitochondria. As a control of our proteomic analysis, we detected a significant increase in LONP1 protein in the overexpression model, whereas we did

not find it in the downregulation model (Figure 5K). Consistent with the above described findings in OXPHOS complex levels, we detected a significant alteration in the amount of complex I proteins in both LONP1-overexpressing and LONP1–knockdown cells (Figure 5K). However, the affected complex I protein components differed between both cells, suggesting a distinct mechanism of regulation in each condition. Thus, all CI proteins were downregulated in LONP1–knockdown cells, while they presented variability in LONP1-overexpressing cells, being some of them upregulated and other downregulated. Furthermore, CI structural proteins, such as NDUFB6, 8, 10 and 11, were the more downregulated proteins in LONP1-knockdown cells, while they were upregulated in LONP1-overexpressing cells. Importantly, these proteins are associated with the assembly and stability of the CI membrane domains and are required for their activity (Andrews et al., 2013; García-Ruiz et al., 2013; Loublier et al., 2011; Perales-Clemente et al., 2010). Conversely, among the most decreased proteins in the LONP1-overexpressing cells, there were four subunits of the NADH dehydrogenase and hydrogenase catalytic modules of CI, such as NDUFV1, NDUFV2, NDUFS3 and NDUFS7. Interestingly, it has been described that these proteins can be removed and replaced in the complex I without degrading the whole complex (Dieteren et al., 2012; Lazarou et al., 2007). These results indicate that the observed complex I decrease in shLon cells was a consequence of loss of stability of this complex, while in LONP1-overexpressing cells the decrease was functional, maintaining the structural domains. Moreover, complex V subunits were clearly downregulated in shLon cells (Figure 5K), which is in line with the observed decrease in complex V dimers (Figure 5F). Interestingly, LONP1-overexpressing cells showed an increase in complex V subunits (Figure 5K), despite the observed decrease in dimers (Figure 5H), which indicates that these cells have a different complex V regulation.

Overall, these data strongly suggest that the apparent convergence in the decrease in aerobic respiration and the subsequent glycolysis activation, by either knockdown or overexpression of LONP1, takes place through different mechanisms. The loss of mitochondrial complexes would operate in shLon cells, while OXPHOS complexes remodeling would underlie the alterations found in LONP1-overexpressing cells.

LONP1 keeps mitochondrial function and induces a global metabolic reprogramming

To further clarify the observed alterations in LONP1-overexpressing and LONP1-knockdown cells, we analyzed other parameters related to mitochondrial function in these cells. We first found that LONP1-knockdown, but not its overexpression, induced a decrease in both mitochondrial membrane potential (Figure 6A) and mtDNA content (Figure 6B). shLon cells also displayed an increase in mitochondrial fragmentation (Figure 6C and Figure S5A) and ROS production (Figure 6D), which caused the proteolytic processing of OPA1 (Figure 6E and Figure S5B). These findings are indicative of a clear mitochondrial dysfunction, which is not observed in LONP1-overexpressing cells. Moreover, knockdown of Lon protease activated the AMPK pathway, exemplified by an increase in AMPK phosphorylation (Figure 6E), which is in line with the low ATP levels and the mitochondrial stress scenario observed in these cells. In contrast, overexpression of LONP1 decreased AMPK activation (Figure 6E). In addition, and consistent with the enhancement of the glycolytic pathway detected in both LONP1-overexpressing and LONP1-knockdown cells, there was an increase in the expression of glycolytic genes in both cases (Figure S5C). However, analysis of lipid synthesis showed a significant decrease in shLon cells, which agrees with the AMPK activation in these cells, whereas LONP1-overexpressing cells displayed similar rates than control cells (Figure 6F and Figure S5D). Interestingly, and despite we did not detect differences in apoptosis (data not shown), we found increased levels of the anti-apoptotic protein Bcl-2 in LONP1-overexpressing cells and decreased levels in shLon cells (Figure 6E), which suggests a possible increase in apoptosis sensitivity in LONP1-deficient cells. We next examined in both LONP1-overexpressing and LONP1-knockdown cells the levels and activity of aconitase (ACO2), a well-established substrate for Lon protease. We found a decrease in ACO2 activity in LONP1-overexpressing cells and an increased activity of this enzyme in shLon cells (Figure S5E). The low expression levels of ACO2 in these cells precluded the detection of clear differences in enzyme levels. However, after transfection of a cDNA encoding ACO2, we detected increased levels and activity of this enzyme in control cells, but not in LONP1-overexpressing cells (Figure S5F-G), indicating that LONP1 processes ACO2 under conditions where this substrate is highly expressed.

Taken together, these results indicate that the absence of LONP1 induces a generalized mitochondrial dysfunction, whereas its overexpression does not alter the mitochondrial homeostasis. To further characterize the cellular alterations induced by the depletion and overexpression of LONP1, we analyzed the global protein changes obtained by quantitative proteomic analysis of the corresponding cells. Thus, we found that LONP1-overexpression increased the levels of proteins related with protein synthesis, such as eukaryotic translation initiation factor complex 3 and ribosomal proteins (Figure 6G). We also found increased levels of proteins related with the spliceosome, proteasome and chaperone-containing T complex (Figure 6H), which is consistent with the increased tumorigenesis observed in LONP1-overexpressing cells. Conversely, LONP1-deficient cells showed reduced levels of all of these proteins (Figure 6G and 6H), which agrees well with the low proliferation rate and tumorigenic potential of these cells. Collectively, these data illustrate the occurrence of marked differences in the process of metabolic adaptation after modulation of LONP1 levels, which leads to a profound mitochondrial dysfunction when cells are depleted of Lon protease and to a global metabolic remodeling when this mitochondrial enzyme is overexpressed.

LONP1 contributes to bypass oncogene-induced senescence

We have described above that knockdown of Lon protease induces growth arrest and mitochondrial dysfunction in melanoma cells, impairing mitochondrial respiration and causing the loss of mitochondrial integrity. Interestingly, besides lower proliferation rates, we observed that shLon cells displayed an increase in size compared with control pLKO1 or LONP1-overexpressing cells, suggesting the occurrence of a cellular senescence phenotype (Figure 7A). Moreover, analysis of β-galactosidase staining, which is a marker of senescent cells, showed an increase in the number of positive cells in those lacking Lonp1, whereas overexpression of LONP1 decreased the number of positive cells (Figure 7B). The induction of cellular senescence is mainly mediated by signals derived from a permanent DNA damage response (DDR). Accordingly, we found that the loss of mitochondrial integrity caused by LONP1 deficiency induced a DDR likely mediated by p53, as assessed by the increased levels of direct

transcriptional targets of this tumor suppressor, including Atf3, Gadd45g and Cdkn1a/p21 (Figure 7C). Interestingly, knockdown of LONP1 in p53-deficient cells resulted in lower proliferation defects when compared to wild-type cells, indicating that p53 contributes to the observed alterations (Figure 7D). Notably, overexpression of LONP1 in B16F10 cells reduced the levels of those markers and β-galactosidase activity (Figure 7B and 7D), indicating a protection against senescence by Lon protease, which was consistent with the observed tumorigenesis increase of these melanoma cells. On the other hand, it is well established that mutations in genes like HRAS or BRAF also induce a senescence phenotype, known as oncogene-induced senescence (OIS), as part of a cell protective response against tumor transformation (Michaloglou et al., 2005; Serrano et al., 1997). On this basis, we explored available cancer transcriptome databases looking for putative differences in LONP1 expression levels during OIS processes. Thus, by analyzing data from previous studies involving transformation of fibroblasts with mutant MEK (Collado et al., 2005), we found that induced OIS did not promote changes in LONP1 expression. However, bypassing senescence in these fibroblasts using viral oncoproteins, significantly increased LONP1 expression (Figure 7E), further supporting the idea that up-regulation of Lon protease may favor oncogenic transformation. Collectively, these results demonstrate that LONP1 is essential to protect against senescence, and reinforce the proposal that levels of this serine protease contribute to modulate the tumorigenic properties of cancer cells.

DISCUSSION

We describe herein the generation and phenotypic characterization of mice deficient in the mitochondrial Lon protease, as well as the functional analysis of this ATP-dependent enzyme in tumor formation and metastasis development. We have found that mice deficient in LONP1 show a lethal phenotype during gastrulation, a period in which a well-fitted mitochondrial function is required to induce profound changes in embryo development (Nagy et al., 2003). At this stage, Lonp1-null embryos display loss of mtDNA and growth arrest, which are features observed in mice deficient in OXPHOS complex subunits, like GRIM19 and SCO2 (Huang et al., 2004; Yang

et al., 2010), or in mtDNA-associated proteins, such as POLG, POLG2 and TFAM (Hance et al., 2005; Humble et al., 2013; Larsson et al., 1998), that also exhibit embryonic lethality. In contrast, Lonp1-heterozygous mice develop normally with no obvious alterations, allowing us to evaluate in vivo the functional and pathological relevance of LONP1 haploinsufficiency. Interestingly, $Lonp1^{+/-}$ mice are protected against chemically-induced colorectal and skin tumors, suggesting an oncogenic function for this mitochondrial protease. Consistent with this hypothesis, LONP1 is up-regulated in human colorectal and skin carcinomas and their levels are associated with poor clinical outcome of the corresponding patients. Accordingly, LONP1-knockdown in HCT116 colorectal cancer cells reduces in vitro cell proliferation and in vivo growth of tumors derived from these cells, whereas ectopic expression of LONP1 increases tumor growth. Moreover, overexpression of LONP1 in melanoma cells increases experimental metastasis formation, whereas knockdown of this protease decreases cell proliferation and lung metastasis. Notably, LONP1 up-regulation does not stimulate cell proliferation, despite the observed increase in tumor growth and metastasis in vivo. The metabolic and stress adaptations undergone by cancer cells during the tumorigenesis process, which are not perfectly replicated in the in vitro experiments, may explain these differences, also observed in similar studies involving other metabolic genes with oncogenic function (Bhalla et al., 2011). Accordingly, we propose that the up-regulation of LONP1 observed in many cancer cell lines and tumor samples (Bernstein et al., 2012; Hu et al., 2005), is probably the consequence of an adaptive metabolic response during malignant transformation.

Metabolic reprogramming of tumor cells has been recently established as a new hallmark of cancer, because of its ability to induce changes in tumor cells that provide them with proliferative advantages and adaptive responses against the stress conditions associated with tumorigenesis (Hanahan and Weinberg, 2011; Ward and Thompson, 2012). Several enzymes have been proposed to act as protumorigenic factors and contribute to this metabolic reprogramming (Chae et al., 2012; Haq et al., 2013; Locasale et al., 2011; Mitsuishi et al., 2012; Vazquez et al., 2013). Furthermore, mutations in genes encoding mitochondrial and metabolic enzymes have been widely reported in human malignancies (Rodríguez et al., 2013; Yan et al., 2009; Zhang et al., 2012), indicating that tumor cells harbor genetic alterations that affect metabolic function and

facilitate tumor formation. The main feature of this reprogramming process is the switch from oxidative to glycolytic metabolism (Vander Heiden et al., 2009). Apparently, both up-regulation and knockdown of Lon protease in melanoma cells are able to induce the same glycolytic switch, turning cells from oxidative to anaerobic metabolism. How is it possible to elicit a similar phenotype with two opposing stimuli? It is well established that up-regulation of the glycolytic pathway is triggered by oncogenic signals during tumor transformation, as well as by many physiological and pathological conditions which cause metabolic changes (Metallo and Vander Heiden, 2013; Rossignol et al., 2004; Wallace et al., 2010). Additionally, a glycolytic shift is also induced by impairment of the mitochondrial respiratory chain (Hu et al., 2012; Landor et al., 2011; López-Ríos et al., 2007; Lu et al., 2012). This impairment of mitochondrial OXPHOS triggers glycolytic metabolism as a survival mechanism which often ends with cell collapse, due to the inability of these damaged cells to reprogram their metabolism (Benard et al., 2007; Wallace, 2005). Accordingly, the glycolytic switch observed in cells lacking LONP1 may be an obligate consequence of their mitochondrial dysfunction, not being related to metabolic reprogramming of cancer cells. Conversely, the switch observed in LONP1-overexpressing cells is a mitochondria-controlled mechanism, which is part of a generalized metabolic reprogramming that contributes to the development and progression of cancer.

Previous studies on different cellular models have provided some insights into the molecular mechanisms that could underlie these LONP1-mediated modulatory functions of mitochondrial activity. Thus, Pim1, a Lon-like serine protease of Saccharomyces cerevisiae, degrades several components of the mitochondrial respiratory chain (Bayot et al., 2010), and its disruption results in accelerated aging (Erjavec et al., 2013). Moreover, a decrease in LONP1 levels in several cell lines induces the formation of mitochondrial aggregates (Bernstein et al., 2012), the oxidation of key mitochondrial enzymes (Bota and Davies, 2002), and the decrease in mitochondrial function (Bota et al., 2005). Similarly, inactivation of Lon protease function with peroxynitrite decreases the activity of some mitochondrial complexes (Stanyer et al., 2008). The metabolic adaptation of shLon cells induces a change in respiration and in the use of electron equivalents, decreasing respiration through CII and favoring the use of NADH electron equivalents feeding CI (Lapuente-Brun et al., 2013). However, the decrease in CI and CIII-

containing supercomplexes due to loss of specific structural subunits implies that it is not a regulated mechanism, but a consequence of defective assembly or mitochondrial membrane destabilization. In addition, the subsequent loss of membrane potential and the alterations in complex V cause a decrease in ATP generation, while the increase in ROS levels – likely due to the defective activity of CI (Murphy, 2009) – exacerbates this mitochondrial dysfunction. These stress conditions induce the OPA1 processing and mitochondrial fragmentation events that may contribute to the decrease in respiration and functional supercomplexes assembly (Cogliati et al., 2013). Moreover, the loss of mitochondrial membrane potential may inhibit the entry of pyruvate into mitochondria (Bricker et al., 2012; Herzig et al., 2012), reducing the Krebs cycle function and the generation of essential metabolites for cell viability. Consequently, the decrease in ATP levels and the mitochondrial stress signals induce AMPK activation, which down-regulates anabolic pathways, such as lipid synthesis, and up-regulates catabolic reactions, like glycolysis, to try to counteract this stress scenario. However, despite the activation of all these stress-response mechanisms, shLon cells are unable to avoid mitochondrial dysfunction due to the dramatic alterations present in them. Interestingly, previous studies have described that mitochondria dysfunction activates a stress response which coordinates a mitochondrial-nuclear retrograde signal aimed at inducing the expression of nuclear genes able to cope with the stressor signals (Butow and Avadhani, 2004; Formentini et al., 2012). Accordingly, the loss of mitochondrial integrity in shLon cells activates a genetic damage response, likely mediated by the p53 tumor suppressor pathway, which finally triggers cell cycle arrest and senescence. This response mechanism induced as a consequence of irreversible mitochondrial damage reinforces the role of LONP1 as a guardian against reduced cellular and organismal fitness by contributing to maintain mitochondrial integrity.

Conversely, the glycolytic switch observed in LONP1-overexpressing cells is triggered by a regulated metabolic reprogramming, maintaining other mitochondrial functions unaltered. The upregulation of LONP1 induces a remodeling of mitochondrial complexes and supercomplexes, decreasing the mitochondrial respiration and favoring the metabolic switch because, under these conditions, respiratory reactions shift towards the glycolytic pathway, being unnecessary to maintain an excess of active mitochondrial complexes (Hsu and Sabatini, 2008;

Wallace, 2012). Moreover, the overexpression of Lon protease reduces the use of NADH equivalents and the respiration through CI, which is frequently mutated and inactivated in tumor cell lines (Bonora et al., 2006; Gasparre et al., 2007; Santidrian et al., 2013). However, despite the reduction of levels and activity of mitochondrial complexes, LONP1 also increases the stability of the CI basic structure, reducing specifically the catalytic active motive. This conversion indicates that the inactivation is regulated and that remodeling could maintain the ability to activate the respiration in order to increase metabolic flexibility when it is required, mechanism proposed in other similar contexts (Dieteren et al., 2012; Lazarou et al., 2007). In agreement with that, CV stability is also reinforced. Lon protease appears to be a key factor in metabolic reprogramming through remodeling of mitochondrial function, supporting the idea that steady-state alterations of this ATP-dependent protease have a significant impact on respiratory chain activity (Figure 7F). The function of LONP1 as a key protease in the regulation of the respiratory complex is consistent with previous studies showing that it degrades COX4-1 in response to HIF1a and leads to the exchange of this subunit with COX4-2, which is more effective under hypoxic conditions (Fukuda et al., 2007). Recent studies have also shown that overexpression of Lon protease induces the expression of the CI subunit NDUFS8 and generates a more aggressive phenotype in cancer cells (Cheng et al., 2013). All of these data illustrate the essential roles of LONP1 in the regulation of mitochondrial and OXPHOS function in tumor cells. We have also observed that metabolic reprogramming promoted by LONP1 enhances protein synthesis and metabolism, and activates different pathways which may contribute to the observed aggressiveness of cancer cells overexpressing LONP1. Nevertheless, because the Lon protease is also increased in response to other stress stimuli (Hori et al., 2002), it is likely that additional proteolytic processing events associated with these stress responses may also contribute to the increased tumorigenesis caused by up-regulation of this enzyme. Further, the increase in LONP1 expression after bypass of OIS highlights the importance of Lon protease in tumor transformation and mitochondrial metabolic reprogramming. Hence, LONP1 emerges as an indispensable protease for cellular life, also being necessary for tumor growth due to its ability to maintain and modulate mitochondrial activity.

In summary, the generation of Lonp1-deficient mice has allowed us to identify the

essential roles of this mitochondrial protease in cell and organismal viability. Additionally, the identification of LONP1 as a key metabolic factor affecting mitochondrial reprogramming and tumor bioenergetics, may open a new way to develop cancer therapies. These results confirm the importance of studying genetic and metabolic alterations in tumor cells, in order to rationalize an effective response to anticipate the development of cancer.

METHODS

Generation of Lonp1$^{-/-}$ mice and genotyping

The Lonp1-heterozygous mice were provided by Texas Institute for Genomic Medicine (Figure S1A). We used genomic DNA from tail samples for PCR genotyping under the following conditions: denaturation at 94 ºC for 15 s, annealing at 62 ºC for 15 s, and extension at 72 ºC for 45 s, 30 cycles. We used the following primers for genotyping: wild type-specific forward 5'-CCCTGACTGCAGAGATTGTGAA-3', mutation-specific forward 5'-CAGGACATAGCGTTG GCTACC-3' and common reverse 5'-TTCAGTGCCAGTGCCTTAGAGT-3'.

Animal studies and carcinogenesis protocols

All animal procedures were approved in accordance with the guidelines of the Committee for Animal Experimentation of the Universidad de Oviedo (Oviedo, Spain). Xenograft studies were performed as previously described (Fraile et al., 2013). Briefly, 2×10^6 HCT116 cells infected with different constructs of pMX or shRNA vectors were injected subcutaneously into the flanks of six-week-old athymic Nude-Foxn1$^{nu/nu}$ mice (Charles River). Tumor size was measured twice a week with a caliper and tumor volume was determined using the formula: $V=0.4 \times A \times B^2$, where A is the largest and B is the smallest dimension of the tumor. Significant differences were assessed by a linear mixed-effects model. For colon carcinogenesis protocol, 6-week-old mice were injected intraperitoneally with 10 mg/kg AOM (azoxymethane; Sigma-Aldrich, St. Louis, MO, USA). 4 days after AOM administration, dextran sodium sulfate (DSS;

MP Biomedicals) at 2% was administered in the drinking water for five consecutive days. Thereafter, mice received reverse osmosis water. Two DSS cycles more were administered with intervals of 16 days on water between cycles at 2% and 1.5% of DSS respectively. During the course of the experiment, mice were monitored for body weight, rectal prolapse, diarrhea, and macroscopic bleeding as indicative of clinical score (Neufert et al., 2007). Ten days after the last DSS cycle, mice were euthanized and colons were resected, flushed with phosphate-buffered saline (PBS) and measured in length. Colons were fixed in 4% paraformaldehyde (PFA) and transversal sections were hematoxylin and eosin (H&E) stained. Number of tumors was count and grade of inflammatory lesions was analyzed in each mice. Skin carcinogenesis was induced using DMBA/TPA as previously described (Balbín et al., 2003). Briefly, 8-week-old mice backs were shaved and treated those 2 days later with a single application of DMBA followed by bi-weekly applications of TPA for 12 weeks. The number and size of papillomas per mouse was recorded weekly. Two weeks after the end of TPA treatment, mice were sacrificed and papillomas were removed, fixed in 4% PFA and subsequently stained with H&E to analyze the grade of lesions**.** The lung metastasis experimental model was performed as previously described (Gutiérrez-Fernández et al., 2008). Briefly, mice were anesthetized and 25,000 B16F10-luc2 tumor cells (100 µl) were injected through the jugular vein. Mice were sacrificed after 21 days and lungs were collected for histological analysis. Serial sections of the lung (at least 10 sections spaced 100 µm) were stained with H&E, and metastatic foci were counted. Metastases were classified in small (<10 cells), medium (between 10 and 50 cells), and large (>50 cells). For histological analysis, tissues were fixed in 4% PFA in PBS and stored in 70% ethanol. Fixed tissues were embedded in paraffin by standard procedures. Blocks were sectioned (5 µm) and stained with H&E.

Immunostaining

Normal and tumor colorectal samples were obtained from the tumor bank of the Instituto Universitario de Oncología del Principado de Asturias (IUOPA) and used to evaluate LONP1 expression. The automated system DISCOVERY® (Ventana Medical Systems) was used to carry out the immunohistochemical protein detection. Sections were deparaffinized and rehydrated in

EZ Prep® (Ventana Medical Systems) for 20 min. Antigen retrieval was done by heating (CC1 HCl-Tris buffer solution, pH 9.0) (Ventana Medical Systems). Endogenous peroxidase activity was blocked with H_2O_2 solution (Inhibitor®, Ventana Medical System) for 4 min. Samples were incubated with primary antibody at 37 ºC: polyclonal anti-LONP1 (Atlas Antibodies). Slides were incubated with the secondary antibody (OmniMap® Ventana Medical Systems) for 30 min at room temperature. Then the samples were visualized with 3-3′-diaminobenzidine (DAB). Finally, samples were counterstained with hematoxylin, dehydrated and mounted in Entellan (Merck). Sections were photographed (20X) under a light microscope (Nikon-Eclipse 80i).

RNA preparation

Cells were washed twice with PBS and immediately homogenized in Trizol (Life Technologies) and processed in the same day through alcohol precipitation according to the manufacturer's instructions. RNA pellets were then washed in cold 80% ethanol and stored at -80 ºC until further use. Following re-suspension of RNA in nuclease-free water (Life Technologies), the samples were quantified and evaluated for purity (260/280 nm ratio) using a NanoDrop ND-1000 spectrophotometer (NanoDrop Technologies).

Real-time quantitative PCR

cDNA was synthesized using 2 µg of total RNA, 0.14 mM random hexamer primer, 0.2 mM of each deoxynucleoside triphosphate and Superscript II reverse transcriptase (Life Technologies). Quantitative PCR (qPCR) was performed using TaqMan® gene expression assay (Life Technologies) or Power SYBR® Green PCR Master Mix (Life Technologies), following manufacturer's instructions, using an Applied Biosystems 7300HT Real-Time PCR System. As an internal control, gene expression was normalized to the β-actin gene using TaqMan® gene expression assay. Relative expression is represented as relative quantification, using RQ value ($RQ=2^{-\Delta\Delta Ct}$).

Cell culture

Cancer cell lines 293T, HCT116, HCT15, HT29, SW480, SW620, DLD-1, RKO and FHC

were purchased from the American Type Culture Collection. The luciferase-expressing cell line B16F10 Luc2 was purchased from Caliper Life Sciences. Cells were routinely maintained in Dulbecco's modified Eagle's medium (DMEM) containing 10% fetal bovine serum (FBS), 100 U/ml penicillin and 100 µg/ml streptomycin (Life Technologies).

DNA constructs

Mouse cDNA from LONP1 was cloned tagged with a FLAG epitope in the carboxy terminus and subcloned into the pMX retroviral vector (pMX). The construct was verified by capillary sequencing. For RNA interference experiments, five shRNA vectors were purchased for human and mouse LONP1 (RHS4533-NM_004793 for human and RMM4534-NM_028782 for mouse; Open Biosystems, Thermo Scientific), and the ability of individual and combinations of the shRNAs to repress the expression of LONP1 was evaluated by Western-blot and quantitative RT-PCR after lentiviral infection.

Viral package and cell infection

Lentiviruses and retrovirus were packaged in HEK-293T cells using a VSVG-based and pCL-Ampho package system respectively, kindly provided by Dr. J.M. Silva (Columbia University, New York, USA). Cells were transfected using TransITs-LT1 Transfection Reagent (Mirus Bio LLC) and a mixture of 2 µg of the desired plasmid and 1 µg of each viral helper, following manufacturer's instructions. Transfection medium was removed 24 h after transfection and fresh medium was added to the plate. Cell supernatants were collected at 24 and 48 h and filtered through a 0.45-µm sterile filter. Cells were seeded in 6-well plates at 20–30% confluence 24 h before infection. The following day, 1 ml of viral supernatant supplemented with 5 mg/ml of polybrene (Millipore) was added to growing cells. This step was repeated twice and cells were left to recover for 24 h in growth media before puromycin selection (2 µg/ml).

Proliferation assay

To quantify cell proliferation, a Cell Titer 96 Non Radioactive cell proliferation kit was

used following manufacturer's instructions (Promega Corp.). Briefly, HCT116 and B16F10 cells infected with the corresponding vectors were seeded into 96-well plates at a density of $5x10^3$ cells per well (100 µl) and incubated at 37ºC, 5% CO_2 for 4 days. Cell proliferation was quantified by measuring the conversion of a tetrazolium salt into formazan in living cells. At the desired time points (0 h, 24 h, 48 h and 72 h), 15 µl of Dye solution was added into each well (n=5) and cells were incubated at 37 ºC for 2 h. Then, 100 µl of solubilization/stop mixture was added into each well. After 1 h of incubation at 37 ºC, absorbance was measured at 570 nm with a Power Wave XS Microplate reader (Biotek). Then, each point was normalized to time 0 h and mean ± SEM was calculated and represented. Statistical significance was assessed using a non-parametric Mann Whitney-Wilcoxon test.

Western blotting

Cultured cells were washed twice with 1× PBS and lysed in RIPA buffer containing 50 mM Tris buffer, pH 7.4, 150 mM NaCl, 1% Triton X-100, 0.1 % SDS, 10 mM EDTA, and complete protease inhibitor cocktail (Roche Applied Science). Once homogenized, lysed cells were centrifuged at 13,000 g at 4 °C for 10 min, and supernatants were collected. The protein concentration of the supernatant was evaluated by bicinchoninic acid technique (BCA protein assay kit; Pierce Biotechnology Inc.). Protein samples (15 µg) were loaded into SDS-polyacrylamide gels. After electrophoresis, gels were electrotransferred onto PVDF membranes, blocked with 5% nonfat dried milk in TBS-T (TBS with 0.05% Tween-20) and incubated with primary antibodies following the commercial instructions. After 3 washes with TBS-T, membranes were incubated with the corresponding secondary antibody in 1.5% milk in TBS-T, and developed with Immobilon Western Chemiluminescent HRP substrate (Millipore) in a LAS-3000 Imaging System (Fujifilm). Antibodies against LONP1 were obtained from Atlas Antibodies; anti-alpha-tubulin and anti-actin were from Sigma-Aldrich; anti-Flag, anti-AMPKα, anti-phospho-AMPKα (Thr172), anti-Bcl-2 and anti-ACO2 were from Cell Signaling; and anti-OPA1 was from BD Bioscience.

Mitochondrial analysis

We quantified mtDNA by real-time PCR using an Applied Biosystems 7300HT Real-Time PCR System and Power SYBR® Green PCR Master Mix (Life Technologies) as previously described (Moreno-Loshuertos et al., 2006). Briefly, total DNA was used as a template and amplified with specific oligodeoxynucleotides for mt-Co2 and Sdha. We calculated the mtDNA copy number per cell using Sdha amplification as a reference for the nuclear genome. Mitochondrial membrane potential, ROS levels, and mitochondrial morphology were determined as previously described (Quirós et al., 2012). Aconitase activity was determined as previously described (Gardner et al., 1994). Briefly, 10 µg of mitochondria were used to measure aconitase activity following the linear increase in absorbance at 340 nm during 60 min at 25 ºC in a reaction mixture containing 50 mM Tris-HCl (pH 7.4), 6 mM sodium citrate, 0.2% Triton X-100, 0.6 mM $MnCl_2$, 0.2 mM NADP and 2 U/mL of NADP-dependent isocitrate dehydrogenase.

Lactate, glucose and ATP measurements

Extracellular lactate levels were measured by a colorimetric assay and glucose levels were determined using the Accu-Chek II glucometer (Roche Diagnostics). Briefly, 5 x 10^4 cells were seeded in triplicates into 24-well plates for 48 hours in the presence or absence of 500 µM of $CoCl_2$. After that, media were collected and the content of glucose and lactate was determined, normalizing to cell number and subtracting the time zero content of each one. Lactate measurement was performed in a hydrazine/glycine buffer (0.5 M glycine, 0.4 M hydrazine, pH 9.0), containing 17 mg/ml NAD and 11.4 mg/ml lactate dehydrogenase (LDH). The absorbance due to formation of NADH was monitored in a Power Wave XS Microplate reader (Biotek) at 340 nm during 1 h at 25 ºC. The presence of lactate on samples was correlated with the lactate concentrations from a standard curve. Cellular ATP levels were determined using the ATP determination kit (Molecular probes, Invitrogen) according to the instructions of the manufacturer. Briefly, cells were collected by trypsinization and lysed using passive lysis buffer (PLB) (Promega). The lysates were centrifuged at 12,000 g at 4 ºC for 5 min, and supernatants were collected. The protein concentration of the supernatant was evaluated by BCA protein assay kit (Pierce Biotechnology). We used 1 µg of lysed material for ATP determination with a D-luciferin/firefly luciferase reaction mix, and luminescence was measured in a Luminometer

TD20/20 and compared to a freshly prepared ATP standard curve.

Electrophoretic analysis of mitochondrial supercomplexes assembly

Mitochondrial membranes were isolated from 5×10^6 cells as previously described (Nijtmans et al., 2002). Mitochondrial membrane proteins were applied and run on a 3-13% first dimension gradient blue native gel electrophoresis (BNGE) as previously described (Schägger, 1995). After electrophoresis, the complexes were electroblotted onto PVDF membranes and sequentially probed with specific antibodies against complex I, anti-NDUFA9; complex III, anti-core1; complex IV, anti-COX5a; complex II, anti-Fp; complex V, anti-F1-ATPase (ATP5B), all from Abcam and anti-Tom20 from Santa Cruz.

Spectrophotometric analysis of mitochondrial complexes

Measurements of mitochondrial complexes enzymatic activities were assessed individually in the spectrophotometer as described elsewhere (Birch-Machin and Turnbull, 2001). Briefly, NADH-dehydrogenase activity rotenone sensitive (CI activity) was measured at 340 nm ($\varepsilon = 6.22\ mM^{-1}cm^{-1}$) in a mix containing 25 mM K_2HPO_4, 5 mM $MgCl_2$, 3 mM KCN, 2.5 mg/ml BSA, pH 7.2; 0.13 mM NADH, 0.13 mM UQ1 and 0.2 µg/ml antimycin A. Rotenone sensitivity was measured under the same conditions adding 5 µM rotenone. Succinate dehydrogenase activity (CII activity) was measured at 600 nm ($\varepsilon = 19.2\ mM^{-1}cm^{-1}$) in a mix containing 25 mM K_2HPO_4, 5 mM $MgCl_2$, 3 mM KCN, 2.5 mg/ml BSA, pH 7.2; 0.03 mM DCPIP (dichlorophenol indophenol), 10 mM succinate, 2 µg/ml antimycin A and 5 µM rotenone. Cytochrome c oxidase activity (COX; CIV activity) was measured at 550 nm ($\varepsilon = 21\ mM^{-1}cm^{-1}$) in a mix containing 100 mM K_2HPO_4 pH 7.4 and reduced cytochrome c (1 mg/ml, freshly made). NADH cytochrome c oxido-reductase activity (CI+III) was measured at 550 nm ($\varepsilon = 21\ mM^{-1}cm^{-1}$) in a mix containing 25 mM K_2HPO_4, 5 mM $MgCl_2$, 3 mM KCN, 2.5 mg/mL BSA, pH 7.2; 0.2 mM KCN, 0.1 mM cytochrome c and 0.1 mM NADH. Succinate cytochrome c oxido-reductase activity (CII+III) was measured at 550 nm ($\varepsilon = 21\ mM^{-1}cm^{-1}$) in a mix containing 25 mM K_2HPO_4, 5 mM $MgCl_2$, 3 mM KCN, 2.5 mg/ml BSA, pH 7.2; 0.2 mM KCN, 0.1 mM cytochrome c, 3 mM succinate and 5 µM rotenone. Citrate synthase activity (CS) was measured at 412 nm ($\varepsilon = 13.6\ mM^{-1}cm^{-1}$) in a

mix containing 10 mM Tris-HCl pH 8, 0.023 mg/ml acetyl CoA, 0.1 mM DTNB (5,5-dithio-bis-2-nitrobenzoic acid), 0.25 mM oxalacetate and 0.1 % Triton X-100.

Seahorse analysis of mitochondrial function

Oxygen consumption was measured in 2 x 10^4 intact cells using a Seahorse Bioscience XF96 extracellular flux analyzer, following manufacturer's instructions. Briefly, after a 12 min equilibration, three measurements of 3 min were performed, separated by 3 minutes of mixing. Maximal membrane potential was assessed by addition of 1 µM oligomycin, and uncoupled mitochondrial respiration was induced by injection of 1 µM CCCP. To stop the mitochondrial dependent oxygen consumption both 1 µM rotenone and antimycin were used.

Fatty acid synthesis assay

Fatty acid synthesis was determined as previously described (Sabbisetti et al., 2009), with some modifications. Briefly, cells were plated in 6-well plate at 3x10^5 cells per dish and incubated overnight. The next day, cells were incubated with 3 µCi of [1-^{14}C] acetate during 4 h. After that, cells were harvested and resuspended in 500 µL of PBS, and 20 µL aliquots were taken to assess protein content. Then, cells were pelleted and lipids were extracted following Folch method, adding 1 mL of chloroform:methanol (2:1) with occasional vortexing. After 20 min incubation, 200 µL of PBS were added, the samples were mixed and centrifuged, and the lower phase was counted for ^{14}C using scintillation counter. Each experiment was performed in triplicates and normalized with protein content.

Protein digestion and iTRAQ labeling

Protein digestion was performed as described (Bonzon-Kulichenko et al., 2011), with minor modifications. The resulting soluble protein extracts from cell lysates or mitochondria-enriched samples were run on a SDS-PAGE gel (10% resolving gel and 4% stacking gel) at 50V. The electrophoresis was stopped when the front dye had barely passed into the resolving gel, ensuring concentration of all proteins into a unique band. Staining was performed using GelCode® Blue Stain Reagent (Thermo Scientific). Gel pieces were cut into cubes (2 mm). For

the protein digestion, modified porcine trypsin (Promega) was added at a final ratio of 1:20 (trypsin-protein). Digestion proceeded overnight at 37 ºC in 100 mM ammonium bicarbonate, pH 8.8. The resulting tryptic peptides were extracted twice by 1 h incubation at room temperature in 100% acetonitrile and 5% formic acid and dried-down. Samples were desalted with C18 RP cartridges and vacuum dried. The concentration of peptides was determined by measuring amide bonds in protein chains with the Direct Detect® Spectrometer (Millipore). A total of 200 µg of each peptide mixture were labeled with different iTRAQ tags according to the manufacturer protocol. LONP1-overxpressed derived samples (LON) were labeled with 115 iTRAQ tag, while the 117 iTRAQ tag was used to label the LONP1-knockdown samples (shLon). The iTRAQ tags 114 and 116 were used to label the corresponding controls, respectively. After labeling, the samples were vacuum dried and finally dissolved in trifluoroacetic acid 1% for both desalting and iTRAQ reagent excess removal in reversed-phase C-18 cartridges.

Identification and quantification of proteins

Tryptic peptide mixtures were subjected to nano-liquid chromatography coupled to mass spectrometry for protein identification and quantification. Peptides were separated on a C-18 reversed phase (RP) nano-column (75 µm I.D. and 50 cm, Acclaim PepMap100, Thermo Scientific) and analyzed in a continuous acetonitrile gradient consisting of 0-30% B in 240 min, 50-90% B in 3 min (B = 90% acetonitrile, 0.5% acetic acid). A flow rate of ca. 200 nL/min was used to elute peptides from the RP nano-column to an emitter nanospray needle for real time ionization and peptide fragmentation on a Q-Exactive mass spectrometer (Thermo Fisher). An enhanced FT-resolution spectrum (resolution=70000) followed by the MS/MS spectra from most intense fifteen parent ions were analyzed along the chromatographic run (272 min). Dynamic exclusion was set at 30 s. For protein identification, tandem mass spectra were extracted and charge state deconvoluted by Proteome Discoverer 1.4.0.288 (Thermo Fisher Scientific). All MS/MS samples were analyzed using SEQUEST^{TM} (Thermo Fisher Scientific). Searching engines were set up to search Mouse_human keratin.fasta (119,718 entries). All searchings were performed assuming full trypsin digestion. Two mixed cleavages were allowed, and an error of 300 ppm or 15 ppm was set for full MS or MS/MS spectra searches, respectively. Oxidation in

M, and deamidation in Q or N were selected as dynamic modifications. Database searching results were analyzed using the probability ratio method (Martínez-Bartolomé et al., 2008) and FDR was calculated using a decoy database and the refined method (Navarro and Vázquez, 2009). Proteins that contained similar peptides and could not be differentiated based on MS/MS analysis alone were grouped to satisfy the principles of parsimony.

Statistical analysis

All experimental data are reported as means and the error bars represent the standard error of the mean (SEM). Differences between mean values were analyzed by two-tailed Student's t test, except in the cases that indicate other statistical test. A value of $P < 0.05$ was considered significant and statistically significant differences are shown with asterisks. All statistical analyses were done using LibreOffice or the statistical package R (http://www.r-project.org/) and the application Rstudio (www.rstudio.org). Statistical analysis of quantitative proteomics data were performed using the QuiXoT package, an in-house developed software based on a statistical model previously described (Jorge et al., 2009). In this model, the accuracy of individual quantifications is taken into account by expressing protein abundance changes in units of standard deviation, using the standardized variable z_q, to which we also refer as the z-score.

ACKNOWLEDGMENTS

We thank J.M. Fraile, J. de la Rosa, A.J. Ramsay, J.M.P. Freije, S. Cal, M. Mittelbrunn and M.T. Fernández-García for helpful comments and advice. We also thank C. Garabaya, A. Moyano, R. Feijoo and I. Martínez for excellent technical assistance, and the Servicio de Histopatología (IUOPA) for histological preparations. This work was supported by grants from Ministerio de Economía y Competitividad-Spain, Ministerio de Ciencia y Educacion-Spain, Instituto de Salud Carlos III (RTICC), Spain and Red Temática de Investigación Cooperativa en Enfermedades Cardiovasculares. The Instituto Universitario de Oncología is supported by Obra Social Cajastur-Asturias. K.W. is supported by the Strategic Young Researcher Overseas Visits Program for Accelerating Brain Circulation from Japan Society for the Promotion of Science. C.L-O. is an Investigator of the Botin Foundation.

FIGURE LEGENDS

Figure 1. Lonp1 deletion causes embryonic lethality. (A) Representative images of Lonp1$^{+/+}$ and Lonp1$^{-/-}$embryos at 8.5 and 9.5 dpc. Scale bar: 1 mm. Right panel shows PCR analysis of Lonp1 embryos' genotypes. (B) Histological analysis of embryos from 5.5 to 7.5 dpc of control and Lonp1-deficient embryos. EX: extraembryonic part; EM: embryonic part; epc: ectoplacental cavity; exc: exocoelomic cavity; ac: amniotic cavity. Scale bar: 100 µm. (C) Analysis of mtDNA quantity expressed as a percentage of levels in control embryos at 3.5 dpc and 7.5 dpc embryos. (n= 10-20), ** $P < 0.01$. (D) Representative images of blastocysts (3.5 dpc embryos) obtained after heterozygous intercrosses of Lonp1 mice. (E) Lonp1-null embryos showed reduced size and delayed development in vitro compared with control blastocysts. ICM: inner cell mass. TB: trophoblastic cells. Scale bar: 50 µm. (F) qPCR and (G) Western-blot analysis of LONP1 expression in MEFs derived from Lonp1$^{+/+}$ and Lonp1$^{+/-}$ mice. ** $P < 0.01$.

Figure 2. Lonp1$^{+/-}$ mice display less susceptibility to AOM-induced colon tumors and skin chemical carcinogenesis induced by DMBA/TPA. (A) Scheme of AOM-induced colon tumor protocol. (B) Percentage of animals with tumors ($P < 0.05$). (C) Average of tumors observed in Lonp1$^{+/+}$ and Lonp1$^{+/-}$ mice. (D) Representative images of H&E staining of colon sections from Lonp1$^{+/+}$ and Lonp1$^{+/-}$ mice at the end of the experiment. Scale bar = 200 µm. (E) Measurement of the length of the colon at the end of the experiment. (F) Clinical score throughout the experiment based on stool consistency and rectal bleeding, as previously described (Wirtz et al., 2007) (n=11-14) * $P < 0.05$. (G) Average number of papillomas per mouse grouped by size (diameter of the lesion in mm), and represented for each genotype, Lonp1$^{+/+}$ (left) and Lonp1$^{+/-}$ (right) (n=10). (H) Inverse Kaplan-Meier analysis of the percentage of mice with papillomas. Log-rank test $P = 0.0439$. (I) Representative pictures of papilloma lesions of Lonp1$^{+/+}$ and Lonp1$^{+/-}$ at week 18. Scale bar = 200 µm.

Figure 3. LONP1 is up-regulated in colon cancer cell lines and colorectal tumors and promotes tumorigenesis in vivo. (A) qPCR analysis of LONP1 expression in colon cancer cell lines, normalized to colon fibroblast and represented with a RQ value. (B) Western-blot analysis and densitometry quantification of LONP1 expression in the same colon cancer cell lines and control colon fibroblasts. (C) Western-blot and densitometry quantification of HCT116 colon cancer cells transduced with LONP1 shRNA vectors (shLon) or with the empty vector as a control (pLKO1), as well as with pMX expressing murine LONP1 (LON) and the empty vector (pMX). LONP1 values correspond to the concomitant expression of endogenous and flagged-transgene. (D) MTT analysis showed decreased proliferation in shLon HCT116 cell lines when compared to control cells; * $P < 0.05$. Tumor xenograft experiments were carried out using HCT116 cells and comparing (E) shLon transduced cells vs. pLKO1 control cells and (F) LONP1 overexpressing cells vs. pMX control cells. Tumor volume was calculated for each group at the indicated times after cancer cells injection, and significant differences were assessed by a linear mixed-effects model; (n=7), * $P < 0.05$. (G) Immunohistochemical analysis of LONP1 expression in normal and tumor colon human samples. (H) Relative expression of LONP1 extracted from a previously reported comparative data set of transcriptomes of 32 adenomas and those of normal mucosa from the same individuals (GEO accession GDS2947) (Sabates-Bellver et al., 2007). (I) Kaplan-Meier survival curves for 64 patients with colorectal cancer expressing high (top 25% of patients) and low (bottom 25% of patients) LONP1 levels. (GSE14333), (Jorissen et al., 2009).

Figure 4. LONP1 expression is essential for tumor development and metastasis formation. (A) Relative expression levels of LONP1 in normal skin, benign nevi and melanoma from data set GDS1375 (Talantov et al., 2005). (B) Kaplan-Meier survival curves for 27 patients with metastatic melanoma expressing high (top 25% of patients) and low (bottom 25% of patients) LONP1 levels. (GSE19234), (Bogunovic et al., 2009). (C) Analysis of LONP1 levels in B16F10-luc2 cells after lentiviral transduction with a control pLKO1 empty vector and shRNA against Lonp1 (shLon) as wells as after retroviral transduction of LON protease (LON) and empty vector pMX, followed by western-blot analysis with densitometry quantification and (D) qPCR

represented with a RQ value. LONP1 levels in the overexpressing cells were the cumulative values of endogenous and flagged-construct expression. (E) MTT analysis showed a decrease in proliferation in shLon B16F10-luc2 cells lines. ** $P < 0.01$. (F) Total number of lung metastasis, generated in the left lung, using pLKO1 control and shLon B16F10-luc2 melanoma cells, and (G) pMX control and overexpression of Lon protease (LON) (n= 10) * $P < 0.05$, *** $P < 0.001$. (F and G; bottom panels) Representative images of lungs at the end of each experiment.

Figure 5. LONP1 controls tumor bioenergetics by remodeling OXPHOS subunits. B16F10 melanoma cells with knockdown (shLon) and overexpression (LON) of Lon protease and their respective controls pLKO1 and pMX were used to study OXPHOS function. (A) Relative ATP levels of the analyzed cells. (B) Oxygen consumption rate (OCR) in basal conditions and after stimulation with FCCP, MRR (maximal respiration rate), represented as OCR per cell relative to each control cell. (C) Percentage of glucose consumption and (D) lactate production during 48 h, relative to control cells. BNGE quantification of OXPHOS subunits (RC complex) using TOM20 as a loading control of isolated mitochondria from (E) shLon and (G) LON cells, relative to each control. BNGE quantification of complexes contained in SC relative to complex free of isolated mitochondria from (F) shLon and (H) LON cells, relative to each control. Combined mitochondrial complexes activities relative to free complexes in order to assess the use of NADH (CI+III/CI) or FAD electron equivalents (CII+III/CII) in (I) shLon cells and (J) LON cells. All experiments were independently carried out at least three times, using triplicates for each cell line; * $P < 0.05$, ** $P < 0.01$, *** $P < 0.001$. (K) Heatmap showing protein abundance changes in subunits of complex I and V, and Lon protease, obtained by high-throughput quantitative proteomics of enriched mitochondrial preparations. The relative abundance changes in LON and shLon cells are expressed using the z-score in relation to each control. ND, not determined.

Figure 6. LONP1 maintains mitochondrial function and promotes a metabolic remodeling process. B16F10 melanoma cells with knockdown (shLon) and overexpression of Lon protease (LON) and their respective controls pLKO1 and pMX were used to study mitochondrial function. (A) Mitochondrial membrane potential ($\Delta\Psi m$) represented as a percentage of TMRM

fluorescence, in normal cells and after CCCP treatment. (B) Mitochondrial DNA (mtDNA) levels represented as percentage relative to each control. (C) Percentage of fragmented mitochondria quantified after mtDsRed2 transfection. (D) ROS levels represented as relative levels of DCF-DA fluorescence. (E) Western-blot analysis showing proteolytic processing of OPA1 long isoforms (a and b) and increase in the short isoforms (c to e), activation of AMPK, and decrease in Bcl-2 in shLon cells. Overexpression of LON causes reduced AMPK activity and an increase in Bcl2 levels. (F) Fatty acid synthesis rate measured as ^{14}C incorporation into cellular lipids represented as relative units (RU). All experiments were independently carried out at least three times, using triplicates for each condition; * $P < 0.05$, *** $P < 0.001$. Heatmap showing abundance changes of proteins belonging to the eukaryotic translation initiation factor 3 (Eif3) and the ribosomal complexes (G), and to the spliceosome, the proteasome and the chaperone-containing T (CCT) complex (H), obtained by high-throughput quantitative proteomics of whole-cell lysates. The relative abundance changes in LON and shLon cells are expressed using the z-score in relation to each control.

Figure 7. LONP1 is necessary to bypass oncogene-induced senescence. (A) Brightfield images of B16F10 melanoma cells used. Scale bar = 100 μm. (B) Percentage of cells positive for β-galactosidase activity as a measure of cellular senescence. (C) Transcriptional qPCR analysis of p53-target genes (Atf3, Gadd45g and Cdkn1a/p21) in these melanoma cells. Data are shown as RQ value. (D) MTT analysis of p53-deficient and wild-type fibroblasts after knockdown of LONP1. The decrease in Lon protease in a background deficient in p53 has less effect than in wild-type background. (E) LONP1 relative expression levels in control, senescence-induced and senescence-bypassed fibroblasts extracted from the data set GSE2484 (Collado et al., 2005). *** $P < 0.001$. (F) Model summarizing the functional relevance of Lon protease in reprogramming mitochondrial activity in cancer.

REFERENCES

Anand, R., Langer, T., and Baker, M.J. (2013). Proteolytic control of mitochondrial function and morphogenesis. Biochim. Biophys. Acta 1833, 195–204.
Andrews, B., Carroll, J., Ding, S., Fearnley, I.M., and Walker, J.E. (2013). Assembly factors for the membrane arm of human complex I. Proc. Natl. Acad. Sci. U. S. A. 110, 18934–18939.
Balbín, M., Fueyo, A., Tester, A.M., Pendás, A.M., Pitiot, A.S., Astudillo, A., Overall, C.M., Shapiro, S.D., and López-Otín, C. (2003). Loss of collagenase-2 confers increased skin tumor susceptibility to male mice. Nat. Genet. 35, 252–257.
Bayot, A., Gareil, M., Rogowska-Wrzesinska, A., Roepstorff, P., Friguet, B., and Bulteau, A.-L. (2010). Identification of novel oxidized protein substrates and physiological partners of the mitochondrial ATP-dependent Lon-like protease Pim1. J. Biol. Chem. 285, 11445–11457.
Benard, G., Bellance, N., James, D., Parrone, P., Fernandez, H., Letellier, T., and Rossignol, R. (2007). Mitochondrial bioenergetics and structural network organization. J. Cell Sci. 120, 838–848.
Bernstein, S.H., Venkatesh, S., Li, M., Lee, J., Lu, B., Hilchey, S.P., Morse, K.M., Metcalfe, H.M., Skalska, J., Andreeff, M., et al. (2012). The mitochondrial ATP-dependent Lon protease: a novel target in lymphoma death mediated by the synthetic triterpenoid CDDO and its derivatives. Blood 119, 3321–3329.
Bhalla, K., Hwang, B.J., Dewi, R.E., Ou, L., Twaddel, W., Fang, H.-B., Vafai, S.B., Vazquez, F., Puigserver, P., Boros, L., et al. (2011). PGC1α promotes tumor growth by inducing gene expression programs supporting lipogenesis. Cancer Res. 71, 6888–6898.
Birch-Machin, M.A., and Turnbull, D.M. (2001). Assaying mitochondrial respiratory complex activity in mitochondria isolated from human cells and tissues. Methods Cell Biol. 65, 97–117.
Bogunovic, D., O'Neill, D.W., Belitskaya-Levy, I., Vacic, V., Yu, Y.-L., Adams, S., Darvishian, F., Berman, R., Shapiro, R., Pavlick, A.C., et al. (2009). Immune profile and mitotic index of metastatic melanoma lesions enhance clinical staging in predicting patient survival. Proc. Natl. Acad. Sci. U. S. A. 106, 20429–20434.
Bonora, E., Porcelli, A.M., Gasparre, G., Biondi, A., Ghelli, A., Carelli, V., Baracca, A., Tallini, G., Martinuzzi, A., Lenaz, G., et al. (2006). Defective oxidative phosphorylation in thyroid oncocytic carcinoma is associated with pathogenic mitochondrial DNA mutations affecting complexes I and III. Cancer Res. 66, 6087–6096.
Bonzon-Kulichenko, E., Pérez-Hernández, D., Núñez, E., Martínez-Acedo, P., Navarro, P., Trevisan-Herraz, M., Ramos, M. del C., Sierra, S., Martínez-Martínez, S., Ruiz-Meana, M., et al. (2011). A robust method for quantitative high-throughput analysis of proteomes by 18O labeling. Mol. Cell. Proteomics 10, M110.003335.
Bota, D. a, and Davies, K.J. a (2002). Lon protease preferentially degrades oxidized mitochondrial aconitase by an ATP-stimulated mechanism. Nat. Cell Biol. 4, 674–680.
Bota, D. a, Ngo, J.K., and Davies, K.J. a (2005). Downregulation of the human Lon protease impairs mitochondrial structure and function and causes cell death. Free Radic. Biol. Med. 38, 665–677.
Bricker, D.K., Taylor, E.B., Schell, J.C., Orsak, T., Boutron, A., Chen, Y.-C., Cox, J.E., Cardon, C.M., Van Vranken, J.G., Dephoure, N., et al. (2012). A mitochondrial pyruvate carrier required for pyruvate uptake in yeast, Drosophila, and humans. Science 337, 96–100.

Bulteau, A.-L., and Bayot, A. (2011). Mitochondrial proteases and cancer. Biochim. Biophys. Acta 1807, 595–601.
Butow, R.A., and Avadhani, N.G. (2004). Mitochondrial signaling: the retrograde response. Mol. Cell 14, 1–15.
Chae, Y.C., Caino, M.C., Lisanti, S., Ghosh, J.C., Dohi, T., Danial, N.N., Villanueva, J., Ferrero, S., Vaira, V., Santambrogio, L., et al. (2012). Control of tumor bioenergetics and survival stress signaling by mitochondrial HSP90s. Cancer Cell 22, 331–344.
Cheng, C.-W., Kuo, C.-Y., Fan, C.-C., Fang, W.-C., Jiang, S.S., Lo, Y.-K., Wang, T.-Y., Kao, M.-C., and Lee, A.Y.-L. (2013). Overexpression of Lon contributes to survival and aggressive phenotype of cancer cells through mitochondrial complex I-mediated generation of reactive oxygen species. Cell Death Dis. 4, e681.
Cheng, X., Kanki, T., Fukuoh, A., Ohgaki, K., Takeya, R., Aoki, Y., Hamasaki, N., and Kang, D. (2005). PDIP38 associates with proteins constituting the mitochondrial DNA nucleoid. J. Biochem. 138, 673–678.
Cipolat, S., Rudka, T., Hartmann, D., Costa, V., Serneels, L., Craessaerts, K., Metzger, K., Frezza, C., Annaert, W., Derks, C., et al. (2006). Mitochondrial rhomboid PARL regulates cytochrome c release during apoptosis via OPA1-dependent cristae remodeling. Cell 126, 163–175.
Cogliati, S., Frezza, C., Soriano, M.E., Varanita, T., Quintana-Cabrera, R., Corrado, M., Cipolat, S., Costa, V., Casarin, A., Gomes, L.C., et al. (2013). Mitochondrial cristae shape determines respiratory chain supercomplexes assembly and respiratory efficiency. Cell 155, 160–171.
Collado, M., Gil, J., Efeyan, A., Guerra, C., Schuhmacher, A.J., Barradas, M., Benguría, A., Zaballos, A., Flores, J.M., Barbacid, M., et al. (2005). Tumour biology: senescence in premalignant tumours. Nature 436, 642.
Dieteren, C.E.J., Koopman, W.J.H., Swarts, H.G., Peters, J.G.P., Maczuga, P., van Gemst, J.J., Masereeuw, R., Smeitink, J.A.M., Nijtmans, L.G.J., and Willems, P.H.G.M. (2012). Subunit-specific incorporation efficiency and kinetics in mitochondrial complex I homeostasis. J. Biol. Chem. 287, 41851–41860.
Erjavec, N., Bayot, A., Gareil, M., Camougrand, N., Nystrom, T., Friguet, B., and Bulteau, A.-L. (2013). Deletion of the mitochondrial Pim1/Lon protease in yeast results in accelerated aging and impairment of the proteasome. Free Radic. Biol. Med. 56, 9–16.
Felk, S., Ohrt, S., Kussmaul, L., Storch, A., and Gillardon, F. (2010). Activation of the mitochondrial protein quality control system and actin cytoskeletal alterations in cells harbouring the MELAS mitochondrial DNA mutation. J. Neurol. Sci. 295, 46–52.
Formentini, L., Sánchez-Aragó, M., Sánchez-Cenizo, L., and Cuezva, J.M. (2012). The mitochondrial ATPase inhibitory factor 1 triggers a ROS-mediated retrograde prosurvival and proliferative response. Mol. Cell 45, 731–742.
Fraile, J.M., Quesada, V., Rodríguez, D., Freije, J.M.P., and López-Otín, C. (2011). Deubiquitinases in cancer: new functions and therapeutic options. Oncogene 31, 2373–2388.
Fraile, J.M., Ordóñez, G.R., Quirós, P.M., Astudillo, A., Galván, J.A., Colomer, D., López-Otín, C., Freije, J.M.P., and Puente, X.S. (2013). Identification of novel tumor suppressor proteases by degradome profiling of colorectal carcinomas. Oncotarget 4, 1931–1932.
Freije, J.M.P., Fraile, J.M., and López-Otín, C. (2011). Protease addiction and synthetic lethality in cancer. Front. Oncol. 1, 25.

Fu, G.K., and Markovitz, D.M. (1998). The human LON protease binds to mitochondrial promoters in a single-stranded, site-specific, strand-specific manner. Biochemistry 37, 1905–1909.
Fukada, K., Zhang, F., Vien, A., Cashman, N.R., and Zhu, H. (2004). Mitochondrial proteomic analysis of a cell line model of familial amyotrophic lateral sclerosis. Mol. Cell. Proteomics 3, 1211–1223.
Fukuda, R., Zhang, H., Kim, J., Shimoda, L., Dang, C. V, and Semenza, G.L. (2007). HIF-1 regulates cytochrome oxidase subunits to optimize efficiency of respiration in hypoxic cells. Cell 129, 111–122.
Galluzzi, L., Kepp, O., and Kroemer, G. (2012). Mitochondria: master regulators of danger signalling. Nat. Rev. Mol. Cell Biol. 13, 780–788.
García-Ruiz, I., Solís-Muñoz, P., Fernández-Moreira, D., Muñoz-Yagüe, T., and Solís-Herruzo, J.A. (2013). Pioglitazone leads to an inactivation and disassembly of complex I of the mitochondrial respiratory chain. BMC Biol. 11, 88.
Gardner, P.R., Nguyen, D.D., and White, C.W. (1994). Aconitase is a sensitive and critical target of oxygen poisoning in cultured mammalian cells and in rat lungs. Proc. Natl. Acad. Sci. U. S. A. 91, 12248–12252.
Gasparre, G., Porcelli, A.M., Bonora, E., Pennisi, L.F., Toller, M., Iommarini, L., Ghelli, A., Moretti, M., Betts, C.M., Martinelli, G.N., et al. (2007). Disruptive mitochondrial DNA mutations in complex I subunits are markers of oncocytic phenotype in thyroid tumors. Proc. Natl. Acad. Sci. U. S. A. 104, 9001–9006.
Granot, Z., Kobiler, O., Melamed-Book, N., Eimerl, S., Bahat, A., Lu, B., Braun, S., Maurizi, M.R., Suzuki, C.K., Oppenheim, A.B., et al. (2007). Turnover of mitochondrial steroidogenic acute regulatory (StAR) protein by Lon protease: the unexpected effect of proteasome inhibitors. Mol. Endocrinol. 21, 2164–2177.
Guillon, B., Bulteau, A.-L., Wattenhofer-Donzé, M., Schmucker, S., Friguet, B., Puccio, H., Drapier, J.-C., and Bouton, C. (2009). Frataxin deficiency causes upregulation of mitochondrial Lon and ClpP proteases and severe loss of mitochondrial Fe-S proteins. FEBS J. 276, 1036–1047.
Gutiérrez-Fernández, A., Fueyo, A., Folgueras, A.R., Garabaya, C., Pennington, C.J., Pilgrim, S., Edwards, D.R., Holliday, D.L., Jones, J.L., Span, P.N., et al. (2008). Matrix metalloproteinase-8 functions as a metastasis suppressor through modulation of tumor cell adhesion and invasion. Cancer Res. 68, 2755–2763.
Hanahan, D., and Weinberg, R.A. (2011). Hallmarks of cancer: the next generation. Cell 144, 646–674.
Hance, N., Ekstrand, M.I., and Trifunovic, A. (2005). Mitochondrial DNA polymerase gamma is essential for mammalian embryogenesis. Hum. Mol. Genet. 14, 1775–1783.
Hansen, J., Corydon, T.J., Palmfeldt, J., Dürr, a, Fontaine, B., Nielsen, M.N., Christensen, J.H., Gregersen, N., and Bross, P. (2008). Decreased expression of the mitochondrial matrix proteases Lon and ClpP in cells from a patient with hereditary spastic paraplegia (SPG13). Neuroscience 153, 474–482.
Haq, R., Shoag, J., Andreu-Perez, P., Yokoyama, S., Edelman, H., Rowe, G.C., Frederick, D.T., Hurley, A.D., Nellore, A., Kung, A.L., et al. (2013). Oncogenic BRAF regulates oxidative metabolism via PGC1α and MITF. Cancer Cell 23, 302–315.

Vander Heiden, M.G., Cantley, L.C., and Thompson, C.B. (2009). Understanding the Warburg effect: the metabolic requirements of cell proliferation. Science 324, 1029–1033.
Herzig, S., Raemy, E., Montessuit, S., Veuthey, J.-L., Zamboni, N., Westermann, B., Kunji, E.R.S., and Martinou, J.-C. (2012). Identification and functional expression of the mitochondrial pyruvate carrier. Science 337, 93–96.
Hori, O., Ichinoda, F., Tamatani, T., Yamaguchi, A., Sato, N., Ozawa, K., Kitao, Y., Miyazaki, M., Harding, H.P., Ron, D., et al. (2002). Transmission of cell stress from endoplasmic reticulum to mitochondria: enhanced expression of Lon protease. J. Cell Biol. 157, 1151–1160.
Hsu, P.P., and Sabatini, D.M. (2008). Cancer cell metabolism: Warburg and beyond. Cell 134, 703–707.
Hu, J., Bianchi, F., Ferguson, M., Cesario, A., Margaritora, S., Granone, P., Goldstraw, P., Tetlow, M., Ratcliffe, C., Nicholson, A.G., et al. (2005). Gene expression signature for angiogenic and nonangiogenic non-small-cell lung cancer. Oncogene 24, 1212–1219.
Hu, Y., Lu, W., Chen, G., Wang, P., Chen, Z., Zhou, Y., Ogasawara, M., Trachootham, D., Feng, L., Pelicano, H., et al. (2012). K-ras(G12V) transformation leads to mitochondrial dysfunction and a metabolic switch from oxidative phosphorylation to glycolysis. Cell Res. 22, 399–412.
Huang, G., Lu, H., Hao, A., Ng, D.C.H., Ponniah, S., Guo, K., Lufei, C., Zeng, Q., and Cao, X. (2004). GRIM-19, a cell death regulatory protein, is essential for assembly and function of mitochondrial complex I. Mol. Cell. Biol. 24, 8447–8456.
Humble, M.M., Young, M.J., Foley, J.F., Pandiri, A.R., Travlos, G.S., and Copeland, W.C. (2013). Polg2 is essential for mammalian embryogenesis and is required for mtDNA maintenance. Hum. Mol. Genet. 22, 1017–1025.
Jorge, I., Navarro, P., Martínez-Acedo, P., Núñez, E., Serrano, H., Alfranca, A., Redondo, J.M., and Vázquez, J. (2009). Statistical model to analyze quantitative proteomics data obtained by 18O/16O labeling and linear ion trap mass spectrometry: application to the study of vascular endothelial growth factor-induced angiogenesis in endothelial cells. Mol. Cell. Proteomics 8, 1130–1149.
Jorissen, R.N., Gibbs, P., Christie, M., Prakash, S., Lipton, L., Desai, J., Kerr, D., Aaltonen, L.A., Arango, D., Kruhøffer, M., et al. (2009). Metastasis-Associated Gene Expression Changes Predict Poor Outcomes in Patients with Dukes Stage B and C Colorectal Cancer. Clin. Cancer Res. 15, 7642–7651.
Kita, K., Suzuki, T., and Ochi, T. (2012). Diphenylarsinic acid promotes degradation of glutaminase C by mitochondrial Lon protease. J. Biol. Chem. 287, 18163–18172.
Kleivi, K., Teixeira, M.R., Eknaes, M., Diep, C.B., Jakobsen, K.S., Hamelin, R., and Lothe, R.A. (2004). Genome signatures of colon carcinoma cell lines. Cancer Genet. Cytogenet. 155, 119–131.
Landor, S.K.-J., Mutvei, A.P., Mamaeva, V., Jin, S., Busk, M., Borra, R., Grönroos, T.J., Kronqvist, P., Lendahl, U., and Sahlgren, C.M. (2011). Hypo- and hyperactivated Notch signaling induce a glycolytic switch through distinct mechanisms. Proc. Natl. Acad. Sci. U. S. A. 108, 18814–18819.
Lapuente-Brun, E., Moreno-Loshuertos, R., Acin-Perez, R., Latorre-Pellicer, A., Colas, C., Balsa, E., Perales-Clemente, E., Quiros, P.M., Calvo, E., Rodriguez-Hernandez, M.A., et al. (2013). Supercomplex Assembly Determines Electron Flux in the Mitochondrial Electron Transport

Chain. Science (80-.). 340, 1567–1570.
Larsson, N.G., Wang, J., Wilhelmsson, H., Oldfors, A., Rustin, P., Lewandoski, M., Barsh, G.S., and Clayton, D.A. (1998). Mitochondrial transcription factor A is necessary for mtDNA maintenance and embryogenesis in mice. Nat. Genet. 18, 231–236.
Lazarou, M., McKenzie, M., Ohtake, A., Thorburn, D.R., and Ryan, M.T. (2007). Analysis of the assembly profiles for mitochondrial- and nuclear-DNA-encoded subunits into complex I. Mol. Cell. Biol. 27, 4228–4237.
Liu, T., Lu, B., Lee, I., Ondrovicová, G., Kutejová, E., and Suzuki, C.K. (2004). DNA and RNA binding by the mitochondrial lon protease is regulated by nucleotide and protein substrate. J. Biol. Chem. 279, 13902–13910.
Locasale, J.W., Grassian, A.R., Melman, T., Lyssiotis, C.A., Mattaini, K.R., Bass, A.J., Heffron, G., Metallo, C.M., Muranen, T., Sharfi, H., et al. (2011). Phosphoglycerate dehydrogenase diverts glycolytic flux and contributes to oncogenesis. Nat. Genet. 43, 869–874.
Lopez-Otin, C., Blasco, M., Partridge, L., Serrano, M., and Kroemer, G. (2013). The Hallmarks of Aging. Cell 153, 1194–1209.
López-Ríos, F., Sánchez-Aragó, M., García-García, E., Ortega, A.D., Berrendero, J.R., Pozo-Rodríguez, F., López-Encuentra, A., Ballestín, C., and Cuezva, J.M. (2007). Loss of the mitochondrial bioenergetic capacity underlies the glucose avidity of carcinomas. Cancer Res. 67, 9013–9017.
Loublier, S., Bayot, A., Rak, M., El-Khoury, R., Bénit, P., and Rustin, P. (2011). The NDUFB6 subunit of the mitochondrial respiratory chain complex I is required for electron transfer activity: a proof of principle study on stable and controlled RNA interference in human cell lines. Biochem. Biophys. Res. Commun. 414, 367–372.
Lu, B., Liu, T., Crosby, J. a., Thomas-Wohlever, J., Lee, I., and Suzuki, C.K. (2003). The ATP-dependent Lon protease of Mus musculus is a DNA-binding protein that is functionally conserved between yeast and mammals. Gene 306, 45–55.
Lu, B., Lee, J., Nie, X., Li, M., Morozov, Y.I., Venkatesh, S., Bogenhagen, D.F., Temiakov, D., and Suzuki, C.K. (2013). Phosphorylation of human TFAM in mitochondria impairs DNA binding and promotes degradation by the AAA+ Lon protease. Mol. Cell 49, 121–132.
Lu, W., Hu, Y., Chen, G., Chen, Z., Zhang, H., Wang, F., Feng, L., Pelicano, H., Wang, H., Keating, M.J., et al. (2012). Novel role of NOX in supporting aerobic glycolysis in cancer cells with mitochondrial dysfunction and as a potential target for cancer therapy. PLoS Biol. 10, e1001326.
Martínez-Bartolomé, S., Navarro, P., Martín-Maroto, F., López-Ferrer, D., Ramos-Fernández, A., Villar, M., García-Ruiz, J.P., and Vázquez, J. (2008). Properties of average score distributions of SEQUEST: the probability ratio method. Mol. Cell. Proteomics 7, 1135–1145.
Matsushima, Y., Goto, Y., and Kaguni, L.S. (2010). Mitochondrial Lon protease regulates mitochondrial DNA copy number and transcription by selective degradation of mitochondrial transcription factor A (TFAM). Proc. Natl. Acad. Sci. U. S. A. 107, 18410–18415.
Metallo, C.M., and Vander Heiden, M.G. (2013). Understanding metabolic regulation and its influence on cell physiology. Mol. Cell 49, 388–398.
Michaloglou, C., Vredeveld, L.C.W., Soengas, M.S., Denoyelle, C., Kuilman, T., van der Horst, C.M.A.M., Majoor, D.M., Shay, J.W., Mooi, W.J., and Peeper, D.S. (2005). BRAFE600-

associated senescence-like cell cycle arrest of human naevi. Nature 436, 720–724.
Mitsuishi, Y., Taguchi, K., Kawatani, Y., Shibata, T., Nukiwa, T., Aburatani, H., Yamamoto, M., and Motohashi, H. (2012). Nrf2 redirects glucose and glutamine into anabolic pathways in metabolic reprogramming. Cancer Cell 22, 66–79.
Moreno-Loshuertos, R., Acín-Pérez, R., Fernández-Silva, P., Movilla, N., Pérez-Martos, A., Rodriguez de Cordoba, S., Gallardo, M.E., and Enríquez, J.A. (2006). Differences in reactive oxygen species production explain the phenotypes associated with common mouse mitochondrial DNA variants. Nat. Genet. 38, 1261–1268.
Murphy, M.P. (2009). How mitochondria produce reactive oxygen species. Biochem. J. 417, 1–13.
Nagy, A., Gertsenstein, M., Vintersten, K., and Behringer, R. (2003). Manipulating the mouse embryo: a laboratory manual (Cold Spring Harbor Laboratory Press).
Navarro, P., and Vázquez, J. (2009). A refined method to calculate false discovery rates for peptide identification using decoy databases. J. Proteome Res. 8, 1792–1796.
Neufert, C., Becker, C., and Neurath, M.F. (2007). An inducible mouse model of colon carcinogenesis for the analysis of sporadic and inflammation-driven tumor progression. Nat. Protoc. 2, 1998–2004.
Ngo, J.K., and Davies, K.J. a (2007). Importance of the lon protease in mitochondrial maintenance and the significance of declining lon in aging. Ann. N. Y. Acad. Sci. 1119, 78–87.
Ngo, J.K., Pomatto, L.C.D., Bota, D.A., Koop, A.L., and Davies, K.J.A. (2011). Impairment of lon-induced protection against the accumulation of oxidized proteins in senescent wi-38 fibroblasts. J. Gerontol. A. Biol. Sci. Med. Sci. 66, 1178–1185.
Nijtmans, L.G.J., Henderson, N.S., and Holt, I.J. (2002). Blue Native electrophoresis to study mitochondrial and other protein complexes. Methods 26, 327–334.
Perales-Clemente, E., Fernández-Vizarra, E., Acín-Pérez, R., Movilla, N., Bayona-Bafaluy, M.P., Moreno-Loshuertos, R., Pérez-Martos, A., Fernández-Silva, P., and Enríquez, J.A. (2010). Five entry points of the mitochondrially encoded subunits in mammalian complex I assembly. Mol. Cell. Biol. 30, 3038–3047.
Quirós, P.M., Ramsay, A.J., Sala, D., Fernández-Vizarra, E., Rodríguez, F., Peinado, J.R., Fernández-García, M.S., Vega, J. a, Enríquez, J. a, Zorzano, A., et al. (2012). Loss of mitochondrial protease OMA1 alters processing of the GTPase OPA1 and causes obesity and defective thermogenesis in mice. EMBO J. 31, 2117–2133.
Rizzuto, R., De Stefani, D., Raffaello, A., and Mammucari, C. (2012). Mitochondria as sensors and regulators of calcium signalling. Nat. Rev. Mol. Cell Biol. 13, 566–578.
Rodríguez, D., Ramsay, A.J., Quesada, V., Garabaya, C., Campo, E., Freije, J.M.P., and López-Otín, C. (2013). Functional analysis of sucrase-isomaltase mutations from chronic lymphocytic leukemia patients. Hum. Mol. Genet. 22, 2273–2282.
Rossignol, R., Gilkerson, R., Aggeler, R., Yamagata, K., Remington, S.J., and Capaldi, R.A. (2004). Energy substrate modulates mitochondrial structure and oxidative capacity in cancer cells. Cancer Res. 64, 985–993.
Rugarli, E.I., and Langer, T. (2012). Mitochondrial quality control: a matter of life and death for neurons. EMBO J. 31, 1336–1349.
Sabates-Bellver, J., Van der Flier, L.G., de Palo, M., Cattaneo, E., Maake, C., Rehrauer, H.,

Laczko, E., Kurowski, M.A., Bujnicki, J.M., Menigatti, M., et al. (2007). Transcriptome profile of human colorectal adenomas. Mol. Cancer Res. 5, 1263–1275.
Sabbisetti, V., Di Napoli, A., Seeley, A., Amato, A.M., O'Regan, E., Ghebremichael, M., Loda, M., and Signoretti, S. (2009). p63 promotes cell survival through fatty acid synthase. PLoS One 4, e5877.
Santidrian, A.F., Matsuno-Yagi, A., Ritland, M., Seo, B.B., LeBoeuf, S.E., Gay, L.J., Yagi, T., and Felding-Habermann, B. (2013). Mitochondrial complex I activity and NAD+/NADH balance regulate breast cancer progression. J. Clin. Invest. 123, 1068–1081.
Schägger, H. (1995). Native electrophoresis for isolation of mitochondrial oxidative phosphorylation protein complexes. Methods Enzymol. 260, 190–202.
Sena, L.A., and Chandel, N.S. (2012). Physiological roles of mitochondrial reactive oxygen species. Mol. Cell 48, 158–167.
Serrano, M., Lin, A.W., McCurrach, M.E., Beach, D., and Lowe, S.W. (1997). Oncogenic ras provokes premature cell senescence associated with accumulation of p53 and p16INK4a. Cell 88, 593–602.
Stanyer, L., Jorgensen, W., Hori, O., Clark, J.B., and Heales, S.J.R. (2008). Inactivation of brain mitochondrial Lon protease by peroxynitrite precedes electron transport chain dysfunction. Neurochem. Int. 53, 95–101.
Talantov, D., Mazumder, A., Yu, J.X., Briggs, T., Jiang, Y., Backus, J., Atkins, D., and Wang, Y. (2005). Novel genes associated with malignant melanoma but not benign melanocytic lesions. Clin. Cancer Res. 11, 7234–7242.
Tatsuta, T. (2009). Protein quality control in mitochondria. J. Biochem. 146, 455–461.
Tian, Q., Li, T., Hou, W., Zheng, J., Schrum, L.W., and Bonkovsky, H.L. (2011). Lon peptidase 1 (LONP1)-dependent breakdown of mitochondrial 5-aminolevulinic acid synthase protein by heme in human liver cells. J. Biol. Chem. 286, 26424–26430.
Vazquez, F., Lim, J.-H., Chim, H., Bhalla, K., Girnun, G., Pierce, K., Clish, C.B., Granter, S.R., Widlund, H.R., Spiegelman, B.M., et al. (2013). PGC1α expression defines a subset of human melanoma tumors with increased mitochondrial capacity and resistance to oxidative stress. Cancer Cell 23, 287–301.
Venkatesh, S., Lee, J., Singh, K., Lee, I., and Suzuki, C.K. (2012). Multitasking in the mitochondrion by the ATP-dependent Lon protease. Biochim. Biophys. Acta 1823, 56–66.
Voos, W. (2013). Chaperone-protease networks in mitochondrial protein homeostasis. Biochim. Biophys. Acta 1833, 388–399.
Wallace, D.C. (2005). A mitochondrial paradigm of metabolic and degenerative diseases, aging, and cancer: a dawn for evolutionary medicine. Annu. Rev. Genet. 39, 359–407.
Wallace, D.C. (2011). Bioenergetic origins of complexity and disease. Cold Spring Harb. Symp. Quant. Biol. 76, 1–16.
Wallace, D.C. (2012). Mitochondria and cancer. Nat. Rev. Cancer 12, 685–698.
Wallace, D.C., Fan, W., and Procaccio, V. (2010). Mitochondrial energetics and therapeutics. Annu. Rev. Pathol. 5, 297–348.
Ward, P.S., and Thompson, C.B. (2012). Metabolic reprogramming: a cancer hallmark even warburg did not anticipate. Cancer Cell 21, 297–308.
Wirtz, S., Neufert, C., Weigmann, B., and Neurath, M.F. (2007). Chemically induced mouse

models of intestinal inflammation. Nat. Protoc. 2, 541–546.
Wu, S.-B., Ma, Y.-S., Wu, Y.-T., Chen, Y.-C., and Wei, Y.-H. (2010). Mitochondrial DNA mutation-elicited oxidative stress, oxidative damage, and altered gene expression in cultured cells of patients with MERRF syndrome. Mol. Neurobiol. 41, 256–266.
Yan, H., Parsons, D.W., Jin, G., McLendon, R., Rasheed, B.A., Yuan, W., Kos, I., Batinic-Haberle, I., Jones, S., Riggins, G.J., et al. (2009). IDH1 and IDH2 mutations in gliomas. N. Engl. J. Med. 360, 765–773.
Yang, H., Brosel, S., Acin-Perez, R., Slavkovich, V., Nishino, I., Khan, R., Goldberg, I.J., Graziano, J., Manfredi, G., and Schon, E. a (2010). Analysis of mouse models of cytochrome c oxidase deficiency owing to mutations in Sco2. Hum. Mol. Genet. 19, 170–180.
Zhang, W.C., Shyh-Chang, N., Yang, H., Rai, A., Umashankar, S., Ma, S., Soh, B.S., Sun, L.L., Tai, B.C., Nga, M.E., et al. (2012). Glycine decarboxylase activity drives non-small cell lung cancer tumor-initiating cells and tumorigenesis. Cell 148, 259–272.

Table 1. Comparison of mitochondrial activities of individual and associated OXPHOS complexes, measured as specific activity (IU/mg) and relative to the citrate synthase activity.

		pLKO1	shLon		pMX	LON	
Specific activity (IU/mg)	**CI**	1.00 ± 0.05	0.66 ± 0.04	***	1.00 ± 0.09	1.23 ± 0.19	
	CII	1.00 ± 0.03	0.93 ± 0.09		1.00 ± 0.02	0.75 ± 0.04	**
	CI+III	1.00 ± 0.08	0.84 ± 0.17		1.00 ± 0.06	0.76 ± 0.03	**
	CII+III	1.00 ± 0.08	0.73 ± 0.08	**	1.00 ± 0.04	0.67 ± 0.07	***
	COX	1.00 ± 0.11	0.96 ± 0.16		1.00 ± 0.11	0.69 ± 0.11	**
	CS	1.00 ± 0.09	0.95 ± 0.07		1.00 ± 0.10	1.16 ± 0.18	
Specific activity relative to CS	**CI**	1.00 ± 0.10	0.70 ± 0.07	***	1.00 ± 0.06	1.16 ± 0.18	
	CII	1.00 ± 0.11	0.99 ± 0.14		1.00 ± 0.11	0.72 ± 0.15	**
	CI+III	1.00 ± 0.08	0.88 ± 0.13		1.00 ± 0.10	0.72 ± 0.15	**
	CII+III	1.00 ± 0.10	0.77 ± 0.10	***	1.00 ± 0.11	0.66 ± 0.21	**
	COX	1.00 ± 0.08	1.01 ± 0.12		1.00 ± 0.03	0.70 ± 0.15	**

Data shown correspond to three independent experiments carried out in triplicated. Statistical significance was performed by analysis of variance (ANOVA). Paired differences were assessed by the post hoc Fisher's protected least significant difference test (PLSD). CI: complex I; CII: complex II; CIII: complex III; COX: complex IV; CS: citrate synthase. ** $P < 0.01$; *** $P < 0.001$.

Figures

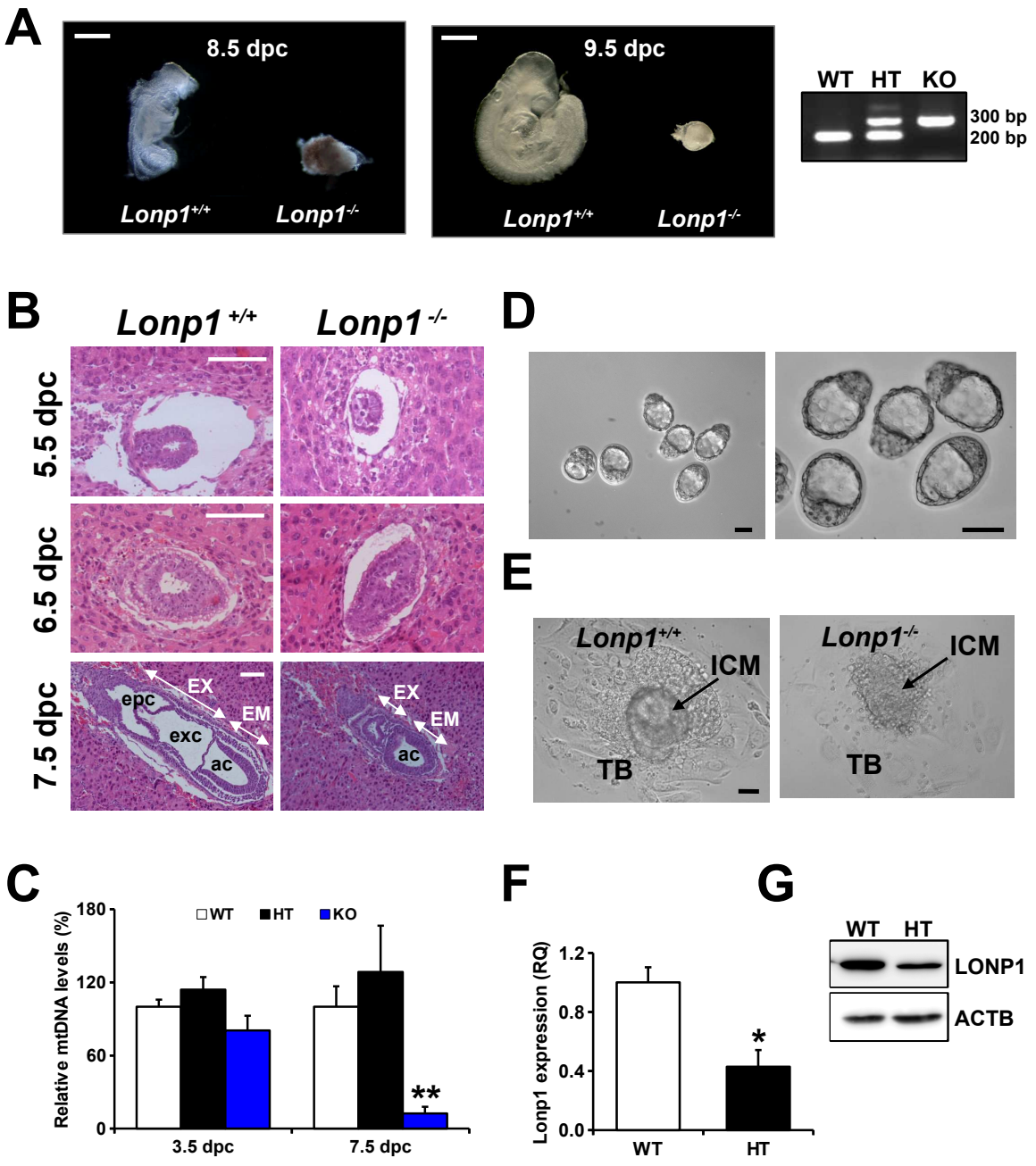

Figure 1; Quiros et al.

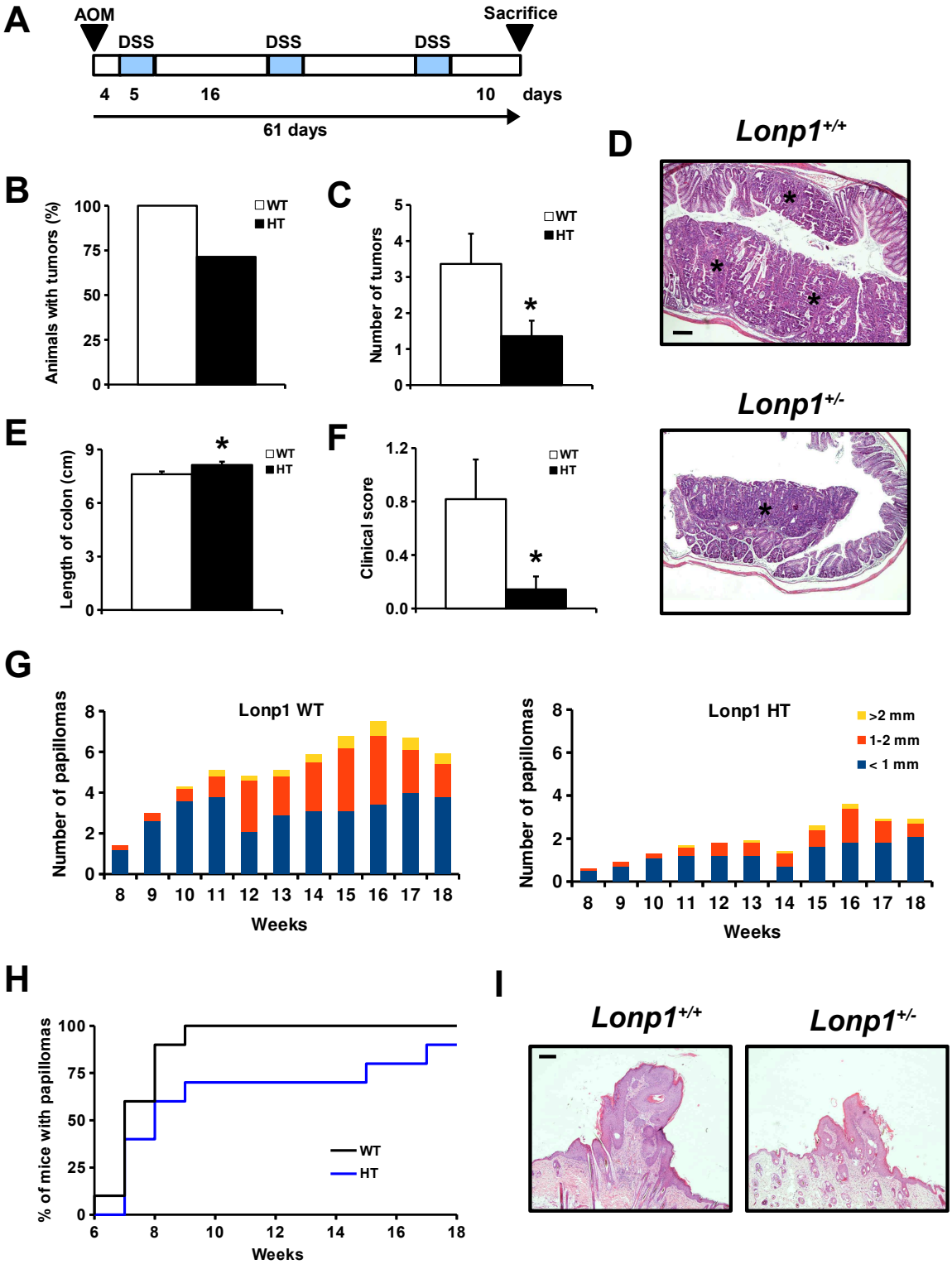

Figure 2; Quiros et al.

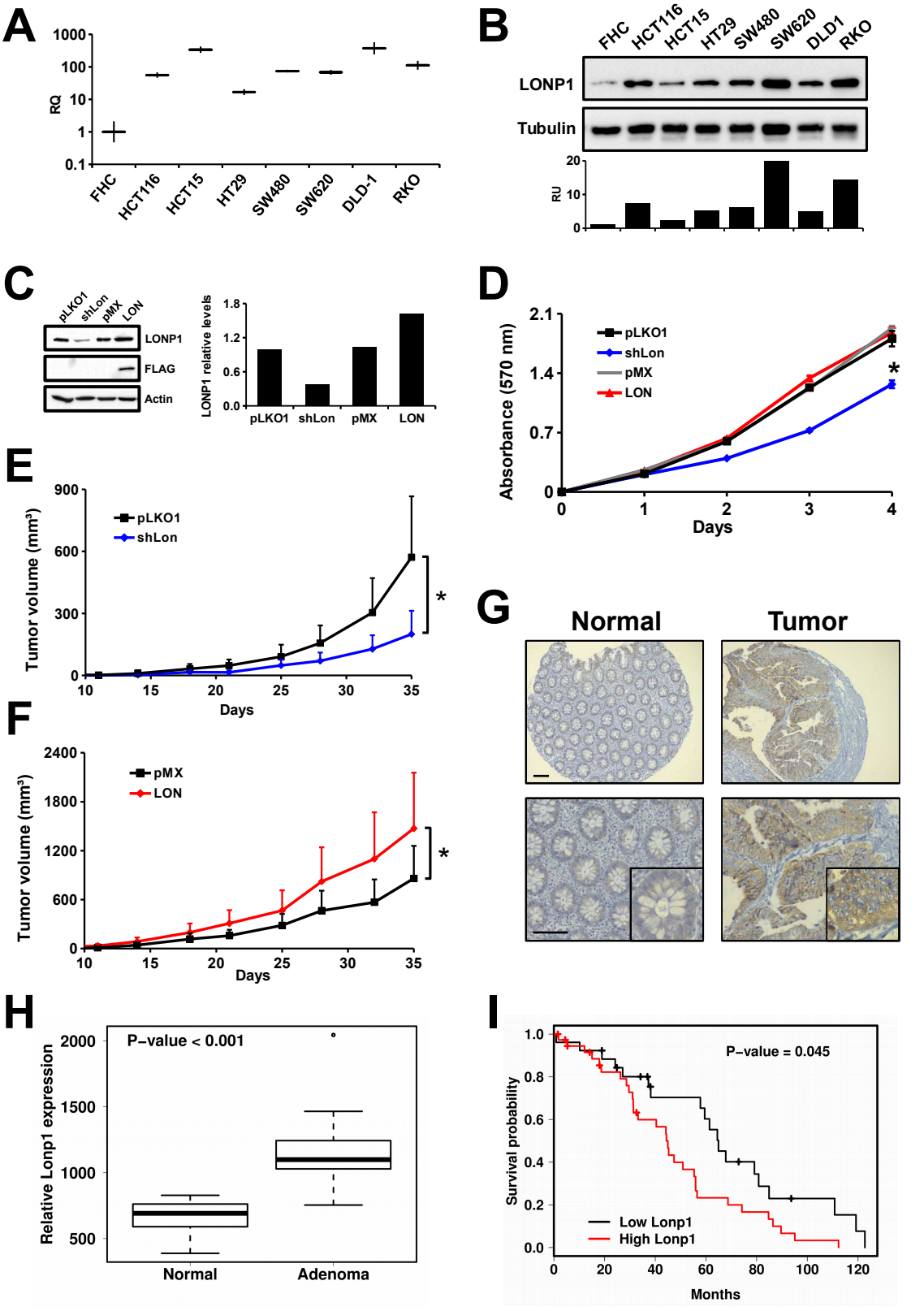

Figure 3; Quiros et al.

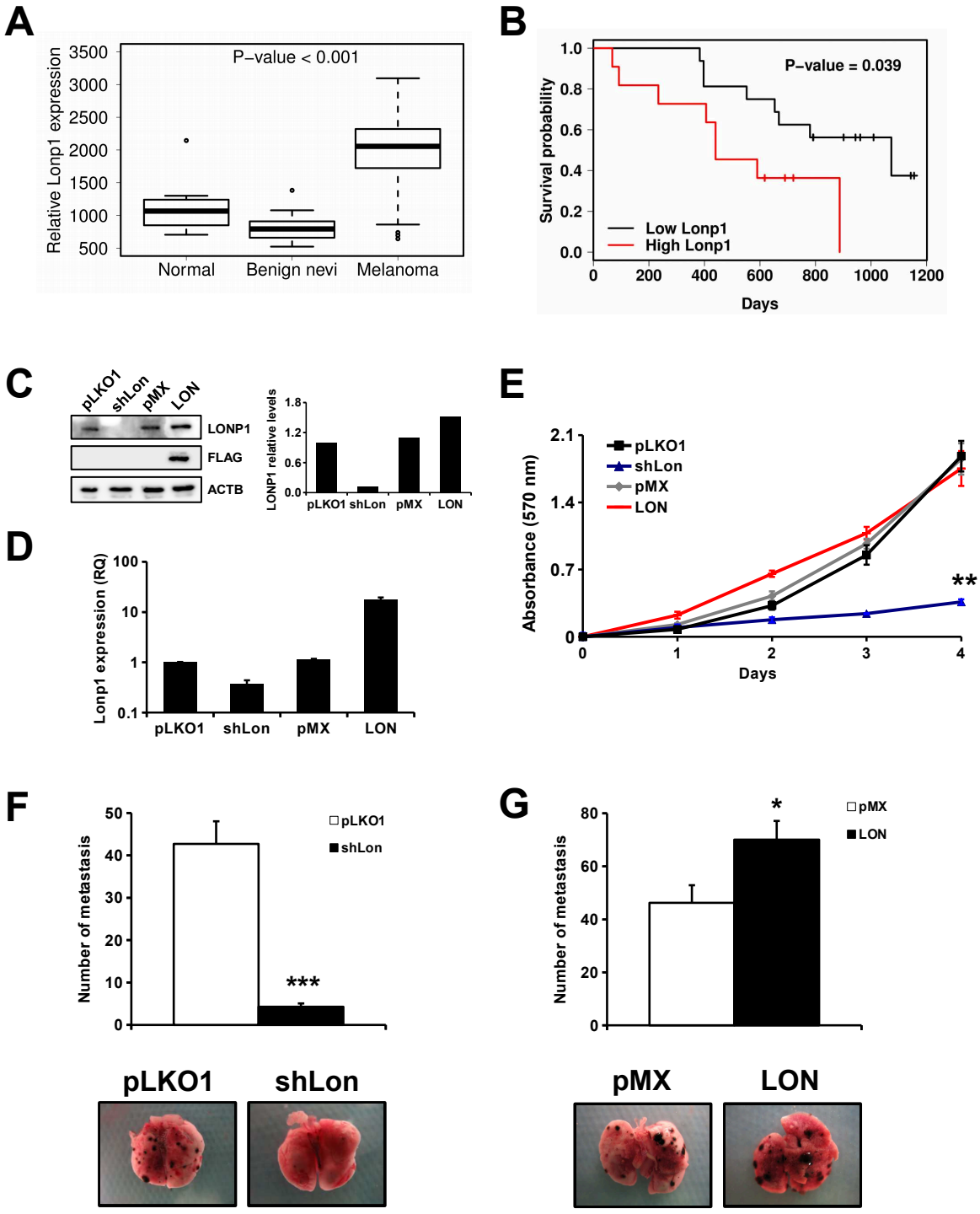

Figure 4; Quiros et al.

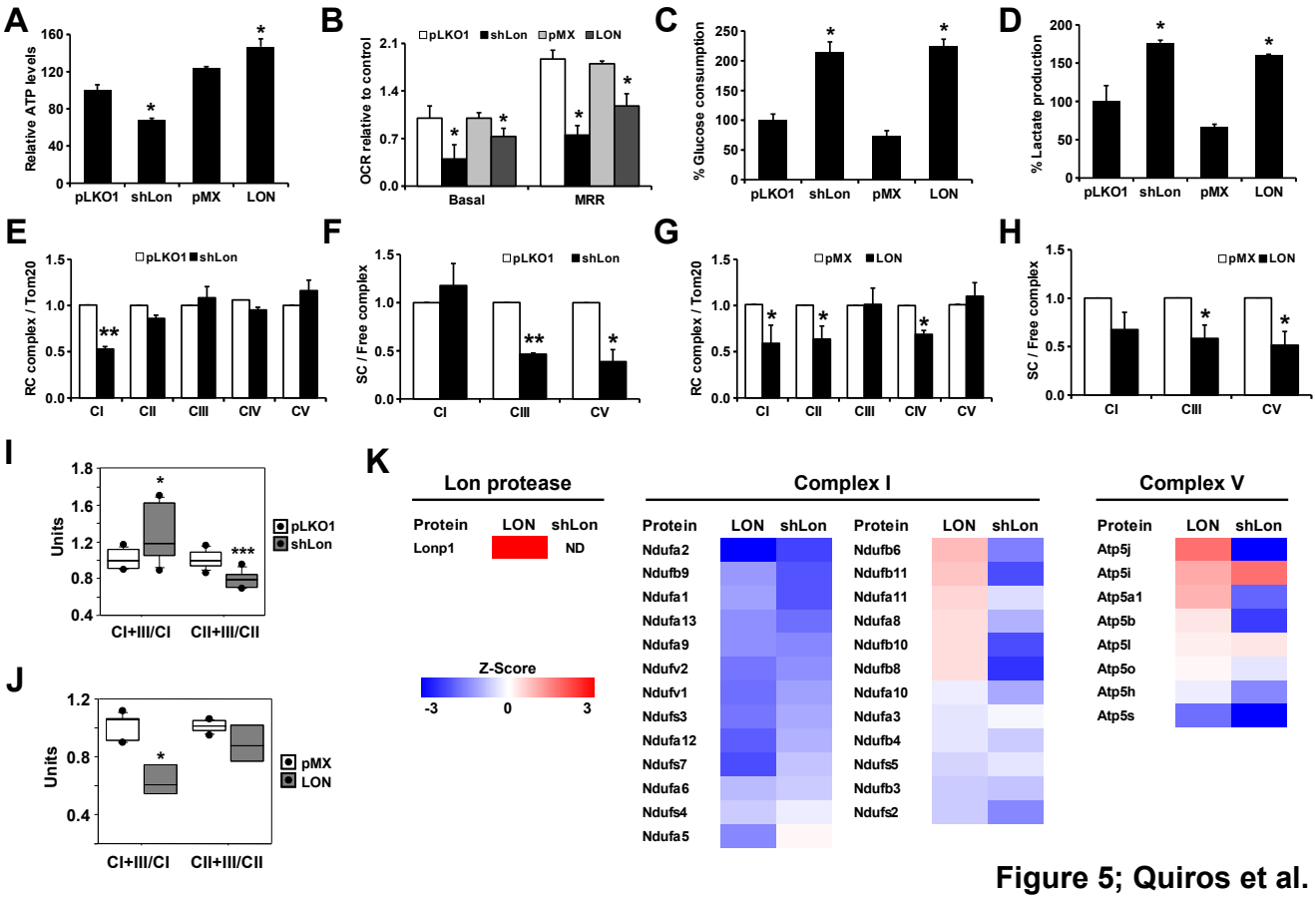

Figure 5; Quiros et al.

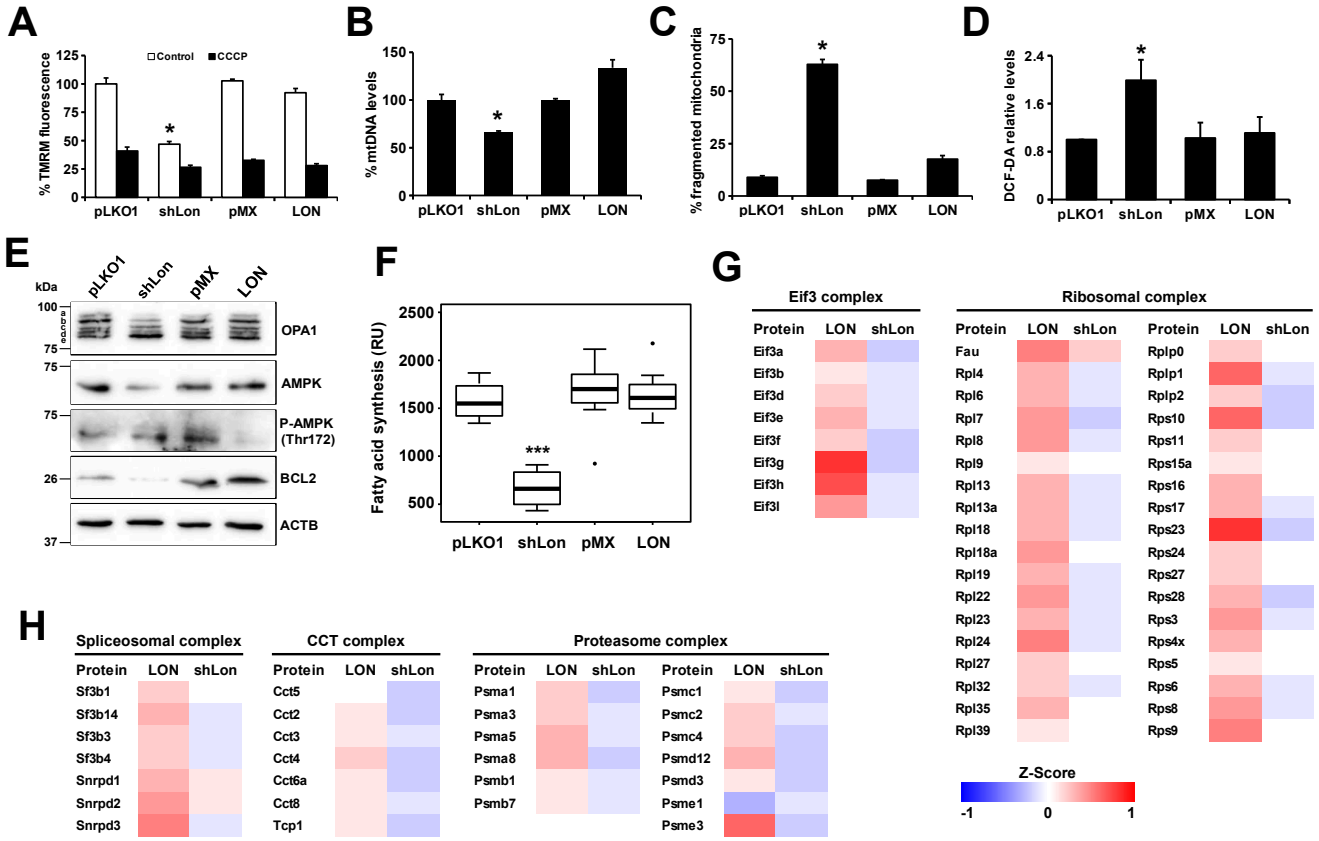

Figure 6; Quiros et al.

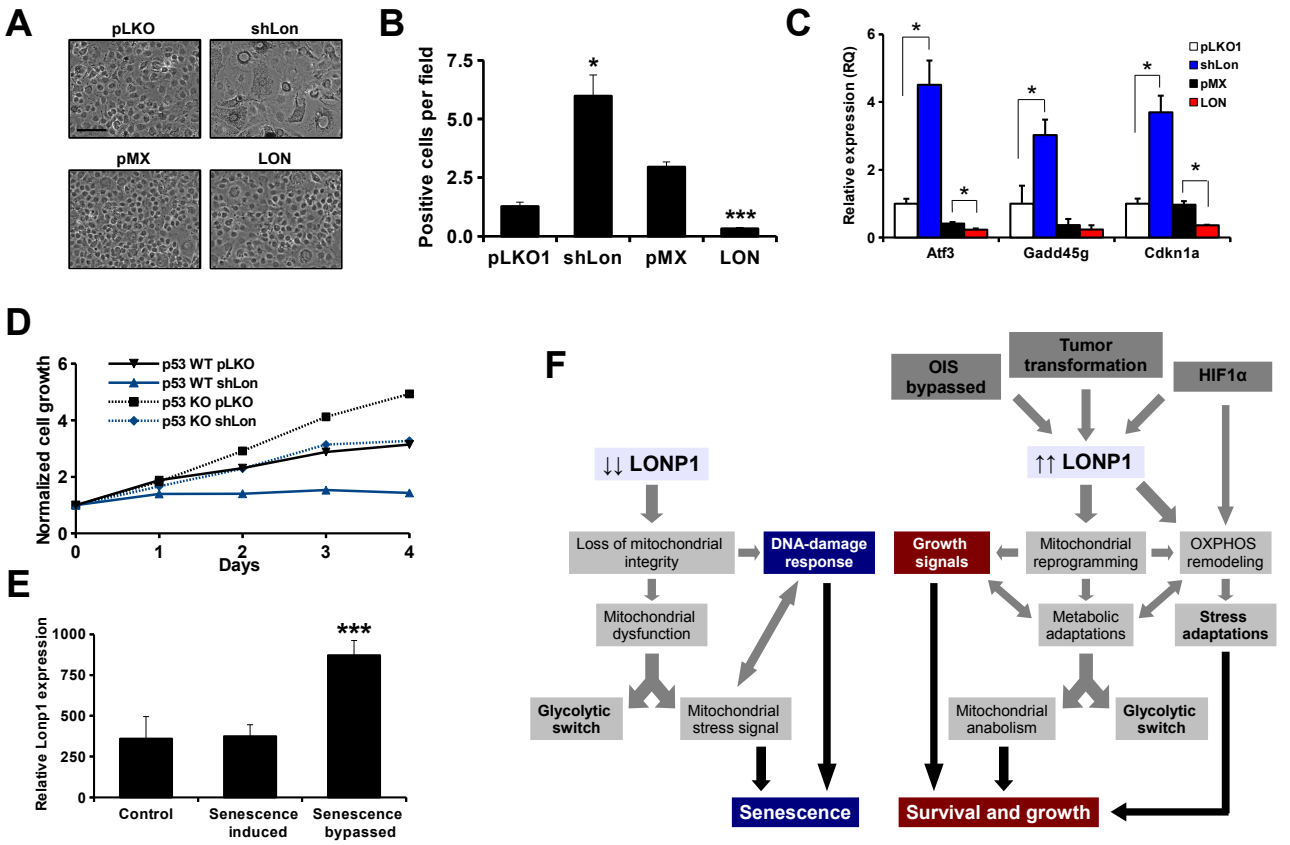

Figure 7; Quiros et al.

SUPPLEMENTAL INFORMATION

Quiros et al. "ATP-dependent Lon protease promotes cancer and metastasis by reprogramming mitochondrial activity"

Supplemental Figures

Supplemental Figure legends

Figure S1, related to Figure 1

A

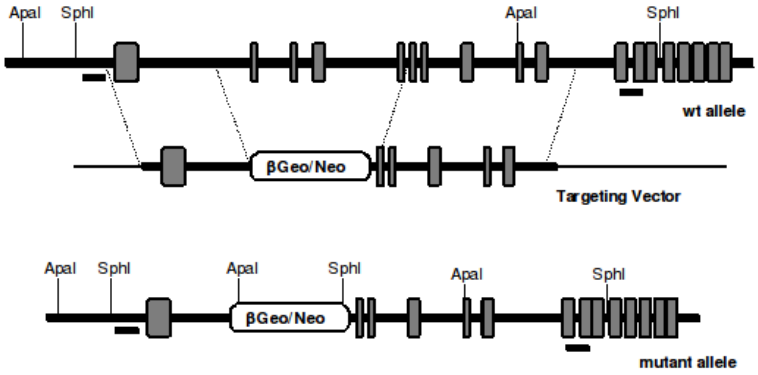

B

Stage	Number of mice				
	+/+ (25%)	+/- (50%)	-/- (25%)	undeterm.	Total
3.5 dpc	43	67	25	24	159
7.5 dpc	23	33	11	3	70
8.5 dpc	12	31	1	3	47
9.5 dpc	7	16	0	1	24
At weaning	96	181	0	0	277

Figure S2, related to Figure 3

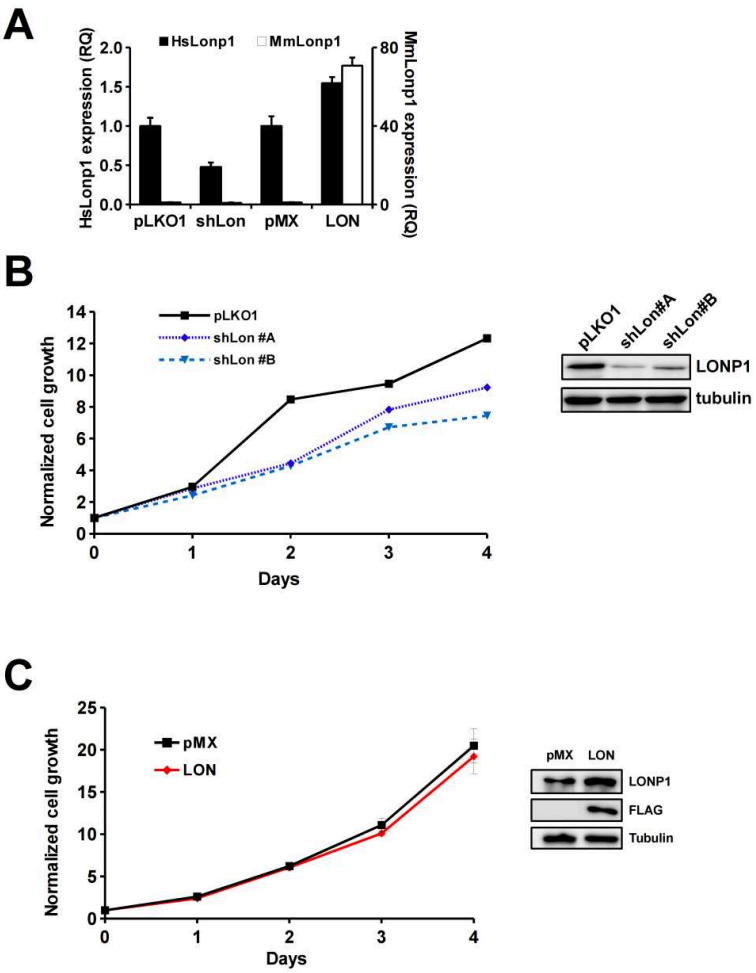

Figure S3, related to Figure 4

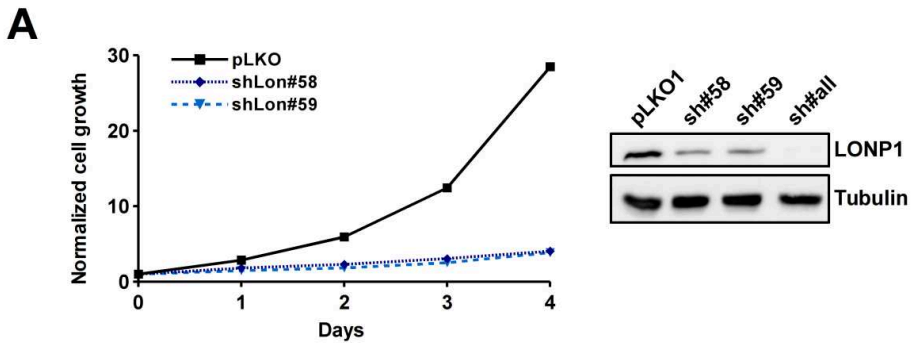

4

Figure S4, related to Figure 5

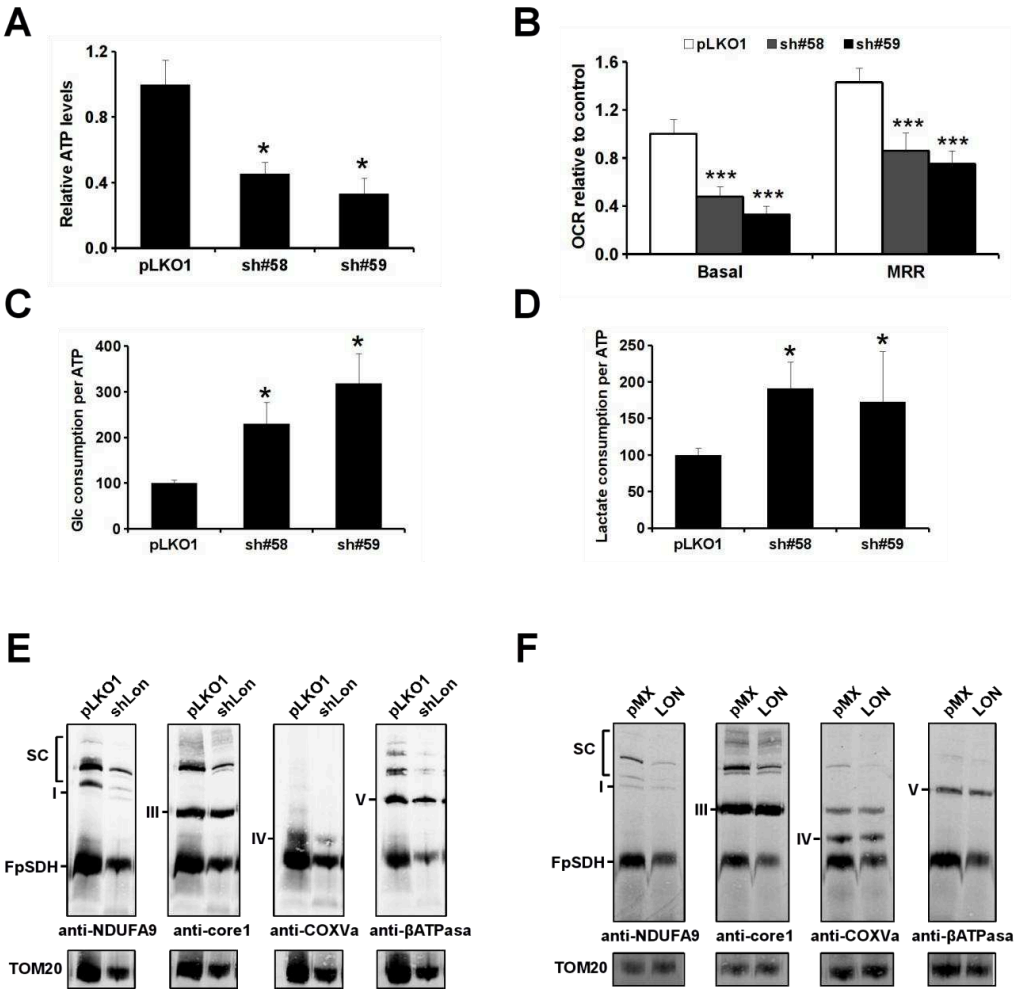

5

Figure S5, related to Figure 6

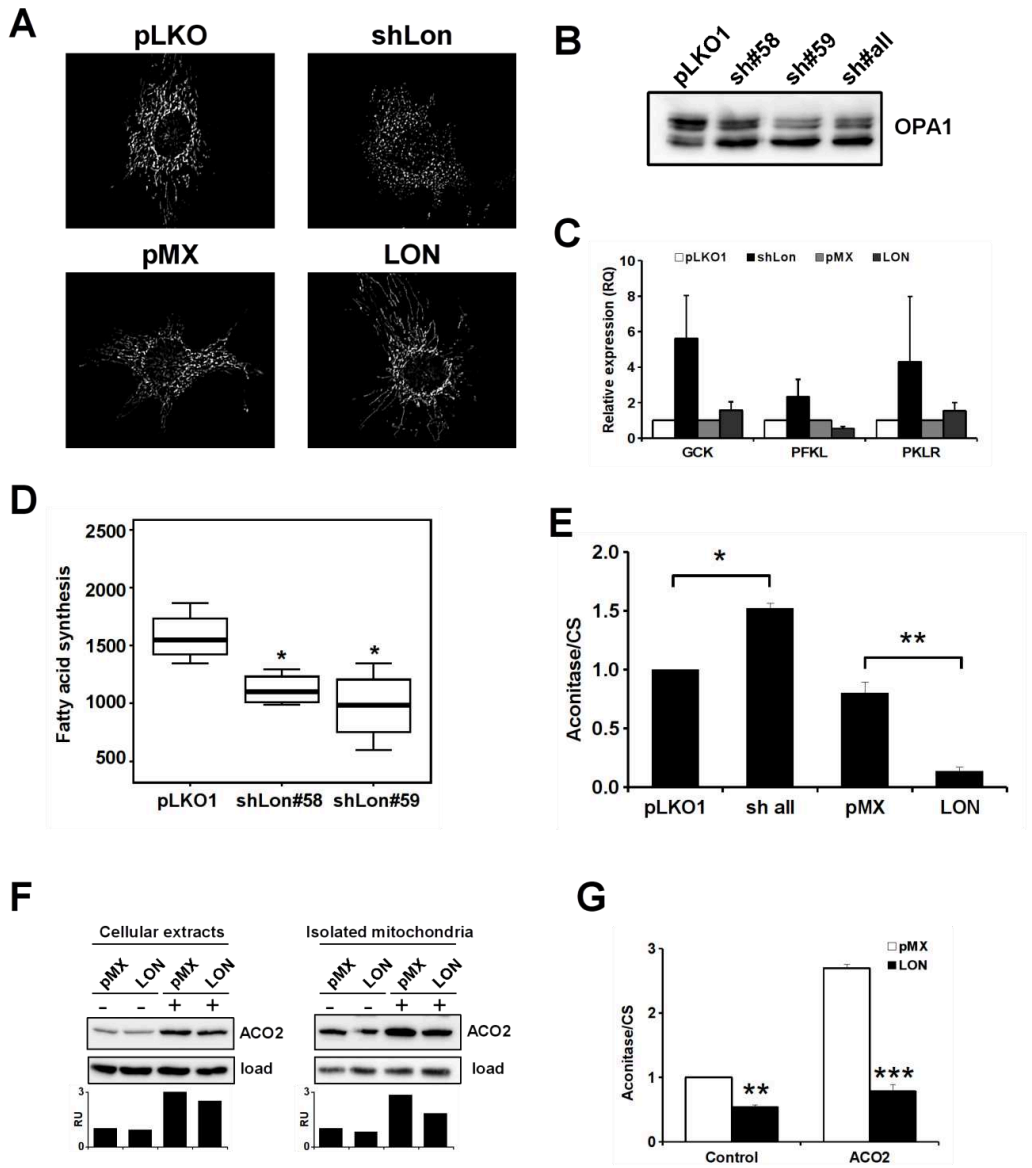

Supplemental Figure legends

Figure S1. (A) Schematic representation of wild-type and mutant Lonp1 alleles, and the targeting vector. The exons are indicated with boxes, the bold solid lines represent introns and the thin solid lines indicate the plasmid backbone in the targeting vector. (B) Analysis of embryos derived from intercrossing of Lonp1 heterozygous mice shows an embryonic lethality at 8.5 dpc. Genotypes were determined by PCR analysis.

Figure S2. (A) qPCR analysis of HCT116 colon cancer cells transduced with LONP1 shRNA vectors (shLon) or with the empty vector as a control (pLKO1), as well as with pMX expressing murine LONP1 (LON) and the empty vector (pMX). qPCR analysis was carried out using two different LONP1 probes to detect endogenous (HsLonp1) and exogenous (MmLonp1) LONP1 expression values. (B) MTT and Western-blot analysis of HCT116 colon cancer cells transduced with two different single shRNA against LONP1. (C) MTT and Western-blot analysis of DLD-1 colon cancer cells transduced with a LONP1-flagged construction and the empty vector pMX.

Figure S3. (A) MTT and Western-blot analysis of B16F10 melanoma cells transduced with two different single shRNA against LONP1, and the complete set of shRNAs. Notice the effect in the use of complete set compared to the use of single shRNA to decrease LONP1 levels.

Figure S4. B16F10 melanoma cells with knockdown of LONP1 using two single shRNAs (sh#58 and sh#59). (A) Relative ATP levels of the analyzed cells. (B) Oxygen consumption rate (OCR) in basal conditions and after stimulation with FCCP, MRR (maximal respiration rate), represented as OCR per cell relative to each control cell. (C) Percentage of glucose consumption and (D) lactate production during 48 h, relative to control. BNGE immunoblots showing distribution of CI, CIII, CIV and CV free and in supercomplexes detected with indicated antibodies in each case, as well as FpSDH (CII) using TOM20 as loading control, in (E) pLKO1 and shLon cells, and (F) pMX and LON cells. All experiments were carried out in triplicate in at least three independent experiments. Bars represent means ± SEM. * $P < 0.05$, *** $P < 0.001$.

Figure S5. (A) Representative pictures of mitochondrial morphology from pLKO1, shLon, pMX and LON cells. Mitochondria were visualized after transfection with a vector containing mito-DsRed2. (B) Western-blot analysis of OPA1 processing in B16F10 melanoma cells with knockdown of LONP1 using two single shRNAs (sh#58 and sh#59) and the complete set of shRNAs (sh#all).

(C) Relative expression levels of glycolytic genes, glucokinase (GCK), phosphofructokinase (PFKL) and pyruvate kinase (PKLR) in the indicated cells. (D) Fatty acid synthesis rate measured as ^{14}C incorporation into cellular lipids represented as relative units (RU). (E) Aconitase (ACO2) activity relative to citrate synthase activity. (F) Western-blot analysis and densitometry quantification of ACO2 levels in control (pMX) and LONP1-overexpressing cells (LON), determined in cellular extracts and isolated mitochondria, after transfection of ACO2 cDNA. (G) ACO2 activity relative to citrate synthase activity of cells previously described. All experiments were carried out in triplicate in at least three independent experiments. Bars represent means ± SEM. * $P < 0.05$, ** $P < 0.01$, *** $P < 0.001$.

8

V. Mitochondrial alterations in a mouse model of premature aging

Lipodystrophy is a pathological condition characterized by loss of adipose tissue. This loss can be localized or generalized and caused by genetic or acquired defects. Mutations in genes encoding the nuclear protein lamin A or its processing enzyme, the metalloprotease Zmpste24, cause diverse human progeroid syndromes and are associated with the development of lipodystrophy. Likewise, mice deficient in Zmpste24 exhibit phenotypic features of accelerated aging, including lipodystrophy. The study of metabolic alterations in these mice may be useful for understanding the molecular mechanisms underlying the adipose tissue dysfunction observed in laminopathies and other lipodystrophic syndromes, as well as to develop novel strategies to prevent or ameliorate these diseases. On this basis, we analyzed the proteomic profiling of the adipose tissue from *Zmpste24*-deficient mice, as a model of lipodystrophy syndrome and premature aging. Using this strategy, we have identified alterations in the protein profile and metabolic state associated with lipoatrophy, highlighting the importance of mitochondrial function for the development of lipodystrophy and aging.

Article 5: Juan R. Peinado, **Pedro M. Quirós**, Marina R. Pulido, Guillermo Mariño, Maria L. Martínez-Chantar, Rafael Vázquez-Martínez, José M. P. Freije, Carlos López-Otín, and María M. Malagón. "Proteomic profiling of adipose tissue from *Zmpste24*$^{-/-}$ mice, a model of lipodystrophy and premature aging, reveals major changes in mitochondrial function and vimentin processing".

Mol Cell Proteomics. 2011 November; 10(11): M111.008094.

Personal contribution to this work

In this work, I was the main responsible of the analysis of the lipoatrophy phenotype of mice, performing all necropsies, extracting the adipose tissue samples and analyzing their histological alterations. In addition, I carried out the determination of ROS levels and collaborated in western-blot analysis of selected proteins. Finally, I contributed to the discussion of the results with Dr. Juan R. Peinado and participated in the writing of the manuscript.

Research

Proteomic Profiling of Adipose Tissue from Zmpste24$^{-/-}$ Mice, a Model of Lipodystrophy and Premature Aging, Reveals Major Changes in Mitochondrial Function and Vimentin Processing*[S]

Juan R. Peinado‡‖, Pedro M. Quirós§, Marina R. Pulido‡, Guillermo Mariño§, Maria L. Martínez-Chantar¶, Rafael Vázquez-Martínez‡, José M. P. Freije§, Carlos López-Otín§, and María M. Malagón‡‡‡

Lipodystrophy is a major disease involving severe alterations of adipose tissue distribution and metabolism. Mutations in genes encoding the nuclear envelope protein lamin A or its processing enzyme, the metalloproteinase Zmpste24, cause diverse human progeroid syndromes that are commonly characterized by a selective loss of adipose tissue. Similarly to humans, mice deficient in Zmpste24 accumulate prelamin A and display phenotypic features of accelerated aging, including lipodystrophy. Herein, we report the proteome and phosphoproteome of adipose tissue as well as serum metabolome in lipodystrophy by using *Zmpste24*$^{-/-}$ mice as experimental model. We show that Zmpste24 deficiency enhanced lipolysis, fatty acid biogenesis and β-oxidation as well as decreased fatty acid re-esterification, thus pointing to an increased partitioning of fatty acid toward β-oxidation and away from storage that likely underlies the observed size reduction of *Zmpste24*-null adipocytes. Besides the mitochondrial proteins related to lipid metabolism, other protein networks related to mitochondrial function, including those involved in tricarboxylic acid cycle and oxidative phosphorylation, were up-regulated in *Zmpste24*$^{-/-}$ mice. These results, together with the observation of an increased mitochondrial response to oxidative stress, support the relationship between defective prelamin A processing and mitochondrial dysfunction and highlight the relevance of oxidative damage in lipoatrophy and aging. We also show that absence of Zmpste24 profoundly alters the processing of the cytoskeletal protein vimentin and identify a novel protein dysregulated in lipodystrophy, High-Mobility Group Box-1 Protein. Finally, we found several lipid derivates with important roles in energy balance, such as Lysophosphatidylcholine or 2-arachidonoylglycerol, to be dysregulated in *Zmpste24*$^{-/-}$ serum. Together, our findings in *Zmpste24*$^{-/-}$ mice may be useful to unveil the mechanisms underlying adipose tissue dysfunction and its overall contribution to body homeostasis in progeria and other lipodystrophy syndromes as well as to develop novel strategies to prevent or ameliorate these diseases. ***Molecular & Cellular Proteomics 10: 10.1074/mcp.M111.008094, 1–16, 2011.***

Adipose tissue has emerged as one of the most important organs regulating body homeostasis as it serves not only for the storage of energy in the form of triglycerides but it is also a source of paracrine and endocrine signals (*i.e.* adipokines) that influence systemic metabolism (1–4). Dysfunction of adipose tissue, as occurs in conditions of excess (obesity) or reduced (lipodystrophy) body fat, results in an abnormal management of triglycerides and alteration of adipokine secretion, leading to several metabolic disturbances such as insulin resistance, dyslipidemia, hepatic steatosis, and type 2 diabetes (4, 5). Accordingly, much effort has been made to elucidate the molecular mechanisms underlying adipose tissue dysfunction and its role in the development of metabolic diseases, including the utilization of proteomic approaches (reviewed in (6, 7)). Indeed, both the number and quality of adipose tissue proteomic studies have notably increased in the last years. Thus, proteome studies have been conducted on adipose tissue biopsies from different fat depots (*i.e.* visceral and subcutaneous adipose tissue) (8) as well as on the two fractions comprising adipose tissue, mature adipocytes and the stromal vascular fraction (9). Isolation of the separate

From the ‡Department of Cell Biology, Physiology and Immunology, University of Córdoba. Instituto Maimónides de Investigación Biomédica de Córdoba (IMIBIC), Córdoba, Spain CIBER Fisiopatología de la Obesidad y Nutrición (CIBERobn), Instituto de Salud Carlos III, Spain; §Department of Biochemistry and Molecular Biology, Universidad de Oviedo, Instituto Universitario de Oncología (IUOPA), Oviedo, Spain; ¶CIC bioGUNE, CIBER de Enfermedades Hepáticas y Digestivas (CIBERehd)

Received January 24, 2011, and in revised form, July 31, 2011
Published, MCP Papers in Press, August 9, 2011, DOI 10.1074/mcp.M111.008094

cellular components of the latter fraction has also enabled to establish the proteome of adipose-derived adult stem cells and adipogenesis (10–12). Moreover, novel adipose tissue secreted peptides and proteins have been identified using proteomic techniques (6, 13, 14) .

Because obesity is the most prevalent condition affecting adipose tissue function, the vast majority of the proteomic studies carried out to date have focused on the molecular characterization of adipose tissue from obese human (8, 15), mouse (16, 17), or rat (18, 19) models. Actually, no other pathological states of adipose tissue have been investigated so far using proteomic techniques. In this regard, lipodystrophy, which includes a variety of distinct syndromes that may be inherited or acquired in origin, is characterized by a generalized or partial lack of adipose tissue (reviewed by (5, 20)). Inherited lipodystrophies are commonly associated to mutations in single genes whereas acquired lipodystrophies develop in patients with certain autoimmune diseases and, more often, in HIV-infected patients under antiretroviral therapy (reviewed by (5, 21–22)).

The most common genetic disorders of inherited lipodystrophies have been linked to mutations in the *LMNA* gene encoding the nuclear envelope A-type lamins, lamins A and C (5). Although these proteins are expressed in nearly all cell types, mutations in *LMNA* are responsible for at least a dozen different disorders with tissue-selective affections and collectively referred to as laminopathies, including Dunnigan-type familial partial lipodystrophy (23). In addition to a structural role, lamins are also involved in the regulation of DNA replication, transcription, and repair (24). In the case of adipose tissue, it has been suggested that lamins play a role in adipocyte differentiation yet the molecular mechanisms responsible for the loss of adipose tissue associated to lamin A/C deficiency are not completely understood (reviewed by (5, 24)). In humans, mutations in the gene encoding the zinc metalloproteinase Zmpste24/FACE1, which is involved in the post-translational cleavage of carboxy-terminal residues of farnesylated prelamin A to form mature lamin A (25) (Fig. 1), cause progeroid syndromes (*i.e.* restrictive dermopathy and mandibuloacral dysplasia) characterized by a generalized loss of fat, especially pronounced in extremities and the truncal region (23, 24). Similarly to humans, mice lacking Zmpste24 accumulate prelamin A and display phenotypic features of progeria including also a generalized lipodystrophy (26), as well as substantial changes in circulating plasma levels of several adipokines (27), hormones and growth factors (28, 29).

In order to investigate the exact impact of the impairment of prelamin A processing on the functioning of adipocytes, we have carried out a proteomic study of adipose tissue from *Zmpste24*$^{-/-}$ mice. Our findings indicate that the absence of Zmpste24 enhances mitochondrial function, especially the tricarboxylic acid (TCA) cycle and electron transport chain, to such a level that it causes oxidative damage. Other metabolic

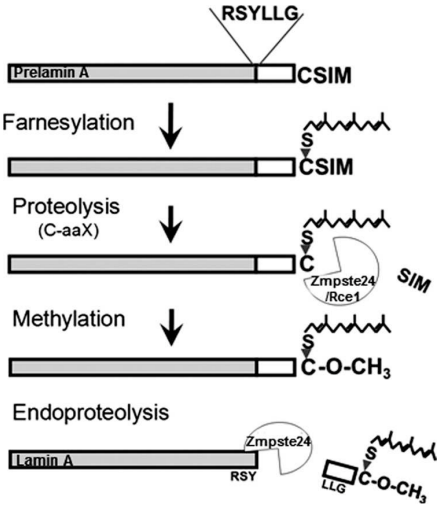

FIG. 1. **Maturation of the lamin A precursor (prelamin A) requires several post-translational processing steps: farnesylation of the C-terminal CaaX motif, proteolysis of the C-terminal aaX residues by endoproteases Zmpste24, and/or Rce1, carboxymethylation of the farnesylated cysteine and endoproteolysis of the 15 C-terminal amino acids by Zmpste24.**

disturbances directly affecting lipid management, such as fatty acid (FA)[1] β-oxidation and re-esterification, together with alterations in vimentin processing, likely contribute to the lipoatrophic state associated with lamin A-related diseases. Finally, serum metabolomics revealed for the first time several markers of lipodystrophy, mostly lipid compounds, further supporting the relevance of the dysregulation of lipid metabolism in the premature aging phenotype.

EXPERIMENTAL PROCEDURES

Animals—Mutant mice deficient in Zmpste24 metalloproteinase have been previously described (26). A total of 38 animals have been used for these studies (18 *Zmpste24*$^{-/-}$ and 20 wild-type males). Animal procedures were conducted in accordance with the guidelines of the Committee on Animal Experimentation of the University of Ov iedo (Oviedo, Spain).

Histological Analysis—For histological analysis, adipose tissue samples from the visceral fat pad obtained from four *Zmpste24*$^{-/-}$ and three wild-type animals were fixed in 4% paraformaldehyde in PBS and stored in 70% ethanol. Fixed tissues were embedded in paraffin by standard procedures. Blocks were sectioned (5 μm) and tissues stained with hematoxylin and eosin. The number of adipocytes and their mean diameter were determined in 5-μm tissue sections by computer-assisted image analysis. For each sample, different microscopic fields were analyzed, and at least 100 adipocytes were measured.

Protein Extraction—For proteomic studies, adipose tissue biopsies from four *Zmpste24*$^{-/-}$ and four wild-type animals were washed in PBS immediately after removal and directly frozen in liquid nitrogen

[1] The abbreviations used are: FA, Fatty acid; CPT1, Carnitine palmitoyltransferase I; HMGB1, High-Mobility Group Box-1 protein; LPC, Lysophosphatidylcholine; TCA, Tricarboxylic acid cycle; UCP-1, Uncoupling protein 1.

and stored at −80 °C. Samples were processed following a specific protocol previously optimized by us for adipose tissue (9). Thus, fat samples were thawed by adding 0.4 ml of cold urea/thiourea buffer (7 M urea, 2 M thiourea, 4% 3-[(3-cholamidopropyl)dimethylammonio]propanesulfonate, 45 mM Tris pH 7.4, 60 mM dithiotreitol, and complete protease inhibitors (1 tablet/20 ml, Roche, Barcelona, Spain)) supplemented with 0.1 mM NaCl, mechanically disrupted and briefly sonicated. Then, they were adjusted to 900 μl with lysis buffer (20 mM Tris pH 7.4, 100 mM NaCl, 1% Triton, and protease inhibitors; Complete, Roche) and incubated for 15 min at 35 °C. After cooling on ice for 10 min, 100 μl of 0.1 M Tris, pH 7, and 50 mM $MgCl_2$ were added to the homogenates, which were then incubated with DNase I (30 U, Sigma) for 10 min on ice. The homogenate was centrifuged (15 min, 10,000 × *g*, 4 °C) and the aqueous phase between the upper lipid phase and lower cellular debris phase was collected. Extensive delipidation was accomplished by Tri-n-butylphosphate-acetone-methanol precipitation. Precipitated proteins were resuspended in 75 μl of urea/thiourea buffer. After Bradford assay for protein quantification, samples were diluted to 7 μg/μl with urea/thiourea buffer and frozen at −20 °C.

Isoelectric Focusing and Two-dimensional-PAGE—Three hundred and fifty micrograms (50 μl) of protein from both wild-type and *Zmpste24*$^{-/-}$ mice, were diluted in 300 μl of Rehydratation Buffer and 0.8% of 3–10NL IPG buffer (GE Healthcare, Barcelona, Spain). Immobilized pH gradient strips (18 cm, pH 3–10 NL) were rehydrated overnight in a Ettan IPGPhor 3 System (GE Healthcare) following a stepwise voltage: 300 V for 3 h, linear gradient to 1000 V for 4 h, linear gradient to 8000 V for 2 h, and 8000 V until total Vh (40,000) is reached. Strips were equilibrated in SDS Equilibration Buffer (75 mM Tris, pH 8.8, 6 M urea, 30% glycerol, 2% SDS) containing 2% dithiothreitol for 15 min, followed by a 15-min wash with equilibration buffer containing 2.5% iodoacetamide. Thereafter, proteins were separated on 12% Tris-glycine gels using an Ettan Dalt Six device (GE Healthcare). These conditions resolved proteins with a MW higher than 20 kDa. After migration, gels were stained with SYPRO Ruby dye and/or 0.1% Coomassie brilliant blue G-250, 10% ammonium sulfate, 2% phosphoric acid, and 20% methanol. Both stainings gave similar results.

Staining of phosphoproteins was performed using Pro-Q Diamond stain (Bio-Rad Laboratories, Hercules, CA) according to manufacturer's instructions. Three hundred micrograms of adipose tissue extracts were set as the minimum protein amount required for a correct identification of phosphorylated proteins. Images of gels stained with Coomassie, SYPRO Ruby or Pro-Q Diamond were captured with the FX system (Bio-Rad).

Matrix-Assisted Laser Desorption Ionization/Time of Flight-MS Analysis—Spots were excised automatically in a ProPic station (Genomic Solutions, Huntingdon, UK) and subjected to MS analysis. MALDI-ToF-MS analysis were carried out on a 4800 MALDI-ToF/ToF Analyzer (Applied Biosystems/MDS SCIEX, Concord, Ontario, Canada). Gel specimens were destained twice (30 min, 37 °C) with 200 mM ammonium bicarbonate/40% acetonitrile. Gel pieces dehydrated for 5 min with pure acetonitrile and dried out over 4 h were automatically digested with trypsin according to standard protocols in a ProGest station (Genomic Solutions). MS and MS/MS analyses of peptides of each sample were analyzed in a 4700 Proteomics Station (Applied Biosystems) in automatic mode. Samples were deposited onto MPep Chips prespotted with α-cyano-4-hydroxy-cinnamic acid (Sunyx, Germany) using the thin layer affinity method and analyzed with the following setting: for the MS data, *m/z* range 800 to 4000 with an accelerating voltage of 20 kV and delayed extraction, peak density of maximum 50 peaks per 200 Da, and minimal signal-to-noise (S/N) ratio of 10 and maximum peak at 65. Peak lists for MS/MS data sets were generated using the 4000 Series Explorer (TM) RAC Software, version 3.5.3 (Applied Biosystems/MDS SCIEX, Concord, Ontario, Canada). For the analysis of vimentin isoforms the *m/z* range was increased from 400 to 4000.

Peak lists were submitted to Mascot database in order to identify the proteins (Database, NCBInr 12012010 (10320603 sequences; 3520860234 residues); taxonomy, Mammalia (757310 sequences)). Analysis was limited to peptides of six or more amino acids and maximum one missed cleavage site. Mass tolerance for precursor ions was set to 100 ppm and mass tolerance for fragment ions to 0.2 Da; oxidation of methionine was searched as variable modification and carbamidomethylation of cysteine was set as fixed modification. MS/MS data were also searched against the ENSEMBL *Mus musculus* database using the open source software X!Tandem (http://www.thegpm.org) with similar settings to those employed for Mascot. Peptide false discovery rates were determined by a target decoy approach using a reversed database concatenated to the parent forward database (30). A cutoff expectation value of ≤1.0 (significance threshold; expressed as the negative logarithm of E-value) was chosen for individual MS/MS spectra that resulted in a false discovery rate of ≤1%. Other post-translational modifications (*i.e.* phosphorylation) were also investigated using Expasy proteomic server (FindMod and Aldente). To determine whether protein carbamylation occurred during the preparation of the samples, representative protein extracts from mouse adipose tissue were analyzed by High-Performance Liquid Chromatography and Tandem Mass spectrometry using LTQ-Orbitrap XL mass spectrometer (Thermo Fisher Scientific Inc.) equipped with a nanoelectrospray ion source (nESI). No carbamylation was detected under these conditions (data not shown).

Immunoblotting—Frozen fat samples from four additional wild-type and *Zmpste24*$^{-/-}$ mice distinct from those employed for 2-DE were disrupted in Triton buffer (20 mM Tris pH 7.4, 150 mM NaCl, 1% Triton, and complete protease inhibitor) and incubated in the presence of 30 units of DNase I (Sigma) for 15 min on ice. Thirty to 70 μg of protein were loaded on 10% SDS-PAGE and transferred to nitrocellulose membranes (Biotrace, Pall, Germany). After Ponceau staining to ensure equal sample loading, membranes were blocked for 1 h with 5% dried milk in TTBS (TBS buffer with 0.05% Tween-20). Antibodies against peroxiredoxin 3 (PRDX3), prelamin A, β-actin, carnitine palmitoyltransferase I (CPT1), uncoupling protein 1 (UCP-1), and phosphoenolpyruvate carboxykinase 1 (PCK1) were purchased from Santa-Cruz Biotechnology (Heidelberg, Germany). Anti-vimentin antibody was purchased from Biomedal SL (Sevilla, Spain) and anti-malic enzyme 1 (ME1) antibody was from Proteintech Group, Inc. (Manchester, UK). After overnight incubation at 4 °C with the corresponding primary antibody, membranes were incubated with the appropriate IgG-HRP-conjugated secondary antibody. Immunoreactive bands were visualized with an enhanced-chemiluminescence reagent (Chemiluminescent HRP substrate, Millipore, MA). Optical densities of the immunoreactive bands were measured using ImageJ 1.40g analysis software.

ROS Determination—The intracellular reactive oxygen species (ROS) levels were determined using the 2,7′-dichloroflourescein diacetate (DCF-DA) dye (Sigma). White adipose tissue was extracted from mice and samples were homogenized using PLB (Promega). The lysates were centrifuged at 12,000 × *g* for 5 min at 4 °C, and supernatants were collected. Protein concentration in the supernatants was evaluated by the bicinchoninic acid technique (BCA protein assay kit, Pierce Biotechnology, Rockford, IL). Supernatants (50 μg) were mixed with 25 μM DCF-DA and then incubated at 37 °C for 30 min in the dark. Fluorescence at 485/535 was measured using a LS55 PerkinElmer LifeScience spectrofluorometer. Adipose tissue samples from at least four different animals of each genotype were used for measurement of ROS generation.

Serum Metabolomics—Sera from eight *Zmpste24*$^{+/+}$ and *Zmpste24*$^{-/-}$ male mice samples were analyzed. A global metabolite

profiling UPLC®-MS methodology was employed, where all endogenous metabolite related features, characterized by mass-to-charge ratio *m*/z and retention time Rt, were included in a subsequent multivariate analysis procedure used to study metabolic differences between the different groups of samples (31). Where possible, Rt-*m*/*z* features corresponding to putative biomarkers were later identified. Sample preparation, LC-MS system, data processing, multivariate data analysis were performed as described previously (32). The top 50 candidate markers resulting from this procedure were selected and subjected to additional statistical testing (fold changes and Wilcoxon rank sum (Mann Whitney) test *p* values). Finally, the following procedures were used in an attempt to identify selected markers: a) Mass spectra recorded in the positive and negative ion modes were analyzed to determine the most likely parent (as opposed to metal adducts or fragments) ion *m*/*z* value and b) The exact mass information obtained, corrected to within a 5 ppm error, was checked against the ChemSpider10 online database, using the subdatabases: KEGG, Lipid Maps and Human Metabolome database. Where possible, hit lists were further reduced by comparison of theoretical/measured isotopic patterns.

Data Analysis—2-DE gel analysis was performed by PDQuest software (Bio-Rad), version 8.0. Spot volume values were normalized in each gel by dividing the raw quantity of each spot by the total volume of all the spots included in the same gel. Other normalizations provided by the PDQuest software were also performed with similar results. Data were log transformed to meet the requirements of a normal distribution and analyzed with Student's *t* test using the statistics tools included in the PDQuest software. Spots which gave significant results ($p < 0.05$) were verified visually to exclude artifacts. Furthermore, statistically significant spots were rechecked by two-tailed unpaired Student's *t* test after reevaluation of density with ImageJ 1.40g software.

Statistical analysis used SSPS statistical software, version 11.0 for WINDOWS (SSPS INC., Chicago, IL). Statistical differences in Western blot experiments were assessed by two-tailed unpaired Student's *t* test. Differences were considered significant at $p < 0.05$. All data are expressed as mean ± S.E. For further evaluation, proteins identified by the proteomic study were analyzed using a pathway analysis software (Ingenuity Pathway Analysis (IPA); Ingenuity Systems, Mountain View, CA) to reveal their potential relationships with other proteins and/or intracellular pathways.

RESULTS

Reduced Adipose Tissue in Zmpste24$^{-/-}$ Mice—Zmpste24-null mice display a lipodystrophic phenotype characterized by the absence of subcutaneous adipose tissue (26). Herein, we have observed that they also suffer from a marked reduction of the visceral fat depot (Fig. 2*A*), which in some cases reached more than a sixfold decrease when compared with that observed in their wild-type littermates. This remaining fat pad can be easily removed together with the gonads (Fig. 2*B*). Histological examination of hematoxylin-eosin stained sections revealed that visceral adipose tissue from *Zmpste24*$^{-/-}$ mice is composed of small adipocytes (Fig. 2*C*), which showed almost half the size of those from wild-type animals. Specifically, minimum diameters of adipocytes from *Zmpste24*-null and wild-type mice were 11 ± 2.9 and 18 ± 1.0 μm, respectively, which likely contributes to the increased number of total adipocytes observed in adipose tissue from *Zmpste24*$^{-/-}$ mice (649.60 ± 83.3 *versus* 443.4 ± 28.5 cells/mm^2 in *Zmpste24*$^{-/-}$ and wild-type mice, respectively).

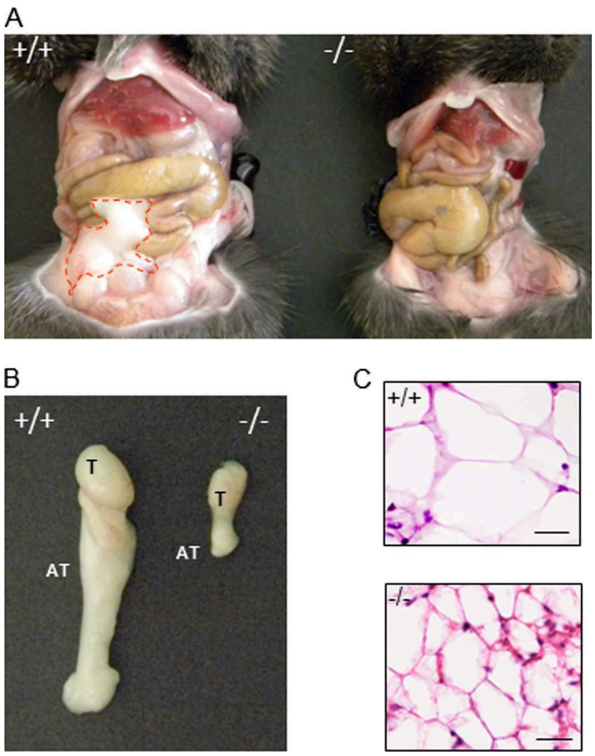

FIG. 2. **Lipoatrophy of visceral adipose tissue in *Zmpste24*$^{-/-}$ mice.** *A*, Representative images showing adipose tissue distribution in 4-month-old *Zmpste24*$^{+/+}$ and *Zmpste24*$^{-/-}$ male mice. Loss of adipose tissue is evident in *Zmpste24*$^{-/-}$ mice (adipose tissue is indicated by a red line). *B*, Visceral adipose tissue removed from *Zmpste24*$^{+/+}$ and *Zmpste24*$^{-/-}$ animals. *C*, Comparisons of hematoxylin and eosin-stained cross sections of adipose tissue of *Zmpste24*$^{+/+}$ and *Zmpste24*$^{-/-}$ mice, showing the decreased size of adipocytes in *Zmpste24*-deficient mice. T, testis; AT, adipose tissue.

Adipose Tissue of Zmpste24$^{-/-}$ Mice Exhibits Altered Metabolic Pathways—Our proteomic analysis of visceral adipose tissue allowed for the identification of ~1,070 spots in a typical two-dimensional gel. Comparative analysis of the proteome of adipose tissue from *Zmpste24*$^{-/-}$ and wild-type mice (four animals per group) revealed that 37 proteins were significantly up-regulated in mutant mice while 9 proteins were down-regulated (Fig. 3*A*). A representative spot corresponding to pyruvate dehydrogenase beta (spot 31) is highlighted in Fig. 3*B* in order to show the reproducibility of the observed differences between adipose tissue proteomes from the two groups of animals. Differences in the proteome of the four different animals analyzed per group were evaluated and average of their density was used to elaborate Table I, where only those proteins with consistent differences ($p < 0.05$) were included. MALDI-TOF identification of the modified proteins showed that the majority of the spots corresponded to proteins participating in known metabolic pathways: 1) glycolysis (ENO1), 2) Acetyl-CoA synthesis and tricarboxylic acid

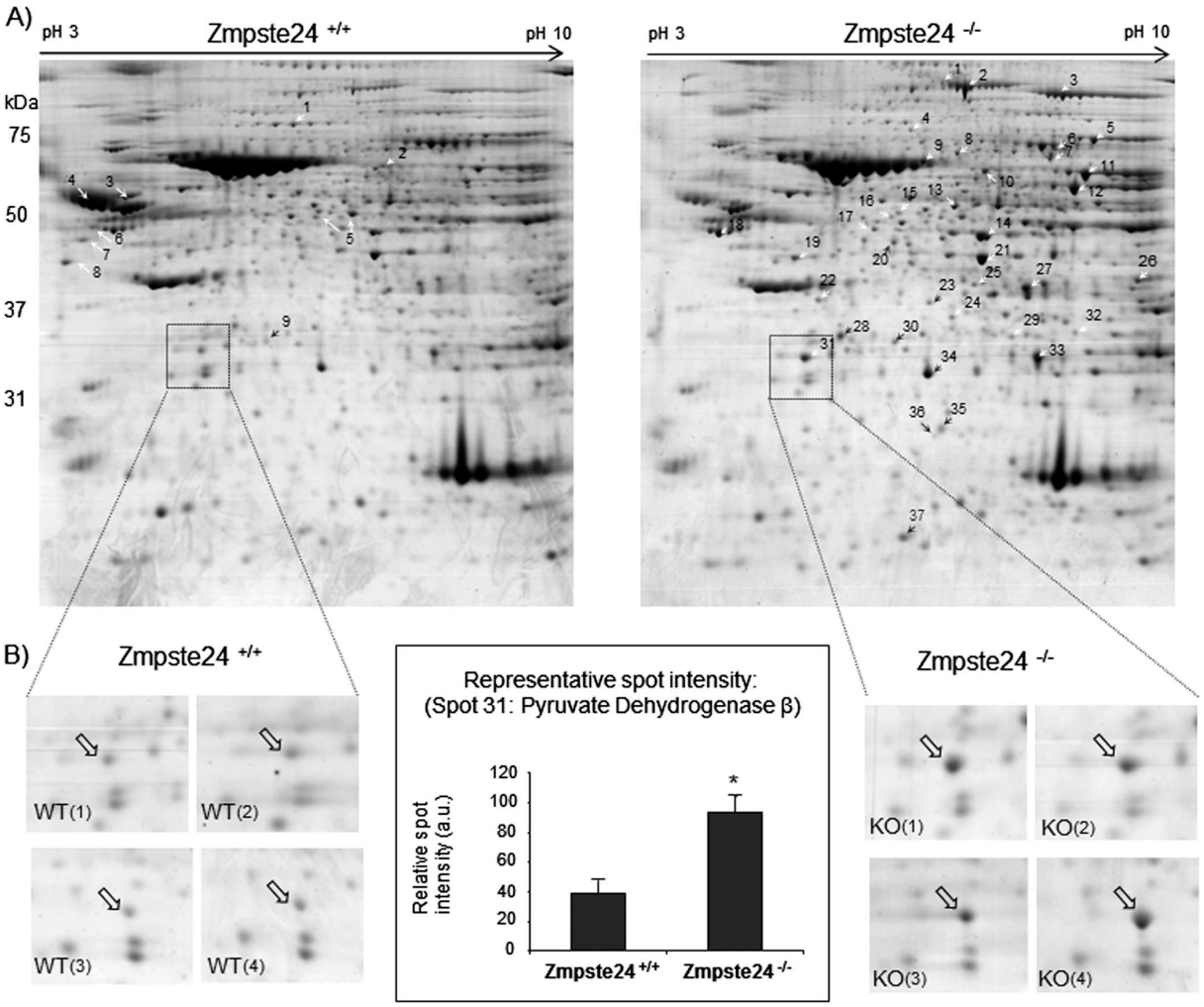

FIG. 3. ***A*, Two-dimensional-PAGE of whole adipose tissue of *Zmpste24*$^{+/+}$ and *Zmpste24*$^{-/-}$ mice.** Proteins were separated on a 2-DE gel using 18 cm pH 3–10 NL strips in the first dimension and 12% SDS-PAGE gels in the second dimension. Molecular weights are indicated (*right*). Differentially expressed proteins between the adipose tissue samples are indicated with *white* or *black* arrows. The numbers correspond to the spot numbers in Table I. *B*, Magnification of the boxed region that contains protein pyruvate dehydrogenase β (quantified in middle graph) in two-dimensional-PAGE gels corresponding to four *Zmpste24*$^{+/+}$ and four *Zmpste24*$^{-/-}$ mice. * $p < 0.05$.

(TCA) cycle-related proteins (PC, PDHB, PDX, CS, ACO2, LDH3A, DLST, SUCLG2, SDHA, ME1, and MDH), 3) pentose phosphate pathway (G6PD, PGD, TKT, and TALDO1), 4) fatty acid synthesis (FAS and ACLY), 5) fatty acid re-esterification (PCK1), 6) β-oxidation of fatty acids (ACSL1 and ACADS), 7) lipolysis (triacylglycerol (TAG) lipase -ATGL- or desnutrin), 8) the glycerol-3-phosphate shuttle (GPD1 and GPD2), and 9) valine, leucine, and isoleucine degradation (PCCA, BCATm, HIBADH, and HIBCH). Furthermore, several proteins of the mitochondrial electron transport chain (NDUFA10, UQCR1, and ATP5B), the mitochondrial response to oxidative stress (PRDX3), cytoskeleton (vimentin and gelsolin), and proteins with not yet known function in adipose tissue (HMGB1) were also identified. Classical components of the serum were also found to be modified in *Zmpste24*$^{-/-}$ mice (A2M and SERPIN1A).

Herein, we have also observed by two-dimensional electrophoresis the accumulation of partially processed lamin A in *Zmpste24*-null mice (Fig 4*A*). MALDI-TOF/TOF analysis of the protein demonstrated that the accumulated protein lacks the -aaX (Figs. 4*B* and 4*C*) which is consistent with previous findings in *Zmpste24*$^{-/-}$ fibroblasts (33), thus suggesting that, in addition to Zmpste24, other protease(s) (*i.e.* Rce1) are likely able to carry out this proteolytic step (Fig. 4*B*). Furthermore, the identified protein contains the sequence including the second proposed cleavage site of Zmpste24 (Figs. 4*B* and

 10.1074/mcp.M111.008094–5

TABLE I

A, Proteins identified by MALDI-TOF/TOF up-regulated in ZMPSTE24$^{-/-}$

Spot num.[a]	Protein name	Symbol	Accesion number[b]	MW (kDa)/pI	% Cover.[c]	Pep.[d]	Protein E-value[e]	Mean fold change[f]	P Student´s t-test[g]
1	Fatty acid synthase	FAS	CH466558	276.7/6.2	12	25	44	3.61	0.002
2	Pyruvate carboxylase	PC	EDL33053	130.3/6.2	48	46	118	2.51	0.001
3	ATP citrate lyase[h]	ACLY	NP_598798	120.5/7.3	40	43	102	2.80	0.002
4	Mitochondrial inner membrane protein	IMMT	NP_083949	84.2/6.2	36	30	33	1.96	0.037
5	Aconitase 2, mitochondrial	ACO2	NP_542364	86.3/8.1	50	37	116	2.38	0.003
6	Lamin A, precursor	PRELA-MIN	NP_733821	74.5/6.5	46	30	66	>10	
7	Acyl-CoA synthetase long-chain family member 1	ACSL1	NP_032007	78.9/6.8	42	27	83	1.88	0.044
8	Propionyl CoA-carboxylase alpha-subunit	PCCA	AAL02364	80.2/7.0	56	37	100	1.98	0.013
9	Glycerol-3-phosphate dehydrogenase, mit. precursor (GPD-M)	GPD2	Q64521	81.4/6.2	55	41	92	2.54	0.001
10	Succinate dehydrogenase	SDHA	NP_075770	73.62/7.1	48	14	15	1.62	0.048
11	Transketolase	TKT	NP_033414	68.3/7.2	63	34	139	1.77	0.010
12	Malic enzyme 1, NADP (+)-dependent, cytosolic	ME1	NP_032641	64.5/7.2	62	33	159	2.34	0.022
13	Glucose-6-phosphate 1-dehydrogenase	G6PD	NP_032088	59.7/6.1	55	40	112	1.64	0.008
14	Mitochondrial aldehyde dehydrogenase 2	ALDH2	EDL19719	55.2/8.3	54	28	159	1.71	0.005
15	Desnutrin[h]	ATGL	AAU33824	54.4/6.0	34	22	37	1.79	0.036
16	mCG3880 [similar to Al-dehyde dehydrogenase family 3 member B1]		EDL32976	52.7/6.2	32	19	36	1.44	0.050
17	Pyruvate dehydrogenase protein X	PDHX	NP_780303	54.2/7.6	35	19	31	1.79	0.020
18	Atp5b protein	ATP5B	AAH37127	56.7/5.2	64	25	112	1.40	0.018
19	Ubiquinol-cytochrome c reductase core protein 1	UQCRC1	NP_079683	53.3/5.7	48	21	86	1.84	0.039
20	2-Oxoglutarate dehydrogenase complex component E2	DLST	Q01205	49.2/8.9	38	19	37	3.55	0.002
21	Enolase 1, alpha non-neuron	ENO1	AAH03891	47.5/6.2	80	24	116	1.35	0.003
22	Succinyl-CoA ligase [GDP-forming] subunit beta	SUCLG2	NP_035637	47.1/6.6	39	16	60	1.78	0.035
23	Acyl-Coenzyme A dehydrogenase, Short/branched chain	ACADS	AAH54428	48.3/8.0	33	19	56	2.25	0.001
24	NADH dehydrogenase (ubiquinone) 1 alpha subcomplex 10[h]	NDUFA10	NP_077159	40.1/6.4	37	23	62	2.19	0.025
25	Acyl-CoA thioesterase 2, mitochondrial precursor	ACOT2	Q9QYR9	49.8/6.9	52	19	48	2.15	0.006
26	Citrate synthase, mitochondrial precursor	CS	NP_080720	51.9/8.7	31	18	42	2.23	0.009
27	Glutamate-ammonia ligase	GLUL	AAA17989	42.8/6.6	54	23	39	1.64	0.010
28	Isocitrate dehydrogena-se 3 (NAD+) alpha,	IDH3B	EDL25822	35.0/5.9	62	25	96	1.68	0.001
29	3-hydroxyisobutyryl-Coenzyme A hydrolase	HIBCH	EDK99981	43.34/8.2	59	24	60	1.63	0.050
30	Transaldolase 1	TALDO1	EDL18063	31.7/7.7	62	19	61	3.27	0.004
31	Pyruvate dehydrogenase (lipoamide) beta	PDHB	NP_077183	39.2/6.4	63	18	69	2.56	0.005
32	Branched-chain- amino-acid aminotransferase, mit.	BCATm	NP_033867	44.7/8.6	40	16	59	3.20	0.035
33	Glycerol-3-phosphate dehydrogenase	GPD1	AAA37726	38.2/6.7	68	26	68	1.74	0.009
34	Malate dehydrogenase, cytoplasmic	MDH1	NP_032644	36.6/6.2	38	13	89	1.41	0.011
35	3-hydroxyisobutyrate dehydrogenase	HIBADH	BAF42049	35.89/8.9	45	17	63	1.68	0.028
36	High mobility group box 1	HMGB1	NP_034569	24.8/6.4	57	16	47	1.87	0.023
37	Peroxiredoxin 3	PRDX3	NP_031478	28.3/7.1	31	11	104	1.45	0.009

TABLE I
B, Proteins identified by MALDI-TOF/TOF down-regulated in ZMPSTE24$^{-/-}$

Spot Num.[a]	Protein name	Symbol	Accesion number[b]	MW (kDa)/pI	% Cover.[c]	Pep.[d]	Protein E-value[e]	Mean fold change[f]	P Student´s t-test[g]
1	Gelsolin precursor	GELSOLIN	NP_666232	86.3/5.83	35	20	31	1.69	0.007
2	Phosphoenolpyruvate carboxykinase 1, cytosolic	PCK1	AAH37629	70.1/6.18	33	23	71	1.54	0.042
3	Vimentin	VIM	NP_035831	51.6/5.0	61	34	100	1.41	0.004
4	Alpha-1-antitrypsin	SERPIN 1A	AAH10988	47.3/5.2	41	17	47	1.55	0.014
5	Phosphoglycerate dehydrogenase	PHGDH	NP_058662	57.3/6.3	26	26	81	1.70	0.001
6	Vimentin	VIM	NP_035831	53.7/5.1 Observed (≈49)	66	33	107	1.88	0.067
7	Vimentin	VIM	NP_035831	53.7/5.1 Observed (≈46)	65	32	85	3.34	0.01
8	Vimentin	VIM	NP_035831	53.7/5.1 Observed (≈43)	64	36	103	5.55	0.009
9	Alpha-2-macroglobulin 35 kDa subunit, precursor	A2M	Q61838	167.1/6.2	43	15	33	1.70	0.01

[a] Spot numbers correspond to those on Fig. 3A, right panel.
[b] Accession number from the NCBInr database.
[c] Coverage of all peptide sequences matched to the identified protein sequence (%).
[d] Pep. corresponds to the number of peptides identified (Mascot).
[e] X!Tandem E-value after reverse database search [Data represented as –Log(E-value].
[f] Mean fold change indicates the average volume ratio of 4 *Zmpste24*$^{+/+}$ and 4 *Zmpste24*$^{-/-}$ animals.
[g] Only those proteins with a $p < 0.05$ (Student's t-test) were considered.
[h] Phosphorylated proteins also detected by ProQ-Diamond Staining.

10.1074/mcp.M111.008094–7

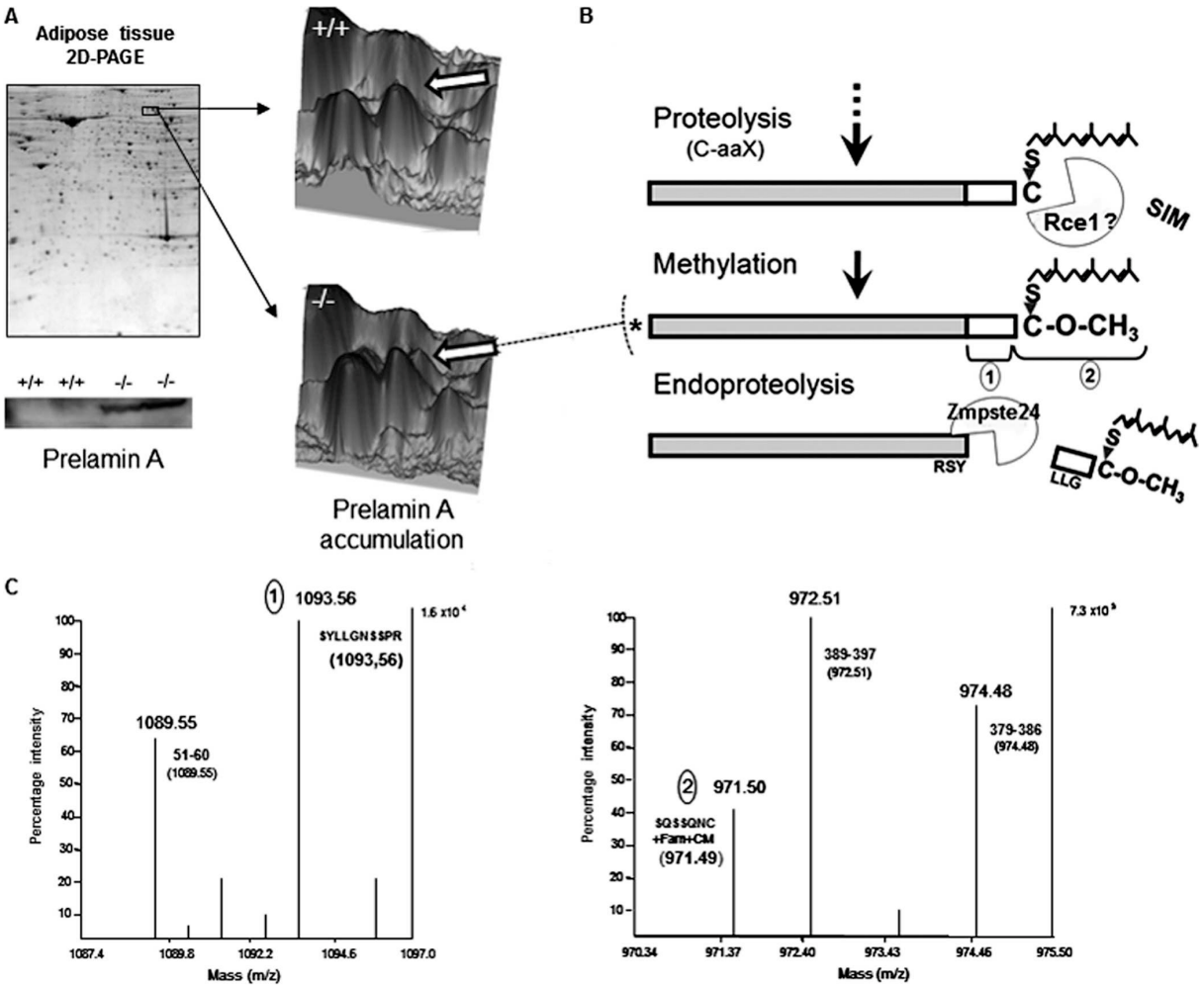

FIG. 4. **Prelamin A accumulation in *Zmpste24*$^{-/-}$ mice.** *A*, Accumulation of partially processed lamin A in *Zmpste24*-null mice could be observed in both bi-dimensional gels (pH: 3–10) and immunoblots (lower panel). *B* and *C*, Analysis of accumulated prelamin A by MALDI-TOF revealed that it corresponded to the methylated form of this protein (*B*), which does not carry the C-terminal aaX amino acids, as observed by MALDI-TOF analysis of the C-terminal tryptic peptides corresponding to the identified forms of prelamin A (1 and 2; *C*). A totally unprocessed form of prelamin A was not detected. Farn, Farnesylated; CM, Carboxymethylated.

4*C*), indicating that the protein accumulated in mutant animals corresponds exclusively to a partially mature form of lamin A (asterisk in Fig. 4*B*).

Western Blot Analysis of Altered Proteins—Immunoblotting using an antibody against β-actin revealed the existence of significant differences in β-actin protein content between *Zmpste24*$^{-/-}$ and wild-type animals (supplemental Fig. S1*A*), thus precluding its use as housekeeping gene for quantitative studies. Furthermore, neither GADPH nor tubulin gave consistent results (data not shown). Consequently, all the experiments were carried out loading equal amounts of proteins from *Zmpste24*$^{-/-}$ and wild-type mice and values were further normalized against Ponceau staining (supplemental Fig. S1*B*).

Several proteins were chosen for validation of the results obtained by two-dimensional electrophoresis: three proteins up-regulated (ME1, PRDX3, and HMGB1; Figs. 5*A*–5*C*) and two down-regulated (PCK1 and vimentin; Fig. 5*D* and Fig. 6, respectively) in *Zmpste24*$^{-/-}$ mice. These analyses revealed that ME1 was 1.5-fold increased in mutant mice (Fig. 5*A*) and PRDX3 reached a fourfold increase (Fig. 5*B*) in these animals when compared with levels observed in wild-type mice. Likewise, HMGB1 protein content was significantly higher in *Zmpste24*$^{-/-}$ mice (1.8-fold *versus* wild-type animals; Fig. 5*C*) whereas PCK1 was diminished in mutant mice (1.9-fold *versus* wild-type animals; Fig. 5*D*). Data from immunoblot studies on vimentin are discussed below.

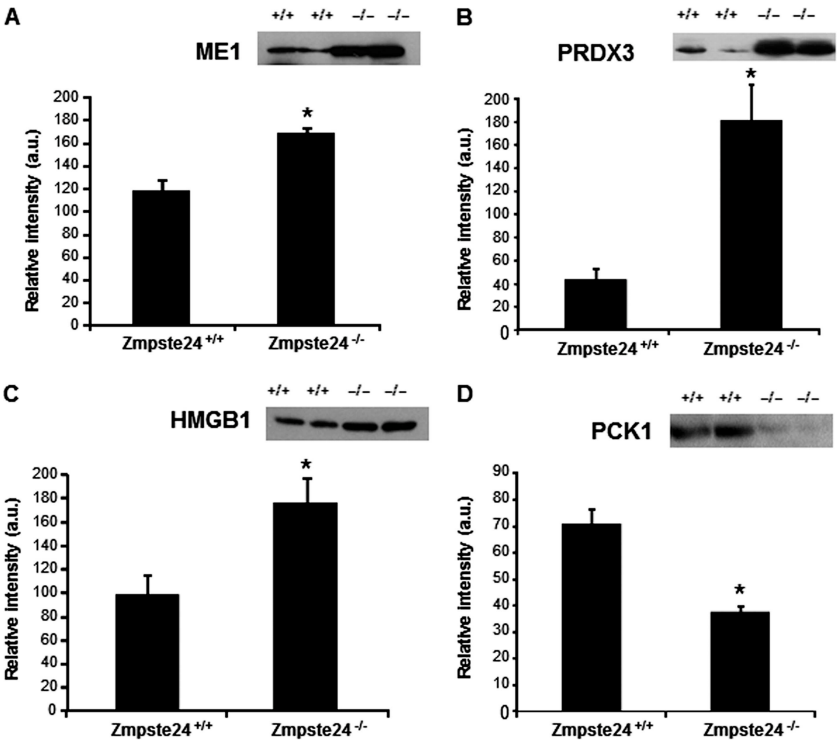

FIG. 5. **Protein abundance (by Western blot) of malic enzyme (ME1; *A*), peroxiredoxin 3 (PRDX3; *B*), high-mobility group box-1 protein (HMGB1; *C*), and phosphoenolpyruvate carboxykinase 1 (PCK1; *D*), in adipose tissue from *Zmpste24*$^{+/+}$ (*n* = 6) and *Zmpste24*$^{-/-}$ (*n* = 4) mice.** * $p < 0.05$, (±S.E.).

Differential Processing of Vimentin in Adipocytes from Zmpste24$^{-/-}$ *Mice*—Immunoblotting of adipose tissue extracts with the antivimentin serum confirmed the data obtained by two-dimensional electrophoresis on the existence of four distinct immunoreactive bands of 53, 49, 46, and 43 kDa in mice adipose tissue (Fig. 6*A*). As observed by the proteomic approach, the smaller isoforms of vimentin were down-regulated in adipose tissue from mutant mice, in particular those of 46 and 43 kDa (Fig. 6*A*). Interestingly, these two short isoforms of vimentin, together with prelamin A, were identified in the two-dimensional electrophoresis experiments as the most differentially expressed proteins between *Zmpste24*$^{-/-}$ and wild-type mice (Table I). Thus, 46-kDa and 43-kDa vimentin forms were reduced by 3.3- and 5.5-fold, respectively, in the proteome of mutant mice with respect to those observed in wild-type animals (Table I). These data are largely in accordance with the results obtained by semiquantitative immunoblotting (Fig. 6*B*).

Although the presence of vimentin isoforms has also been depicted in proteomic studies of human subcutaneous adipose tissue (15), their origin is not known and no information is yet available as to whether they may arise from alternative splicing or post-translational processing. To address this issue, we first analyzed vimentin isoforms by MALDI-TOF/TOF. The identified proteins correspond to N-terminal truncated variants within the region spanning the first 100 amino acid residues of vimentin (supplemental Fig. S2). Fig. 6*C* shows the first N-terminal tryptic peptide identified in each isoform, including their predicted molecular weight and isoelectric point. No cleavage was observed at the C-terminal end since the tryptic product was readily detected in the MALDI mass spectrum of all isoforms (supplemental Fig. S2).

Analysis of Mitochondrial Function in Zmpste24$^{-/-}$ *Adipose Tissue*—Given the finding that two proteins potentially involved in mitochondrial fatty acid β-oxidation, long-chain acyl-CoA synthetase-1 (ACSL1) and acyl-coenzymeA dehydrogenase, short chain (ACADS), were up-regulated in adipose tissue of *Zmpste24*$^{-/-}$ mice, we investigated whether mitochondrial fatty acid import could be also affected in these animals by quantifying protein levels of the key enzyme mediating this process, carnitine palmitoyltransferase I (CPT1) (34). Western immunoblotting of adipose tissue protein extracts revealed that *Zmpste24*$^{-/-}$ mice did indeed contain significantly higher levels of CPT1 than wild-type mice (Fig. 7*A*).

Since proteomic studies revealed that several proteins of the mitochondrial electron transport chain were up-regulated in the adipose tissue of *Zmpste24*-null mice, including a subunit of the mitochondrial ATP synthase complex, we hypothesized that ATP levels could be altered in *Zmpste24*-null mice. However, ATP content was not significantly modified in mutant mice (data not shown). In order to evaluate whether an increase in thermogenesis, via induction of uncoupling protein 1 (UCP-1; (35, 36)), could occur in *Zmpste24*-null mice, we investigated its expression by Western blot. No immunoreac-

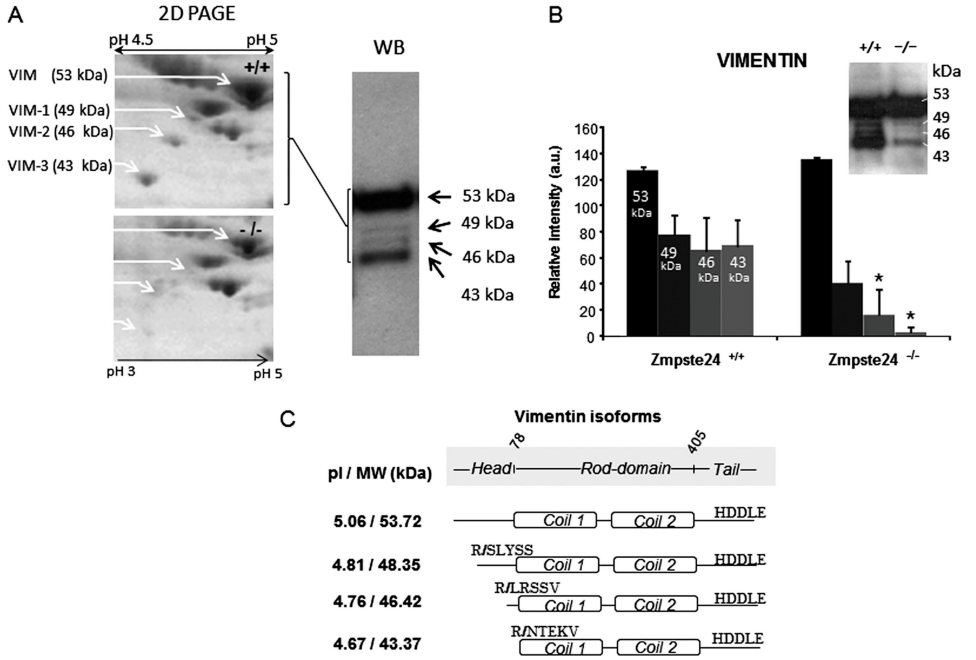

FIG. 6. ***A,* Magnification of a representative two-dimensional-PAGE gel from *Zmpste24*$^{+/+}$ and *Zmpste24*$^{-/-}$ animals showing the area of the gel containing the four identified isoforms of vimentin (53, 49, 46, and 43 kDa approximately, *left* panel).** All the isoforms were identified by Western blot using the vimentin antibody (*right* panel). Two of the identified isoforms showed significant expression differences between the two groups of animals when evaluated by Western blot (*B*). *C*, Predicted molecular weight and isoelectric point of the identified forms of vimentin on the basis of MALDI-TOF identification.

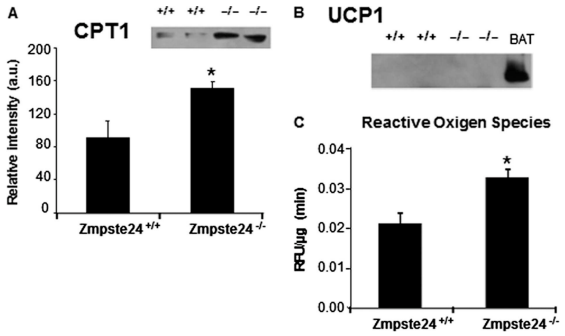

FIG. 7. **Western blot for carnitine palmitoyltransferase I (CPT1; *A*, and uncoupling protein 1 (UCP1; *B*, in adipose tissue extracts.** *C*, Analysis of ROS levels measured as relative fluorescence units (RFU) of DCF-DA, per μg of protein and minute. *Zmpste24*$^{+/+}$ ($n = 6$) and *Zmpste24*$^{-/-}$ ($n = 4$) mice * $p < 0.05$, ($\pm$S.E.).

tive band for UCP-1 was observed in these samples whereas this protein was clearly visible in immunoblots from paired samples of brown adipose tissue (Fig. 7*B*).

Finally, the increased levels of mitochondrial PRDX3 found in *Zmpste24*$^{-/-}$ fat prompted us to evaluate the occurrence of oxidative damage in the tissue. As shown in Fig. 7*C*, ROS levels were significantly enhanced in adipose tissue of *Zmpste24*$^{-/-}$ mice as compared with wild-type animals, indicating that Zmpste24 deficiency increases oxidative stress.

Analysis of the Phosphoproteome of Adipose Tissue—Phosphorylation is a ubiquitous and fundamental reversible, regulatory mechanism that enables to modify protein function by altering protein stability, cellular location, substrate affinity, complex formation, or activity (37). Herein, together with the analysis of adipose tissue from *Zmpste24*$^{-/-}$ and wild-type mice by two-dimensional-PAGE, we also employed a phosphoproteomic approach to establish the phosphorylation fingerprint of adipose tissue proteins in the presence or absence of the metalloprotease (Fig. 8*A*). This has enabled us to identify, for the first time, six proteins that are regulated in adipose tissue at the post-translational level: the mitochondrial complex I subunit NDUFA10, the ATP citrate lyase (ACLY), the rate-limiting enzyme for triglyceride catabolism in mice, desnutrin (human ATGL1), phosphoglucomutase 1 (PGM-1), desmin, and pyruvate dehydrogenase alpha 1 (PDHA1). In addition, the potential phosphorylation sites of three of these proteins were also identified (Fig. 8*B*), including three sites already described in PGM-1 (S95, T96, and T115), one in desmin (T42), and a novel phosphothreonine residue in desnutrin (T452), which is close to the two C-terminal serine residues previously reported to be phosphorylated in this protein (38). Finally, three out of the six proteins found to be highly phosphorylated in mouse adipose tissue were also identified by two-dimensional-PAGE on the basis of their overexpression in mutant animals: NDUFA10, ACLY, and desnutrin (Table I).

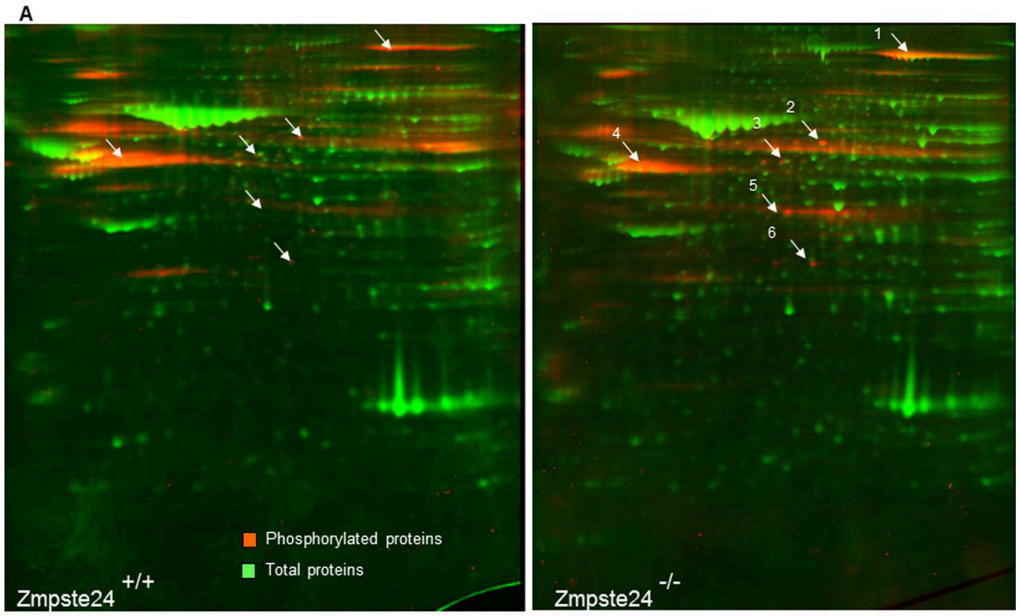

B

Name	Phospho.Detected Peptide	Score deviation (Da)
1) ACLY-1	Not Determined	
2) PGM-1	108-130 AIGGIILTASHNPGGPNGDFGIK,	0.0207.
	86-105 LVIGQNGILSTPAVSCIIRK,	0.0068 (C)[8].
3) Desnutrin	444-462 QLLLGLFCTNVAFPPDALR,	-0.001 (C)[8].
4) Desmin	38 52 AGFGTKGSSSSMTSR	0.059 (M_OX)[12]
5) PDHA1	Not Determined	
6) NDUFA10	Not Determined	

FIG. 8. ***A*, Phosphoproteomic analysis of adipose tissue from *Zmpste24*$^{+/+}$ and *Zmpste24*$^{-/-}$ mice.** *B*, The phospho-peptides identified by MALDI-TOF are indicated in the table. Potential phosphorylation sites are underlined. C: Carbamidomethyl. M_OX: *M*ethionine *O*xidated.

Serum Metabolic Profile of Zmpste24$^{-/-}$ *Mice*—Although microscopy and proteomic analysis of adipose tissue of *Zmpste24*-null mice, together with previous data on the occurrence of hepatic steatosis in these animals (27), pointed to the inability of adipocytes to properly store lipids, we observed no changes in serum FA levels in mutant mice (data not shown). To get further clues about the metabolic biomarkers associated to genetic lipodystrophy, we employed a metabolomic strategy. Serum metabolic profiling revealed 32 metabolites up-regulated in *Zmpste24*$^{-/-}$ mice whereas 22 were found to be down-regulated. Of the identified metabolites, 67% corresponded to known compounds (supplemental Table S3). Analysis of the altered metabolites by a software for pathway analysis revealed major perturbations in lipid metabolism and oxidative scavenging (Fig. 9). Remarkably, most of the down-regulated metabolites corresponded to lysophospholipids and, in particular to several molecular species of lysophosphatidylcholine (LPC). Increased levels of several steroids including corticosterone (1.9-fold change) and aldosterone (4.4- to 12.9-fold change) were also observed in *Zmpste24*$^{-/-}$ mice, suggestive of alterations in adrenal gland function in these animals. Finally, in agreement with previous observations (27), lower levels of glucose were found in mutant mice as compared with wild-type animals.

DISCUSSION

Lipodystrophy is a major disease involving severe alterations of adipose tissue distribution and metabolism. Mutations in genes encoding the nuclear protein lamin A or its processing enzyme, the metalloproteinase Zmpste24, cause diverse human progeroid syndromes and are associated with the development of lipodystrophy. By using mice deficient in Zmpste24, we report for the first time the protein fingerprint of lipoatrophy. We demonstrate that adipose tissue of *Zmpste24*$^{-/-}$ mice exhibit marked alterations in key proteins involved in lipid management and energy expenditure. This, together with an abnormal processing of the cytoskeletal protein vimentin in *Zmpste24*$^{-/-}$ adipocytes, may underlie the lipodystrophic phenotype associated with the loss of functional Zmpste24. Microscopic data revealed that *Zmpste24*$^{-/-}$ mice contained significantly smaller adipocytes than wild-type mice, thus indicating an impaired fat storage

Top Networks

ID	Associated Network Functions	Score
1	Free Radical Scavenging, Lipid Metabolism, Small Molecule Biochemistry	25
2	Cardiovascular System Development and Function, Cell Morphology, Embryonic Development	1
3	Small Molecule Biochemistry, Gene Expression, Lipid Metabolism	0

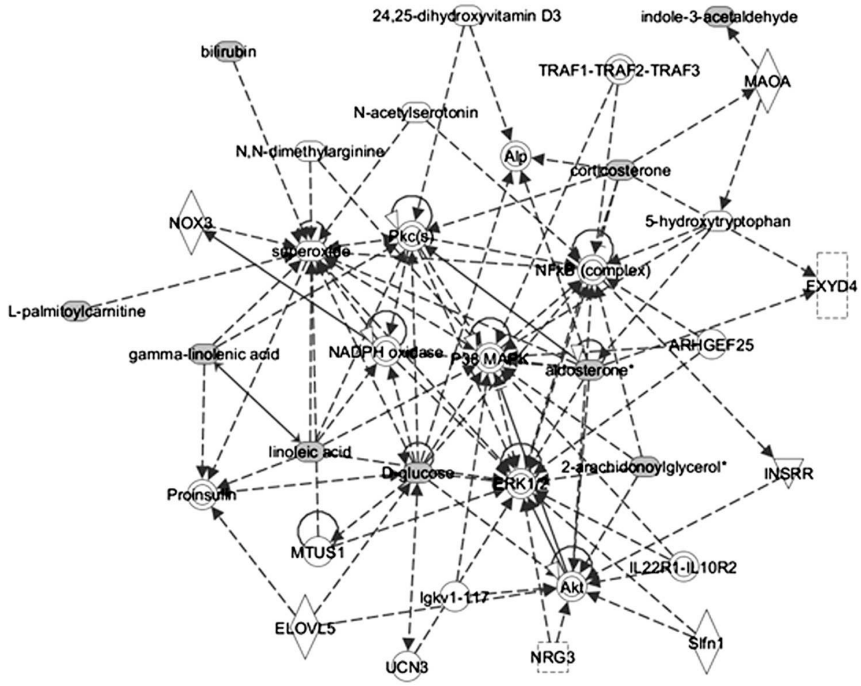

FIG. 9. **Metabolic pathway analysis of the serum metabolomics experiments allowed for the identification of one statistically significant interaction map corresponding to free radical scavenging, lipid metabolism, and small molecule biochemistry (*top*).** Nine of the identified metabolites were identified to belong to this pathway (*bottom*).

capacity in these cells. Several processes may contribute to decreased TAG accumulation: increased TAG lipolysis, decreased FA uptake or synthesis, decreased FA re-esterification and increased FA release or oxidation. Our proteomic data support the view that several of these processes may occur in *Zmpste24*-null adipocytes (Fig. 10). Thus, the observed up-regulation of the rate-limiting lipolytic enzyme adipose triglyceride lipase (human ATGL/murine desnutrin) (39) in mutant mice strongly suggest that TAG lipolysis is enhanced in these animals. Intriguingly, we have identified a novel phosphorylation site in desnutrin (T452), which is close to the two C-terminal region serines previously reported to be phosphorylated in this protein (S406 and S430) (38). It has been recently shown that phosphorylation at S406 or S430 is not necessary for the hydrolase activity of desnutrin although the C-terminal region appears to be important for TAG hydrolysis (40). Thus, it seems likely that phosphorylation at T452 plays a role in the regulation of desnutrin activity.

One of the most increased proteins in adipose tissue of null mice was fatty acid synthase (FAS), an enzyme that plays a central role in *de novo* FA biogenesis. FAS converts acetyl-CoA and malonyl-CoA into palmitate in a process that requires NADPH, which is supplied by both the pentose phosphate pathway and the pyruvate cycle (41). Interestingly, many of the enzymes participating in these pathways were also enhanced in adipose tissue of *Zmpste24*$^{-/-}$ mice. Taken together, these findings suggest that *de novo* lipogenesis is increased in mutant mice. In this scenario, the bulk of FA synthesized *de novo* or generated by TAG hydrolysis does not seem to be redirected for esterification into TAG in *Zmpste24*-null adipocytes since, besides the aforementioned reduced size of these cells, adipose tissue from mutant mice exhibited diminished levels of the key enzyme involved in glyceroneogenesis and FA re-esterification in adipocytes, PCK1 (42). In line with these findings, targeted ablation of PCK1 expression in white adipose tissue in mice reduced body fat pads and,

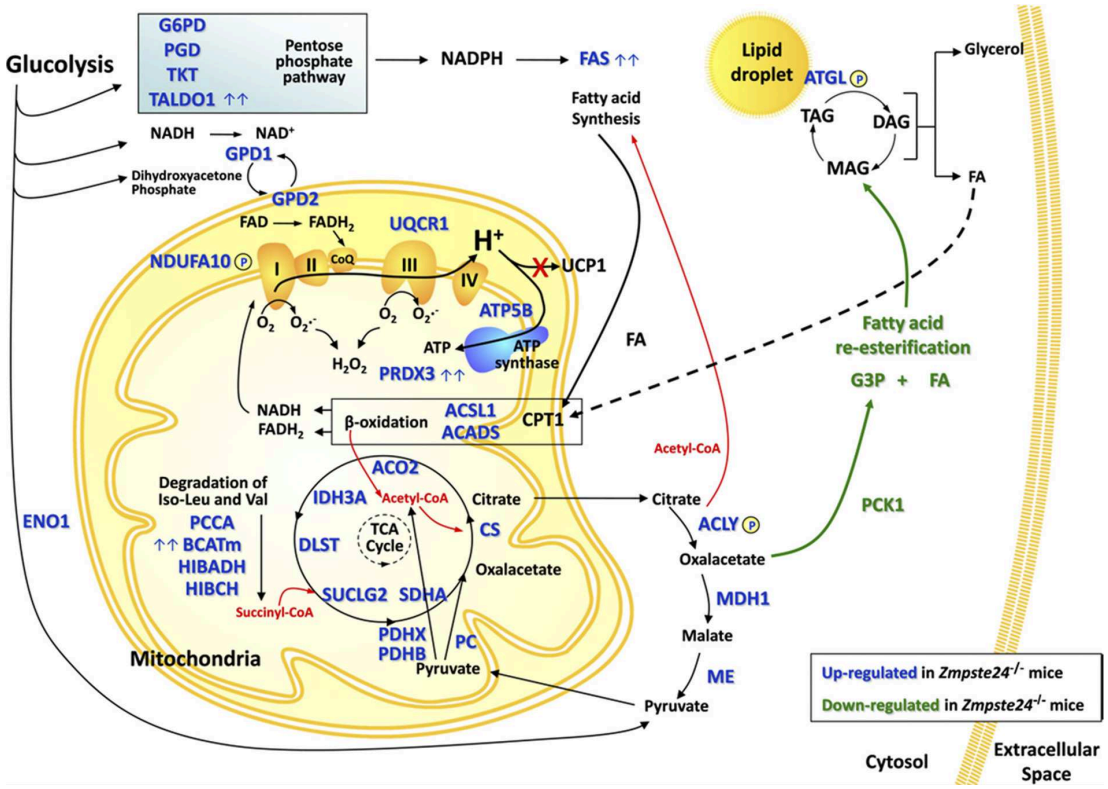

FIG. 10. **Schematic representation of the metabolic pathways altered in adipose tissue of *Zmpste24*$^{-/-}$ mice.** Up-regulated (*blue*) and down-regulated (*green*) proteins are highlighted. Proteins with more than a threefold increase between wild type and null mice are indicated with a double arrow.

more notably, nearly 25% of the mutant mice were lipodystrophic (43). Likewise, ritonavir, a common component of the antiretroviral therapy associated with the development of lipodystrophy in HIV patients (38), decreased PCK1 expression in murine 3T3-L1 adipocytes (44). Collectively, these observations favor PCK1 as a common player in the development of lipodystrophy.

Impaired FA re-esterification resulting from down-regulation of PCK1 could lead to enhanced FA efflux from *Zmpste24*-null adipocytes and subsequent ectopic deposition of lipids. Indeed, *Zmpste24*-null mice display a clear hepatic steatosis (27). Nevertheless, we (data not shown) and others (27) have found that serum FA levels are not elevated in *Zmpste24*-null mice and thus, it is unlikely that FA from adipose tissue contribute to the extensive lipid accumulation observed in mutant mice liver (27). Instead, lack of Zmpste24 seems to cause a shift within adipocytes toward increased FA utilization and energy expenditure. Thus, mutant mice exhibited enhanced levels of two enzymes involved in FA β-oxidation (ACSL1 and ACADS). These data, which are consistent with the observed up-regulation of CPT1, the enzyme responsible of FA translocation across the mitochondrial membrane (45), support the view that adipocyte shrinkage in mutant mice is due, at least in part, to an increased partitioning of FA toward β-oxidation and away from storage as TAG. Furthermore, the increased expression of several proteins associated with oxidative phosphorylation suggests that adipose tissue metabolism in mutant mice could be remodeled toward ATP production, which is rapidly mobilized to sustain the enhanced rate of FA synthesis. Notably, expression of UCP-1, normally found only in brown adipose tissue but that can be induced in white adipocytes by different stimuli (35, 36) was not altered in *Zmpste24*$^{-/-}$ mice thus suggesting that excess energy is not likely dissipated as heat, at least via UCP-1.

Taken together, our results reveal that the lack of Zmpste24 alters mitochondrial function and oxidative capacity of adipocytes. Indeed, a total of 21 out of the 37 proteins overexpressed in *Zmpste24*$^{-/-}$ mice corresponded to mitochondrial proteins involved in oxidative metabolism. Considering the prominent role of adipose tissue mitochondria in lipogenesis and adipogenesis (46), it is reasonable to propose that mitochondrial alterations caused by Zmpste24 depletion contribute to the lipoatrophic phenotype of mutant mice. Remarkably, antiretroviral treatment of HIV patients which causes severe lipoatrophies, altered the expression of genes involved in FA oxidation, TCA cycle and oxidative phosphorylation in

adipose tissue (47–49). These changes were associated to up-regulation of genes involved in oxidative stress (49, 50). In particular, HIV antiretroviral protease inhibitors (PIs), which inhibit Zmpste24 activity and lead to prelamin A accumulation (51), induce the expression of oxidative stress markers in adipose tissue in a manner comparable to that observed in patients with *LMNA* mutations (52). In accordance with these observations, evidence supporting the occurrence of oxidative stress in adipose tissue of *Zmpste24*$^{-/-}$ mice is provided by our findings of increased ROS levels. Taking into account that PRDX3 provides a primary antioxidant defense of mitochondrial respiratory chain (53, 54), increased ROS levels may account for the significant up-regulation of this peroxidase. Taken together, these findings evidence the relationship between defective prelamin A processing and oxidative stress and highlight the relevance of oxidative damage in the development of lipoatrophy. Interestingly, mitochondrial dysfunction and oxidative stress induced by antiretroviral drugs or prelamin A accumulation have been proposed to promote premature cellular senescence of preadipocytes (52). Our data on *Zmpste24*$^{-/-}$ mice, which exhibit clear features of accelerated senescence, reinforce the notion of a functional link between defective lamin A maturation, mitochondrial alterations and premature aging (55). Notably, Zmpste24 also altered normal processing of the cytoskeletal protein vimentin, an intermediate filament that has been suggested to regulate mitochondrial function by mediating the interaction of mitochondria with microtubules (56). In addition, vimentin has a prominent role in the development of lipid droplets during adipocyte differentiation (57, 58) and in the control of lipid metabolism in differentiated adipocytes (59) and, consequently, the presence of vimentin variants may be necessary to provide plasticity to the adipocyte for correct lipid management. Our proteomic analysis has enabled the identification of a novel protein dysregulated in *Zmpste24*$^{-/-}$ mice, HMGB1, whose expression in adipose tissue has not been documented previously. HMGB1 is a chromatin-binding nuclear protein implicated in DNA repair mechanisms (60), and has been also proposed to play a role in sustaining autophagy (61). Notably, previous studies have demonstrated that *Zmpste24*$^{-/-}$ mice exhibit an extensive basal activation of autophagy, which primarily represents a prosurvival mechanism, in liver, skeletal muscle and heart (27, 62). In fact, despite the progeroid phenotype of *Zmpste24*$^{-/-}$ mice, these animals also display transcriptional alterations in metabolism regulatory genes in the liver and profound changes in circulating glucose and hormone levels indicative of an activated antiaging response (27–29). In line with these findings, the shift in the expression profile of metabolic proteins found in *Zmpste24*$^{-/-}$ mice highly resembles that observed in adipose tissue from old rats subjected to calorie restriction (18). Collectively, our proteomic data support the original proposal by Mariño *et al.* (27) that a protective metabolic response is triggered in *Zmpste24*$^{-/-}$ mice in order to attenuate the deleterious consequences associated to partially processed lamin A accumulation. Despite this adaptive response, continuous mitochondrial overload and subsequent oxidative stress and, presumably, increased autophagy, would finally lead to the loss of adipose tissue observed in mutant mice.

Metabolomic analysis revealed significant changes in plasma metabolites in *Zmpste24*$^{-/-}$ mice. These include the adrenal steroids corticosterone and aldosterone, which were up-regulated in mutant animals. Interestingly, A-ZIP/F-1 mice, a mouse model of lipodystrophy, display high corticosterone serum levels, which can be partially reverted upon leptin treatment (63). Taking into account that circulating leptin is strongly diminished in *Zmpste24*$^{-/-}$ mice (27), its deficiency may contribute, at least in part, to reduce the inhibitory tone on corticosterone secretion by the adrenal gland in these animals. Circulating levels of the endocannabinoid 2-arachidonoylglycerol were highly enhanced in *Zmpste24*$^{-/-}$ animals. There are evidences that endocannabinoids, which control food intake and energy expenditure *via* central actions and are also produced by fat cells and regulate adipose tissue metabolism, are increased in plasma and adipose tissue of obese rodents and human (64). Our present findings support the view that, as in conditions of excess of body fat, the endogenous endocannabinoid system is also dysregulated in conditions of adipose tissue deficiency. Finally, mutant mice also exhibited a strong down-regulation of different species of the phosphatidylcholine derivate LPC, and both anti-inflammatory (65, 66) and pro-inflammatory (67) properties have been attributed for LPCs. Irrespectively of their function, LPCs are increased in obese rats (68) and human (69). Considering the observed LPC depletion in lipoatrophic mice, LPC may therefore constitute a new marker of adipose tissue dysfunction.

In summary, proteomic analysis of adipose tissue from *Zmpste24*$^{-/-}$ mice and measurement of several metabolites in both adipose tissue and serum has enabled us to identify the changes in the protein expression profile and metabolic state associated with lipodystrophy. Our results shed new light on the importance of mitochondrial function for the development of lipodystrophy and for the aging process and link the accumulation of a partially mature form of lamin A to the dysregulation of lipid metabolism and oxidative stress in adipocytes. This, together with our novel findings on the regulation of HMGB1 expression and vimentin processing by Zmpste24, may be useful to unveil the mechanisms underlying adipose tissue dysfunction in laminopathies and other lipodystrophic syndromes as well as to develop novel strategies that may help to prevent or ameliorate these diseases.

Acknowledgments—Mass spectrometry was performed at the Proteomics Facility (SCAI) of the University of Córdoba, which is Node 6 of the ProteoRed Consortium financed by Genoma España and belongs to the Andalusian Platform for Genomics, Proteomics and Bioinformatics. We thank Dr. M.S. Fernández-García for help with histopathological analysis.

* This work was supported by Ministerio de Ciencia e Innovación (MICINN)/FEDER (BFU2007-60180; BFU2010-17116), Junta de Andalucía/FEDER (CTS-03039, and BIO-0139), and CIBER Obesidad y Nutrición (CIBERobn), Instituto de Salud Carlos III, Spain. C.L.-O. laboratory is supported by grants from MICINN, Fundación M. Botín, and the European Union (FP7-Microenvimet). The Instituto Universitario de Oncología is supported by Obra Social Cajastur-Asturias, Spain. Metabolomics was performed by the Unit mix CIC bioGUNE- OWL Genomics.

S This article contains supplemental Figs. S1 and S2 and supplemental table S3.

‖ To whom correspondence should be addressed: Department of Cell Biology, Physiology and Immunology, Campus Universitario de Rabanales, Edificio Severo-Ochoa, Pl. 3, University of Córdoba. E-14014 Córdoba, Spain. Tel.: +34-957-21-22-56; Fax: +34-957-21-86-34; E-mail: bc2pemej@uco.es.

‡‡ E-mail: bc1mapom@uco.es.

REFERENCES

1. Kershaw, E. E., and Flier, J. S. (2004) Adipose tissue as an endocrine organ. *J Clin Endocrinol. Metab.* **89,** 2548–2556
2. de Luca, C., and Olefsky, J. M. (2006) Stressed out about obesity and insulin resistance. *Nat. Med.* **12,** 41–42
3. Waki, H., and Tontonoz, P. (2007) Endocrine functions of adipose tissue. *Annu. Rev. Pathol.* **2,** 31–56
4. Frühbeck, G. (2008) Overview of adipose tissue and its role in obesity and metabolic disorders. *Methods Mol. Biol.* **456,** 1–22
5. Huang-Doran, I., Sleigh, A., Rochford, J., O'Rahilly, S., and Savage, D. (2010) Lipodystrophy: Metabolic insights from a rare disorder. *J. Endocrinol.* **207,** 245–255
6. Chen, X., and Hess, S. (2008) Adipose proteome analysis: focus on mediators of insulin resistance. *Expert Rev. Proteomics* **5,** 827–839
7. Peral, B., Camafeita, E., Fernández-Real, J. M., and Lápez, J. A. (2009) Tackling the human adipose tissue proteome to gain insight into obesity and related pathologies. *Expert Rev. Proteomics* **6,** 353–361
8. Pérez-Pérez, R., Ortega-Delgado, F. J., García-Santos, E., López, J. A., Camafeita, E., Ricart, W., Fernández-Real, J. M., and Peral, B. (2009) Differential proteomics of omental and subcutaneous adipose tissue reflects their unalike biochemical and metabolic properties. *J. Proteome Res.* **8,** 1682–1693
9. Peinado, J. R., Jimenez-Gomez, Y., Pulido, M. R., Ortega-Bellido, M., Diaz-Lopez, C., Padillo, F. J., Lopez-Miranda, J., Vazquez-Martinez, R., and Malagón, M. M. (2010) The stromal-vascular fraction of adipose tissue contributes to major differences between subcutaneous and visceral fat depots. *Proteomics* **10,** 3356–3366
10. DeLany, J. P., Floyd, Z. E., Zvonic, S., Smith, A., Gravois, A., Reiners, E., Wu, X., Kilroy, G., Lefevre, M., and Gimble, J. M. (2005) Proteomic analysis of primary cultures of human adipose-derived stem cells: modulation by Adipogenesis. *Mol. Cell. Proteomics* **4,** 731–740
11. Roche, S., Delorme, B., Oostendorp, R. A., Barbet, R., Caton, D., Noel, D., Boumediene, K., Papadaki, H. A., Cousin, B., Crozet, C., Milhavet, O., Casteilla, L., Hatzfeld, J., Jorgensen, C., Charbord, P., and Lehmann, S. (2009) Comparative proteomic analysis of human mesenchymal and embryonic stem cells: towards the definition of a mesenchymal stem cell proteomic signature. *Proteomics* **9,** 223–232
12. Kheterpal, I., Ku, G., Coleman, L., Yu, G., Ptitsyn, A. A., Floyd, Z. E., and Gimble, J. M. (2011) Proteome of human subcutaneous adipose tissue stromal vascular fraction cells versus mature adipocytes based on DIGE. *J. Proteome Res.* **10,** 1519–1527
13. Zhong, J., Krawczyk, S. A., Chaerkady, R., Huang, H., Goel, R., Bader, J. S., Wong, G. W., Corkey, B. E., and Pandey, A. (2010) Temporal profiling of the secretome during adipogenesis in humans. *J. Proteome Res.* **9,** 5228–5238
14. Roca-Rivada, A., Alonso, J., Al-Massadi, O., Castelao, C., Peinado, J. R., Seoane, L. M., Casanueva, F. F., and Pardo, M. (2011) Secretome analysis of rat adipose tissues shows location-specific roles for each depot type. *J. Proteomics.* **74,** 1068–1079
15. Boden, G., Duan, X., Homko, C., Molina, E. J., Song, W., Perez, O., Cheung, P., and Merali, S. (2008) Increase in endoplasmic reticulum stress-related proteins and genes in adipose tissue of obese, insulin-resistant individuals. *Diabetes* **57,** 2438–2444
16. Jiang, L., Wang, Q., Yu, Y., Zhao, F., Huang, P., Zeng, R., Qi, R. Z., Li, W., and Liu, Y. (2009) Leptin contributes to the adaptive responses of mice to high-fat diet intake through suppressing the lipogenic pathway. *PLoS One* **4,** e6884
17. de Roos, B., Rungapamestry, V., Ross, K., Rucklidge, G., Reid, M., Duncan, G., Horgan, G., Toomey, S., Browne, J., Loscher, C. E., Mills, K. H., and Roche, H. M. (2009) Attenuation of inflammation and cellular stress-related pathways maintains insulin sensitivity in obese type I interleukin-1 receptor knockout mice on a high-fat diet. *Proteomics* **9,** 3244–3256
18. Valle, A., Sastre-Serra, J., Roca, P., and Oliver, J. (2010) Modulation of white adipose tissue proteome by aging and calorie restriction. *Aging Cell* **9,** 882–894
19. Joo, J. I., Kim, D. H., Choi, J. W., and Yun, J. W. (2010) Proteomic analysis for antiobesity potential of capsaicin on white adipose tissue in rats fed with a high fat diet. *J. Proteome Res.* **9,** 2977–2987
20. Jeninga, E. H., and Kalkhoven, E. (2010) Central players in inherited lipodystrophies. *Trends Endocrinol. Metab.* **21,** 581–588
21. Garg, A. (2004) Acquired and inherited lipodystrophies. *N. Engl. J. Med.* **350,** 1220–1234
22. Domingo, P., and Villarroya, F. (2010) Targets of Metabolic Toxicity of HIV Antiretroviral Drugs: The Multiple Roads to Lipodystrophy and Metabolic Syndrome. *Curr. Pharm. Des.* **16,** 3337–3338
23. Worman, H. J., Fong, L. G., Muchir, A., and Young, S. G. (2009) Laminopathies and the long strange trip from basic cell biology to therapy. *J. Clin. Invest.* **119,** 1825–1836
24. Dechat, T., Pfleghaar, K., Sengupta, K., Shimi, T., Shumaker, D. K., Solimando, L., and Goldman, R. D. (2008) Nuclear lamins: major factors in the structural organization and function of the nucleus and chromatin. *Genes Dev.* **22,** 832–853
25. Barrowman, J., and Michaelis, S. (2009) ZMPSTE24, an integral membrane zinc metalloprotease with a connection to progeroid disorders. *Biol. Chem.* **390,** 761–773
26. Pendas, A. M., Zhou, Z., Cadiñanos, J., Freije, J. M., Wang, J., Hultenby, K., Astudillo, A., Wernerson, A., Rodriguez, F., Tryggvason, K., and Lopez-Otin, C. (2002) Defective prelamin A processing and muscular and adipocyte alterations in Zmpste24 metalloproteinase-deficient mice. *Nat. Genet.* **31,** 94–99
27. Mariño, G., Ugalde, A. P., Salvador-Montoliu, N., Varela, I., Quirós, P. M., Cadiñanos, J., van der Pluijm, I., Freije, J. M., and Lopez-Otín, C. (2008) Premature aging in mice activates a systemic metabolic response involving autophagy induction. *Hum. Mol. Genet.* **17,** 2196–2211
28. Mariño, G., Ugalde, A. P., Fernández, A. F., Osorio, F. G., Fueyo, A., Freije, J. M., and López-Otin, C. (2010) Insulin-like growth factor 1 treatment extends longevity in a mouse model of human premature aging by restoring somatotroph axis function. *Proc. Natl. Acad. Sci. U.S.A.* **107,** 16268–16273
29. Ugalde, A. P., Mariño, G., and López-Otín, C. (2010) Rejuvenating somatotropic signaling: a therapeutical opportunity for premature aging? *Aging* **2,** 1017–1022
30. Elias, J. E., and Gygi, S. P. (2007) Target-decoy search strategy for increased confidence in large-scale protein identifications by mass spectrometry. *Nat. Methods* **4,** 207–214
31. Theodoridis, G., Gika, H. G., and Wilson, I. D. (2008) LC-MS-based methodology for global metabolite profiling in metabonomics/metabolomics. *Trends Analyt. Chem.* **27,** 251–260
32. Barr, J., Vázquez-Chantada, M., Alonso, C., Pérez-Cormenzana, M., Mayo, R., Galán, A., Caballeria, J., Martin-Duce, A., Tran, A., Wagner, C., Luka, Z., Lu, S. C., Castro, A., Le Marchand-Brustel, Y., Martínez-Chantar, M. L., Veyrie, N., Clement, K., Tordjman, J., Gual, P., and Mato, J. M. (2010) Liquid chromatography-mass spectrometry-based parallel metabolic profiling of human and mouse model serum reveals putative biomarkers associated with the progression of nonalcoholic fatty liver disease. *J. Proteome Res.* **9,** 4501–4512
33. Varela, I., Pereira, S., Ugalde, A. P., Navarro, C. L., Suárez, M. F., Cau, P., Cadiñanos, J., Osorio, F. G., Foray, N., Cobo, J., de Carlos, F., Lévy, N., Freije, J. M., and Lopez-Otin, C. (2008) Combined treatment with statins and aminobisphosphonates extends longevity in a mouse model of human premature aging. *Nat. Med.* **14,** 767–772
34. Rufer, A. C., Thoma, R., and Hennig, M. (2009) Structural insight into

function and regulation of carnitine palmitoyltransferase. *Cell. Mol. Life Sci.* **66,** 2489–2501
35. Orci, L., Cook, W. S., Ravazzola, M., Wang, M. Y., Park, B. H., Montesano, R., and Unger, R. H. (2004) Rapid transformation of white adipocytes into fat-oxidizing machines. *Proc. Natl. Acad. Sci. U.S.A.* **101,** 2058–2063
36. Bogacka, I., Ukropcova, B., McNeil, M., Gimble, J. M., and Smith, S. R. (2005) Structural and functional consequences of mitochondrial biogenesis in human adipocytes in vitro. *J. Clin. Endocrinol. Metab.* **90,** 6650–6656
37. Ozlu, N., Akten, B., Timm, W., Haseley, N., Steen, H., and Steen, J. A. (2010) Phosphoproteomics. *Wiley Interdiscip. Rev. Syst. Biol. Med.* **2,** 255–276
38. Kim, S. C., Chen, Y., Mirza, S., Xu, Y., Lee, J., Liu, P., and Zhao, Y. (2006) A clean, more efficient method for in-solution digestion of protein mixtures without detergent or urea. *J. Proteome Res.* **5,** 3446–3452
39. Haemmerle, G., Lass, A., Zimmermann, R., Gorkiewicz, G., Meyer, C., Rozman, J., Heldmaier, G., Maier, R., Theussl, C., Eder, S., Kratky, D., Wagner, E. F., Klingenspor, M., Hoefler, G., and Zechner, R. (2006) Defective lipolysis and altered energy metabolism in mice lacking adipose triglyceride lipase. *Science* **312,** 734–737
40. Duncan, R. E., Wang, Y., Ahmadian, M., Lu, J., Sarkadi-Nagy, E., and Sul, H. S. (2010) Characterization of desnutrin functional domains: critical residues for triacylglycerol hydrolysis in cultured cells. *J. Lipid Res.* **51,** 309–317
41. Menendez, J. A., Vazquez-Martin, A., Ortega, F. J., and Fernandez-Real, J. M. (2009) Fatty acid synthase: association with insulin resistance, type 2 diabetes, and cancer. *Clin. Chem.* **55,** 425–438
42. Beale, E. G., Hammer, R. E., Antoine, B., and Forest, C. (2002) Glyceroneogenesis comes of age. *FASEB J.* **16,** 1695–1696
43. Olswang, Y., Cohen, H., Papo, O., Cassuto, H., Croniger, C. M., Hakimi, P., Tilghman, S. M., Hanson, R. W., and Reshef, L. (2002) A mutation in the peroxisome proliferator-activated receptor gamma-binding site in the gene for the cytosolic form of phosphoenolpyruvate carboxykinase reduces adipose tissue size and fat content in mice. *Proc. Natl. Acad. Sci. U.S.A.* **99,** 625–630
44. Adler-Wailes, D. C., Guiney, E. L., Wolins, N. E., and Yanovski, J. A. (2010) Long-term ritonavir exposure increases fatty acid and glycerol recycling in 3T3-L1 adipocytes as compensatory mechanisms for increased triacylglycerol hydrolysis. *Endocrinology* **151,** 2097–2105
45. Brown, N. F., Hill, J. K., Esser, V., Kirkland, J. L., Corkey, B. E., Foster, D. W., and McGarry, J. D. (1997) Mouse white adipocytes and 3T3-L1 cells display an anomalous pattern of carnitine palmitoyltransferase (CPT) I isoform expression during differentiation. Inter-tissue and interspecies expression of CPT I and CPT II enzymes. *Biochem. J.* **327,** 225–231
46. De Pauw, A., Tejerina, S., Raes, M., Keijer, J., and Arnould, T. (2009) Mitochondrial (dys)function in adipocyte (de)differentiation and systemic metabolic alterations. *Am. J. Pathol.* **175,** 927–939
47. Mallon, P. W., Unemori, P., Sedwell, R., Morey, A., Rafferty, M., Williams, K., Chisholm, D., Samaras, K., Emery, S., Kelleher, A., Cooper, D. A., and Carr, A. (2005) In vivo, nucleoside reverse-transcriptase inhibitors alter expression of both mitochondrial and lipid metabolism genes in the absence of depletion of mitochondrial DNA. *J. Infect. Dis.* **191,** 1686–1696
48. Boothby, M., McGee, K. C., Tomlinson, J. W., Gathercole, L. L., McTernan, P. G., Shojaee-Moradie, F., Umpleby, A. M., Nightingale, P., and Shahmanesh, M. (2009) Adipocyte differentiation, mitochondrial gene expression and fat distribution: differences between zidovudine and tenofovir after 6 months. *Antivir. Ther.* **14,** 1089–1100
49. Sievers, M., Walker, U. A., Sevastianova, K., Setzer, B., Wågsäter, D., Eriksson, P., Yki-Järvinen, H., and Sutinen, J. (2009) Gene expression and immunohistochemistry in adipose tissue of HIV type 1-infected patients with nucleoside analogue reverse-transcriptase inhibitor-associated lipoatrophy. *J. Infect. Dis.* **200,** 252–262
50. Kim, M. J., Jardel, C., Barthélémy, C., Jan, V., Bastard, J. P., Fillaut-Chapin, S., Houry, S., Capeau, J., and Lombès, A. (2008) Mitochondrial DNA content, an inaccurate biomarker of mitochondrial alteration in human immunodeficiency virus-related lipodystrophy. *Antimicrob. Agents Chemother.* **52,** 1670–1676
51. Coffinier, C., Hudon, S. E., Farber, E. A., Chang, S. Y., Hrycyna, C. A., Young, S. G., and Fong, L. G. (2007) HIV protease inhibitors block the zinc metalloproteinase ZMPSTE24 and lead to an accumulation of prelamin A in cells. *Proc. Natl. Acad. Sci. U.S.A.* **104,** 13432–13437
52. Caron, M., Auclair, M., Donadille, B., Béréziat, V., Guerci, B., Laville, M., Narbonne, H., Bodemer, C., Lascols, O., Capeau, J., and Vigouroux, C. (2007) Human lipodystrophies linked to mutations in A-type lamins and to HIV protease inhibitor therapy are both associated with prelamin A accumulation, oxidative stress and premature cellular senescence. *Cell Death Differ.* **14,** 1759–1767
53. Cox, A. G., Peskin, A. V., Paton, L. N., Winterbourn, C. C., and Hampton, M. B. (2009) Redox potential and peroxide reactivity of human peroxiredoxin 3. *Biochemistry* **48,** 6495–6501
54. Kang, S. W., Chae, H. Z., Seo, M. S., Kim, K., Baines, I. C., and Rhee, S. G. (1998) Mammalian peroxiredoxin isoforms can reduce hydrogen peroxide generated in response to growth factors and tumor necrosis factor-alpha. *J. Biol. Chem.* **273,** 6297–6302
55. Findeisen, H. M., Pearson, K. J., Gizard, F., Zhao, Y., Qing, H., Jones, K. L., Cohn, D., Heywood, E. B., De Cabo, R., and Bruemmer, D. (2011) Oxidative Stress Accumulates in Adipose Tissue during Aging and Inhibits Adipogenesis. *PLoS One* **6,** e18532
56. Tang, H. L., Lung, H. L., Wu, K. C., Le, A. H., Tang, H. M., and Fung, M. C. (2008) Vimentin supports mitochondrial morphology and organization. *Biochem. J.* **410,** 141–146
57. Lieber, J. G., and Evans, R. M. (1996) Disruption of the vimentin intermediate filament system during adipose conversion of 3T3-L1 cells inhibits lipid droplet accumulation. *J. Cell Sci.* **109,** 3047–3058
58. Franke, W. W., Hergt, M., and Grund, C. (1987) Rearrangement of the vimentin cytoskeleton during adipose conversion: formation of an intermediate filament cage around lipid globules. *Cell* **49,** 131–141
59. Kumar, N., Robidoux, J., Daniel, K. W., Guzman, G., Floering, L. M., and Collins, S. (2007) Requirement of vimentin filament assembly for beta3-adrenergic receptor activation of ERK MAP kinase and lipolysis. *J. Biol. Chem.* **282,** 9244–9250
60. Prasad, R., Liu, Y., Deterding, L. J., Poltoratsky, V. P., Kedar, P. S., Horton, J. K., Kanno, S., Asagoshi, K., Hou, E. W., Khodyreva, S. N., Lavrik, O. I., Tomer, K. B., Yasui, A., and Wilson, S. H. (2007) HMGB1 is a cofactor in mammalian base excision repair. *Mol. Cell* **27,** 829–841
61. Kang, R., Livesey, K. M., Zeh, H. J., Loze, M. T., and Tang, D. (2010) HMGB1: A novel Beclin 1-binding protein active in autophagy. *Autophagy* **6,** 1209–1211
62. Mariño, G., Fernandez, A. F., and López-Otín, C. (2010) Autophagy and aging: lessons from progeria models. *Adv. Exp. Med. Biol.* **694,** 61–68
63. Lamounier-Zepter, V., Bornstein, S. R., Kunes, J., Zicha, J., Krsek, M., Ehrhart-Bornstein, M., Ziegler, C. G., Kiessling, A., Funk, R. H., and Haluzik, M. (2008) Adrenocortical changes and arterial hypertension in lipoatrophic A-ZIP/F-1 mice. *Mol. Cell. Endocrinol.* **280,** 39–46
64. Vettor, R., and Pagano, C. (2009) The role of the endocannabinoid system in lipogenesis and fatty acid metabolism. *Best Pract. Res. Clin. Endocrinol. Metab.* **23,** 51–63
65. Huang, L. S., Hung, N. D., Sok, D. E., and Kim, M. R. (2010) Lysophosphatidylcholine containing docosahexaenoic acid at the sn-1 position is anti-inflammatory. *Lipids* **45,** 225–236
66. Cunningham, T. J., Yao, L., and Lucena, A. (2008) Product inhibition of secreted phospholipase A2 may explain lysophosphatidylcholines' unexpected therapeutic properties. *J. Inflamm.* **5,** 17
67. Matsumoto, T., Kobayashi, T., and Kamata, K. (2007) Role of lysophosphatidylcholine (LPC) in atherosclerosis. *Curr. Med. Chem.* **14,** 3209–3220
68. Damian, D., Oresic, M., Verheij, E., Meulman, J. J., Friedman, J., Adourian, A., Morel, N., Smilde, A., and Greef, J. (2007) Applications of a new subspace clustering algorithm (COSA) in medical systems biology. *Metabolomics* **3,** 69–77
69. Pietiläinen, K. H., Sysi-Aho, M., Rissanen, A., Seppanen-Laakso, T., Yki-Järvinen, H., Kaprio, J., and Oresic, M. (2007) Acquired obesity is associated with changes in the serum lipidomic profile independent of genetic effects–a monozygotic twin study. *PLoS One* **2,** e218

VI. Other works related to this Doctoral Thesis period

Article 6: Guillermo Mariño, Alejandro P. Ugalde, Natalia Salvador-Montoliu, Ignacio Varela, **Pedro M. Quirós**, Juan Cadiñanos, Ingrid van der Pluijm, José M.P. Freije and Carlos López-Otín. "Premature aging in mice activates a systemic metabolic response involving autophagy induction". Hum Mol Genet. 2008; 17:2196-211.

Article 7: Alejandro P. Ugalde, Gonzalo R. Ordóñez, **Pedro M. Quirós**, Xose S. Puente, Carlos López-Otín. "Metalloproteases and the degradome". Methods Mol Biol. 2010; 622:3-29.

Article 8: Fernando G. Osorio, Claire L. Navarro, Juan Cadiñanos, Isabel C. López-Mejía, **Pedro M. Quirós**, Catherine Bartoli, José Rivera, Jamal Tazi, Gabriela Guzmán, Ignacio Varela, Danielle Depetris, Félix de Carlos, Juan Cobo, Vicente Andrés, Annachiara De Sandre-Giovannoli, José M. P. Freije, Nicolas Lévy, and Carlos López-Otín. "Splicing-directed therapy in a new mouse model of human accelerated aging". Science Transl Med. 2011; 3:106ra107.

Article 9: Alejandro Vazquez-Martin, Luciano Vellon, **Pedro M. Quirós**, Sílvia Cufí, Eunate Ruiz de Galarreta, Cristina Oliveras-Ferraros, Ángel G. Martín, Begoña Martin-Castillo, Carlos López-Otín, Javier A. Menendez. "Activation of AMP-activated protein kinase (AMPK) provides a metabolic barrier to reprogramming somatic cells into stem cells". Cell Cycle. 2012; 11(5):974-89.

Article 10: Esther Lapuente-Brun, Raquel Moreno-Loshuertos, Rebeca Acín-Pérez, Ana Latorre-Pellicer, Carmen Colás, Eduardo Balsa, Ester Perales-Clemente, **Pedro M. Quirós**, Enrique Calvo, M. A. Rodríguez-Hernández, Plácido Navas, Raquel Cruz, Ángel Carracedo, Carlos López-Otín, Acisclo Pérez-Martos, Patricio Fernández-Silva, Erika Fernández-Vizarra, and José Antonio Enríquez. "Supercomplex assembly determines electron flux in the mitochondrial electron transport chain". Science. 2013; 340:1567-70.

Article 11: Julia M. Fraile, Gonzalo R. Ordóñez, **Pedro M. Quirós**, Aurora Astudillo, José A. Galván, Dolors Colomer, Carlos López-Otín, José M.P. Freije and Xose S. Puente "Identification of novel tumor suppressor proteases by degradome profiling of colorectal carcinomas". Oncotarget. 2013 4:1919-32.

Article 12: Tania Fontanil, Susana Rúa, María Llamazares, Angela Moncada-Pazos, **Pedro M. Quirós**, Olivia García-Suárez, Jose A. Vega, Takako Sasaki, Yamina Mohamedi, Manuel M. Esteban, Alvaro J. Obaya and Santiago Cal. "Interaction between the ADAMTS-12 metalloprotease and fibulin-2 induces tumor-suppressive effects in breast cancer cells". Oncotarget. 2013 (in press)

Discussion

The study of mitochondrial function has acquired great interest over the last decades due to its large impact on human disease. Mitochondria are the core of energy production in the cell and defects in their function have consequences for all metabolic pathways. Cellular metabolism regulates, integrates and connects all these pathways, and defects in one cellular function could have consequences in other parts of the metabolic network. Thus, the role played by bioenergetics and mitochondria in the cellular and physiological functions explains why metabolic defects underlie a broad range of human diseases. Therefore, it is not surprising that, due to the importance in the regulation of cellular bioenergetics, the study of mitochondrial function has grown during the last years in parallel with that of metabolism. Moreover, the increase in metabolic disorders, likely due to lifestyle changes, has impulsed the study of metabolism and its regulation to first line of research. Furthermore, the growing observations linking metabolic dysfunctions with many common diseases have generated a new concept by which many of these pathological conditions can be redefined as metabolic disorders. For instance cancer, which has been historically viewed as a cell proliferative disorder, can also be considered as a metabolic disease, and many of the new anti-tumor therapies are based on metabolic targets (Galluzzi et al., 2013).

Mitochondrial form and function depends closely on metabolic state and vice versa (Liesa and Shirihai, 2013). Thus, the analysis of how mitochondria regulate their function is essential to understand the defects observed in several metabolic diseases. In this regard, the mitochondrial quality control system plays a key role controlling mitochondrial function (ANdreux2013). The molecular study of this system gained additional interest with the discovery of different neurological diseases caused by mutations in mitochondrial proteins, such as OPA1 or SPG7, related to this control mechanism (Casari et al., 1998; Delettre et al., 2000). Further studies of this quality control system also found relationships with other different pathological conditions (Tatsuta and Langer, 2008). However, despite the progress in this field, the physiological function of several of these proteins, including different mitochondrial proteases, remains unknown. On this basis, the first part of this Thesis has been aimed at the functional characterization of two of these mitochondrial enzymes by using mouse models (**I-IV**).

There are several mitochondrial proteases associated with the quality control system whose physiological function remains unknown. Among them, we first focused on OMA1, a zinc metalloprotease located in the mitochondrial inner membrane. This enzyme belongs to the M48 family, which also includes FACE1/ZMPSTE24, a very interesting metalloprotease associated with premature aging disorders (Navarro et al., 2005; Varela et al., 2005). Yeast OMA1 seems to play a role in mitochondrial quality control by degrading misfolded proteins in the inner membrane in cooperation with m-AAA protease (Kaser et al., 2003). This function has been proposed as a salvage system under stress conditions where the activity of

AAA protease is reduced, similarly to its homologous protease in *Escherichia coli*, HtpX, which is a stress-controlled protease located in the plasma membrane and whose activity overlaps with the AAA protease, FtsH (Shimohata et al., 2002). However, *in vitro* studies have demonstrated that in mammals OMA1 participates in the proteolytic processing of the fusion protein OPA1, together with m-AAA protease (Ehses et al., 2009; Head et al., 2009). On this basis, and to address the first two main objectives of the present Thesis, we generated mice deficient in OMA1. These mice would serve us to analyze both the molecular and physiological relevance of this mitochondrial quality control protease.

Mice deficient in OPA1 or in some proteases related to its proteolytic processing, such as SPG7, AFG3L2 or PARL, displayed severe alterations ranging from neurological disorders to embryonic lethality (Cipolat et al., 2006; Davies et al., 2007; Ferreirinha and Quattrini, 2004; Maltecca et al., 2008). However, mice deficient in OMA1 were viable, fertile and did not display any obvious alteration (**I**). This primary observation suggested a possible redundancy in the mitochondrial inner membrane proteolysis mediated by OMA1. However, a deep analysis of these mice revealed an unexpected contribution of this protease to metabolic homeostasis. *Oma1*-deficient mice displayed a diet-induced obesity phenotype, accompanied by a marked hypertrophy of adipocytes, hepatic steatosis as well as an increase in plasma triglycerides and leptin levels (**I**). In addition, *Oma1*-deficient mice also exhibited reduced energy expenditure and altered thermogenic response, common characteristics of several obesity phenotypes (Feldmann et al., 2009). The most frequent causes of obesity are increased food intake and reduced energy expenditure (Tschöp et al., 2012). Since these mice did not show increase in food intake, the reduced energy expenditure could explain the cause of obesity. Interestingly, under normal diet these mice showed increased insulin sensitivity, feature that was lost under obesity phenotype, suggesting that some metabolic conditions, such as high-fat diet, may alter the normal physiology of mice.

The *in vivo* functional relevance of OMA1 in mitochondrial function was analyzed in cells and tissues derived from Oma1 mutant mice. Thus, we established that OMA1 participates in the physiological processing of OPA1 (**I**), generating short isoforms (S-OPA1) required for the normal mitochondrial fusion. Notably, one of these short isoforms is generated exclusively by OMA1 (**I**). More importantly, we demonstrated that OMA1 plays an essential and non-redundant role in the proteolytic inactivation of OPA1, inhibiting the mitochondrial fragmentation under stress conditions (**I**). Accordingly, the absence of OMA1 induces an increase in the mitochondrial network connection, showing a highly connected and less-fragmented mitochondria, as well as a protection against mitochondrial fragmentation under stress conditions (**I**). Interestingly, the inhibition of the proteolytic inactivation of OPA1 under stress conditions also induces protection against apoptosis (**I**), because under those conditions, the stabilization of the long OPA1 isoforms (L-OPA1) prevents

cytochrome c release and mitochondrial depolarization (Cipolat et al., 2006; Freeman et al., 2006; Olichon et al., 2007). However, despite OPA1 is involved in the OXPHOS remodeling (Cogliati et al., 2013), mitochondria deficient in OMA1 did not display marked respiratory defects (**I**), indicating that OMA1 is dispensable for OXPHOS function and does not participate in the protein quality control at molecular level. Similar situation was observed in mitochondria deficient in the rhomboid PARL1 protease, also associated with the OPA1 processing and L-OPA1 stabilization (Cipolat et al., 2006). Conversely, we detected defects in beta-oxidation in Oma1-deficient cells, a process which depends on the OPA1 levels, indicating that the system OMA1-OPA1 plays a key role regulating lipid metabolism (**I**).

There is growing evidence that a number of metabolic disorders are caused by alterations of mitochondrial function and dynamics (Archer, 2013). Moreover, different studies have evidenced that changes in mitochondrial morphology can be induced as a metabolic response due to adaptations of cellular bioenergetics (Liesa and Shirihai, 2013). For example, conditions that require high energy demand, such as limited nutrient availability, induce mitochondrial elongation (Gomes et al., 2011). Conversely, excess of energy supply, such as pancreatic beta cells exposed to excess nutrients, induce mitochondrial fragmentation (Molina et al., 2009). Furthermore, changes in mitochondrial dynamics in specific tissues can influence in the general metabolic homeostasis (Kasahara et al., 2013; Sebastián et al., 2012; Shenouda et al., 2011) and for example, specific changes in neuronal circuits can have impact in the general metabolic status of mice (Dietrich et al., 2013; Schneeberger et al., 2013). Therefore, specific alterations in mitochondrial dynamics caused by OMA1 in one specific tissue may have a great impact in general homeostasis. In our analysis, we observed that the major alterations in mitochondrial function were in brown adipose tissue (BAT), where, among other defects, we found a mitochondrial dynamics alteration caused by OPA1-processing deficiency as well as defects in beta-oxidation (**I**).

The control of temperature and energy expenditure, as well as fat mass, is carried out by brown adipose tissue. Brown fat uses its high mitochondrial content and UCP1 protein to uncouple respiration and dissipates chemical energy as heat (Seale et al., 2009). This function occurs in response to the β-adrenergic stimulation induced by cold exposure and spontaneous hyperphagia, although this diet-induced thermogenesis is still controversial (Kozak, 2010). The non-shivering thermogenesis induced by cold-stress is a main regulator of energy expenditure and depends on mitochondrial dynamics (Liesa and Shirihai, 2013). Mice deficient in OMA1 showed a low night basal temperature and cold intolerance, both correlated with a decrease in heat production (**I**). Interestingly, a recent study has shown that this cold-induced adrenergic stimulation leads to mitochondrial fragmentation in BAT, which is necessary to amplify the uncoupling signal in brown adipocytes. Accordingly, defects in mitochondrial fragmentation reduce the uncoupling whereas inhibition of mitochondrial

fusion increases this process (Wikstrom et al., 2014). These data strongly support our model in which defects in mitochondrial dynamics regulation alter metabolism in brown adipose tissue explaining the obesity phenotype, the low energy expenditure and the cold intolerance observed in *Oma1*-deficient mice (**I**). Therefore, we propose that OMA1 participates in mitochondrial quality control regulating mitochondrial dynamics, and its absence induces mitochondrial dysfunctions, which have an important impact on mouse metabolic homeostasis (**I, II**).

The generation of the Oma1 mouse model has allowed us the discovery of an unexpected role of this mitochondrial quality control protease as a new key regulator of metabolic homeostasis (**II**). Interestingly, due to the fact that *Oma1*-deficient mice are not lethal, we were able to analyze the physiological and pathological relevance of this mitochondrial protease. As we demonstrated, the function of OMA1 seems to be critical under stress condition, whereas in normal situations the existence of other proteases that process OPA1 seems enough to maintain the mitochondrial dynamics equilibrium in a normal range. Interestingly, OMA1 is active under normal conditions, but highly active under stress situations, which indicates that their physiological function must be perfectly regulated to avoid OPA1 overprocessing under non-stress conditions. Although the regulation and stability of OMA1 is not completely well understood, it has been proposed that this protein remains sequestered by prohibitin complex and is released under stress conditions (Ehses et al., 2009). However, the molecular mechanisms are not yet clear and additional studies will be required to address the functional regulation of OMA1 in the mitochondrial inner membrane dynamics under pathological conditions.

The function of OMA1 under stress conditions correlates perfectly with the origin of OMA1 as a stress protease. In general, the stress signals induce healthy responses to counteract some deleterious effects. However, continuous stress signals could induce a dysfunction or aggravate the initial damage. In this context, the function of OMA1 as “backup protease” could be harmful in some pathological stress conditions. This paradoxical effect could be explained because the mitochondrial fragmentation generated after a cell injury causes apoptosis and cell death when the mitochondrial function cannot be rescued. Thus, under normal conditions, the stress response leads to mitochondrial fragmentation mediated by OMA1 to protect cell function, facilitating the recovery of mitochondria. However, under some pathological conditions, the stress response could induce a generalized cell death because the damage is constant and the cells are unable to restore their function, aggravating the initial injury and promoting a pathological situation. This hypothesis has been demonstrated in additional experiments performed in collaboration with the group of Dr. Zheng Dong in the context of renal injury (**III**). Some renal diseases such as acute kidney injury and chronic kidney disease are characterized by renal tissue injury and a decline of

renal function. The healthy renal cells display a tubular mitochondrial morphology, but the mitochondrial network becomes fragmented in the context of these renal pathologies (Zhan et al., 2013). This mitochondrial fragmentation has been demonstrated in experimental models of acute kidney injury as well as diabetic nephropathy, in both kidney cells and tissues. Importantly, this fragmentation is accompanied by cell death, suggesting that the pathogenic role of mitochondrial fragmentation is very important in renal diseases (Brooks et al., 2009).

Several signals can contribute or cause the observed mitochondrial fragmentation, including Bcl2 family proteins, over-activation of Drp1, deregulation of calcium metabolism, reactive oxygen species or mitochondrial permeability transition (Youle and van der Bliek, 2012). Interestingly, the intrinsic apoptotic pathway, characterized by the BAX/BAK-mediated mitochondrial membrane permeabilization, plays an important role under this pathological condition because mice deficient in BAX or BAK proteins are protected from acute kidney injury (Wei et al., 2013). However, the observation that mitochondrial fragmentation precedes the activation of apoptosis supports the pathogenic role of this fragmentation upstream BAX/BAK function. Thus, the over-activation of OMA1, due to an excess of damage in renal cells, could underlie the pathogenesis of these diseases. In this regard, we demonstrated that OMA1 plays a key role in OPA1 proteolysis and mitochondrial fragmentation during renal tubular cell apoptosis (**III**). Importantly, mice deficient in OMA1 exhibited better kidney function, less tubular damage and less apoptosis in response to ischemic challenge in a model of renal injury (**III**). This health improvement was associated with the stabilization of L-OPA1 isoforms, the suppression of mitochondrial fragmentation, and the decrease of cytochrome c release and apoptosis (**III**). Collectively, these data strongly suggest that the proteolytic inactivation of OPA1 mediated by OMA1 contributes to mitochondrial fragmentation and the subsequent mitochondrial damage and cell death in pathological conditions. Additionally, the inhibition of mitochondrial fragmentation or the increase in mitochondrial fusion, preventing mitochondrial damage and apoptosis, supports the relevance of mitochondrial dynamics in several pathological conditions, including renal diseases.

In summary, the generation and characterization of *Oma1*-deficient mice has contributed to clarifying the *in vivo* functional role of this metalloproteinase in mitochondrial quality control, metabolic homeostasis and pathological conditions. Thus, we have demonstrated that OMA1 deficiency causes a profound perturbation of the mitochondrial fusion–fission equilibrium that has important implications for metabolic homeostasis (**I, II**). These alterations are especially significant under metabolic stress conditions, indicating that an intact OMA1/OPA1 system is essential for developing the appropriate adaptive response to some metabolic stressors (**I, II**). Additionally, our results in the study of renal

diseases have demonstrated that the mitochondrial stress response mediated by OMA1 can contribute to cellular damage, due to an excessive stress response of mitochondrial dynamic system (**III**). Therefore, the function of OMA1 seems to be critical under some metabolic or pathological conditions reinforcing the key role of mitochondrial dynamics for human disease. Future studies with *Oma1*-deficient mice in different diseases affecting mitochondrial dynamics will help to clarify the possible clinical relevance of OMA1 inhibitors or activators to treat these pathological conditions.

To continue with the study of mitochondrial proteases and expand the knowledge on mitochondrial quality control system, we next focused on the Lon protease. LONP1 is a serine protease located in the mitochondrial matrix and whose function has been associated with quality control at molecular level. Despite Lon protease is very well known and is a conserved protein from bacteria to eukaryotic cells, its physiological role in mammals is largely unknown. To address the third and fourth objectives of this Thesis, we first generated mice deficient in this proteolytic enzyme. In contrast to Oma1, the absence of LONP1 in mice induced embryonic lethality. In addition, *Lonp1*-deficient embryos showed an almost total loss of mtDNA before dying (**IV**). These results confirm the essential function of this protease for mitochondrial function, supporting previous findings in yeast and bacteria, where the disruption of Lon protease induces serious defects (Erjavec et al., 2013). Furthermore, the inability to generate cells deficient in Lon protease and the observed decrease in the *in vitro* growth of embryos lacking LONP1 suggested that this enzyme was essential for cell life (**IV**). This embryonic lethality and some of the observed characteristics in *Lonp1*-deficient embryos were also common in other critical proteins for mitochondrial function, such as OXPHOS complex subunits or mtDNA-associated proteins, supporting the essential roles of mitochondrial function for embryonic development (Hance et al., 2005; Huang et al., 2004).

Many works have described changes in the expression levels of Lon protease in several diseases including cancer (Venkatesh et al., 2012). The putative function of LONP1 as a mitochondrial quality control protease suggests that increased expression of this proteolytic enzyme would have beneficial effects for cancer cells facilitating their survival under some stress conditions. However, all these works suggesting a link between LONP1 function and cancer were exclusively based on *in vitro* experiments or in its association with putative substrates of interest in cancer (Bernstein et al., 2012; Cheng et al., 2013; Fukuda et al., 2007). To clarify the role of LONP1 in tumor development, we studied the susceptibility of *Lonp1*-happloinsufficient mice to different chemical carcinogenesis protocols. We found that heterozygous mice for Lon protease were protected against colorectal tumors and skin papillomas (**IV**). Accordingly, the expression levels of LONP1 in human colorectal and melanoma tumor samples were increased and the survival of the corresponding patients was

lower. This essential function of LONP1 was confirmed in cell-based experiments using colorectal and melanoma cells lines, where a decrease in levels of this protease induced a reduction in cell proliferation and tumor growth, while its upregulation enhanced the tumorigenic properties of those cells (**IV**). All these data confirm *in vivo* the oncogenic properties of this quality control protease.

The function of LONP1 seems to be critical for mitochondrial function because disruption of this protease generates embryonic lethality and reduced proliferation in tumor cell lines, whereas high levels of LONP1 increase the oncogenic properties of tumor cells. Interestingly, the study of mitochondrial function in the cellular models of gain- and loss-of function of Lon protease have allowed us to find an unexpected and paradoxical situation. Thus, using melanoma cell lines we found that both upregulation and knockdown of LONP1 induced a glycolytic switch (**IV**). However, the convergence on this glycolytic switch was not caused by the same mechanism. While the glycolytic switch in cells lacking LONP1 was induced as a consequence of their mitochondrial dysfunction, the switch observed in LONP1-overexpressing cells was generated by a metabolic reprogramming. This situation has been described in other cell models and is explained because the glycolytic shift can be induced by different situations such as impairment of the mitochondrial respiratory chain, oncogenic signals during tumor transformation, or metabolic adaptations under different physiological and pathological conditions (Landor et al., 2011; Metallo and Vander Heiden, 2013; Wallace et al., 2010).

Functional analysis of cells deficient in LONP1 has also allowed us to describe an essential role for Lon protease in maintaining mitochondrial and OXPHOS function. The disruption of Lon protease induced a destabilization of complex I and some supercomplexes, due to the specific loss of structural subunits of complex I (**IV**). These alterations, consequence of the defective assembly or the mitochondrial membrane destabilization, promoted an increase in ROS, likely mediated by the defective activity of CI (Murphy, 2009), as well as loss of membrane potential and the decrease in complex V and ATP generation. In addition, both OPA1 processing and mitochondrial fragmentation were induced as a consequence of this mitochondrial dysfunction (**IV**). These subsequent alterations contributed to the decrease in respiration and functional supercomplexes assembly (Cogliati et al., 2013). Thus, the observed glycolytic switch was induced by the dysfunctional mitochondrial respiration. In addition, the continuous stress promoted a deleterious cellular signal that activates a genetic damage response which finally triggers cell cycle arrest and senescence (**IV**). This mitochondrial dysfunction and the subsequent defects in respiration have also been reported in yeast as well as in some cellular models (Bayot et al., 2010; Bota et al., 2005).

On the other hand, we found that upregulation of LONP1 induced a remodeling of mitochondrial OXPHOS system, characterized by a general decrease in all mitochondrial complexes and supercomplexes as well as in the global respiration. However, it is noteworthy that the reduction in complex I was mainly due to a decrease in functional subunits, whereas other structural subunits, which were reduced in *Lonp1*-knockdown cells, were increased (**IV**). These changes that increase the stability and reduce the activity of complex I support a molecular control mechanism under low mitochondrial respiration requirements. Thus, this regulated inactivation could maintain the ability to activate the respiration in order to increase metabolic flexibility when it is required, a mechanism which has been proposed in other similar contexts (Dieteren et al., 2012). Accordingly, the decrease in mitochondrial respiration favors the glycolytic switch because under glycolytic metabolism is unnecessary to maintain an excess of active mitochondrial complexes (Hsu and Sabatini, 2008). These changes are part of a metabolic reprogramming response which favors tumor cells under some conditions, explaining why increased levels of LONP1 are very common in tumor cell lines. In fact, the metabolic reprogramming of cancer cells has been recently established as a new hallmark of cancer, due to its ability to induce changes in tumor cells that provide them with proliferative advantages and adaptive responses against the stress conditions associated with tumorigenesis (Ward and Thompson, 2012). Interestingly, as part of this reprogramming mediated by LONP1, we have also observed increased levels of different components of protein synthesis machinery, as well as a series of chromatin remodelers and components of the spliceosome, proteasome and chaperone-containing complexes (**IV**). Notably, all of these proteins were found decreased in the Lonp1-knockdown cells, indicating that those changes were mediated by this mitochondrial protease (**IV**). The upregulation of these proteins together with the glycolytic switch explains the enhanced of the tumorigenic properties observed in these cells. Collectively, our results highlight the role of LONP1 as an essential protease for cell life contributing to the maintenance of mitochondrial integrity, as well as a necessary protease for tumor growth due to its ability to maintain and modulate mitochondrial activity and metabolic reprogramming.

In summary, the generation of *Lonp1*-deficient mice has allowed us to identify the key roles of this mitochondrial quality control protease for cell life and organismal viability. In addition, we have demonstrated the functional in vivo roles of this mitochondrial protease in tumor development, identifying this enzyme as an oncogenic protease in both human and mice. Additionally, we have characterized LONP1 as a quality control protease that maintains the functionality of OXPHOS system and dynamics contributing to the metabolic reprogramming of cancer cells. Finally, the identification of Lon protease as a key metabolic regulator affecting mitochondrial reprogramming and tumor bioenergetics, may open a new way to develop cancer therapies targeting this essential protease.

The generation of mouse models deficient in selected mitochondrial proteases has allowed us to analyze mitochondrial alterations caused by defects in components of the mitochondrial quality control. However, some mitochondrial dysfunctions are not only caused by defects or mutations in mitochondrial proteins, but can also be a consequence of different cellular alterations. In particular, mitochondrial dysfunction induced during aging as an initial response to the damage, becomes deleterious when the damage or stress conditions are persistent (Lopez-Otin et al., 2013). The availability in our laboratory of a mouse model of accelerated aging, caused by defects in the metalloproteinase Zmpste24 (Pendás et al., 2002), encouraged us to study the mitochondrial and metabolic alterations underlying the adipose tissue dysfunctions observed in these mice. *Zmpste24*-deficient mice accumulate prelamin A and are a reliable model of human Hutchinson-Gilford progeria syndrome (HGPS), which is caused by a mutation in the *LMNA* gene that generates a toxic form of the protein called progerin (Gordon et al., 2014). One common feature in progeroid syndromes is the development of lipodystrophy, characterized by the generalized loss of fat deposits. Lipodystrophy involves severe alterations of adipose tissue distribution and metabolism, and can be caused by genetic or metabolic defects. On this basis, the last objective of this Thesis was to describe the protein fingerprint of the lipoatrophy observed in *Zmpste24*-deficient mice in order to characterize the mitochondrial and metabolic alterations underlying this lipodystrophic syndrome.

Mice deficient in *Zmpste24* display a decrease in fat deposits accompanied with a reduction in the adipocyte size, which suggests the occurrence of an impairment of the fat storage capacity in these animals (**V**). To unravel the causes underlying this lipodystrophic phenotype, we analyzed the proteomic profile of the white adipose tissue obtained from these mice to characterize the different altered pathways. Several processes may contribute to the decrease in lipid accumulation such as an increase in triacylglyceride lipolysis; a decrease in fatty-acid synthesis, uptake or re-esterification; or an increase in fatty-acid oxidation or release. In this regard, several proteins of lipolysis and beta-oxidation were found increased whereas some enzymes of fatty acid re-esterification were decreased in *Zmpste24*-deficient mice. Surprisingly, we also found increased levels of fatty acid synthase, an enzyme that plays a central role in *de novo* fatty acid biogenesis, as well as enzymes of the pentose phosphate pathway and pyruvate cycle, which supply NADPH to the fatty acid synthesis (Menendez and Lupu, 2007). These data strongly suggest an increase in fatty acid oxidation using lipids generated by lipolysis or synthesized *de novo*, which explains the reduction in adipocyte size likely contributing to the lipodystrophic phenotype (**V**). In addition, there were increased levels of several proteins associated with oxidative phosphorylation, suggesting that the adipose tissue metabolism from these mutant mice has increased OXPHOS function powered by lipids (**V**). Additionally, *Zmpste24*-deficient mice also showed an increase in ROS levels, which could contribute to the damage in adipose

tissue function. Thus, these data suggest that the metabolic reprogramming observed in the mitochondria of adipose tissue could be inefficient, generating an uncoupling respiration due to the molecular alterations produced by the toxic effects of prelamin A. In this regard, the increase in peroxidase PRDX3 could provide a primary antioxidant defense against mitochondrial respiratory chain (Cox et al., 2009). Moreover, considering the prominent role of the mitochondria from adipose tissue in lipogenesis and adipogenesis (De Pauw et al., 2009), we propose that mitochondrial alterations caused by Zmpste24 depletion contribute to the lipoatrophic phenotype of mutant mice. Interestingly, a recent study using skin fibroblasts derived from HGPS mouse models has demonstrated a mitochondrial dysfunction induced by the expression of progerin or prelamin A (Rivera-Torres et al., 2013). This study has shown a decrease in mitochondrial respiration, characterized by a loss of OXPHOS subunits, and decrease in complex IV activity and ATP production, together with an increase in glycolytic enzymes. In addition, a similar study has shown a decrease in complex IV and mitochondrial ATP production in heart tissue samples (Villa-Bellosta et al., 2013). While these data could represent differences with our model regarding mitochondrial function, the tissue functionality may explain those changes.

The increase in lipolysis and beta-oxidation observed in our model could be induced as a response to counteract the decrease in ATP production and energy mediated by local or systemic effects. In this regard, an increase in beta-oxidation was observed in the liver of these mice to counteract the upregulation of the gluconeogenic pathway and the low levels of glucose present in these mice (Mariño et al., 2008). It is noteworthy that the metabolic alterations previously described in *Zmpste24*-deficient mice have been proposed as prosurvival mechanisms activated in response to the extensive damage. For instance, the basal activation of autophagy in liver, skeletal muscle and heart, the metabolic transcriptional changes in liver, and the profound changes in circulating glucose and hormone levels, suggest an activation of an anti-aging response (Mariño et al., 2008; Ugalde et al., 2010). Interestingly, the changes in the expression profile of metabolic proteins found in our study highly resemble those observed in adipose tissue from old rats subjected to calorie restriction (Valle et al., 2010). Therefore, our data strongly support the original proposals by which a protective metabolic response is triggered in *Zmpste24*-deficient mice in order to attenuate the deleterious consequences associated with prelamin A accumulation.

Additionally, along with the proteomic approach, we also conducted a serum metabolomic analysis which revealed several markers of lipodystrophy, mostly lipid compounds belonging to the free radical scavenging, lipid metabolism, and small molecule biochemistry categories, further supporting that the changes in these proteins are relevant to the deregulation of lipid metabolism in the premature aging phenotype (**V**). On the other hand, we found an alteration in the processing of the cytoskeletal protein vimentin which could

provide another alteration in the lipid droplets of the adipocytes deficient in *Zmpste24*. It has been suggested that vimentin regulates mitochondrial function by mediating the interaction of mitochondria with microtubules (Tang et al., 2008). In addition, vimentin plays a role in the development of lipid droplets during adipocyte differentiation and in the control of lipid metabolism in differentiated adipocytes (Shen et al., 2012). Therefore, the absence of short isoforms of vimentin in *Zmpste24*-deficient mice could contribute to the alterations in the lipid metabolism.

Taken together, our findings shed new light on the importance of mitochondrial function for the development of lipodystrophy as well as for the aging process, and link the accumulation of an immature form of lamin A to the deregulation of lipid metabolism and oxidative stress in adipocytes. Moreover, our data suggesting an increase in mitochondrial function and ROS production together with alterations in lipid metabolism may be useful to unveil the mechanisms underlying adipose tissue dysfunction in laminopathies and other lipodystrophic syndromes, as well as to develop novel strategies that may help to prevent or ameliorate these diseases.

In summary, in this Thesis we have tried to increase the knowledge on mitochondrial function and the links of these organelles with relevant diseases such as metabolic disorders and cancer. Thus, the generation of mouse models deficient in mitochondrial proteases OMA1 and LONP1 have allowed us to underscore the physiological and pathological relevance of both proteolytic enzymes. In the first part of this work, we have analyzed the *Oma1*-deficient mice identifying an unexpected role of this mitochondrial protease in metabolic homeostasis. In addition, we have found that OMA1 plays a non-redundant regulatory function of mitochondrial dynamics under stress conditions, and that this protective role can be deleterious under pathological steady stress conditions such as those occurring in acute renal injury. Additionally, we have generated mice deficient in the Lon protease that have allowed us to characterize the essential role of this proteolytic enzyme in mitochondrial function and cell life. Further, we have identified LONP1 as an oncogenic protease that participates in the maintenance of mitochondrial function. Moreover, we have demonstrated that LONP1 plays a key role regulating OXPHOS function and participates in the metabolic reprogramming of cancer cells. Finally, by using a mouse model of accelerated aging, we have characterized the mitochondrial and metabolic alterations in the adipose tissue of these progeroid mice, which likely underlie the lipodystrophic phenotype characteristic of these animals and of patients with accelerated aging syndromes. Collectively, our work has tried to highlight the relevance of mitochondrial proteases and metabolic and mitochondrial regulation in human life and disease, and hopefully, may contribute to improve some aspects of devastating pathological conditions associated with these processes.

Conclusions

1. OMA1 plays an essential and non-redundant role in the *in vivo* proteolytic inactivation of OPA1.

2. OMA1 is a new metabolic factor which controls energy expenditure and thermogenesis in mice through the regulation of mitochondrial dynamics.

3. OMA1 function results detrimental under mitochondrial stress conditions in acute kidney injury contributing to renal cell death.

4. LONP1 is a mitochondrial protease essential for embryonic development and cell viability, whose loss induces mitochondrial dysfunction and triggers cellular senescence.

5. LONP1 is an oncogenic protease that controls metabolic reprogramming through remodeling of mitochondrial function

6. The lipodystrophic phenotype observed of *Zmpste24*-deficient mice is caused by the defective processing of the cytoskeletal protein vimentin together with mitochondrial dysfunction and severe metabolic alterations.

Bibliography

Acín-Pérez R, Bayona-Bafaluy MP, Bueno M, Machicado C, Fernández-Silva P, Pérez-Martos A, Montoya J, López-Pérez MJ, Sancho J, Enríquez JA (2003) An intragenic suppressor in the cytochrome c oxidase I gene of mouse mitochondrial DNA. *Hum. Mol. Genet.* 12:329–39.

Acin-Perez R, Enriquez JA (2013) The function of the respiratory supercomplexes: The plasticity model. *Biochim. Biophys. Acta* .

Acín-Pérez R, Fernández-Silva P, Peleato ML, Pérez-Martos A, Enriquez JA (2008) Respiratory active mitochondrial supercomplexes. *Mol. Cell* 32:529–39.

Anand R, Langer T, Baker MJ (2013) Proteolytic control of mitochondrial function and morphogenesis. *Biochim. Biophys. Acta* 1833:195–204.

Andreux PA, Houtkooper RH, Auwerx J (2013) Pharmacological approaches to restore mitochondrial function. *Nat. Rev. Drug Discovery* 12:465–83.

Antinozzi PA, Segall L, Prentki M, McGarry JD, Newgard CB (1998) Molecular or pharmacologic perturbation of the link between glucose and lipid metabolism is without effect on glucose-stimulated insulin secretion. A re-evaluation of the long-chain acyl-CoA hypothesis. *J. Biol. Chem.* 273:16146–54.

Archer SL (2013) Mitochondrial dynamics–mitochondrial fission and fusion in human diseases. *N. Engl. J. Med.* 369:2236–51.

Autret A, Martin SJ (2009) Emerging role for members of the Bcl-2 family in mitochondrial morphogenesis. *Mol. Cell* 36:355–63.

Baker BM, Haynes CM (2011) Mitochondrial protein quality control during biogenesis and aging. *Trends Biochem Sci* 36:254–61.

Baker MJ, Tatsuta T, Langer T (2011) Quality control of mitochondrial proteostasis. *Cold Spring Harb Perspect Biol* 3:1–19.

Balbín M, Fueyo A, Tester AM, Pendás AM, Pitiot AS, Astudillo A, Overall CM, Shapiro SD, López-Otín C (2003) Loss of collagenase-2 confers increased skin tumor susceptibility to male mice. *Nat. Genet.* 35:252–7.

Barr J, Vázquez-Chantada M, Alonso C, Pérez-Cormenzana M, Mayo R, Galán A, Caballería J, Martín-Duce A, Tran A, Wagner C, Luka Z, Lu SC, Castro A, Le Marchand-Brustel Y, Martínez-Chantar ML, Veyrie N, Clément K, Tordjman J, Gual P, Mato JM (2010) Liquid chromatography-mass spectrometry-based parallel metabolic profiling of

human and mouse model serum reveals putative biomarkers associated with the progression of nonalcoholic fatty liver disease. *J. Proteome Res.* 9:4501–12.

Bayot A, Gareil M, Rogowska-Wrzesinska A, Roepstorff P, Friguet B, Bulteau AL (2010) Identification of novel oxidized protein substrates and physiological partners of the mitochondrial ATP-dependent Lon-like protease Pim1. *J. Biol. Chem.* 285:11445–57.

Bernstein SH, Venkatesh S, Li M, Lee J, Lu B, Hilchey SP, Morse KM, Metcalfe HM, Skalska J, Andreeff M, Brookes PS, Suzuki CK (2012) The mitochondrial ATP-dependent Lon protease: a novel target in lymphoma death mediated by the synthetic triterpenoid CDDO and its derivatives. *Blood* 119:3321–9.

Bonifati V, Rizzu P, van Baren MJ, Schaap O, Breedveld GJ, Krieger E, Dekker MCJ, Squitieri F, Ibanez P, Joosse M, van Dongen JW, Vanacore N, van Swieten JC, Brice A, Meco G, van Duijn CM, Oostra BA, Heutink P (2003) Mutations in the DJ-1 gene associated with autosomal recessive early-onset parkinsonism. *Science* 299:256–9.

Bonn F, Tatsuta T, Petrungaro C, Riemer J, Langer T (2011) Presequence-dependent folding ensures MrpL32 processing by the m-AAA protease in mitochondria. *EMBO J.* 30:2545–56.

Bonzon-Kulichenko E, Pérez-Hernández D, Núñez E, Martínez-Acedo P, Navarro P, Trevisan-Herraz M, Ramos MdC, Sierra S, Martínez-Martínez S, Ruiz-Meana M, Miró-Casas E, García-Dorado D, Redondo JM, Burgos JS, Vázquez J (2011) A robust method for quantitative high-throughput analysis of proteomes by 18O labeling. *Mol. Cell. Proteomics* 10:M110.003335.

Bota Da, Davies KJa (2002) Lon protease preferentially degrades oxidized mitochondrial aconitase by an ATP-stimulated mechanism. *Nat. Cell Biol.* 4:674–80.

Bota Da, Ngo JK, Davies KJa (2005) Downregulation of the human Lon protease impairs mitochondrial structure and function and causes cell death. *Free Radical Biol Med* 38:665–77.

Braschi E, Zunino R, McBride HM (2009) MAPL is a new mitochondrial SUMO E3 ligase that regulates mitochondrial fission. *EMBO Rep.* 10:748–54.

Bratic A, Larsson NG (2013) The role of mitochondria in aging. *J. Clin. Invest.* 123:951–7.

Brooks C, Wei Q, Cho SG, Dong Z (2009) Regulation of mitochondrial dynamics in acute kidney injury in cell culture and rodent models. *J. Clin. Invest.* 119:1275–85.

Casari G, De Fusco M, Ciarmatori S, Zeviani M, Mora M, Fernandez P, De Michele G, Filla A, Cocozza S, Marconi R, Dürr A, Fontaine B, Ballabio A (1998) Spastic paraplegia and

OXPHOS impairment caused by mutations in paraplegin, a nuclear-encoded mitochondrial metalloprotease. *Cell* 93:973–83.

Chae YC, Caino MC, Lisanti S, Ghosh JC, Dohi T, Danial NN, Villanueva J, Ferrero S, Vaira V, Santambrogio L, Bosari S, Languino LR, Herlyn M, Altieri DC (2012) Control of tumor bioenergetics and survival stress signaling by mitochondrial HSP90s. *Cancer Cell* 22:331–44.

Chen H, Detmer SA, Ewald AJ, Griffin EE, Fraser SE, Chan DC (2003) Mitofusins Mfn1 and Mfn2 coordinately regulate mitochondrial fusion and are essential for embryonic development. *J. Cell Biol.* 160:189–200.

Cheng CW, Kuo CY, Fan CC, Fang WC, Jiang SS, Lo YK, Wang TY, Kao MC, Lee AYL (2013) Overexpression of Lon contributes to survival and aggressive phenotype of cancer cells through mitochondrial complex I-mediated generation of reactive oxygen species. *Cell death & disease* 4:e681.

Cipolat S, Martins de Brito O, Dal Zilio B, Scorrano L (2004) OPA1 requires mitofusin 1 to promote mitochondrial fusion. *Proc. Natl. Acad. Sci. U.S.A.* 101:15927–15932.

Cipolat S, Rudka T, Hartmann D, Costa V, Serneels L, Craessaerts K, Metzger K, Frezza C, Annaert W, Derks C, Dejaegere T, Pellegrini L, Scorrano L, Strooper BD, D'Adamio L, D'Hooge R, De Strooper B (2006) Mitochondrial rhomboid PARL regulates cytochrome c release during apoptosis via OPA1-dependent cristae remodeling. *Cell* 126:163–75.

Civitarese AE, MacLean PS, Carling S, Kerr-Bayles L, McMillan RP, Pierce A, Becker TC, Moro C, Finlayson J, Lefort N, Newgard CB, Mandarino L, Cefalu W, Walder K, Collier GR, Hulver MW, Smith SR, Ravussin E (2010) Regulation of skeletal muscle oxidative capacity and insulin signaling by the mitochondrial rhomboid protease PARL. *Cell Metab.* 11:412–26.

Claypool SM (2009) Cardiolipin, a critical determinant of mitochondrial carrier protein assembly and function. *Biochim. Biophys. Acta* 1788:2059–68.

Cogliati S, Frezza C, Soriano ME, Varanita T, Quintana-Cabrera R, Corrado M, Cipolat S, Costa V, Casarin A, Gomes LC, Perales-Clemente E, Salviati L, Fernandez-Silva P, Enriquez JA, Scorrano L (2013) Mitochondrial cristae shape determines respiratory chain supercomplexes assembly and respiratory efficiency. *Cell* 155:160–71.

Cox AG, Peskin AV, Paton LN, Winterbourn CC, Hampton MB (2009) Redox potential and peroxide reactivity of human peroxiredoxin 3. *Biochemistry* 48:6495–501.

Davies VJ, Hollins AJ, Piechota MJ, Yip W, Davies JR, White KE, Nicols PP, Boulton ME, Votruba M (2007) Opa1 deficiency in a mouse model of autosomal dominant optic atrophy

impairs mitochondrial morphology, optic nerve structure and visual function. *Hum. Mol. Genet.* 16:1307–18.

De Pauw A, Tejerina S, Raes M, Keijer J, Arnould T (2009) Mitochondrial (dys)function in adipocyte (de)differentiation and systemic metabolic alterations. *Am. J. Pathol.* 175:927–39.

Delettre C, Lenaers G, Griffoin JM, Gigarel N, Lorenzo C, Belenguer P, Pelloquin L, Grosgeorge J, Turc-Carel C, Perret E, Astarie-Dequeker C, Lasquellec L, Arnaud B, Ducommun B, Kaplan J, Hamel CP (2000) Nuclear gene OPA1, encoding a mitochondrial dynamin-related protein, is mutated in dominant optic atrophy. *Nat. Genet.* 26:207–210.

Di Bella D, Lazzaro F, Brusco A, Plumari M, Battaglia G, Pastore A, Finardi A, Cagnoli C, Tempia F, Frontali M, Veneziano L, Sacco T, Boda E, Brussino A, Bonn F, Castellotti B, Baratta S, Mariotti C, Gellera C, Fracasso V, Magri S, Langer T, Plevani P, Di Donato S, Muzi-Falconi M, Taroni F (2010) Mutations in the mitochondrial protease gene AFG3L2 cause dominant hereditary ataxia SCA28. *Nat. Genet.* 42:313–21.

Dieteren CEJ, Koopman WJH, Swarts HG, Peters JGP, Maczuga P, van Gemst JJ, Masereeuw R, Smeitink JAM, Nijtmans LGJ, Willems PHGM (2012) Subunit-specific incorporation efficiency and kinetics in mitochondrial complex I homeostasis. *J. Biol. Chem.* 287:41851–60.

Dietrich MO, Liu ZW, Horvath TL (2013) Mitochondrial dynamics controlled by mitofusins regulate agrp neuronal activity and diet-induced obesity. *Cell* 155:188–99.

Ehses S, Raschke I, Mancuso G, Bernacchia A, Geimer S, Tondera D, Martinou JC, Westermann B, Rugarli EI, Langer T (2009) Regulation of OPA1 processing and mitochondrial fusion by m-AAA protease isoenzymes and OMA1. *J. Cell Biol.* 187:1023–36.

Elias JE, Gygi SP (2007) Target-decoy search strategy for increased confidence in large-scale protein identifications by mass spectrometry. *Nat. Methods* 4:207–14.

Erjavec N, Bayot A, Gareil M, Camougrand N, Nystrom T, Friguet B, Bulteau AL (2013) Deletion of the mitochondrial Pim1/Lon protease in yeast results in accelerated aging and impairment of the proteasome. *Free Radical Biol Med* 56:9–16.

Falkevall A, Alikhani N, Bhushan S, Pavlov PF, Busch K, Johnson KA, Eneqvist T, Tjernberg L, Ankarcrona M, Glaser E (2006) Degradation of the amyloid beta-protein by the novel mitochondrial peptidasome, PreP. *J. Biol. Chem.* 281:29096–104.

Fasshauer M, Klein J, Ueki K, Kriauciunas KM, Benito M, White MF, Kahn CR (2000) Essential role of insulin receptor substrate-2 in insulin stimulation of Glut4 translocation and glucose uptake in brown adipocytes. *J. Biol. Chem.* 275:25494–501.

Feldmann HM, Golozoubova V, Cannon B, Nedergaard J (2009) UCP1 ablation induces obesity and abolishes diet-induced thermogenesis in mice exempt from thermal stress by living at thermoneutrality. *Cell Metab.* 9:203–9.

Ferreirinha F, Quattrini A (2004) Axonal degeneration in paraplegin-deficient mice is associated with abnormal mitochondria and impairment of axonal transport. *J. Clin. Invest.* 113:231–242.

Fischer F, Weil A, Hamann A, Osiewacz HD (2013) Human CLPP reverts the longevity phenotype of a fungal ClpP deletion strain. *Nat. Commun.* 4:1397.

Fraile JM, Ordóñez GR, Quirós PM, Astudillo A, Galván JA, Colomer D, López-Otín C, Freije JMP, Puente XS (2013) Identification of novel tumor suppressor proteases by degradome profiling of colorectal carcinomas. *Oncotarget* 4:1931–2.

Frank S, Gaume B, Bergmann-Leitner ES, Leitner WW, Robert EG, Catez F, Smith CL, Youle RJ (2001) The role of dynamin-related protein 1, a mediator of mitochondrial fission, in apoptosis. *Dev. Cell* 1:515–25.

Freeman H, Shimomura K, Horner E, Cox RD, Ashcroft FM (2006) Nicotinamide nucleotide transhydrogenase: a key role in insulin secretion. *Cell Metab.* 3:35–45.

Frezza C, Cipolat S, Martins de Brito O, Micaroni M, Beznoussenko GV, Rudka T, Bartoli D, Polishuck RS, Danial NN, De Strooper B, Scorrano L (2006) OPA1 controls apoptotic cristae remodeling independently from mitochondrial fusion. *Cell* 126:177–89.

Friedman JR, Nunnari J (2014) Mitochondrial form and function. *Nature* 505:335–43.

Fukuda R, Zhang H, Kim Jw, Shimoda L, Dang CV, Semenza GL (2007) HIF-1 regulates cytochrome oxidase subunits to optimize efficiency of respiration in hypoxic cells. *Cell* 129:111–22.

Gakh O, Cavadini P, Isaya G (2002) Mitochondrial processing peptidases. *Biochim. Biophys. Acta* 1592:63–77.

Galluzzi L, Kepp O, Vander Heiden MG, Kroemer G (2013) Metabolic targets for cancer therapy. *Nat. Rev. Drug Discovery* 12:829–46.

Gardner PR, Nguyen DD, White CW (1994) Aconitase is a sensitive and critical target of oxygen poisoning in cultured mammalian cells and in rat lungs. *Proc. Natl. Acad. Sci. U.S.A.* 91:12248–52.

Gerdes F, Tatsuta T, Langer T (2012) Mitochondrial AAA proteases–towards a molecular understanding of membrane-bound proteolytic machines. *Biochim. Biophys. Acta* 1823:49–55.

Gomes LC, Di Benedetto G, Scorrano L (2011) During autophagy mitochondria elongate, are spared from degradation and sustain cell viability. *Nat. Cell Biol.* 13:589–98.

Gordon LB, Rothman FG, López-Otín C, Misteli T (2014) Progeria: a paradigm for translational medicine. *Cell* 156:400–7.

Gutierrez-Fernandez A, Fueyo A, Folgueras AR, Garabaya C, Pennington CJ, Pilgrim S, Edwards DR, Holliday DL, Jones JL, Span PN, Sweep FCGJ, Puente XS, Lopez-Otin C (2008) Matrix metalloproteinase-8 functions as a metastasis suppressor through modulation of tumor cell adhesion and invasion. *Cancer Res.* 68:2755–63.

Hanahan D, Weinberg RA (2011) Hallmarks of cancer: the next generation. *Cell* 144:646–74.

Hance N, Ekstrand MI, Trifunovic A (2005) Mitochondrial DNA polymerase gamma is essential for mammalian embryogenesis. *Hum. Mol. Genet.* 14:1775–83.

Hansen J, Svenstrup K, Ang D, Nielsen MN, Christensen JH, Gregersen N, Nielsen JrE, Georgopoulos C, Bross P (2007) A novel mutation in the HSPD1 gene in a patient with hereditary spastic paraplegia. *J Neurol* 254:897–900.

Haynes CM, Petrova K, Benedetti C, Yang Y, Ron D (2007) ClpP mediates activation of a mitochondrial unfolded protein response in C. elegans. *Dev. Cell* 13:467–80.

Haynes CM, Ron D (2010) The mitochondrial UPR - protecting organelle protein homeostasis. *J. Cell Sci.* 123:3849–55.

Head B, Griparic L, Amiri M, Gandre-Babbe S, van der Bliek AM (2009) Inducible proteolytic inactivation of OPA1 mediated by the OMA1 protease in mammalian cells. *J. Cell Biol.* 187:959–66.

Hirschey MD, Shimazu T, Goetzman E, Jing E, Schwer B, Lombard DB, Grueter Ca, Harris C, Biddinger S, Ilkayeva OR, Stevens RD, Li Y, Saha AK, Ruderman NB, Bain JR, Newgard CB, Farese RV, Alt FW, Kahn CR, Verdin E (2010) SIRT3 regulates mitochondrial fatty-acid oxidation by reversible enzyme deacetylation. *Nature* 464:121–5.

Houtkooper RH, Mouchiroud L, Ryu D, Moullan N, Katsyuba E, Knott G, Williams RW, Auwerx J (2013) Mitonuclear protein imbalance as a conserved longevity mechanism. *Nature* 497:451–7.

Hsu PP, Sabatini DM (2008) Cancer cell metabolism: Warburg and beyond. *Cell* 134:703–7.

Huang G, Lu H, Hao A, Ng DCH, Ponniah S, Guo K, Lufei C, Zeng Q, Cao X (2004) GRIM-19, a cell death regulatory protein, is essential for assembly and function of mitochondrial complex I. *Mol. Cell. Biol.* 24:8447–56.

Ishihara N, Fujita Y, Oka T, Mihara K (2006) Regulation of mitochondrial morphology through proteolytic cleavage of OPA1. *EMBO J.* 25:2966–77.

Itoh K, Nakamura K, Iijima M, Sesaki H (2013) Mitochondrial dynamics in neurodegeneration. *Trends Cell Biol* 23:64–71.

Jenkinson EM, Rehman AU, Walsh T, Clayton-Smith J, Lee K, Morell RJ, Drummond MC, Khan SN, Naeem MA, Rauf B, Billington N, Schultz JM, Urquhart JE, Lee MK, Berry A, Hanley NA, Mehta S, Cilliers D, Clayton PE, Kingston H, Smith MJ, Warner TT, Black GC, Trump D, Davis JRE, Ahmad W, Leal SM, Riazuddin S, King MC, Friedman TB, Newman WG (2013) Perrault syndrome is caused by recessive mutations in CLPP, encoding a mitochondrial ATP-dependent chambered protease. *Am. J. Hum. Genet.* 92:605–13.

Jin SM, Lazarou M, Wang C, Kane La, Narendra DP, Youle RJ (2010) Mitochondrial membrane potential regulates PINK1 import and proteolytic destabilization by PARL. *J. Cell Biol.* 191:933–42.

Jorge I, Navarro P, Martínez-Acedo P, Núñez E, Serrano H, Alfranca A, Redondo JM, Vázquez J (2009) Statistical model to analyze quantitative proteomics data obtained by 18O/16O labeling and linear ion trap mass spectrometry: application to the study of vascular endothelial growth factor-induced angiogenesis in endothelial cells. *Mol. Cell. Proteomics* 8:1130–49.

Karbowski M, Lee YJ, Gaume B, Jeong SY, Frank S, Nechushtan A, Santel A, Fuller M, Smith CL, Youle RJ (2002) Spatial and temporal association of Bax with mitochondrial fission sites, Drp1, and Mfn2 during apoptosis. *J. Cell Biol.* 159:931–8.

Kasahara A, Cipolat S, Chen Y, Dorn GW, Scorrano L (2013) Mitochondrial fusion directs cardiomyocyte differentiation via calcineurin and Notch signaling. *Science* 342:734–7.

Kaser M, Kambacheld M, Kisters-Woike B, Langer T (2003) Oma1, a novel membrane-bound metallopeptidase in mitochondria with activities overlapping with the m-AAA protease. *J. Biol. Chem.* 278:46414–23.

Kitada T, Asakawa S, Hattori N, Matsumine H, Yamamura Y, Minoshima S, Yokochi M, Mizuno Y, Shimizu N (1998) Mutations in the parkin gene cause autosomal recessive juvenile parkinsonism. *Nature* 392:605–8.

Koopman WJH, Distelmaier F, Smeitink JaM, Willems PHGM (2013) OXPHOS mutations and neurodegeneration. *EMBO J.* 32:9–29.

Koopman WJH, Willems PHGM, Smeitink JAM, Ph D (2012) Monogenic mitochondrial disorders. *N. Engl. J. Med.* 366:1132–41.

Koppen M, Metodiev MD, Casari G, Rugarli EI, Langer T (2007) Variable and tissue-specific subunit composition of mitochondrial m-AAA protease complexes linked to hereditary spastic paraplegia. *Mol. Cell. Biol.* 27:758–67.

Kozak LP (2010) Brown fat and the myth of diet-induced thermogenesis. *Cell Metab.* 11:263–7.

Kwong JQ, Beal MF, Manfredi G (2006) The role of mitochondria in inherited neurodegenerative diseases. *J. Neurochem.* 97:1659–75.

Landes T, Leroy I, Bertholet A, Diot A, Khosrobakhsh F, Daloyau M, Davezac N, Miquel MC, Courilleau D, Guillou E, Olichon A, Lenaers G, Arnauné-Pelloquin L, Emorine LJ, Belenguer P (2010) OPA1 (dys)functions. *Semin. Cell Dev. Biol.* 21:593–8.

Landor SKJ, Mutvei AP, Mamaeva V, Jin S, Busk M, Borra R, Grönroos TJ, Kronqvist P, Lendahl U, Sahlgren CM (2011) Hypo- and hyperactivated Notch signaling induce a glycolytic switch through distinct mechanisms. *Proc. Natl. Acad. Sci. U.S.A.* 108:18814–9.

Lapuente-Brun E, Moreno-Loshuertos R, Acin-Perez R, Latorre-Pellicer A, Colas C, Balsa E, Perales-Clemente E, Quiros PM, Calvo E, Rodriguez-Hernandez MA, Navas P, Cruz R, Carracedo A, Lopez-Otin C, Perez-Martos A, Fernandez-Silva P, Fernandez-Vizarra E, Enriquez JA (2013) Supercomplex Assembly Determines Electron Flux in the Mitochondrial Electron Transport Chain. *Science* 340:1567–1570.

Liesa M, Shirihai OS (2013) Mitochondrial dynamics in the regulation of nutrient utilization and energy expenditure. *Cell Metab.* 17:491–506.

Lin J, Wu PH, Tarr PT, Lindenberg KS, St-Pierre J, Zhang CY, Mootha VK, Jäger S, Vianna CR, Reznick RM, Cui L, Manieri M, Donovan MX, Wu Z, Cooper MP, Fan MC, Rohas LM, Zavacki AM, Cinti S, Shulman GI, Lowell BB, Krainc D, Spiegelman BM (2004) Defects in adaptive energy metabolism with CNS-linked hyperactivity in PGC-1alpha null mice. *Cell* 119:121–35.

Lopez-Otin C, Blasco Ma, Partridge L, Serrano M, Kroemer G, López-Otín C (2013) The Hallmarks of Aging. *Cell* 153:1194–1209.

López-Otín C, Bond JS (2008) Proteases: multifunctional enzymes in life and disease. *J. Biol. Chem.* 283:30433–7.

López-Otín C, Hunter T (2010) The regulatory crosstalk between kinases and proteases in cancer. *Nat. Rev. Cancer* 10:278–92.

López-Otín C, Overall CM (2002) Protease degradomics: a new challenge for proteomics. *Nat. Rev. Mol. Cell Biol.* 3:509–19.

Losón OC, Song Z, Chen H, Chan DC (2013) Fis1, Mff, MiD49, and MiD51 mediate Drp1 recruitment in mitochondrial fission. *Mol. Biol. Cell* 24:659–67.

Lu B, Liu T, Crosby Ja, Thomas-Wohlever J, Lee I, Suzuki CK (2003) The ATP-dependent Lon protease of Mus musculus is a DNA-binding protein that is functionally conserved between yeast and mammals. *Gene* 306:45–55.

Luce K, Osiewacz HD (2009) Increasing organismal healthspan by enhancing mitochondrial protein quality control. *Nat. Cell Biol.* 11:852–8.

Magen D, Georgopoulos C, Bross P, Ang D, Segev Y, Goldsher D, Nemirovski A, Shahar E, Ravid S, Luder A, Heno B, Gershoni-Baruch R, Skorecki K, Mandel H (2008) Mitochondrial hsp60 chaperonopathy causes an autosomal-recessive neurodegenerative disorder linked to brain hypomyelination and leukodystrophy. *Am. J. Hum. Genet.* 83:30–42.

Maltecca F, Aghaie A, Schroeder DG, Cassina L, Taylor BA, Phillips SJ, Malaguti M, Previtali S, Guénet JL, Quattrini A, Cox GA, Casari G (2008) The mitochondrial protease AFG3L2 is essential for axonal development. *J. Neurosci.* 28:2827–36.

Mariño G, Niso-Santano M, Baehrecke EH, Kroemer G (2014) Self-consumption: the interplay of autophagy and apoptosis. *Nat. Rev. Mol. Cell Biol.* 15:81–94.

Mariño G, Ugalde AP, Salvador-Montoliu N, Varela I, Quirós PM, Cadiñanos J, van der Pluijm I, Freije JMP, López-Otín C (2008) Premature aging in mice activates a systemic metabolic response involving autophagy induction. *Hum. Mol. Genet.* 17:2196–211.

Martínez-Bartolomé S, Navarro P, Martín-Maroto F, López-Ferrer D, Ramos-Fernández A, Villar M, García-Ruiz JP, Vázquez J (2008) Properties of average score distributions of SEQUEST: the probability ratio method. *Mol. Cell. Proteomics* 7:1135–45.

Matsushima Y, Goto Yi, Kaguni LS (2010) Mitochondrial Lon protease regulates mitochondrial DNA copy number and transcription by selective degradation of mitochondrial transcription factor A (TFAM). *Proc. Natl. Acad. Sci. U.S.A.* 107:18410–5.

McBride HM, Neuspiel M, Wasiak S (2006) Mitochondria: more than just a powerhouse. *Curr Biol* 16:R551–60.

Menendez JA, Lupu R (2007) Fatty acid synthase and the lipogenic phenotype in cancer pathogenesis. *Nat. Rev. Cancer* 7:763–77.

Metallo CM, Vander Heiden MG (2013) Understanding metabolic regulation and its influence on cell physiology. *Mol. Cell* 49:388–98.

Miyake N, Yano S, Sakai C, Hatakeyama H, Matsushima Y, Shiina M, Watanabe Y, Bartley J, Abdenur JE, Wang RY, Chang R, Tsurusaki Y, Doi H, Nakashima M, Saitsu H, Ogata K, Goto YI, Matsumoto N (2013) Mitochondrial complex III deficiency caused by a homozygous UQCRC2 mutation presenting with neonatal-onset recurrent metabolic decompensation. *Hum. Mutat.* 34:446–52.

Molina AJA, Wikstrom JD, Stiles L, Las G, Mohamed H, Elorza A, Walzer G, Twig G, Katz S, Corkey BE, Shirihai OS (2009) Mitochondrial networking protects beta-cells from nutrient-induced apoptosis. *Diabetes* 58:2303–15.

Mouchiroud L, Houtkooper RH, Moullan N, Katsyuba E, Ryu D, Cantó C, Mottis A, Jo YS, Viswanathan M, Schoonjans K, Guarente L, Auwerx J (2013) The NAD(+)/Sirtuin Pathway Modulates Longevity through Activation of Mitochondrial UPR and FOXO Signaling. *Cell* 154:430–41.

Murphy MP (2009) How mitochondria produce reactive oxygen species. *Biochem J* 417:1–13.

Nakamura N, Hirose S (2008) Regulation of mitochondrial morphology by USP30, a deubiquitinating enzyme present in the mitochondrial outer membrane. *Mol. Biol. Cell* 19:1903–1911.

Navarro CL, Cadiñanos J, De Sandre-Giovannoli A, Bernard R, Courrier S, Boccaccio I, Boyer A, Kleijer WJ, Wagner A, Giuliano F, Beemer FA, Freije JM, Cau P, Hennekam RCM, López-Otín C, Badens C, Lévy N (2005) Loss of ZMPSTE24 (FACE-1) causes autosomal recessive restrictive dermopathy and accumulation of Lamin A precursors. *Hum. Mol. Genet.* 14:1503–13.

Navarro P, Vázquez J (2009) A refined method to calculate false discovery rates for peptide identification using decoy databases. *J. Proteome Res.* 8:1792–6.

Neufert C, Becker C, Neurath MF (2007) An inducible mouse model of colon carcinogenesis for the analysis of sporadic and inflammation-driven tumor progression. *Nat. Protoc.* 2:1998–2004.

Nijtmans LGJ, Henderson NS, Holt IJ (2002) Blue Native electrophoresis to study mitochondrial and other protein complexes. *Methods (San Diego, Calif.)* 26:327–34.

Nunnari J, Suomalainen A (2012) Mitochondria: in sickness and in health. *Cell* 148:1145–59.

Olichon a, Elachouri G, Baricault L, Delettre C, Belenguer P, Lenaers G (2007) OPA1 alternate splicing uncouples an evolutionary conserved function in mitochondrial fusion from a vertebrate restricted function in apoptosis. *Cell Death Differ.* 14:682–92.

Osman C, Merkwirth C, Langer T (2009) Prohibitins and the functional compartmentalization of mitochondrial membranes. *J. Cell Sci.* 122:3823–30.

O'Toole JF, Liu Y, Davis EE, Westlake CJ, Attanasio M, Otto EA, Seelow D, Nurnberg G, Becker C, Nuutinen M, Kärppä M, Ignatius J, Uusimaa J, Pakanen S, Jaakkola E, van den Heuvel LP, Fehrenbach H, Wiggins R, Goyal M, Zhou W, Wolf MTF, Wise E, Helou J, Allen SJ, Murga-Zamalloa CA, Ashraf S, Chaki M, Heeringa S, Chernin G, Hoskins BE, Chaib H, Gleeson J, Kusakabe T, Suzuki T, Isaac RE, Quarmby LM, Tennant B, Fujioka H, Tuominen H, Hassinen I, Lohi H, van Houten JL, Rotig A, Sayer JA, Rolinski B, Freisinger P, Madhavan SM, Herzer M, Madignier F, Prokisch H, Nurnberg P, Jackson PK, Jackson P, Khanna H, Katsanis N, Hildebrandt F (2010) Individuals with mutations in XPNPEP3, which encodes a mitochondrial protein, develop a nephronophthisis-like nephropathy. *J. Clin. Invest.* 120:791–802.

Owusu-Ansah E, Song W, Perrimon N (2013) Muscle mitohormesis promotes longevity via systemic repression of insulin signaling. *Cell* 155:699–712.

Pagliarini DJ, Calvo SE, Chang B, Sheth Sa, Vafai SB, Ong SE, Walford Ga, Sugiana C, Boneh A, Chen WK, Hill DE, Vidal M, Evans JG, Thorburn DR, Carr Sa, Mootha VK (2008) A mitochondrial protein compendium elucidates complex I disease biology. *Cell* 134:112–23.

Pagliarini DJ, Rutter J (2013) Hallmarks of a new era in mitochondrial biochemistry. *Genes Dev* 27:2615–27.

Park YY, Lee S, Karbowski M, Neutzner A, Youle RJ, Cho H (2010) Loss of MARCH5 mitochondrial E3 ubiquitin ligase induces cellular senescence through dynamin-related protein 1 and mitofusin 1. *J. Cell Sci.* 123:619–26.

Payne M, Yang Z, Katz BJ, Warner JEA, Weight CJ, Zhao Y, Pearson ED, Treft RL, Hillman T, Kennedy RJ, Meire FM, Zhang K (2004) Dominant optic atrophy, sensorineural hearing loss, ptosis, and ophthalmoplegia: a syndrome caused by a missense mutation in OPA1. *Am J Ophthalmol* 138:749–55.

Pendás AM, Zhou Z, Cadiñanos J, Freije JMP, Wang J, Hultenby K, Astudillo A, Wernerson A, Rodríguez F, Tryggvason K, López-Otín C (2002) Defective prelamin A processing and muscular and adipocyte alterations in Zmpste24 metalloproteinase-deficient mice. *Nat. Genet.* 31:94–9.

Petek E, Windpassinger C, Vincent JB, Cheung J, Boright AP, Scherer SW, Kroisel PM, Wagner K (2001) Disruption of a novel gene (IMMP2L) by a breakpoint in 7q31 associated with Tourette syndrome. *Am. J. Hum. Genet.* 68:848–58.

Pierson TM, Adams D, Bonn F, Martinelli P, Cherukuri PF, Teer JK, Hansen NF, Cruz P, Mullikin For The Nisc Comparative Sequencing Program JC, Blakesley RW, Golas G, Kwan J, Sandler A, Fuentes Fajardo K, Markello T, Tifft C, Blackstone C, Rugarli EI, Langer T, Gahl WA, Toro C (2011) Whole-exome sequencing identifies homozygous AFG3L2 mutations in a spastic ataxia-neuropathy syndrome linked to mitochondrial m-AAA proteases. *PLoS Genet.* 7:e1002325.

Pinho CM, Björk BF, Alikhani N, Bäckman HG, Eneqvist T, Fratiglioni L, Glaser E, Graff C (2010) Genetic and biochemical studies of SNPs of the mitochondrial A beta-degrading protease, hPreP. *Neurosci. Lett.* 469:204–8.

Poole AC, Thomas RE, Andrews LA, McBride HM, Whitworth AJ, Pallanck LJ (2008) The PINK1/Parkin pathway regulates mitochondrial morphology. *Proc. Natl. Acad. Sci. U.S.A.* 105:1638–43.

Powers ET, Morimoto RI, Dillin A, Kelly JW, Balch WE (2009) Biological and chemical approaches to diseases of proteostasis deficiency. *Annu. Rev. Biochem.* 78:959–91.

Rivera-Torres J, Acín-Perez R, Cabezas-Sánchez P, Osorio FG, Gonzalez-Gómez C, Megias D, Cámara C, López-Otín C, Enríquez JA, Luque-García JL, Andrés V (2013) Identification of mitochondrial dysfunction in Hutchinson-Gilford progeria syndrome through use of stable isotope labeling with amino acids in cell culture. *J Proteomics* 91:466–77.

Rugarli EI, Langer T (2012) Mitochondrial quality control: a matter of life and death for neurons. *EMBO J.* 31:1336–49.

Sabbisetti V, Di Napoli A, Seeley A, Amato AM, O'Regan E, Ghebremichael M, Loda M, Signoretti S (2009) p63 promotes cell survival through fatty acid synthase. *PLoS One* 4:e5877.

Schägger H (1995) Native electrophoresis for isolation of mitochondrial oxidative phosphorylation protein complexes. *Methods Enzymol* 260:190–202.

Schmidt O, Pfanner N, Meisinger C (2010) Mitochondrial protein import: from proteomics to functional mechanisms. *Nat. Rev. Mol. Cell Biol.* 11:655–67.

Schneeberger M, Dietrich MO, Sebastián D, Imbernón M, Castaño C, Garcia A, Esteban Y, Gonzalez-Franquesa A, Rodríguez IC, Bortolozzi A, Garcia-Roves PM, Gomis R, Nogueiras R, Horvath TL, Zorzano A, Claret M (2013) Mitofusin 2 in POMC Neurons Connects ER Stress with Leptin Resistance and Energy Imbalance. *Cell* 155:172–87.

Schon EA, DiMauro S, Hirano M (2012) Human mitochondrial DNA: roles of inherited and somatic mutations. *Nat. Rev. Genet.* 13:878–90.

Seale P, Kajimura S, Spiegelman BM (2009) Transcriptional control of brown adipocyte development and physiological function–of mice and men. *Genes Dev* 23:788–97.

Sebastián D, Hernández-Alvarez MI, Segalés J, Sorianello E, Muñoz JP, Sala D, Waget A, Liesa M, Paz JC, Gopalacharyulu P, Orešič M, Pich S, Burcelin R, Palacín M, Zorzano A (2012) Mitofusin 2 (Mfn2) links mitochondrial and endoplasmic reticulum function with insulin signaling and is essential for normal glucose homeostasis. *Proc. Natl. Acad. Sci. U.S.A.* 109:5523–8.

Sharpley MS, Marciniak C, Eckel-Mahan K, McManus M, Crimi M, Waymire K, Lin CS, Masubuchi S, Friend N, Koike M, Chalkia D, MacGregor G, Sassone-Corsi P, Wallace DC (2012) Heteroplasmy of mouse mtDNA is genetically unstable and results in altered behavior and cognition. *Cell* 151:333–43.

Shen WJ, Zaidi SK, Patel S, Cortez Y, Ueno M, Azhar R, Azhar S, Kraemer FB (2012) Ablation of vimentin results in defective steroidogenesis. *Endocrinology* 153:3249–57.

Shenouda SM, Widlansky ME, Chen K, Xu G, Holbrook M, Tabit CE, Hamburg NM, Frame AA, Caiano TL, Kluge MA, Duess MA, Levit A, Kim B, Hartman ML, Joseph L, Shirihai OS, Vita JA (2011) Altered mitochondrial dynamics contributes to endothelial dysfunction in diabetes mellitus. *Circulation* 124:444–53.

Shi G, Lee JR, Grimes DA, Racacho L, Ye D, Yang H, Ross OA, Farrer M, McQuibban GA, Bulman DE (2011) Functional alteration of PARL contributes to mitochondrial dysregulation in Parkinson's disease. *Hum. Mol. Genet.* 20:1966–74.

Shimohata N, Chiba S, Saikawa N, Ito K, Akiyama Y (2002) The Cpx stress response system of Escherichia coli senses plasma membrane proteins and controls HtpX, a membrane protease with a cytosolic active site. *Genes to cells : devoted to molecular & cellular mechanisms* 7:653–62.

Smirnova E, Shurland DL, Ryazantsev SN, van der Bliek AM (1998) A human dynamin-related protein controls the distribution of mitochondria. *J. Cell Biol.* 143:351–8.

Song Z, Chen H, Fiket M, Alexander C, Chan DC (2007) OPA1 processing controls mitochondrial fusion and is regulated by mRNA splicing, membrane potential, and Yme1L. *J. Cell Biol.* 178:749–55.

Soung YH, Lee JW, Kim SY, Sung YJ, Park WS, Nam SW, Kim SH, Lee JY, Yoo NJ, Lee SH (2005) Caspase-8 gene is frequently inactivated by the frameshift somatic mutation 1225_1226delTG in hepatocellular carcinomas. *Oncogene* 24:141–7.

Stahl A, Moberg P, Ytterberg J, Panfilov O, Brockenhuus Von Lowenhielm H, Nilsson F, Glaser E (2002) Isolation and identification of a novel mitochondrial metalloprotease (PreP) that degrades targeting presequences in plants. *J. Biol. Chem.* 277:41931–9.

Stiburek L, Cesnekova J, Kostkova O, Fornuskova D, Vinsova K, Wenchich L, Houstek J, Zeman J (2012) YME1L controls the accumulation of respiratory chain subunits and is required for apoptotic resistance, cristae morphogenesis, and cell proliferation. *Mol. Biol. Cell* 23:1010–23.

Strauss KM, Martins LM, Plun-Favreau H, Marx FP, Kautzmann S, Berg D, Gasser T, Wszolek Z, Müller T, Bornemann A, Wolburg H, Downward J, Riess O, Schulz JB, Krüger R (2005) Loss of function mutations in the gene encoding Omi/HtrA2 in Parkinson's disease. *Hum. Mol. Genet.* 14:2099–111.

Sun T, Gao Y, Tan W, Ma S, Shi Y, Yao J, Guo Y, Yang M, Zhang X, Zhang Q, Zeng C, Lin D (2007) A six-nucleotide insertion-deletion polymorphism in the CASP8 promoter is associated with susceptibility to multiple cancers. *Nat. Genet.* 39:605–13.

Tanaka A, Cleland MM, Xu S, Narendra DP, Suen DF, Karbowski M, Youle RJ (2010) Proteasome and p97 mediate mitophagy and degradation of mitofusins induced by Parkin. *J. Cell Biol.* 191:1367–80.

Tang HL, Lung HL, Wu KC, Le AHP, Tang HM, Fung MC (2008) Vimentin supports mitochondrial morphology and organization. *Biochem J* 410:141–6.

Tatsuta T, Langer T (2008) Quality control of mitochondria: protection against neurodegeneration and ageing. *EMBO J.* 27:306–14.

Theodoridis G, Gika HG, Wilson ID (2008) LC-MS-based methodology for global metabolite profiling in metabonomics/metabolomics. *TrAC Trends in Analytical Chemistry* 27:251–260.

Tschöp MH, Speakman JR, Arch JRS, Auwerx J, Brüning JC, Chan L, Eckel RH, Farese RV, Galgani JE, Hambly C, Herman MA, Horvath TL, Kahn BB, Kozma SC, Maratos-Flier E, Müller TD, Münzberg H, Pfluger PT, Plum L, Reitman ML, Rahmouni K, Shulman GI, Thomas G, Kahn CR, Ravussin E (2012) A guide to analysis of mouse energy metabolism. *Nat. Methods* 9:57–63.

Twig G, Elorza A, Molina AJa, Mohamed H, Wikstrom JD, Walzer G, Stiles L, Haigh SE, Katz S, Las G, Alroy J, Wu M, Py BF, Yuan J, Deeney JT, Corkey BE, Shirihai OS (2008) Fission and selective fusion govern mitochondrial segregation and elimination by autophagy. *EMBO J.* 27:433–46.

Ugalde AP, Mariño G, López-Otín C (2010) Rejuvenating somatotropic signaling: a therapeutical opportunity for premature aging? *Aging* 2:1017–22.

Valente EM, Abou-Sleiman PM, Caputo V, Muqit MMK, Harvey K, Gispert S, Ali Z, Del Turco D, Bentivoglio AR, Healy DG, Albanese A, Nussbaum R, González-Maldonado R, Deller T, Salvi S, Cortelli P, Gilks WP, Latchman DS, Harvey RJ, Dallapiccola B, Auburger G, Wood NW (2004) Hereditary early-onset Parkinson's disease caused by mutations in PINK1. *Science* 304:1158–60.

Valle A, Sastre-Serra J, Roca P, Oliver J (2010) Modulation of white adipose tissue proteome by aging and calorie restriction. *Aging Cell* 9:882–94.

Vander Heiden MG, Cantley LC, Thompson CB (2009) Understanding the Warburg effect: the metabolic requirements of cell proliferation. *Science* 324:1029–33.

Varela I, Cadiñanos J, Pendás AM, Gutiérrez-Fernández A, Folgueras AR, Sánchez LM, Zhou Z, Rodríguez FJ, Stewart CL, Vega Ja, Tryggvason K, Freije JMP, López-Otín C (2005) Accelerated ageing in mice deficient in Zmpste24 protease is linked to p53 signalling activation. *Nature* 437:564–8.

Varfolomeev EE, Schuchmann M, Luria V, Chiannilkulchai N, Beckmann JS, Mett IL, Rebrikov D, Brodianski VM, Kemper OC, Kollet O, Lapidot T, Soffer D, Sobe T, Avraham KB, Goncharov T, Holtmann H, Lonai P, Wallach D (1998) Targeted disruption of the mouse Caspase 8 gene ablates cell death induction by the TNF receptors, Fas/Apo1, and DR3 and is lethal prenatally. *Immunity* 9:267–76.

Venkatesh S, Lee J, Singh K, Lee I, Suzuki CK (2012) Multitasking in the mitochondrion by the ATP-dependent Lon protease. *Biochim. Biophys. Acta* 1823:56–66.

Villa-Bellosta R, Rivera-Torres J, Osorio FG, Acín-Pérez R, Enriquez Ja, López-Otín C, Andrés V (2013) Defective extracellular pyrophosphate metabolism promotes vascular calcification in a mouse model of Hutchinson-Gilford progeria syndrome that is ameliorated on pyrophosphate treatment. *Circulation* 127:2442–51.

Vögtle FN, Wortelkamp S, Zahedi RP, Becker D, Leidhold C, Gevaert K, Kellermann J, Voos W, Sickmann A, Pfanner N, Meisinger C (2009) Global analysis of the mitochondrial N-proteome identifies a processing peptidase critical for protein stability. *Cell* 139:428–39.

von der Malsburg K, Müller JM, Bohnert M, Oeljeklaus S, Kwiatkowska P, Becker T, Loniewska-Lwowska A, Wiese S, Rao S, Milenkovic D, Hutu DP, Zerbes RM, Schulze-Specking A, Meyer HE, Martinou JC, Rospert S, Rehling P, Meisinger C, Veenhuis M, Warscheid B, van der Klei IJ, Pfanner N, Chacinska A, van der Laan M (2011) Dual role of mitofilin in mitochondrial membrane organization and protein biogenesis. *Dev. Cell* 21:694–707.

Wallace DC (2011) Bioenergetic origins of complexity and disease. *Cold Spring Harbor Symp. Quant. Biol.* 76:1–16.

Wallace DC (2005) A mitochondrial paradigm of metabolic and degenerative diseases, aging, and cancer: a dawn for evolutionary medicine. *Annu. Rev. Genet.* 39:359–407.

Wallace DC (2012) Mitochondria and cancer. *Nat. Rev. Cancer* 12:685–98.

Wallace DC (2013) A mitochondrial bioenergetic etiology of disease. *J. Clin. Invest.* 123:1405–12.

Wallace DC, Fan W, Procaccio V (2010) Mitochondrial energetics and therapeutics. *Annual review of pathology* 5:297–348.

Ward PS, Thompson CB (2012) Metabolic reprogramming: a cancer hallmark even warburg did not anticipate. *Cancer Cell* 21:297–308.

Waterham HR, Koster J, van Roermund CWT, Mooyer PAW, Wanders RJA, Leonard JV (2007) A lethal defect of mitochondrial and peroxisomal fission. *N. Engl. J. Med.* 356:1736–41.

Wei Q, Dong G, Chen JK, Ramesh G, Dong Z (2013) Bax and Bak have critical roles in ischemic acute kidney injury in global and proximal tubule-specific knockout mouse models. *Kidney Int.* 84:138–48.

Wei Q, Dong Z (2012) Mouse model of ischemic acute kidney injury: technical notes and tricks. *Am. J. Physiol. Renal Physiol.* 303:F1487–94.

Westermann B (2010) Mitochondrial fusion and fission in cell life and death. *Nat. Rev. Mol. Cell Biol.* 11:872–84.

Wikstrom JD, Mahdaviani K, Liesa M, Sereda SB, Si Y, Las G, Twig G, Petrovic N, Zingaretti C, Graham A, Cinti S, Corkey BE, Cannon B, Nedergaard J, Shirihai OS (2014) Hormone-induced mitochondrial fission is utilized by brown adipocytes as an amplification pathway for energy expenditure. *EMBO J.* .

Yan H, Parsons DW, Jin G, McLendon R, Rasheed BA, Yuan W, Kos I, Batinic-Haberle I, Jones S, Riggins GJ, Friedman H, Friedman A, Reardon D, Herndon J, Kinzler KW, Velculescu VE, Vogelstein B, Bigner DD (2009) IDH1 and IDH2 mutations in gliomas. *N. Engl. J. Med.* 360:765–73.

Youle RJ, Narendra DP (2011) Mechanisms of mitophagy. *Nat. Rev. Mol. Cell Biol.* 12:9–14.

Youle RJ, van der Bliek AM (2012) Mitochondrial fission, fusion, and stress. *Science* 337:1062–5.

Zhan M, Brooks C, Liu F, Sun L, Dong Z (2013) Mitochondrial dynamics: regulatory mechanisms and emerging role in renal pathophysiology. *Kidney Int.* 83:568–81.

Zhang WC, Shyh-Chang N, Yang H, Rai A, Umashankar S, Ma S, Soh BS, Sun LL, Tai BC, Nga ME, Bhakoo KK, Jayapal SR, Nichane M, Yu Q, Ahmed DA, Tan C, Sing WP, Tam J, Thirugananam A, Noghabi MS, Pang YH, Ang HS, Mitchell W, Robson P, Kaldis P, Soo RA, Swarup S, Lim EH, Lim B (2012) Glycine decarboxylase activity drives non-small cell lung cancer tumor-initiating cells and tumorigenesis. *Cell* 148:259–72.

Zhang Z, Wakabayashi N, Wakabayashi J, Tamura Y, Song WJ, Sereda S, Clerc P, Polster BM, Aja SM, Pletnikov MV, Kensler TW, Shirihai OS, Iijima M, Hussain MA, Sesaki H (2011) The dynamin-related GTPase Opa1 is required for glucose-stimulated ATP production in pancreatic beta cells. *Mol. Biol. Cell* 22:2235–45.

Zhao J, Zhang J, Yu M, Xie Y, Huang Y, Wolff DW, Abel PW, Tu Y (2013) Mitochondrial dynamics regulates migration and invasion of breast cancer cells. *Oncogene* 32:4814–24.

Züchner S, De Jonghe P, Jordanova A, Claeys KG, Guergueltcheva V, Cherninkova S, Hamilton SR, Van Stavern G, Krajewski KM, Stajich J, Tournev I, Verhoeven K, Langerhorst CT, de Visser M, Baas F, Bird T, Timmerman V, Shy M, Vance JM (2006) Axonal neuropathy with optic atrophy is caused by mutations in mitofusin 2. *Annals of neurology* 59:276–81.

Züchner S, Mersiyanova IV, Muglia M, Bissar-Tadmouri N, Rochelle J, Dadali EL, Zappia M, Nelis E, Patitucci A, Senderek J, Parman Y, Evgrafov O, Jonghe PD, Takahashi Y, Tsuji S, Pericak-Vance MA, Quattrone A, Battaloglu E, Polyakov AV, Timmerman V, Schröder JM, Vance JM, Battologlu E (2004) Mutations in the mitochondrial GTPase mitofusin 2 cause Charcot-Marie-Tooth neuropathy type 2A. *Nat. Genet.* 36:449–51.

Zunino R, Schauss A, Rippstein P, Andrade-Navarro M, McBride HM (2007) The SUMO protease SENP5 is required to maintain mitochondrial morphology and function. *J. Cell Sci.* 120:1178–88.